NASA CONTRACTOR REPORT 177330

Parametric Study of Supersonic STOVL Flight Characteristics

David C. Rapp
General Dynamics Corporation

CONTRACT NAS2-11753
March 1985

NASA

NASA CONTRACTOR REPORT 177330

Parametric Study of Supersonic STOVL Flight Characteristics

David C. Rapp
General Dynamics Corporation
Forth Worth, Texas

Prepared for
Ames Research Center
Under Contract NAS2-11753

National Aeronautics and
Space Administration

Ames Research Center
Moffett Field, California 94035

FOREWORD

The author wishes to acknowledge the devotion of George Kidwell in pressing through the obstacles encountered in releasing the RFP for this contract. Special thanks is given to Dr. W. H. Foley for the opportunity to execute this contract under the General Dynamics E-7 Program. Specific recognition is given to Art Sheridan and Bernard Beard for contributions of technical guidance.

For the sake of clarity, U.S. Customary Units have been used throughout this report in lieu of S.I. (Metric) Units. A conversion table is provided in Appendix L.

TABLE OF CONTENTS

TABLE OF CONTENTS (Concluded)

LIST OF FIGURES

LIST OF FIGURES (Continued)

LIST OF FIGURES (Continued)

LIST OF FIGURES (Concluded)

LIST OF TABLES

LIST OF SYMBOLS

Symbol	Description
A/B	Afterburner.
a/g	Flight-path acceleration divided by gravitational constant, g.
AGL	Above ground level.
AOA	Angle of attack.
BLC	Boundary layer control.
C_D	Drag coefficient.
$C_{D_{00}}$	Zero-lift zero-camber drag coefficient.
C.G.	Center of gravity.
C_L	Lift coefficient.
$C_{L_{MAX}}$	Maximum lift coefficient.
C_M	Moment coefficient.
$C_{M_{\dot{\alpha}}}$	Aerodynamic-pitch-damping coefficient.
C_{m_q}	Pitch-damping coefficient.
g	Gravitational constant, 32.174 ft/sec^2
IRT	Intermediate rated thrust.
k	Ejector mass-split fraction. Aft-nozzle airflow divided by total fan airflow.
K	Gear air-spring force.
NASA	National Aeronautics and Space Administration.
P_s	Specific excess power.
R	Gear total reaction force.
RCR	Runway condition reading.
RCS	Reaction control system.
S	Wing area.

LIST OF SYMBOLS (Concluded)

Symbol	Description
S_g	Ground-roll distance.
SI	International System (of Units)
S_{REF}	Reference wing area.
STO	Short takeoff.
STOVL	Short takeoff and vertical landing.
TOGW	Takeoff gross weight.
V_{MIN}	Minimum level-flight speed.
V_{LO}	Liftoff speed.
W	Gross weight.
$\dot{z}$	Gear deflection rate.
α	Angle of attack.
ϕ	Ejector-augmentation ratio.
σ	Multiplicative factor that is applied to aerodynamic-ground-effect increments, which is a function of the height of the trailing-edge of the wing divided by the wing span.
ξ	Gear damping coefficient.

1. INTRODUCTION

Early in 1980, General Dynamics began a program to investigate the possibility of designing a V/STOL fighter/attack aircraft that would incorporate an existing engine, rather than designing a conceptual aircraft to given missions, which generally require new engines. Such a demonstrator aircraft could be built much sooner and at less cost than one requiring an engine development program.

Under a contract to NASA/Ames Research Center, General Dynamics designed Configuration E-7, a short takeoff and vertical landing (STOVL) aircraft with a design specification similar to that of the F-18A. The short-takeoff capability is made possible through the use of an ejector system that was developed under contract to NASA/Ames (References 1 through 4). In this system, two ejectors yield a respectable and dependable augmentation ratio that has been verified by a large-scale engine-driven model at Ames.

1.1 AIRCRAFT DESCRIPTION

The most prominent feature of the E-7 design is the propulsion system. As can be seen in Figure 1-1 the engine is installed such that the fan air and core flows are split into separate ducts. The core flow is ducted aft to a vectorable ventral nozzle. The fan air is ducted either forward to ejectors in the wing root (for propulsive lift) or aft to an axisymmetric nozzle in the tail (for forward thrust). Figures 1-2 through 1-4 illustrate the thrust-vectoring modes of hover, transition, and up-and-away flight, respectively.

The E-7 general arrangement and design parameters are shown in Figure 1-5. E-7 and its propulsion system are fully described in References 5 and 6.

1.2 PERFORMANCE METHODOLOGY

An important consideration during the E-7 design process was its performance at low speed. Typical required performance parameters during a design analysis are critical field length, landing ground roll, single-engine rate of climb, approach speed, and time from brake release to climbout speed. General Dynamics has, over the last few years, emphasized the development of its Mission Analysis and Performance System (MAPS) computer program. Three of the options in MAPS provide the performance engineer with a tool to analyze the low-speed capabilities of an aircraft. The goal of these low-speed performance options is to provide flexible tools for use during configuration analysis and selection. Flexibility during analysis is attained through user control over the input data. The input data controls not only

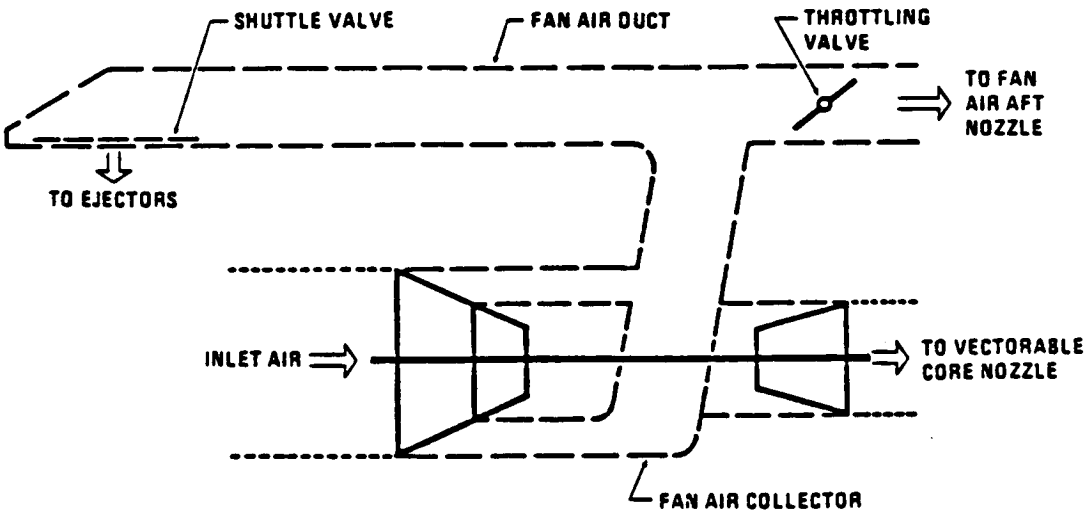

Figure 1-1, Propulsive System Schematic.

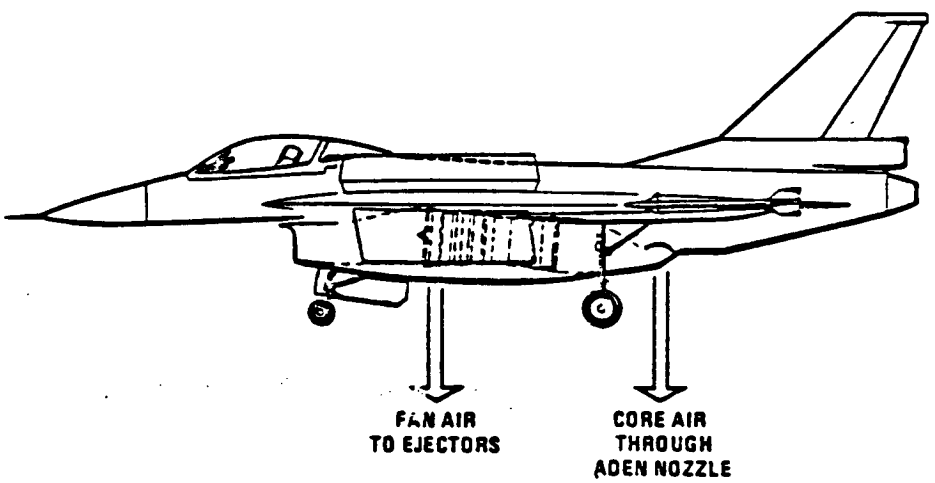

Figure 1-2, Propulsion System - Hover Configuration.

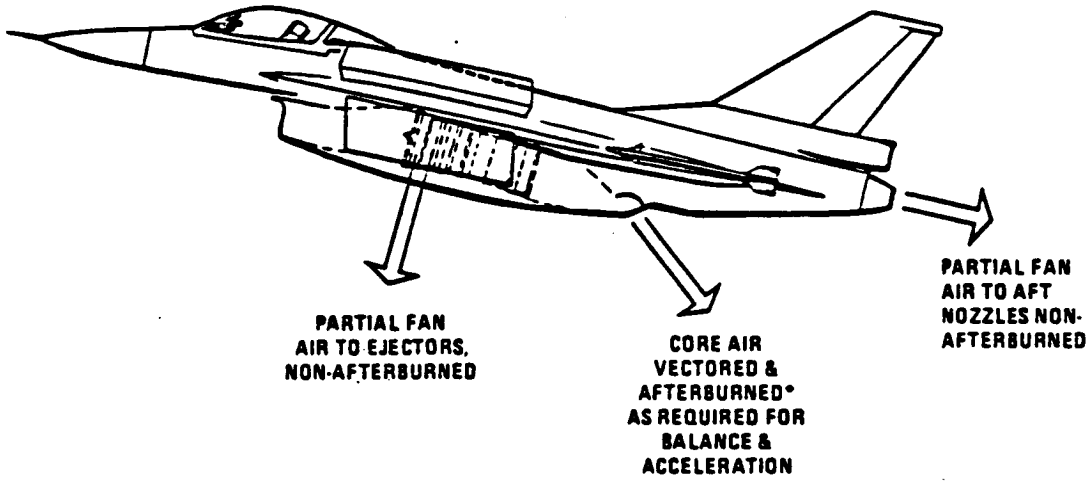

*CORE AFTERBURNED ONLY ON F101-DFE CONFIGURATIONS

Figure 1-3, Propulsion System - STO and Transition Configuration.

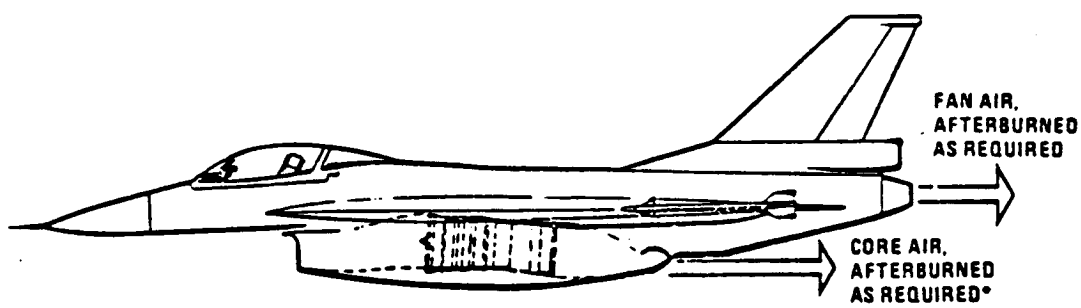

*ONLY ON F101-DFE CONFIGURATIONS

Figure 1-4, Propulsion System - Up-and-Away Configuration.

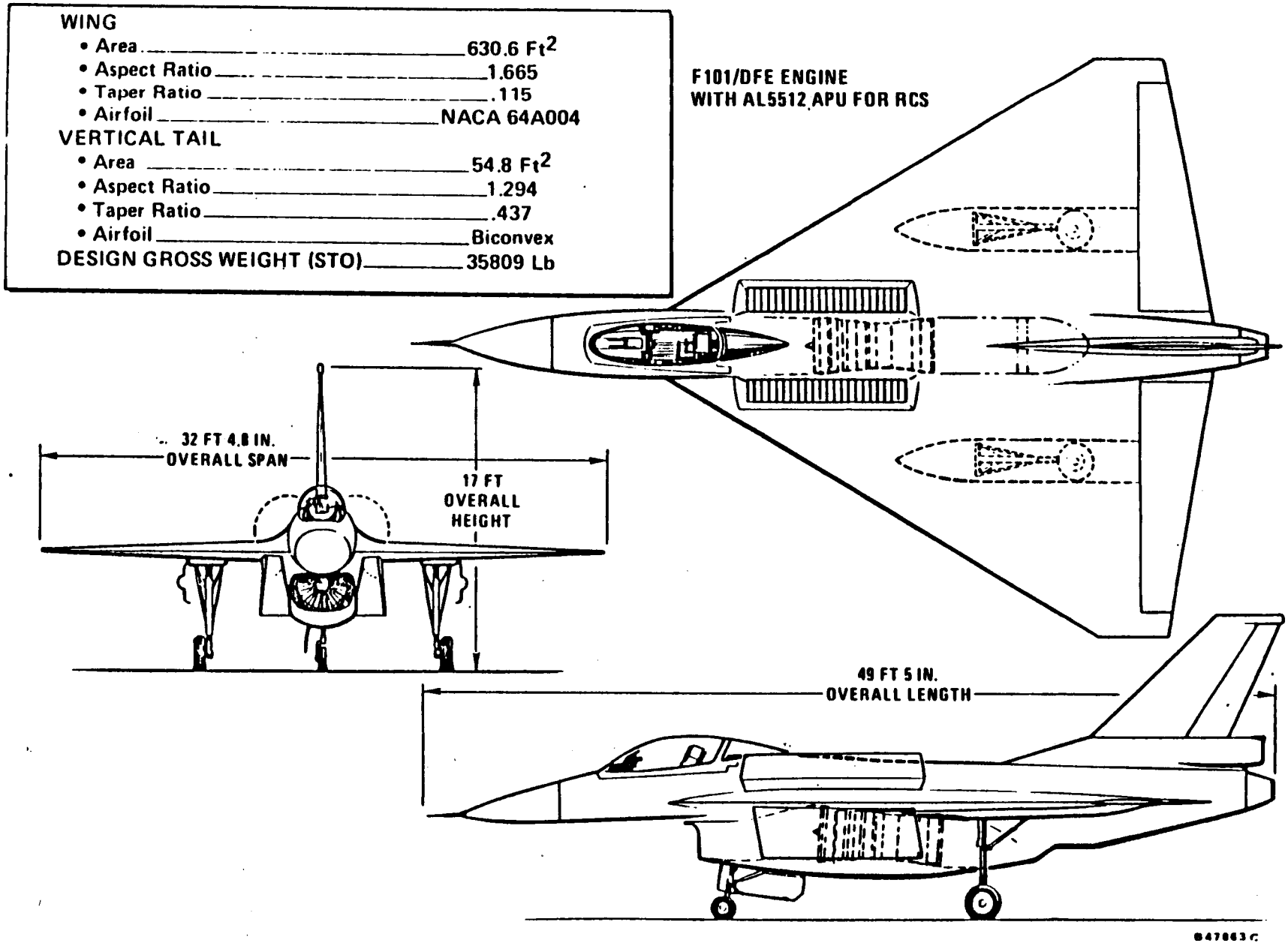

Figure 1-5. Configuration F-7 Three-View

the analysis performed, but the format of the output data as well. Each option analyzes a dif-ferent aspect of low-speed performance: flight-path performance (Option 70), point performance (Option 71), and some special performance parameters such as liftoff speed (Option 72).

1.2.1 Flight-Path Performance

The flight-path performance section numerically integrates the equations of motion. It is restricted to two-dimensional maneuvers (i.e., flight in the vertical plane). This section has the capability to simulate almost any operational technique or low-speed maneuver provided the aircraft remains in the vertical plane.

Many different low-speed maneuvers (such as takeoffs, accel-stops, and pop-ups), although complex as a whole, can be divided or partitioned into less complex segments. Each segment then becomes relatively simple to define in terms of the state and control variables as functions of time.

These segment definitions are guidance commands. In other words, the program varies the controls of the aircraft in an attempt to follow the segment definition. For example, during rotation, the guidance commands may be military power and a pitch rate of 2 deg/sec; during a cruise, they may be an altitude of 20,000 feet and a Mach number of 0.80. The guidance commands can specify a variable as a quadratic function of time, which allows almost any type of maneuver to be defined.

Since the path is segmented, a flexible method to terminate each segment and transfer to the next one is provided. In Option 70, the user can specify up to five different final conditions. Each final condition is stated in terms of a check variable, a termination value, and a segment to which to transfer. The variable can be any normal output variable such as time, distance, velocity, pitch angle, or angle of attack. Furthermore, the user has the option to define his own special output variables, as mathematical combinations of the normal output variables, which may be used to specify final conditions.

The use of guidance commands and final conditions in a conventional takeoff is shown in Figure 1-6. Initial conditions must be provided for the first segment. For subsequent seg-ments, the path is assumed to be continuous (though discontinu-ities in weight and time are allowed). In the first segment, the controls are specified directly; that is, the power setting is at maximum power and the elevator deflection is at 0 deg. After the aircraft has accelerated to 120 knots calibrated airspeed, the elevator is used to rotate the aircraft at a 2-deg/sec pitch rate until a pitch angle of 10 deg is reached. The program then solves for the elevator deflection necessary to achieve and maintain a 2-deg/sec pitch rate. The last segment specifies a constant 10-deg pitch angle until a 50-foot altitude is reached.

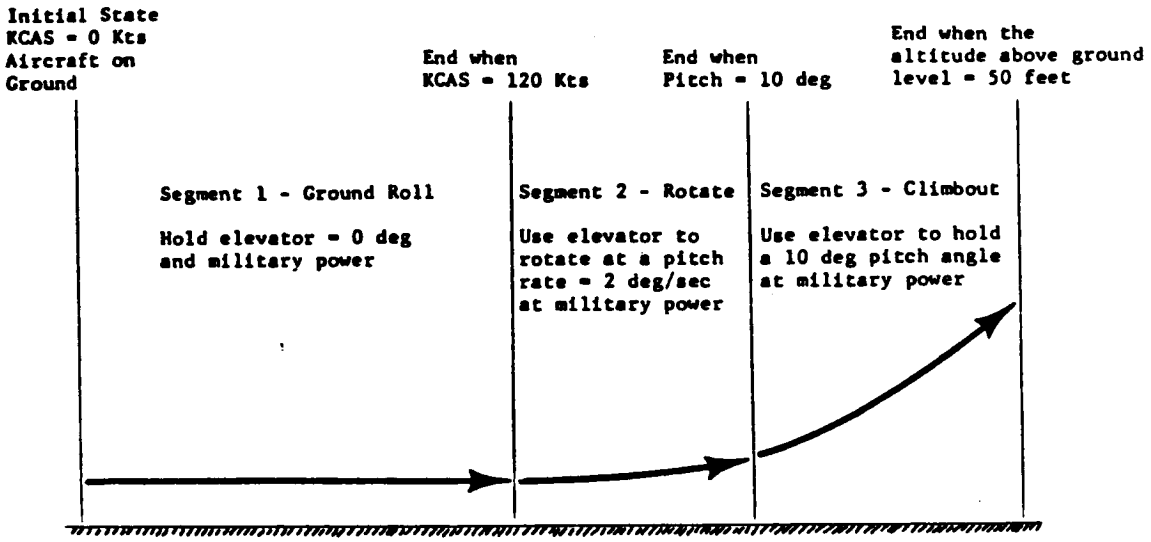

Figure 1-6, Sample Path Description.

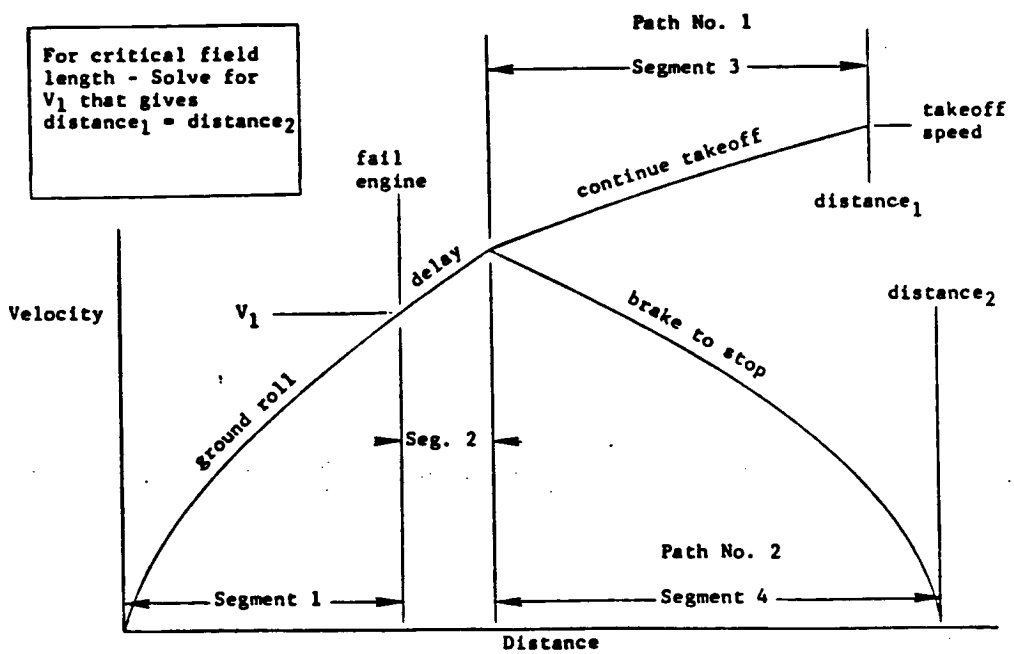

Figure 1-7, Sample Path Constraints.

Path control variables are not restricted to those variables associated with the flight controls (such as elevator deflection and power setting). Also, user-defined variables can be employed to control such items as ground effect, landing gear retraction, speed brakes, and other configuration-related variables.

By segmenting the path and by allowing flexible segment termination conditions, one can define nearly any type of flight path. However, it is often required to compare two paths (e.g., critical field lengths) or to satisfy path constraints (e.g., maximum brake-energy limits). Therefore, an option is available that allows one to define a second path; instead of transferring to a single segment after a final condition is encountered, one can transfer to two different segments. Figure 1-7 illustrates a method of calculating critical field length. A numerical search routine satisfies constraints by varying a parameter on one of the segments. In the example shown in Figure 1-7, the final condition for Segment 1 is the velocity that sets the distance at the end of Path 1 equal to the distance at the end of Path 2. A numerical search for this velocity is made until the two distances are equal. The user must specify which variable is being varied and the constraint that is being satisfied. Up to three searches can be performed on a path.

During a design analysis it is often required to analyze the effect of a certain design parameter on the low-speed performance (i.e., to perform a trade-off study). This is easily accomplished by allowing the user to define survey loops that systematically vary parameters defining the path or controlling the forces. The program generates a flight path for each of the presecribed combinations of the design parameters.

The user can define summary variables that compare data among surveyed paths. These variables are useful in obtaining incremental data by comparing paths generated in a survey to a reference or baseline path. This data allows the effect of a single parameter on the flight path to be studied, and it aids in the generation of performance substantiation and flight manual plots.

The path-performance section contains three different methods (or levels of analysis) for calculating aircraft performance within a segment. The most detailed level of analysis assumes that the aircraft is a rigid body with forces and moments acting on it. Untrimmed aerodynamic data and landing gear reaction data are required at this level.

The next level of analysis assumes that the aircraft is a point mass and, consequently, does not include rotational dynamics. The aircraft is assumed to be trimmed. Therefore, trimmed or untrimmed aerodynamics data may be input, and no landing gear reaction data is required. If untrimmed aerodynamic data is input, the program will trim it at the flight conditions prior to use.

At the remaining level of analysis, the conceptual level, additional assumptions are made in order to simplify the calculations. The same equations of motion are used as for the point-mass simulation; however, the integration method is much simpler and the forces are approximated. For example, the drag polar is assumed to be parabolic and the lift curve is assumed to be linear. The lift and drag curves can be input directly or they can be curve fits of tabulated library data. Other forces are assumed to be constant during the segment. Furthermore, some of the flexibility in guidance laws has been eliminated in order to simplify the calculations. For example, the user selects a segment type such as ground roll, where the guidance commands have been assumed to be a constant pitch angle (or angle of attack) and a constant power setting. In the other, more detailed methods, the user can specify the segment to be flown in a variety of ways.

Theoretically, the rigid body analysis should be the most accurate and, in practice, this has proven to be true. However, for certain types of segments, the point mass simulation and the conceptual level of analysis produce results with adequate accuracy. For example, for a ground-roll segment on a takeoff, results from all three levels of analysis are generally within 0.5 percent. Since the simplified methods are less expensive to calculate, it is desirable to allow levels of analysis to change from segment to segment. This feature has been provided to reduce the cost of a simulation with minimal loss of accuracy. The only restriction is that library data (describing the forces) must be provided in the form required by the most detailed analysis that is used anywhere in a given flight path. For example, if the conceptual level is used for the ground roll and the detailed level for the rotation in a takeoff maneuver, untrimmed aerodynamic data must be available to the program so that it can compute the rotation properly.

A variety of different types of output are provided by the flight-path performance section. The normal program output gives the user flight-path data (such as airspeed, altitude and pitch angle), force data (such as lift coefficients, drag coefficients, and thrust), and control data (such as power setting and elevator deflection). Data is normally presented at each integration step. A briefer output form is available to give data only at the beginning and end of each segment. It is useful in reducing the amount of output from large surveys.

A special output form is available wherein the user can specify the variables he wants printed out for each integration step. He also has the option to define new output variables that are mathematical combinations of the existing output variables.

As noted previously, special summary output variables can be defined when surveys are used. These variables can be any mathematical combination of the existing output variables; furthermore, they can reference output variables on another path in the survey.

1.2.2 Point Performance

The point performance section is used to calculate rates of climb, climb gradients, and approach glide-slope angles. The aircraft is assumed to be airborne, non-accelerating, and trimmed. Thus, the summation of both forces and moments acting on the aircraft are zero. Given the airspeed, altitude, weight, power setting, and configuration, the point performance section solves for the flight-path angle and angle of attack that satisfy these conditions. From this information, the rate of climb and climb gradients can be determined. Single-engine rates of climb can be calculated simply by specifying the number of inoperative engines.

In the point performance section, the level of analysis is determined by the method used to define the forces. Trimmed or untrimmed aerodynamic data can be supplied. If untrimmed data is input, then the user must also give data describing the controls used to trim the aircraft.

Options are available to survey almost any combination of state variables (such as true airspeed or weight), control variables (such as power setting or flap deflection), and configuration indicators (such as wing-sweep angle or payload). Several variables can be modified on the same survey loop, giving the user additional flexibility and allowing him to avoid unnecessary calculations.

1.2.3 Special Performance

Some low-speed calculations required for design analysis do not fit into the point-performance or flight-path performance categories. Therefore, a special performance section was created to meet these requirements. Currently, this section can be used to calculate four specific design parameters: (1) the maximum-aft-center-of-gravity location that can be used before the aircraft tips back, (2) the nose gear unstick speed, (3) the liftoff speed, and (4) the stall speed.

The maximum-aft-center-of-gravity location is computed by varying the center of gravity until the force on the nose gear is zero. The weight, speed, configuration, and controls are specified by the user.

The nose gear unstick speed is obtained by searching for the velocity at which the force on the nose gear is zero. Generally, the user specifies the controls to generate the maximum positive moment about the center of gravity. The weight, configuration, and controls are held constant during the calculation.

The liftoff speed is computed by varying the velocity until the total force perpendicular to the runway is equal to zero. The aircraft is assumed to be just touching the runway, in a trimmed condition, and at a specified liftoff angle of attack. The weight and configuration are held constant.

The stall speed is obtained in a similar manner, except that the velocity is varied until the total force perpendicular to the velocity vector is zero. The aircraft is assumed to be in level flight, at the runway altitude, and trimmed. The weight and configuration are assumed to be constant.

It should be noted that these quantities can be pre-computed by the flight path performance section for use as segment final conditions. Survey loops can be defined by the user to vary gross weight and the configuration. These are set up similarly to the survey loops in the other sections.

2. BASELINE DATA MODEL

The E-7 data model for MAPS reflects a complete accounting of all aerodynamic coefficients, propulsive forces and mass properties.

A new aerodynamics data base was created to reflect the most recent results from the 1/9-scale E-7 wind-tunnel test performed in the General Dynamics Low-Speed Test Facility. Based on the test data, new untrimmed polars and moment curves were loaded into MAPS libraries. Baseline library data plots are included in Appendix A. These most recent results are superior to those of the 1981 baseline. Figure 2-1 shows a drag-coefficient comparison between the 1981 and 1984 baselines. The minimum drag in the 1981 baseline is shown to be constant because of the assumption that its use would be restricted to sea level. The 1984 data predict drag at sea level and higher altitudes to allow analysis of transition to hover. Figure 2-1 also shows a drag-due-to-lift comparison for a 20-deg elevon deflection. The drag due to lift of the 1984 baseline is improved over the 1981 baseline for all lift coefficients. Additionally, the test data indicate that the configuration is aerodynamically stable up to an angle of attack (AOA) of 27 deg, which is now assumed as the new stability limit. The 1981 database has an assumed 20-deg operational AOA limit. Figure 2-2 shows the actual gain in usable AOA.

All force values or coefficients are loaded into tabular libraries that can be accessed by MAPS and interpolated or extrapolated as required. All aerodynamic coefficients are functions of ground effect. Rather than interpolating the data as a function of h/b (height of the wing above ground divided by the span of the wing), the ground-effect parameter, σ, is utilized (Reference 8). Linear interpolation of σ better represents the non-linear effects of ground interaction. Definition of σ is also included in Appendix A.

Table 2-1 lists all of the force components that are included in the data model, the independent parameters used to define them, and the points (fuselage stations and water lines) at which the forces are assumed act.

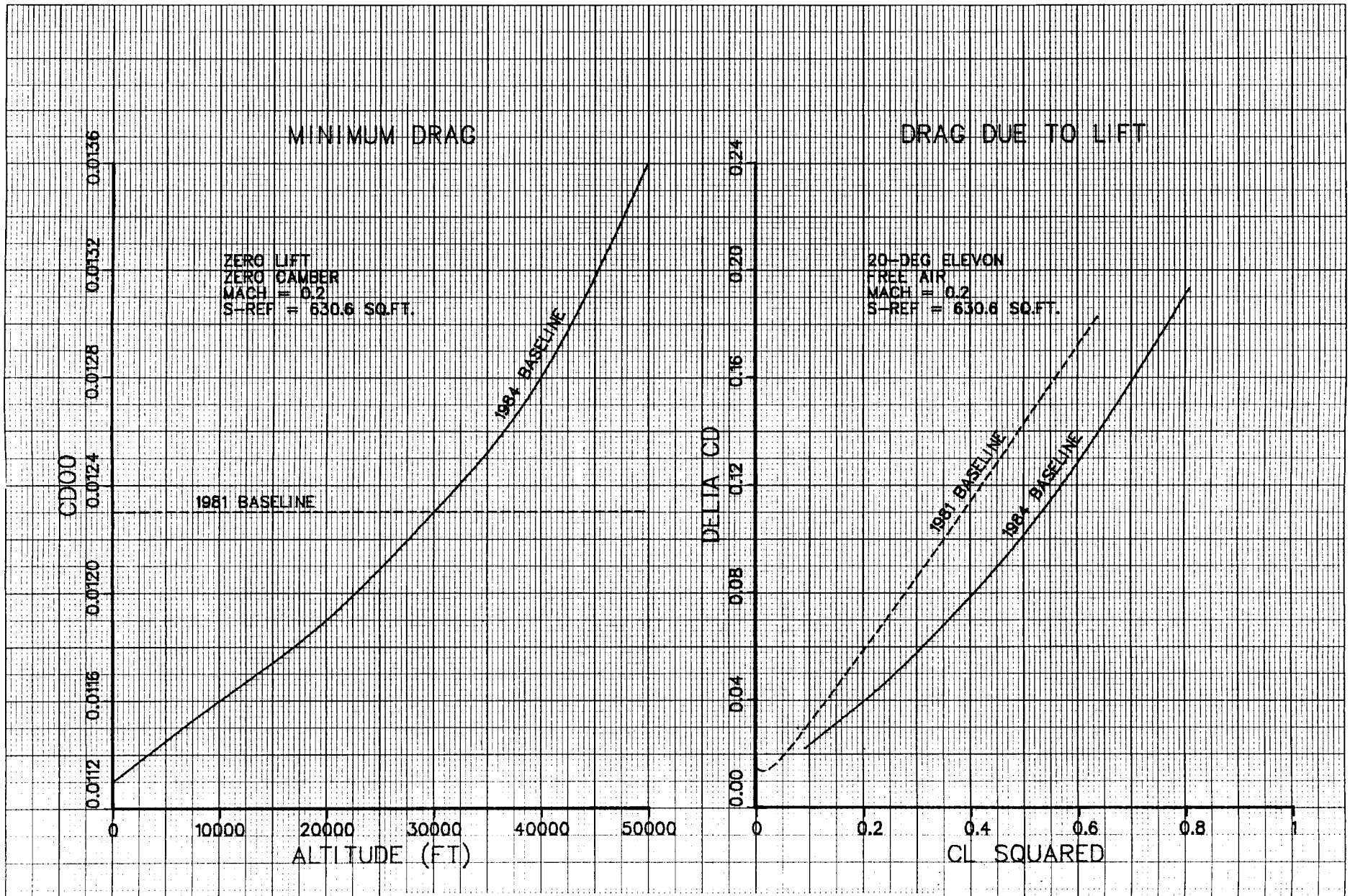

Figure 2-1, Drag-Database Comparison.

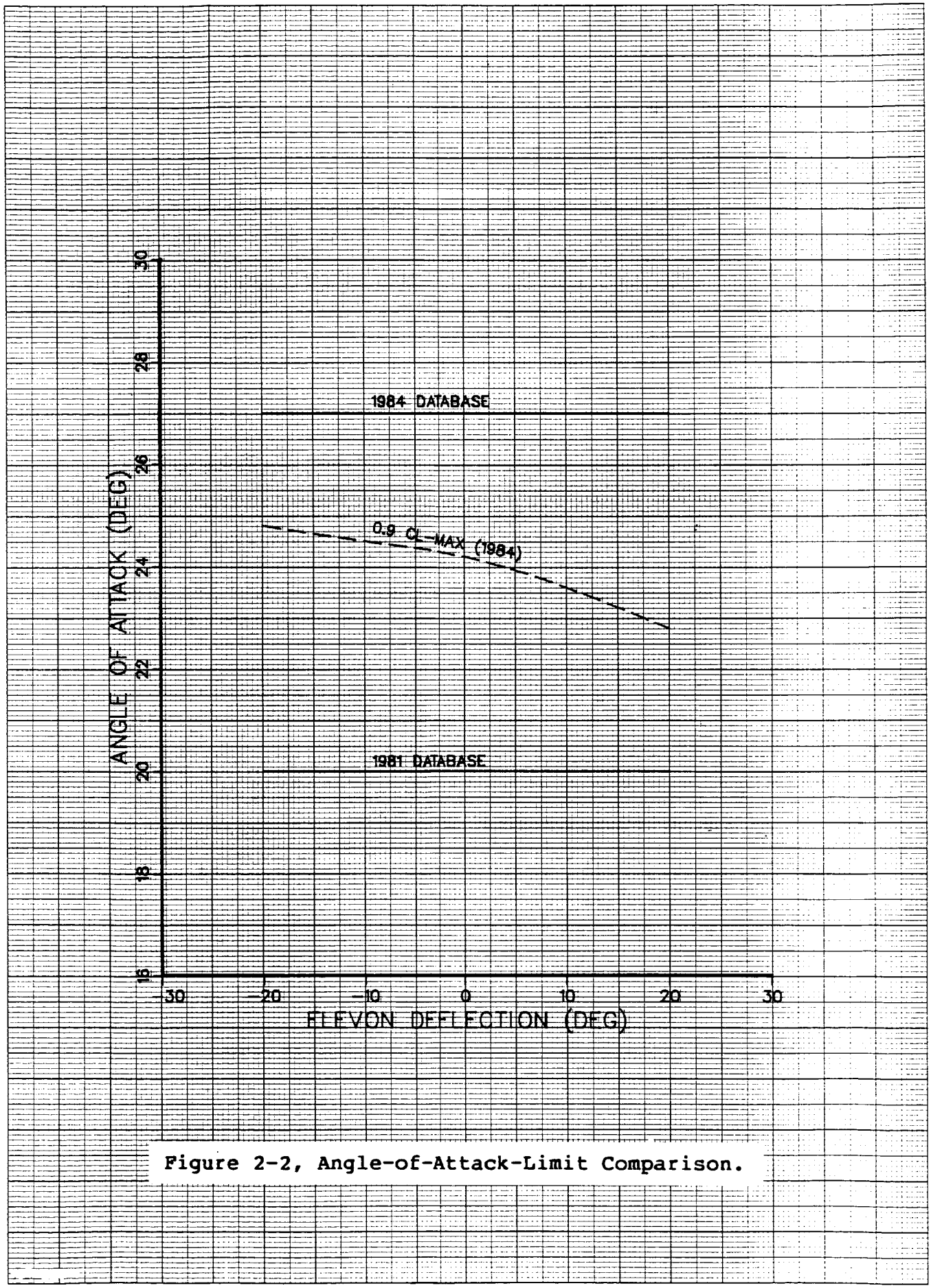

Figure 2-2, Angle-of-Attack-Limit Comparison.

Table 2-1, Data Library Structure

AERODYNAMICS

Dependent Variables	Independent Variables	Fuselage Station	Water Line
Drag due to lift	Lift coefficient Elevon deflection Sigma (h/b parameter)	312.9	91.0
Zero-lift zero-camber Drag	Altitude	312.9	91.0
Gear drag	Gear indicator	312.9	91.0
Ejector-door drag	Ejector-door indicator	312.9	91.0
Lift coefficient	Angle of attack Elevon deflection Sigma	312.9	91.0
Moment coefficient	Lift coefficient Elevon deflection Sigma		
$C_{m_{\dot{\alpha}}}$	Constant		
C_{m_q}	Constant		

Table 2-1, Data Library Structure (Cont.)

PROPULSION

Dependent Variables	Independent Variables	Fuselage Station	Water Line
Core thrust	Mach Vector angle Core afterburner indicator	389.8	54.7
Aft thrust	Mach Ejector setting Aft afterburner indicator	559.4	98.7
Ejector thrust	Mach Ejector setting	253.7	87.5
RCS thrust	Constant	C.G.	C.G.
Inlet drag	Mach	162.2	65.5
Ejector drag	Ejector thrust Mach	253.7	101.9
Fuel flow	Mach Core afterburner indicator Aft afterburner indicator		

Table 2-1, Data Library Structure (Cont.)

MASS PROPERTIES

Dependent Variables	Independent Variables
C.G. fuselage station	Weight
	Payload indicator
	Gear indicator
C.G. water line	Weight
	Payload indicator
	Gear indicator
Pitch inertia	Weight
	Payload indicator
	Gear indicator

Table 2-1, Data Library Structure (Concluded)

LANDING GEAR

Dependent Variable	Independent Variable	Fuselage Station	Water Line
Nose-gear friction coefficient	Constant	175.1	3.1-15.5
Main gear friction coefficient	Brake indicator Runway RCR Value Ground speed	356.9	0.5-18.7
Maximum brake force	Brake energy	356.9	0.5-18.7
Nose-gear reaction	Deflection Deflection rate	175.1	3.1-15.5
Main-gear reaction	Deflection Deflection rate	356.9	0.5-18.7

3. BASELINE ANALYSIS

Because a new data baseline was assumed, a revised maximum STO weight was determined. Previous studies of the E-7 low-speed performance showed that the optimum elevon deflection is +20 deg. The carpet plot of minimum level-flight speed (V_{MIN}) vs. ejector setting and elevon deflection (Figure 3-1) shows that the horizontal acceleration (a/g) requirement creates a strong downward trend of V_{MIN} as elevon deflection increases.

Figure 3-2 shows carpet plots of V_{MIN} which are used to optimize the angle of attack (AOA). Each plot shows V_{MIN} vs. AOA and ejector setting at a fixed gross weight. Figure 3-3 shows the minimum level-flight speed as a function of gross weight and ejector setting. A constraint line traces the horizontal-acceleration requirement of 0.065. For this part of the analysis, the angle of attack was fixed at 22.8 deg, which is equivalent to a 0.9 times the $C_{L_{MAX}}$ limit for a 20-deg elevon deflection (this condition is optimum over the majority of the weight range).

The objective of several elements of this study is to calculate a takeoff-performance figure of merit called STO weight. STO weight is defined as the maximum gross weight that can takeoff from a 400-ft long aircraft carrier deck at sea level in tropical-day conditions and satisfy the following limits:

1. The sink-over-bow must not exceed ten feet.
2. The lift coefficient, C_L, must not exceed 0.9 times $C_{L_{MAX}}$.
3. The horizontal acceleration must not drop below 0.065 a/g (2.1 ft/sec/sec).

STO weight was calculated by conducting a survey of takeoff gross weights during an Option 70 simulation to achieve the requirements above. Figure 3-4 shows flight-path summaries of altitude, AOA, airspeed, and a/g versus distance. The altitude plot shows that the airplane began to rise before the edge of the deck. This rise was completely due to rotation, i.e., the center of gravity rose but the main gear remained on the deck. Beyond the deck edge, the center of gravity sank ten feet. The AOA plot also shows the pitch increase before the deck edge and the continued rotation to the AOA limit. After reaching the AOA limit, a point-mass analysis is assumed because control rate and angular velocity are very small and the simpler analysis allows the user to have better control of AOA and a/g with reduced computation time. The airspeed increased smoothly and leveled off after rotation. The a/g plot shows a smooth acceleration for the first 260 feet, at which point, the ejector was activated and caused the a/g to drop drastically. Up to 580 feet, the a/g wavered as the elevons and thrust vector angle controlled the rotation. This summary predicts that 34,700 lb is the correct

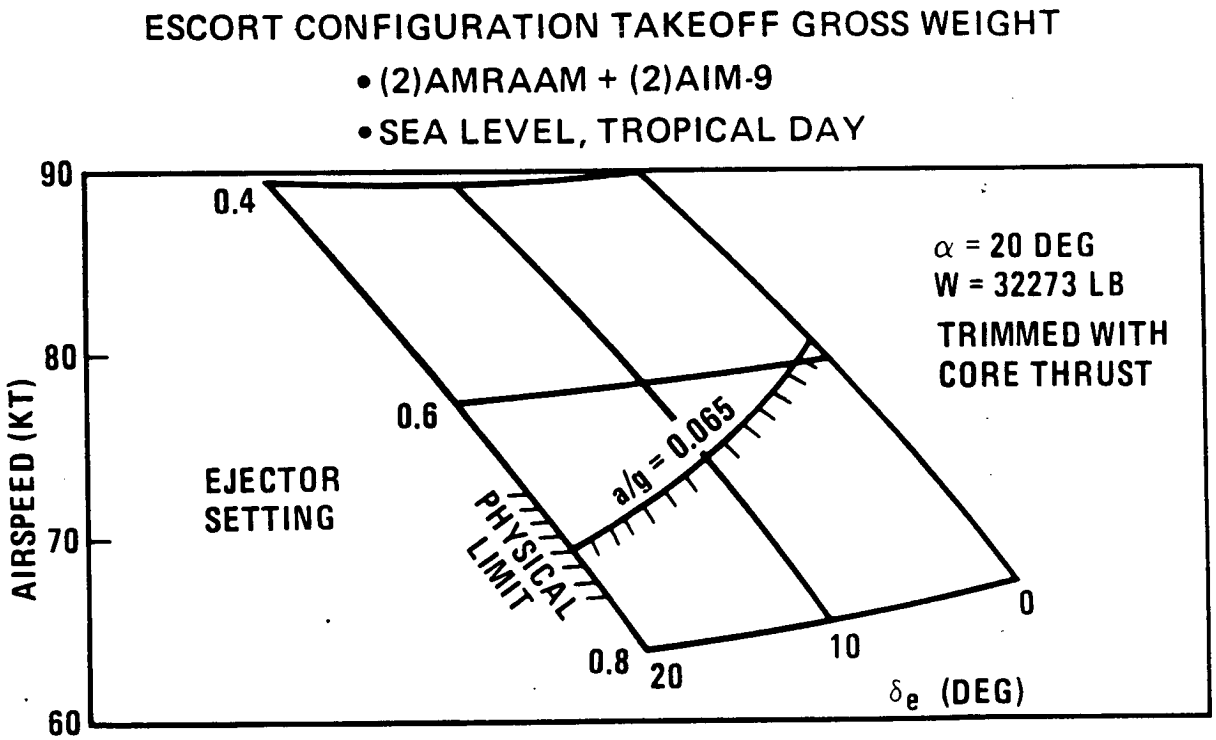

Figure 3-1, Elevon Optimization.

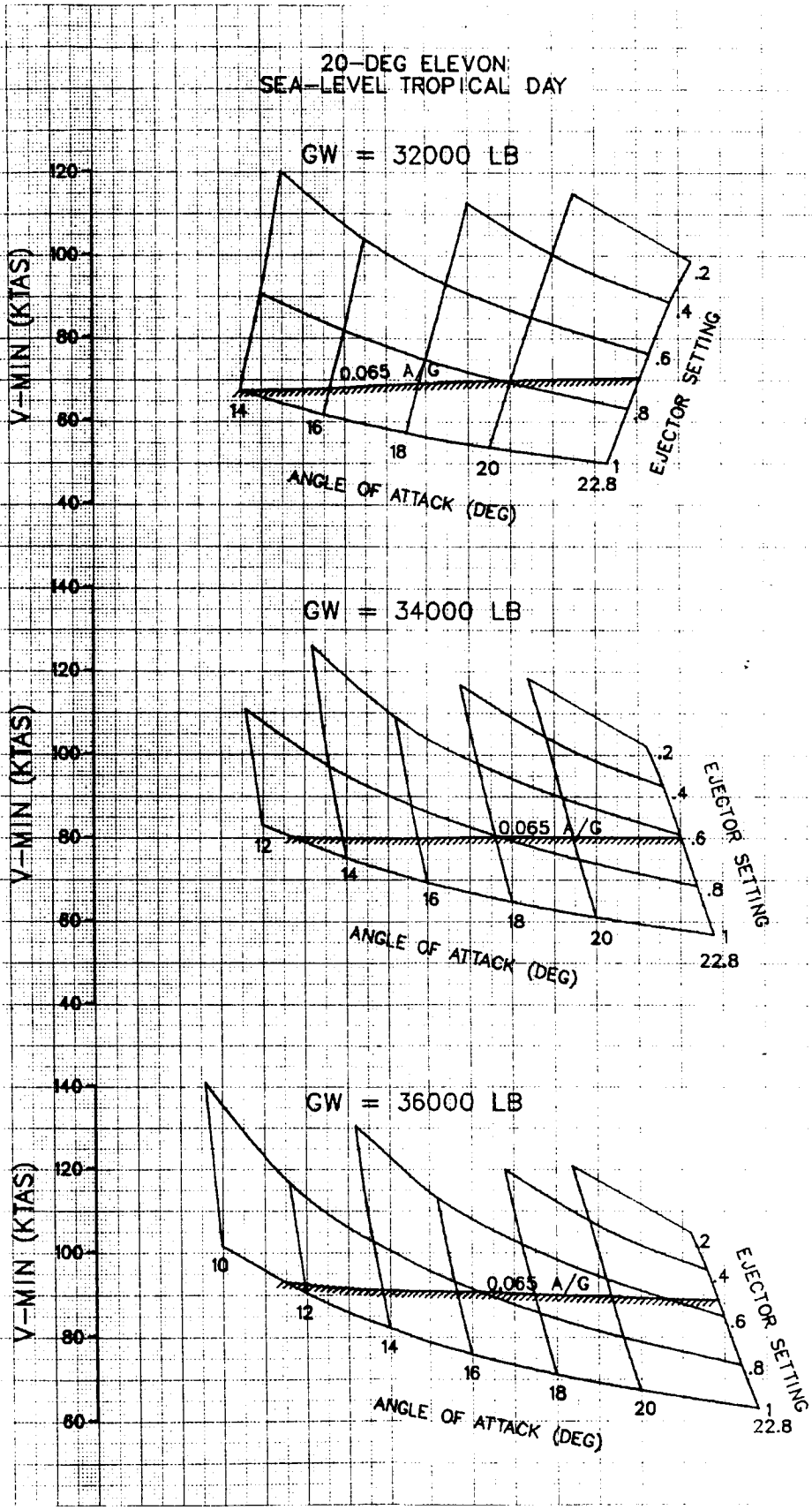

Figure 3-2, Angle-of-Attack Optimization.

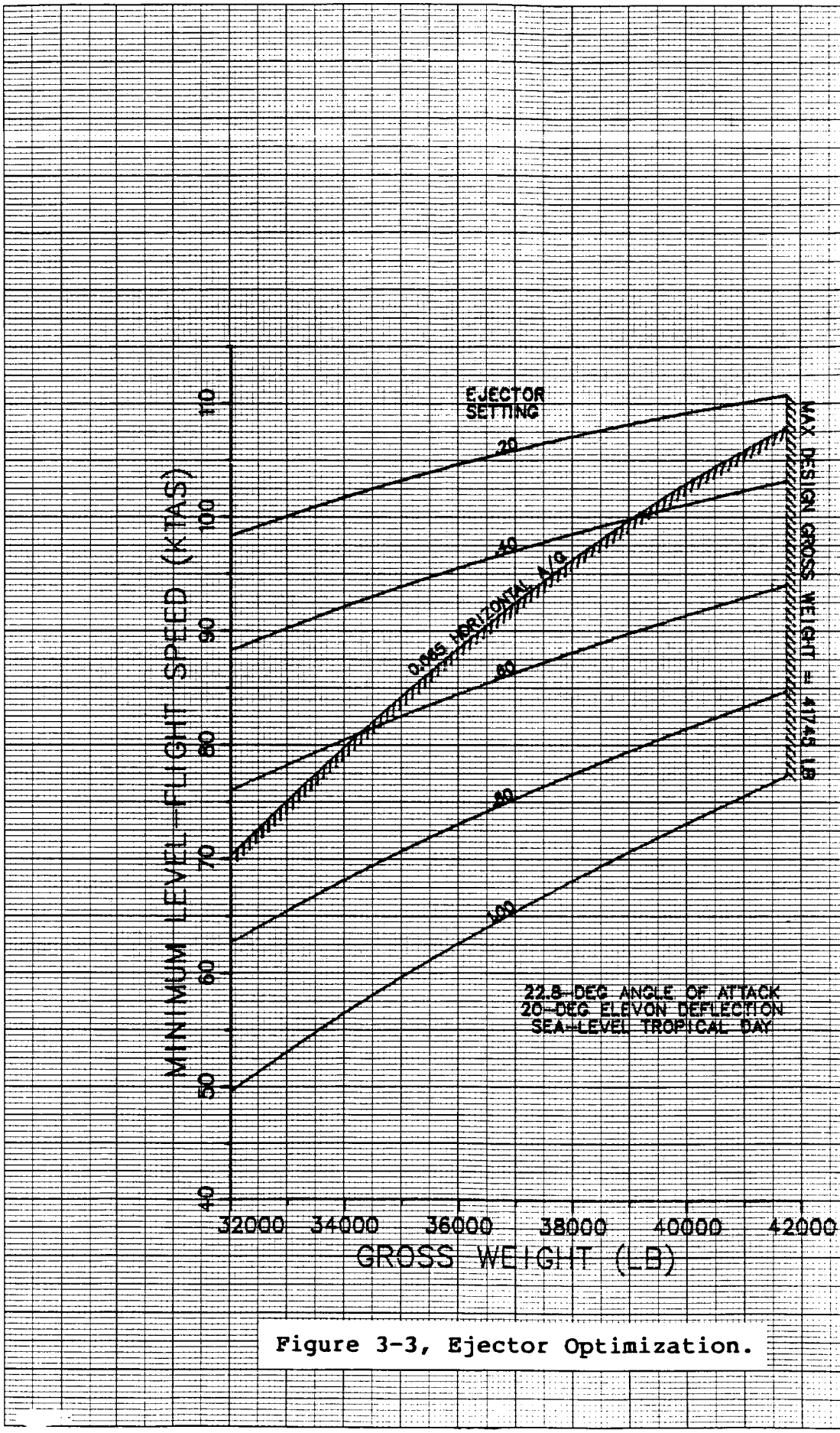

Figure 3-3, Ejector Optimization.

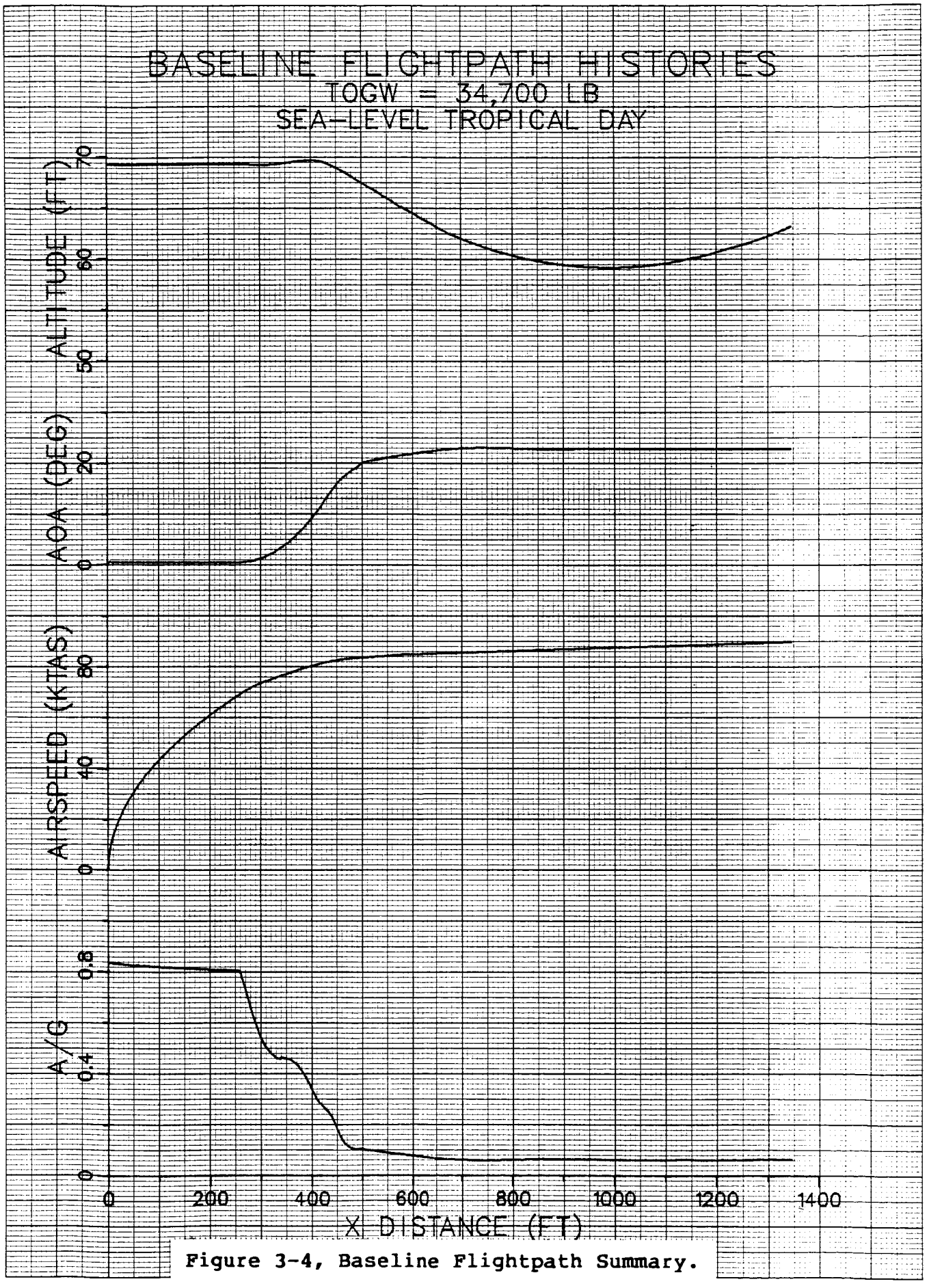

Figure 3-4, Baseline Flightpath Summary.

STO weight for the new baseline; it simultaneously meets all three limits: sink over bow, 0.9 $C_{L_{MAX}}$, and 0.065 a/g.

Time histories of pertinent parameters are included in Appendix G, which contains the histories of takeoff and transition to wing-borne flight studied in Section 8.

4. AFT THRUST VECTOR

A convergent-divergent two-dimensional (2D-CD) vectorable aft nozzle was incorporated on predecessors to E-7. At the time that the low-speed characteristics of those configurations were investigated, the optimum deflection was found to be full down to allow as much ejector thrust as possible. This assumption was not made on this configuration because optimum deflection can be very dependent on airplane weight and design.

The vectorable nozzle installed for this investigation is assumed to maintain the same thrust location (i.e., fuselage station and water line). The associated weight increment is estimated to be 200 lb. This weight increment does not affect the calculation of STO weight but does affect the resulting useful load. The afterbody nozzle drag is assumed to be identical to the baseline nozzle. Thrust loss caused by deflection of the nozzle is modeled as an attenuation of 0.1 percent per degree of nozzle deflection.

For the expected range of STO weight, maximum angle of attack (AOA) is assumed to be optimum. The optimum elevon deflection is +20 deg. To optimize the aft-thrust-vector deflection, minimum level-flight speed, V_{MIN}, is calculated as a function of weight and thrust deflection for a horizontal acceleration of 0.065 g. As can be seen in Figure 4-1, the optimum aft-vector angle varies with gross weight. Note that the zero-deflection line is identical to the 0.065-a/g line in Figure 3-3. At the baseline STO weight, the optimum deflection is about zero; therefore, the vectoring capability adds no advantage concerning the minimum speed. This relationship is described in Figure 4-2. Data are presented for E-7 in level flight at fixed speed, weight, AOA, and elevon deflection. These data trends are plotted as functions of aft-thrust vector. Note that the a/g curve reaches a maximum. The core vector is the key to the a/g trend: the a/g is very dependent on the horizontal component of the 17,000-lb thrust from the core.

The ejectors and aft nozzle are both supplied with fan air, therefore, as more ejector thrust is used, the aft thrust decreases. At light takeoff gross weights, which utilize nearly full ejector thrust, the thrust that is vectorable by the aft nozzle is very small.

However, the aft vector does add more pitch authority, which can allow a faster rotation during the takeoff sequence. This added advantage, however, only increases the STO weight by 200 lb, just enough to compensate for the weight increase caused by the heavier nozzle. A flight path summary of the takeoff sequence is shown in Figure 4-3. Time histories of pertinent parameters are included in Appendix B.

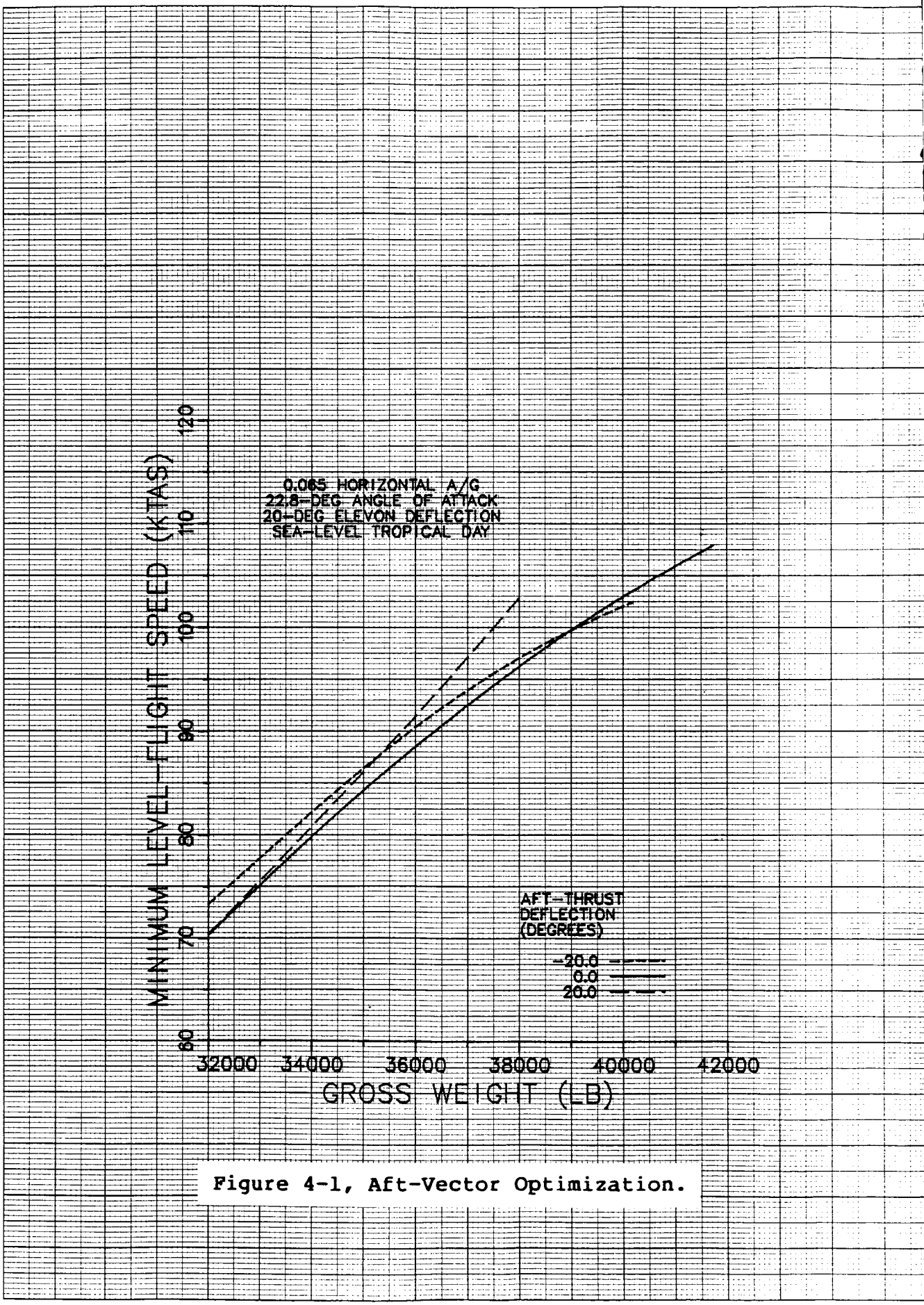

Figure 4-1, Aft-Vector Optimization.

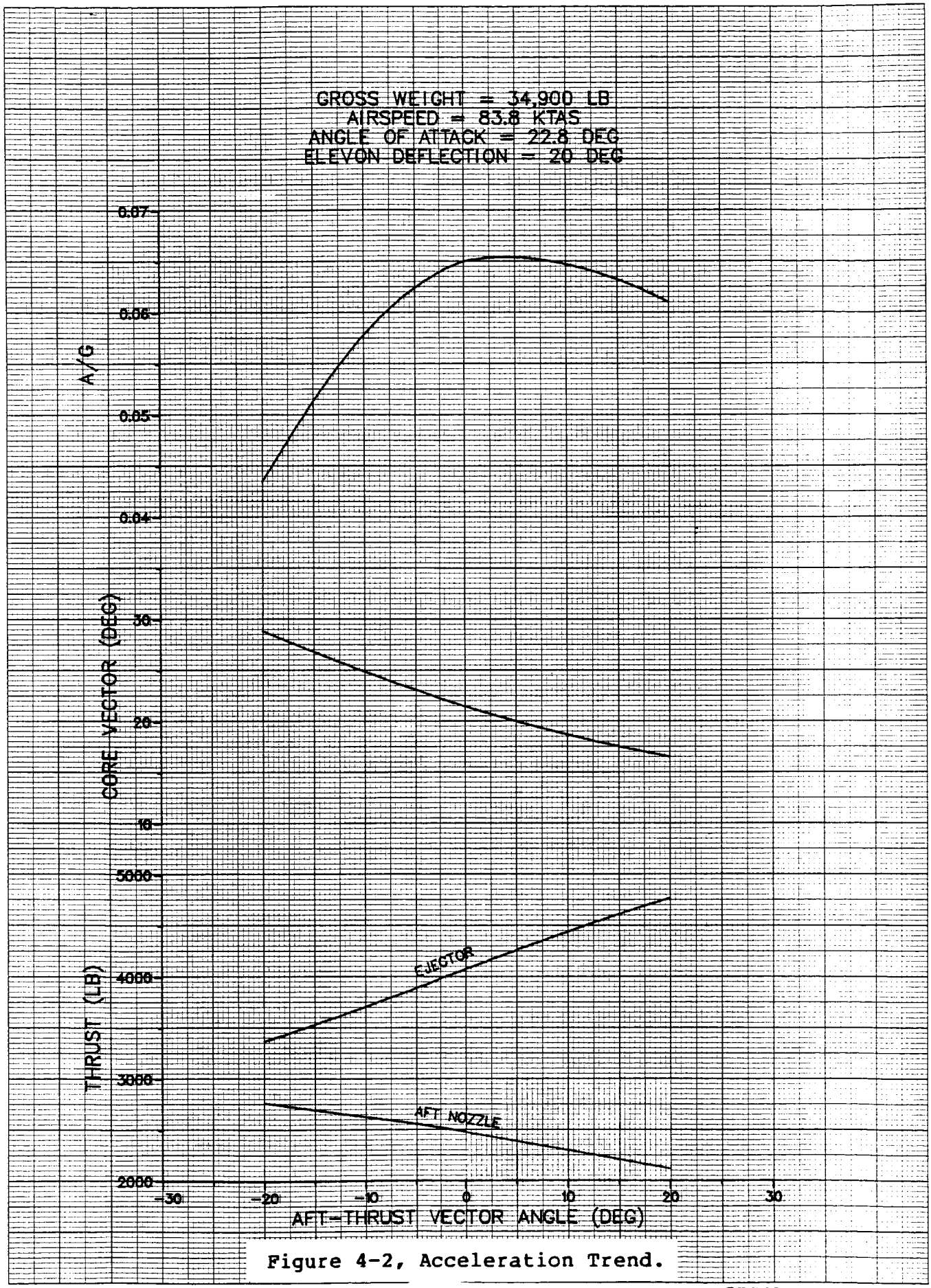

Figure 4-2, Acceleration Trend.

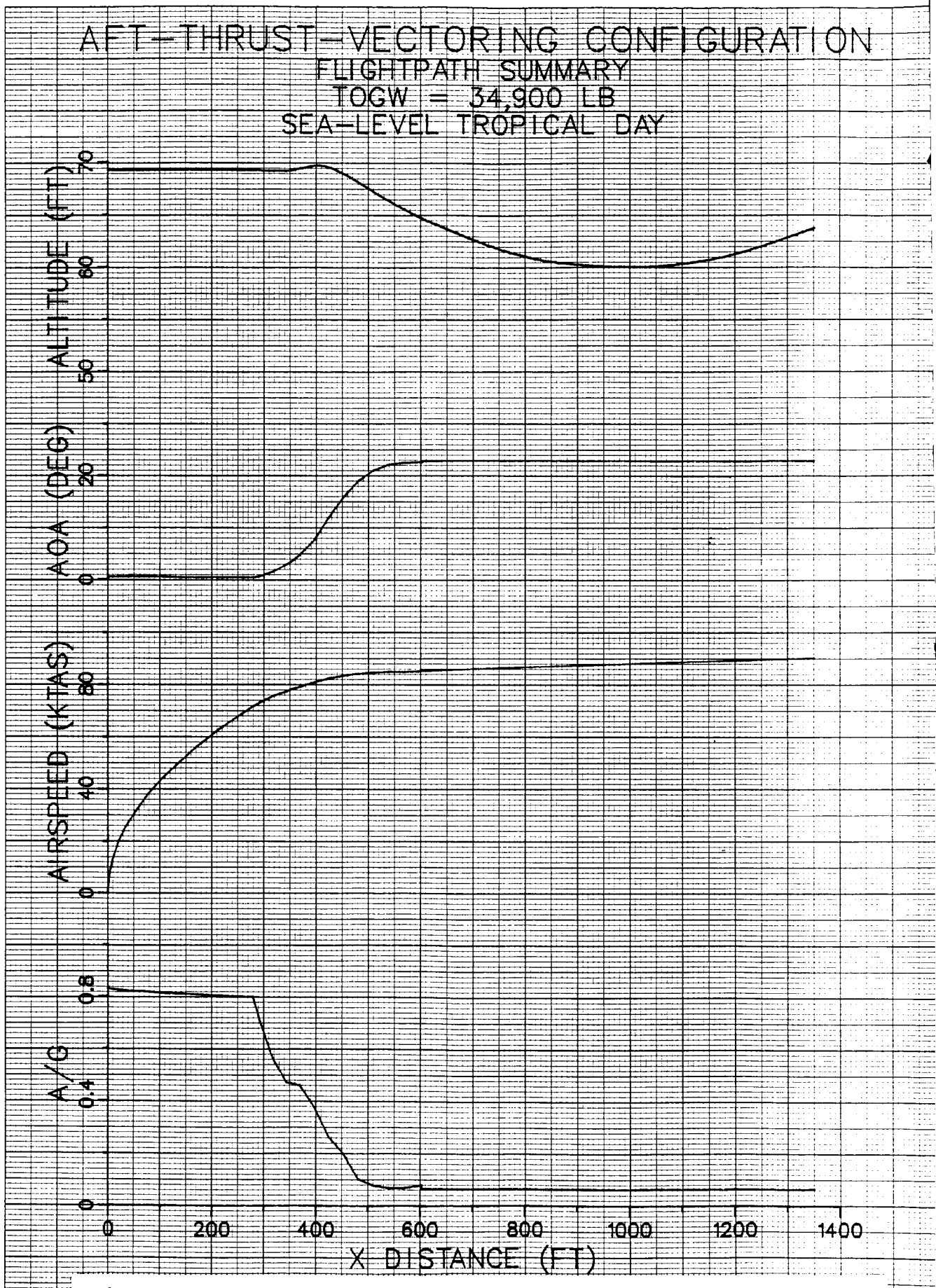

Figure 4-3, Aft-Vectoring-Configuration Flightpath Summary.

Other advantages of a vectorable nozzle are:

1. Increased transient maneuverability in combat situations.

2. Thrust reversing capability that can be used in short landings (e.g., landings at gross weights greater than hover weight).

3. Increased performance in non-ejector takeoffs.

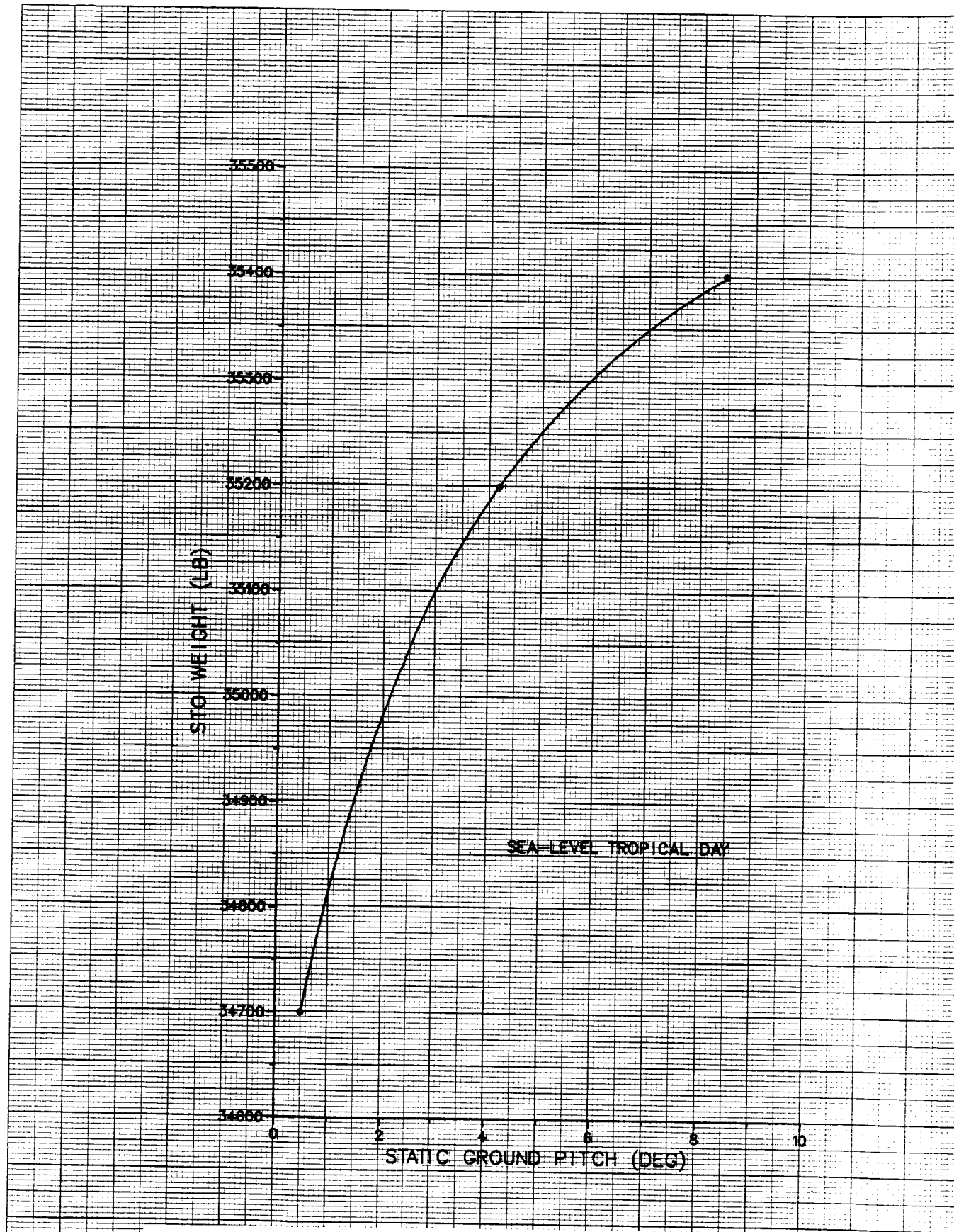

Figure 5-1, STO Weight vs. Static Ground Pitch.

5. INCREASED STATIC PITCH

The purpose in increasing the static pitch of the airplane is to investigate the trade between (1) decreasing the required change in angle of attack during the takeoff sequence which thereby decreases the time required to rotate and (2) the degradation caused by increased drag and reduced longitudinal thrust. The increased pitch can be physically achieved by simply lengthening the nose-gear strut. In this investigation, two static pitches were studied, +4.2 and +8.5 deg achieved by increasing the length of the nose gear by 10 and 20 in, respectively. Increasing the static pitch does not affect the optimization of the ejector or elevon because the flying configuration is unchanged. The STO weight is calculated as in Section 3. A plot of STO weight vs. static ground pitch is shown in Figure 5-1. Over the range of pitches tested, the benefits of increasing the static pitch continue to increase beyond 8 deg. The downward concavity of the trend indicates that an optimum static ground pitch exists in the vicinity of 15 deg. A flight-path summary of the takeoff sequence for the +8.5-deg case is shown in Figure 5-2. Time histories of pertinent parameters are shown in Appendix C.

It is apparent that the benefits in increasing the static pitch are worth the slight increase in dry weight. The STO weight increases by more than 500 lb whereas the dry weight increases on the order of 50 lb. The fuel volume may decrease slightly. Adding to the takeoff performance benefits, the modification may also have a positive effect toward orienting the pilot during vertical landings. Lengthening of the nose gear probably would not affect the deck-handling characteristics.

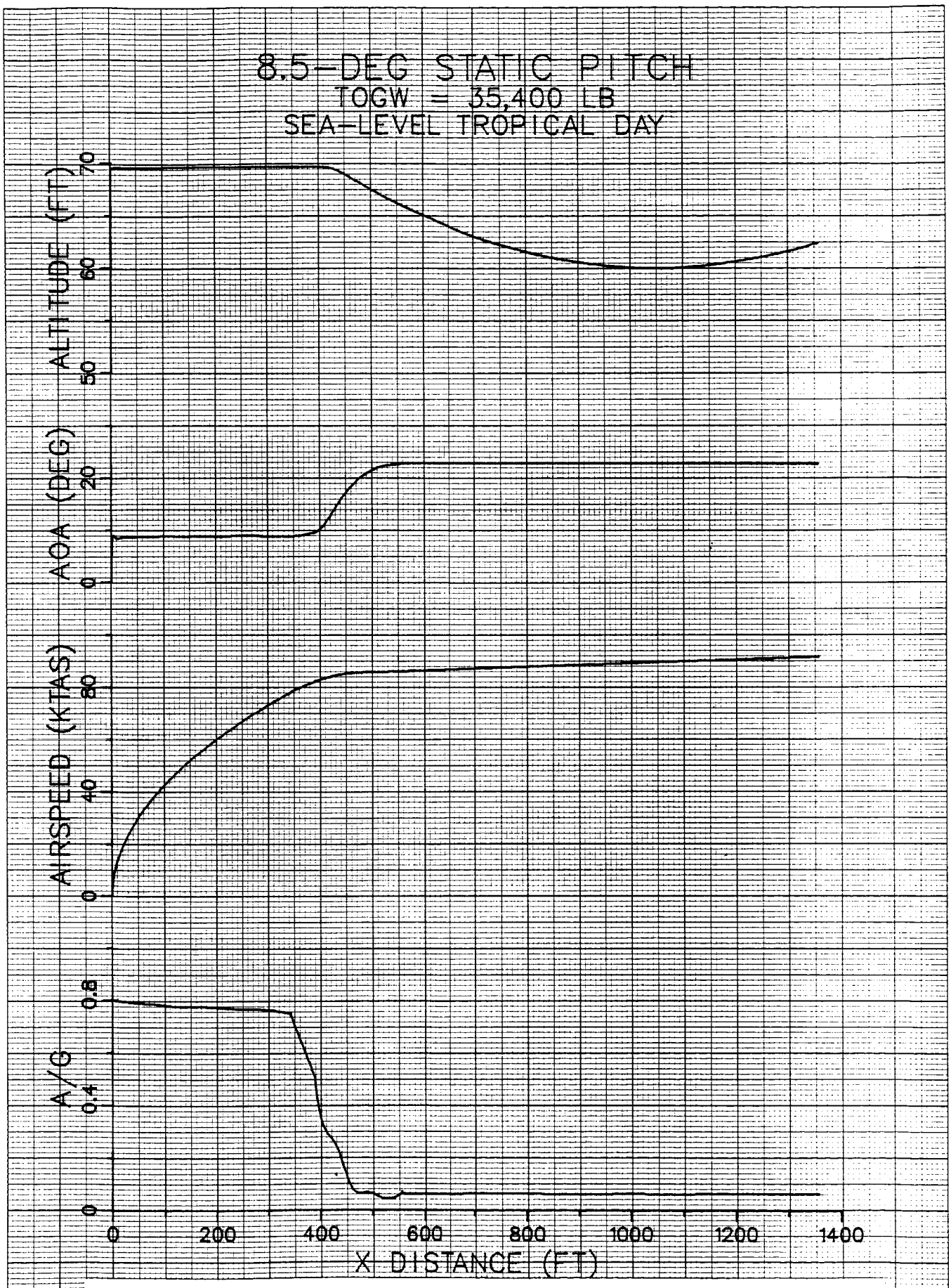

Figure 5-2, 8.5-deg Static Ground Pitch Fightpath Summary.

6. INCREMENTAL PERFORMANCE OF PROPULSIVE-LIFT ELEMENTS

This study addresses the two sources of propulsive lift of the baseline E-7, the ejector and the core thrust vector, and a third component, a vectorable aft thrust. The objective of this task is to first study each component individually and then combinations of two components to determine which items have the highest leverage for improving the STO performance.

The combination of the three components listed above form a matrix of eight possible takeoff configurations. This matrix is shown in Table 6-1. For future reference, each combination of lifting components is assigned a Case number, e.g., the baseline configuration is Case 7.

Table 6-1, Propulsive-Lift Combinations

CASE NUMBER	PROPULSIVE LIFT COMPONENTS		
	Aft-Thrust Vectoring	Core-Thrust Vectoring	Ejector Thrust
1	-	-	-
2	X	-	-
3	-	X	-
4	-	-	X
5	X	X	-
6	X	-	X
7	-	X	X
8	X	X	X

For the analysis described in the sections above, STO weight is the figure of merit of takeoff performance. In this section, the field-takeoff (as apposed to carrier) ground-roll distance (S_g) is calculated for the escort weight and loading.

For the E-7 configuration, lift-off speed is defined as the maximum of the three following speeds:

The level-flight speed in ground effect at the tail-bump angle of attack, (20 deg for the E-7).

1.1 times the minimum level-flight speed (V_{MIN}) at $C_{L_{MAX}}$ in free air.

The speed at which the climb gradient potential is equal to 0.005 out of ground effect.

Case 1 (no propulsive-lift components) represents a standard CTOL airplane. The performance of Case 1 is used as a comparison point for Cases 2 through 4. For the Case-1 configuration, the liftoff speed, as defined above, is 93 KTAS. However, the nose-gear unstick speed (the minimum speed at which there exists sufficient control power to rotate the airplane) is 74.4 KTAS, which makes the actual liftoff speed 118 KTAS. Therefore, the minimum takeoff distance is 735 ft. This distance is very short by most aircraft standards. The most significant way to decrease the takeoff distance is to decrease the unstick speed.

Adding the vectorable aft thrust (Case 2) allows much more pitch authority than Case 1 and thereby greatly decreases the nose-gear-unstick speed. Though the lift-off speed is lowered only slightly, the takeoff distance is greatly decreased. Rather than being rotation limited, as in Case 1, the liftoff speed is set by the free-air V_{MIN}.

In Case 3, the core-thrust vector has no ability to reduce the unstick speed, and thereby has very little effect on decreasing the takeoff distance. The takeoff distance does decrease slightly relative to Case 1 because the core nozzle adds to controllability in the latter half of rotation and adds slightly more lift which allows liftoff at a reduced angle of attack. The optimum core vector angle can be determined from Figure 6-1. In this case, the takeoff velocity is determined by V_{MIN} in ground effect, which is minimized at a core-vector angle of 17 deg.

Adding the ejector (Case 4), like the aft vector, reduces the nose-gear-unstick speed relative to Case 1; in fact, it reduces it to zero. Adding the ejector does have a major drawback: use of the ejector disallows use of the afterburner in the aft nozzle. The lift-off velocity of Case 4 is actually higher than that of Case 1 because the slight amount of ejector thrust that can be trimmed with the elevon is less than the vertical component of afterburning the aft thrust, even when not vectored. (Because the ejector thrust acts forward of the center of gravity and the core and aft thrusts are not vectorable, only the elevon is available to trim the airplane. The elevon can trim about 200 lb of ejector thrust. Activating the ejector reduces the aft thrust by more than 7000 lb, which has a lifting component of over 3000 lb.) Because of the loss of aft thrust, the Case-4 configuration must accelerate to a higher speed with less accelerating force.

An interesting result arises with Case 5 in which the ejector is not used. Only the two vectorable nozzles are available for propulsive lift. These components can be used to trim each other. Because the aft thrust is further from the center of gravity, it can be deflected upwards, creating a small

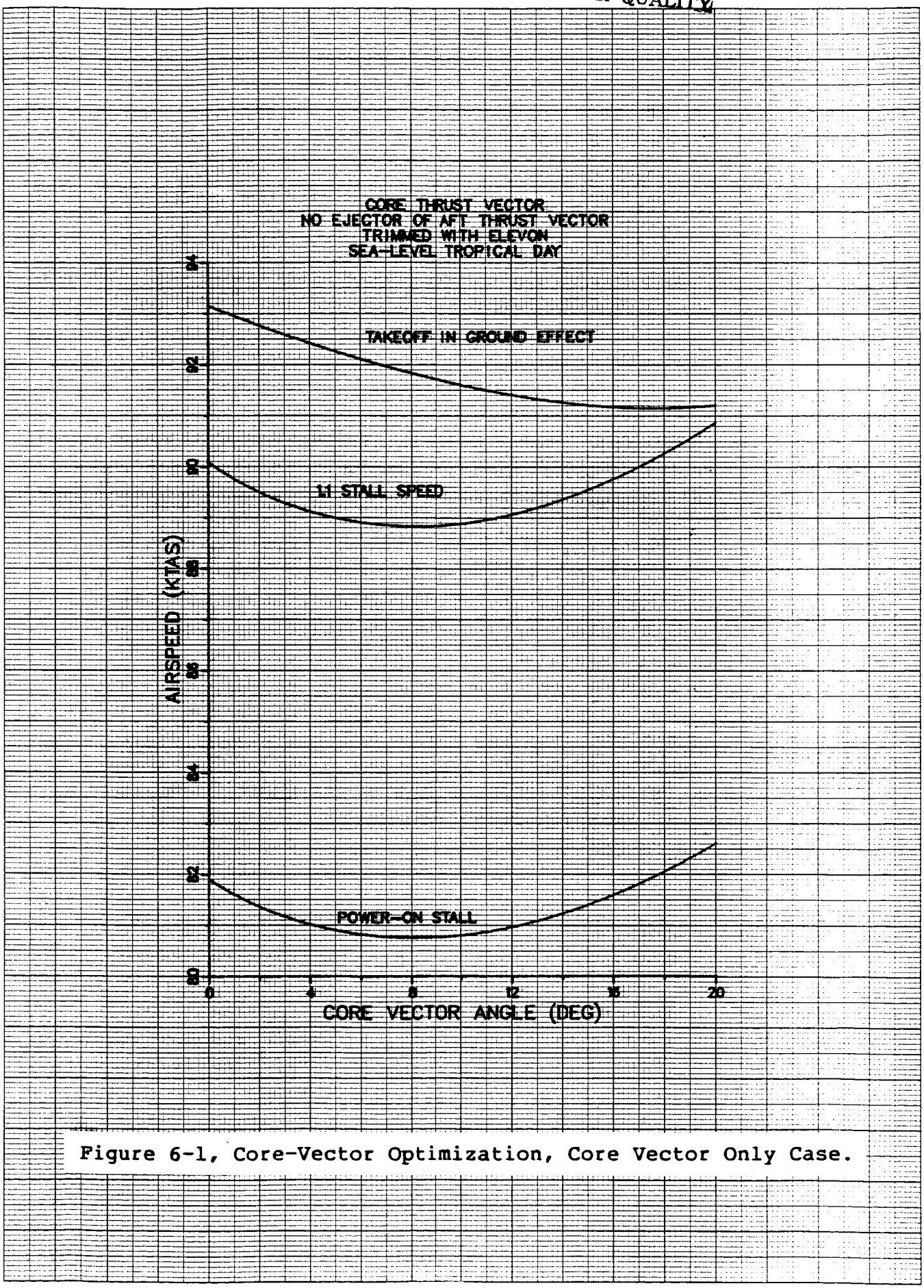

Figure 6-1, Core-Vector Optimization, Core Vector Only Case.

down load, while the core vector can be deflected downwards to create a greater lifting force that maintains the airplane trim. Figure 6-2 shows the data used to optimize the core vector angle. In this case, the liftoff speed is limited by 1.1 V_{MIN}. Though the lift-off speed is not as low as the baseline (Case 7 described below) a similar S_g is achieved because the afterburned aft thrust allows greater acceleration.

When the ejector is used with only the aft vector to maintain thrust balance (Case 6), the takeoff performance is severely impacted. Most of the ability to trim the ejector thrust comes from the core thrust as is Cases 7 and 8. The elevon and aft vector are deflected downward to allow as much ejector thrust as possible. Since the liftoff speed is relatively low, the optimum method is to increase the AOA to the maximum allowable. The liftoff velocity, defined by 1.1 V_{MIN}, is greater than 90 KTAS. The resulting ground roll is greater than 500 ft, which is even longer than the ground roll for Case 2.

Case 7 is the baseline E-7 configuration. Based on the results in Section 3, the takeoff speed is optimized with full ejector thrust and full-down elevon. Figure 6-3 shows the data used to optimize the angle of attack. Here the required climb gradient becomes a limiting constraint. The optimum AOA is determined by indexing it to a climb gradient of 0.005, which in this case occurs at about 17 deg. The takeoff sequence is then performed to achieve liftoff at 1.1 times V_{MIN}. The resulting takeoff speed is 67 knots, which is more than twenty knots less than that of any of Cases 1 through 4. Likewise the S_g is about 300 ft, which is half the S_g of Cases 1, 3, and 4. It is interesting to note the comparison between Case 7 and Case 5 (aft and core vectoring with no ejector). The Case-7 takeoff velocity is almost ten knots less than that of Case-5, but, the S_g is only ten feet shorter.

Case 8 (all three propulsive-lift components) is identical to the configuration that was studied in Section 4. In this investigation, the field-takeoff distance is being investigated rather than STO weight. As shown in Section 3, for relatively light takeoff gross weights (TOGW), the optimum takeoff configuration uses full ejector thrust and operates at a reduced angle of attack (AOA). Again, the use of full ejector thrust eliminates all aft thrust, therefore, the vectorable aft nozzle has no effect on takeoff speed. In that respect, Case 8 is identical to Case 7 and has the same takeoff speed. The vectorable nozzle does add more authority in pitch and enables the aircraft to initiate a faster rotation. This feature, however, only shortens S_g by ten feet.

A tabular summary of all cases is listed in Table 6-2. Figure 6-4 shows a summary of the entire task by comparing the lift-off speeds (as defined above) and ground roll distances for all eight configurations. This representation shows the value of accelerating force and the importance of rotation speed. Time histories of pertinent parameters are shown in Appendix D.

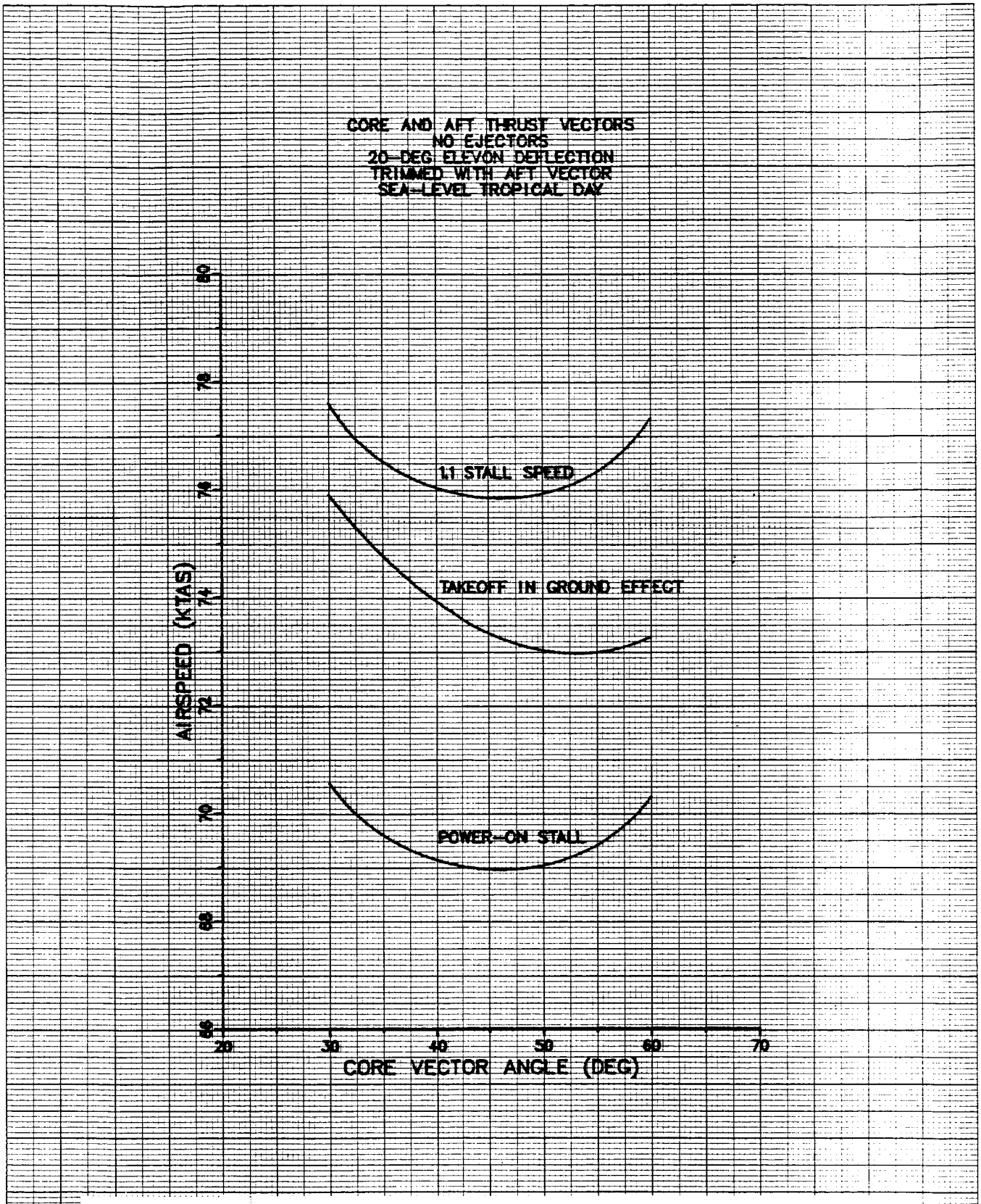

Figure 6-2, Core-Vector Optimization, Aft and Core Vectors.

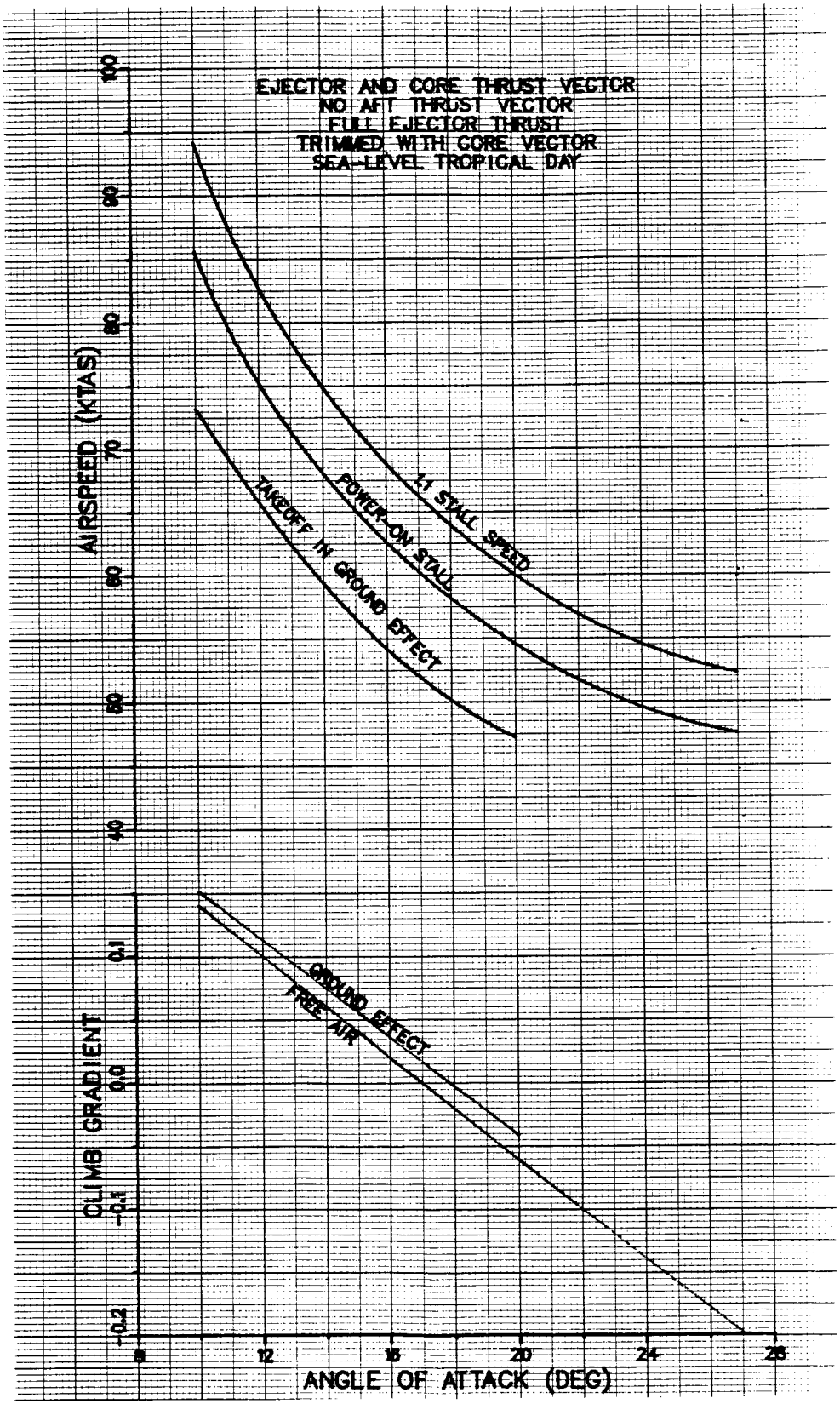

Figure 6-3, Angle-of-Attack Optimization, Ejector and Core Vector.

Table 6-2 Ground-Roll Distance Summary

CASE NO.	PROPULSIVE-LIFT COMPONENTS			TAKEOFF SPEED (ktas)			GROUND-ROLL DISTANCE (ft)	COMMENTS
	Aft-Thrust Vectoring	Core Thrust Vectoring	Ejector Thrust	1.1 x Free-Air V_{min}	At Tail Bump	Actual		
1	-	-	-	90	93	118	735	Rotation limited
2	X	-	-	89	86	89	431	
3	-	X	-	89	91	114	95	Rotation limited
4	-	-	X	96	86	96	588	Only 200 lb ejector thrust
5	X	X	-	76	73	76	327	Aft thrust vectored up
6	X	-	X	92	82	92	535	
7	-	X	X	67*	59*	67	317	Baseline
8	X	X	X	67*	59*	67	307	

*CLIMB GRADIENT POTENTIAL = 0.005

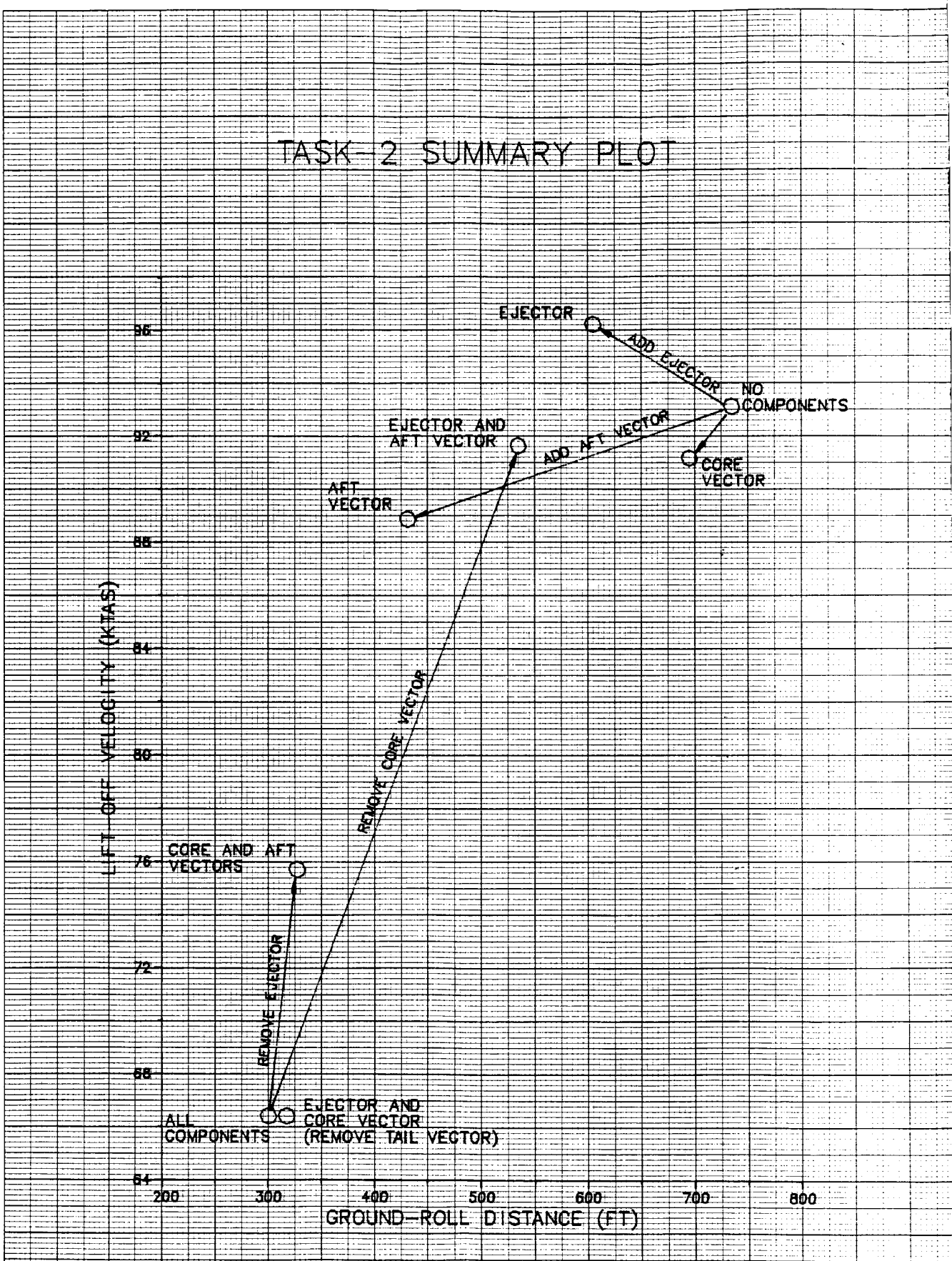

Figure 6-4, Propulsive-Lift-Comparison Summary.

The aft thrust vector is the most advantageous component when used singly. The advantage occurs primarily because this particular airplane design is rotation limited. This limitation can be cured by other means: installation of a jump strut or increasing the elevon effectiveness. A secondary advantage of the vectorable aft nozzle is the ability to gain a larger vertical thrust component from the afterburning fan flow.

Naturally, the two-components cases have superior takeoff performance to the one-component cases. With the exception of the core-vector removed case, the ground roll distances are very similar. On the surface, the ejector-removed case looks attractive, at least for pure takeoff considerations, but, the ejector must be used to perform hover.

By far, the largest synergism occurs when the ejector and core vector are combined. This effect is most prominent at light gross weights because it is optimum to operate at full ejector.

This task reveals the afterburning of the aft thrust to be very advantageous. In some cases, increased energy rate nearly equals the benefits of the ejector. Because this is such a high leverage item, it would be very advantageous to afterburn the fan flow even at partial ejector settings. Note that this would only gain slight benefit at light TOGWs because all of the fan flow is directed to the ejector at lift-off. However, with the ability to afterburn partial fan flow, it may be optimum to operate at maximum angle of attack rather than at full ejector. Another advantage of the vectorable aft nozzle was identified when combined with the core nozzle. Takeoff performance similar to the baseline configuration is achieved with a simpler takeoff sequence.

Another area of high leverage is marked by the considerable synergism between the ejector and core nozzle. The takeoff performance may be very sensitive to thrust magnitude and placement. These parameters, however, are very constrained by the requirement to balance in hover. Any improvement in one component would require an improvement or redesign of the other.

7. CANARD SURFACE

This task was originally intended to investigate the effects of a canard simply as a lifting surface. This approach, however, does not include the first-order effects of wing/canard coupling. To model this arrangement, totally new low-speed and trimmed aerodynamics data models were required, which were based on Convair Model 200/218 wind-tunnel-test results in References 9 through 12. A three-view drawing of model 200/218 is shown in Figure 7-1.

One must realize that this analysis is totally theoretical because it is not possible to add a canard to E-7 for the following reasons:

1. No physical attachment point exists that would not obstruct the pilot's vision.

2. The additional weight would upset the hover balance. Either ballast would have to be added or the entire airplane would have to be redesigned. As is the case with all vertical-landing aircraft, any additional dry weight decreases hover useful load. Adding a canard to E-7 nearly eliminates the fuel available for hover because of canard and ballast weight.

3. The additional lifting surface disrupts the static margin of stability. The airplane would have to be redesigned to regain the same flight characteristics.

For purposes of this task, the canard is assumed to be added without regard to pilot visibility or structural integrity (attachment is in the immediate vicinity of the canopy). The canard is assumed to weigh 700 lb. A ballast of 700 lb is added to the tail fairing without affecting the internal arrangement or fuel volume. The aerodynamic prediction is based on the resulting increased negative static margin. Figure 7-2 shows the hypothetical position of the canard. Note that the surface has no physical attachment and obstructs the pilots downward side vision.

The data curves that are incorporated in the Option 70 model are shown in Appendix E. Note that detailed design was not performed on the canard. The canard-area/wing-area ratio is assumed to be the same as that of Model 200. The results of a detailed design probably would be more favorable than the results of this study.

Similar to the procedure used in Section 3, the ejector setting, and canard deflection were optimized for a range of takeoff gross weights (TOGW). For this case, the optimum elevon deflection and the optimum angle of attack (AOA) are assumed to be 20 and 22.8 deg, respectively. In Figure 7-3, minimum level

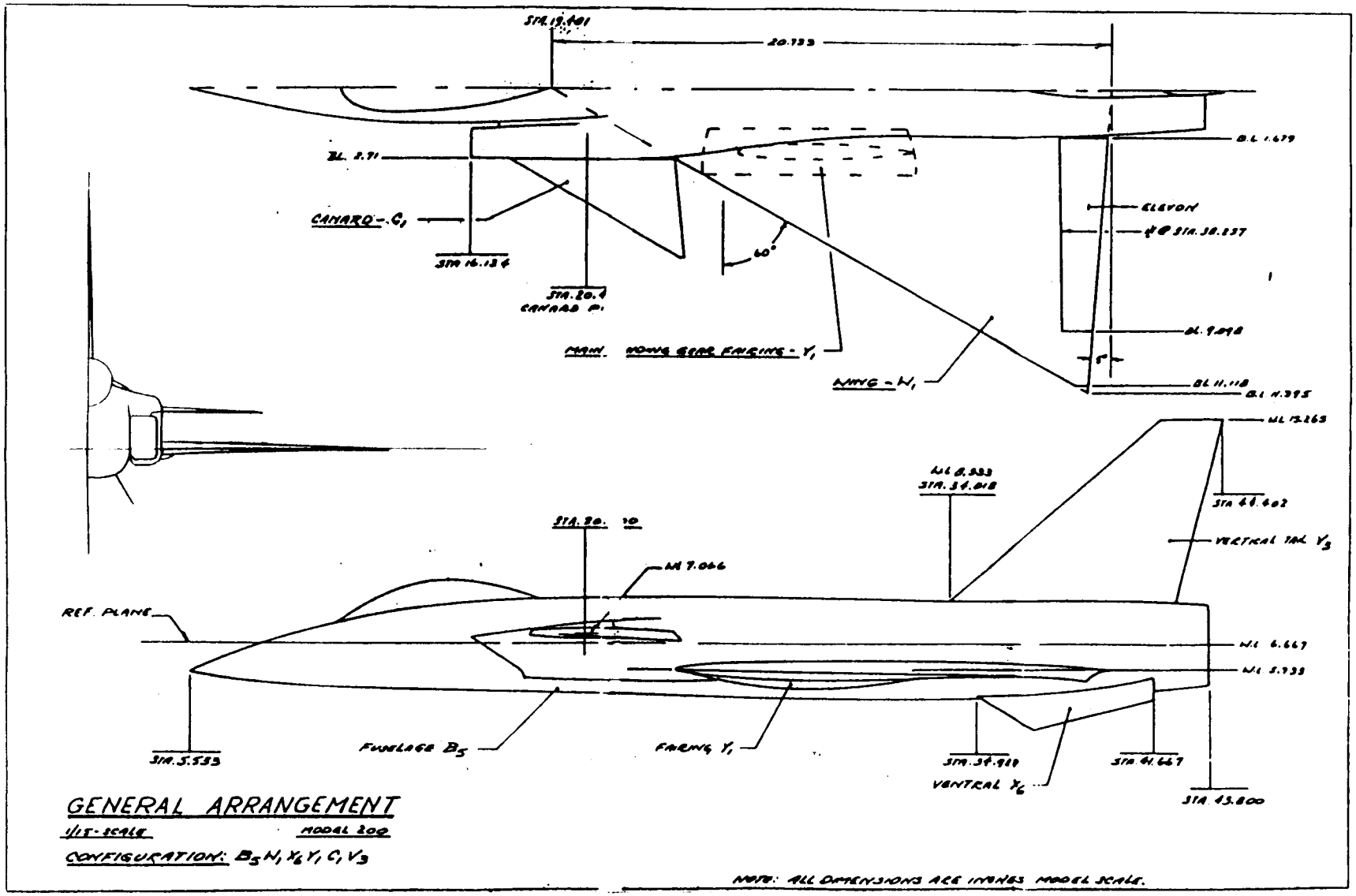

Figure 7-1, Model 200/218 Three View

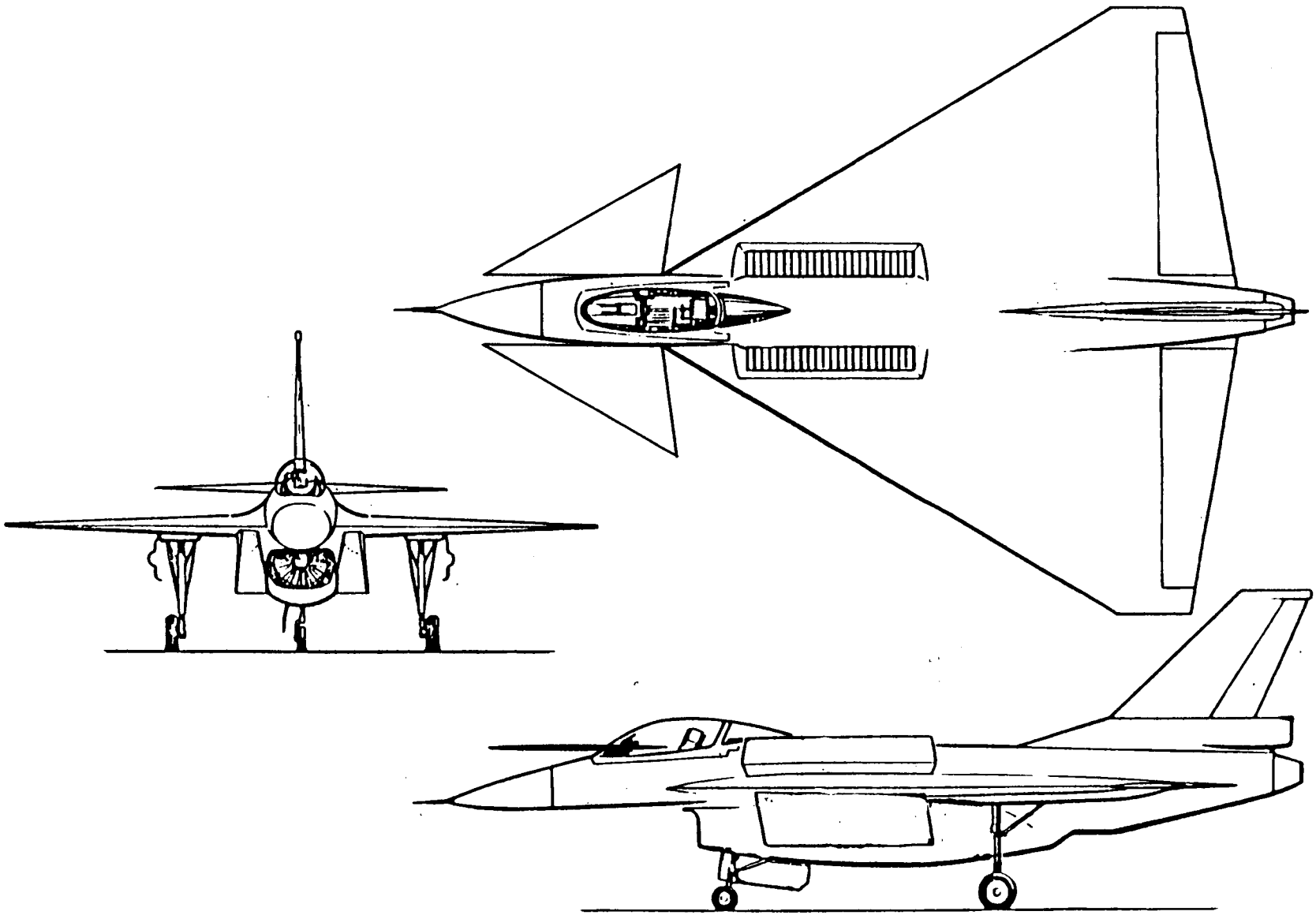

Figure 7-2, E-7 with Canards.

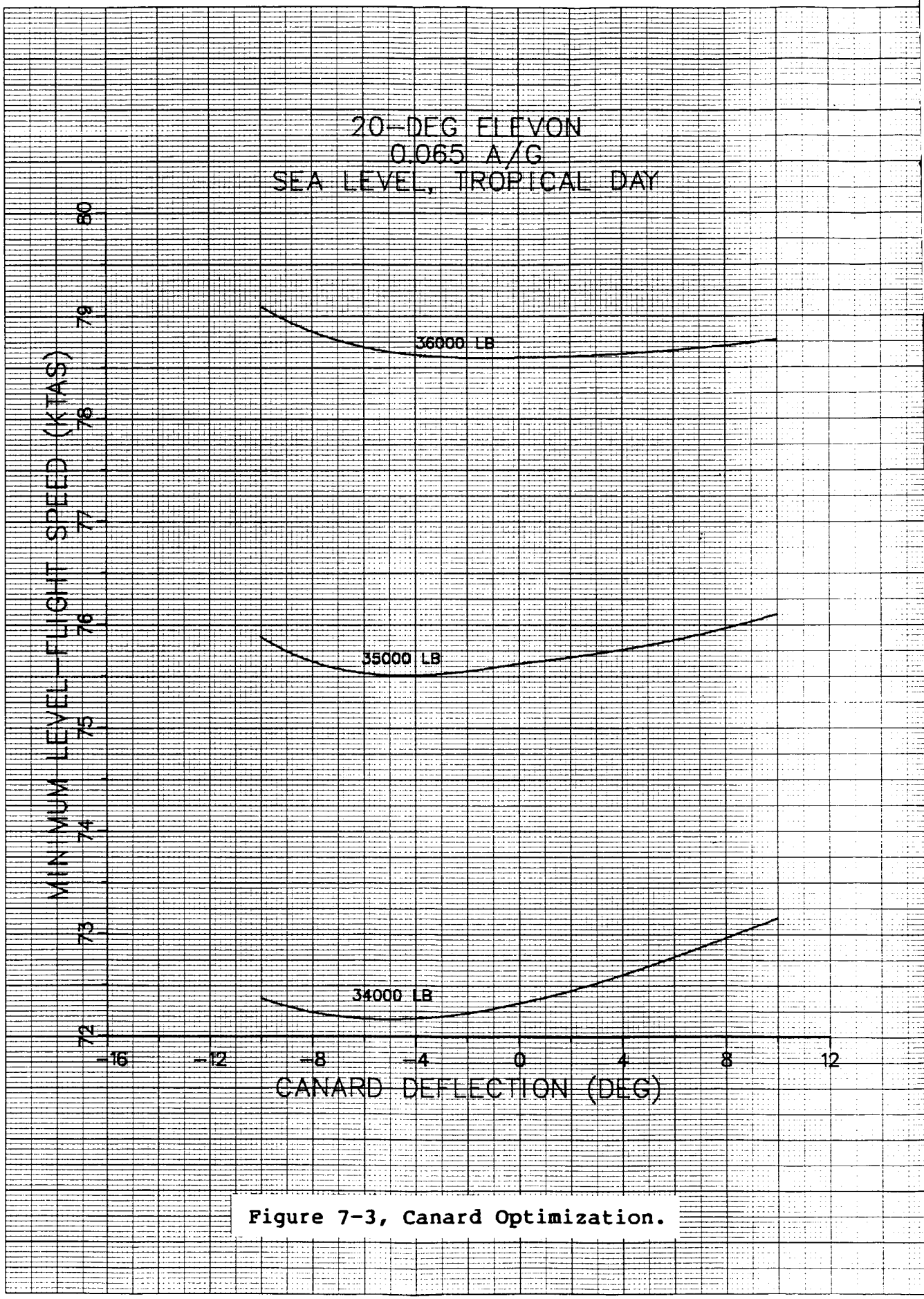

Figure 7-3, Canard Optimization.

flight speed, V_{MIN}, is plotted for a range of TOGW and canard deflection. These results show that the optimum canard deflection varies with gross weight. Once the optimum canard deflection is selected, the optimum ejector setting can be selected by referring to Figure 7-4 where the ejector is referenced to canard deflection and gross weight. As in Section 3, the STO weight is determined by the maximum TOGW that yields a carrier takeoff with 10 ft sink over bow and a minimum horizontal acceleration of 0.065 g. STO weight for the canard configuration is 36,500 lb. A summary of the flight path of the launch is shown in Figure 7-5, and, time histories of pertinent parameters are in Appendix F. In the flight path summary, one can see that the canard is used to initiate rotation and then moves to the optimum position for minimum level-flight speed. The canard has the effect of increasing the STO weight by 1600 lb, which compensates for the 1400-lb dry-weight increase of this particular configuration.

Besides the effect on STO weight, the effect on combat performance must be considered. The close coupled canard yields an added advantage, not only in increasing the effective lifting surface by 60 sq. ft. but also allows a higher L/D that can be exploited in high lift condiions. Table 7-1 lists the prominent combat characteristics for the E-7 with and without canards. Adding the canard is advantageous mostly in sustained turn load factor because of higher L/D capability. Otherwise, there is little difference with the exception of the degredation in acceleration time caused by increased wave drag. Note that the overall effect of the canard is that it is generally able to compensate for its additional 1400 lb of gross weight.

The use of a canard has a positive overall effect on the aircraft performance; it would be an asset to most STOVL aircraft if it can be properly integrated into the design. In particular, redesign would be able to improve the acceleration performance by reworking the area distribution. The dry-weight penalty could be reduced by rebalancing the airplane in hover. However, this task would be a major redesign for E-7.

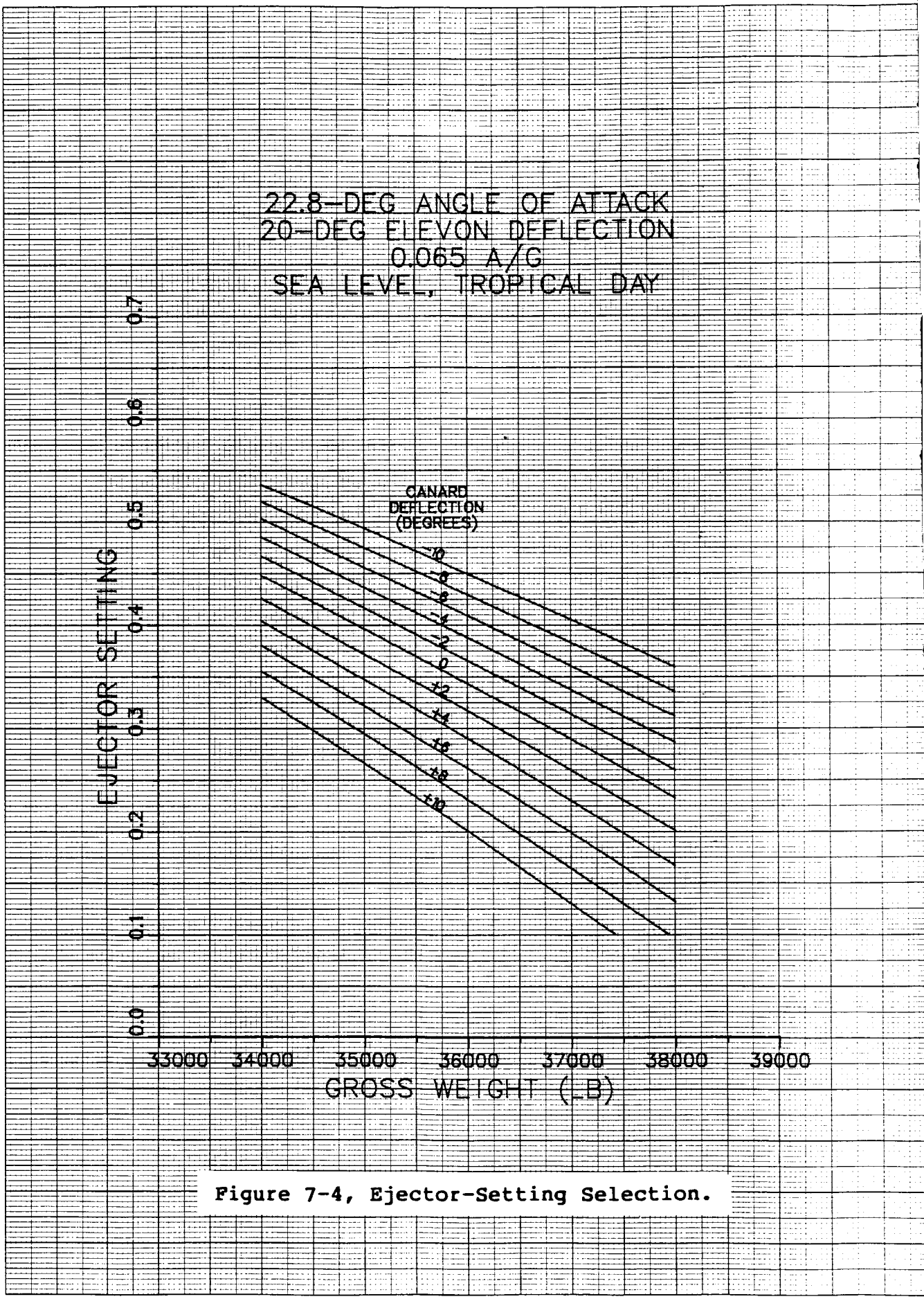

Figure 7-4, Ejector-Setting Selection.

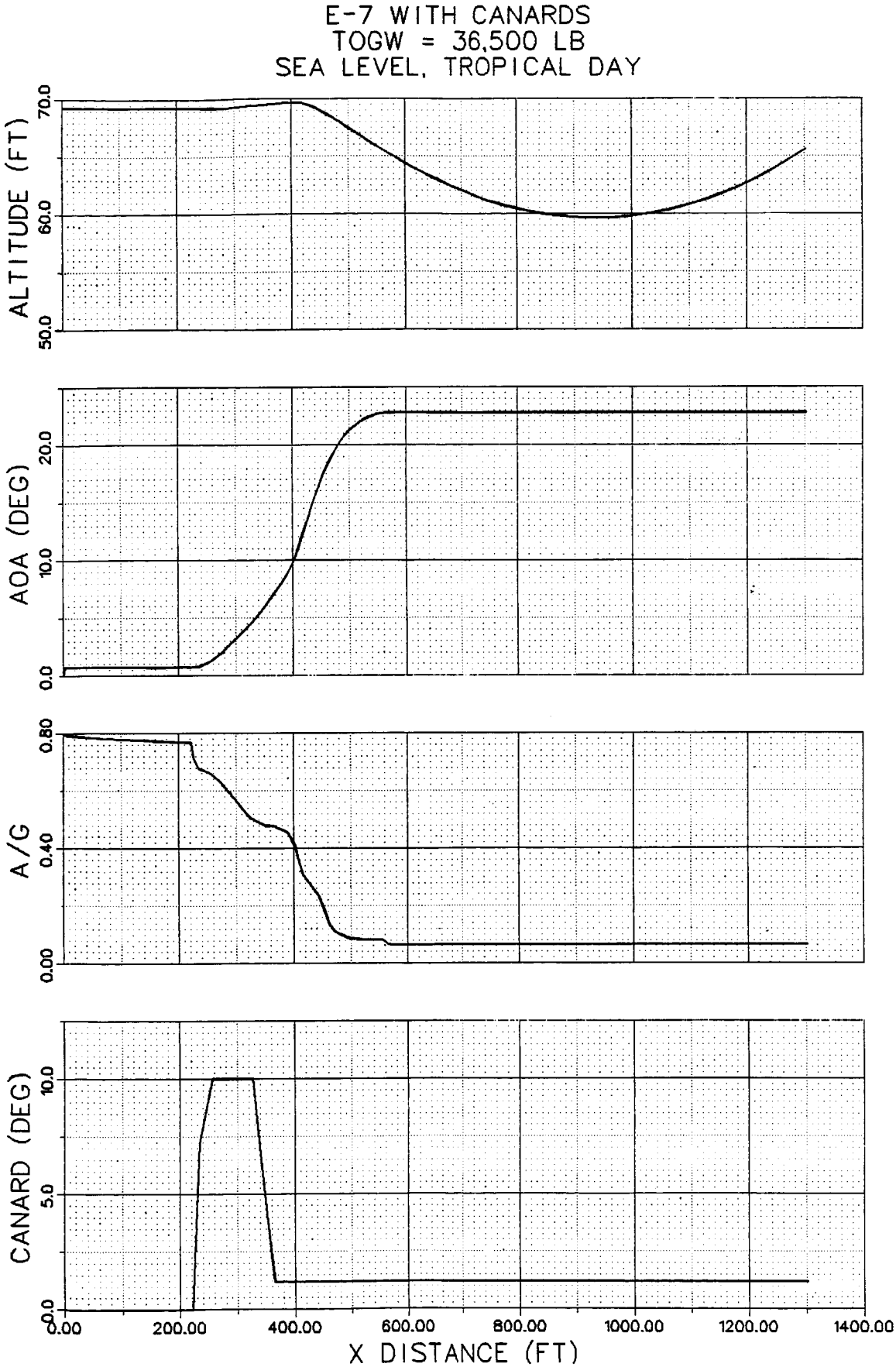

Figure 7-5, Canard Flightpath Summary.

Table 7-1, Combat Comparison

	Baseline E-7	E-7 With Canards
Combat Weight (lb)	27354	28754
Sustained Turn Loadfactor Mach .65/10,000 ft Max Power	5.25	5.55
Acceleration Time (sec) 35,000 ft, max power		
Mach 0.8 to 1.2	36.6	39.7
Mach 0.8 to 1.6	89.0	101.4
Maximum Mach		
35,000 ft, max power	1.735	1.715
10,000 ft, int power	1.032	1.074
Combat Ceiling, int power (ft)	46700	45800
Specific Excess Power (ft/sec) 1g, Mach 0.9, 10,000 ft	775	725

8. TRANSITION TO WING-BORNE FLIGHT

Transition is defined as the passage between jet-borne flight and wing-borne flight. In the case of a STOVL airplane, transition to wing-borne flight (also referred to as accelerating transition) begins when the gear lifts off the ground or deck and ends when the propulsive system is in the up-and-away configuration.

When optimizing the transition to wing-borne flight, the primary objective is to minimize the time from brake release to completion. For the E-7 configuration, wing-borne flight is defined as the minimum level-flight speed with no ejector thrust. This flight condition defines a unique specific energy. Therefore, the minimum time to wing-borne flight is achieved by maintaining the highest average specific excess power, P_s. The highest P_s is maintained when the ejector is not employed and the afterburner can be maintained on the aft nozzle. The analysis procedure is very similar to the determination of STO weight as performed for the baseline case in Section 3. To minimize the transition time, the airplane must hold at the bottom of the 10-ft sink to convert all of the P_s into velocity rather than into altitude. Analysis of the STO weight case is simply a continuation of the simulation for the baseline takeoff. A summary of the flight path is shown in Figure 8-1. After rolling off the deck edge, the airplane sinks ten feet and reaches level flight. As the speed increases, the ejector must be cut back to maintain level flight because aerodynamic lift is increasing. To keep the airplane trimmed, the core-thrust vector angle must be reduced, which thereby increases the flight path acceleration and speeds-up the transition process. When the core nozzle is fully aft the elevon is used to maintain the trim. At STO weight, the transition time from brake release is about 16 sec.

When operating at less than STO weight, the airplane has added freedom to use the sink over bow to aid the acceleration. In the case of the escort mission weight, 32,073 lb, rotation can be initiated right before the deck edge. Minimum level-flight speed is nearly reached by the end of the deck. The ejector is used only to help rotate and can be shut off very quickly once near the level-flight condition. The resulting transition time is only nine seconds. A summary of the escort-weight transition is shown in Figure 8-2, and, transition time histories are included in Appendix G.

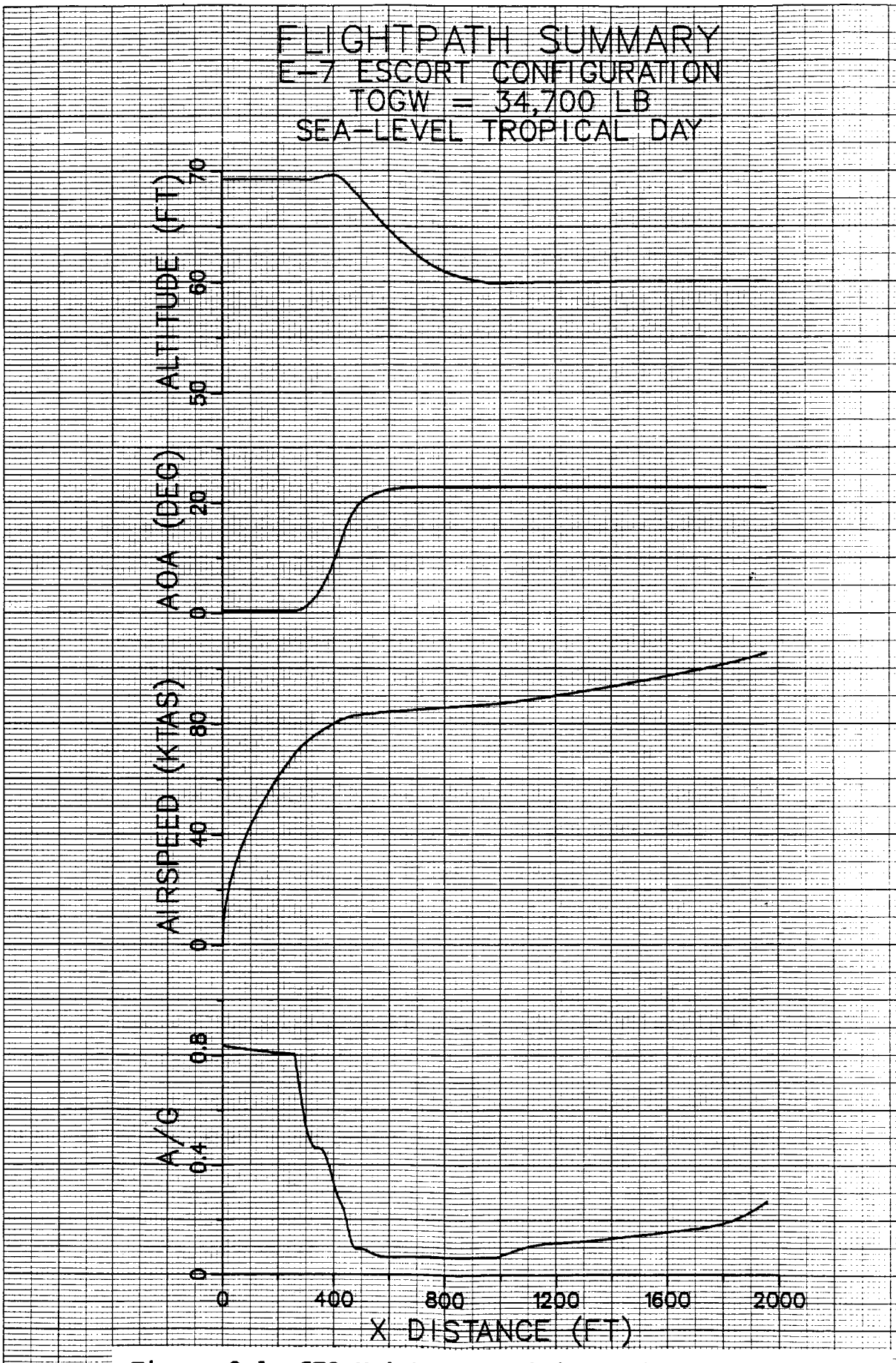

Figure 8-1, STO Weight Transition Flightpath Summary.

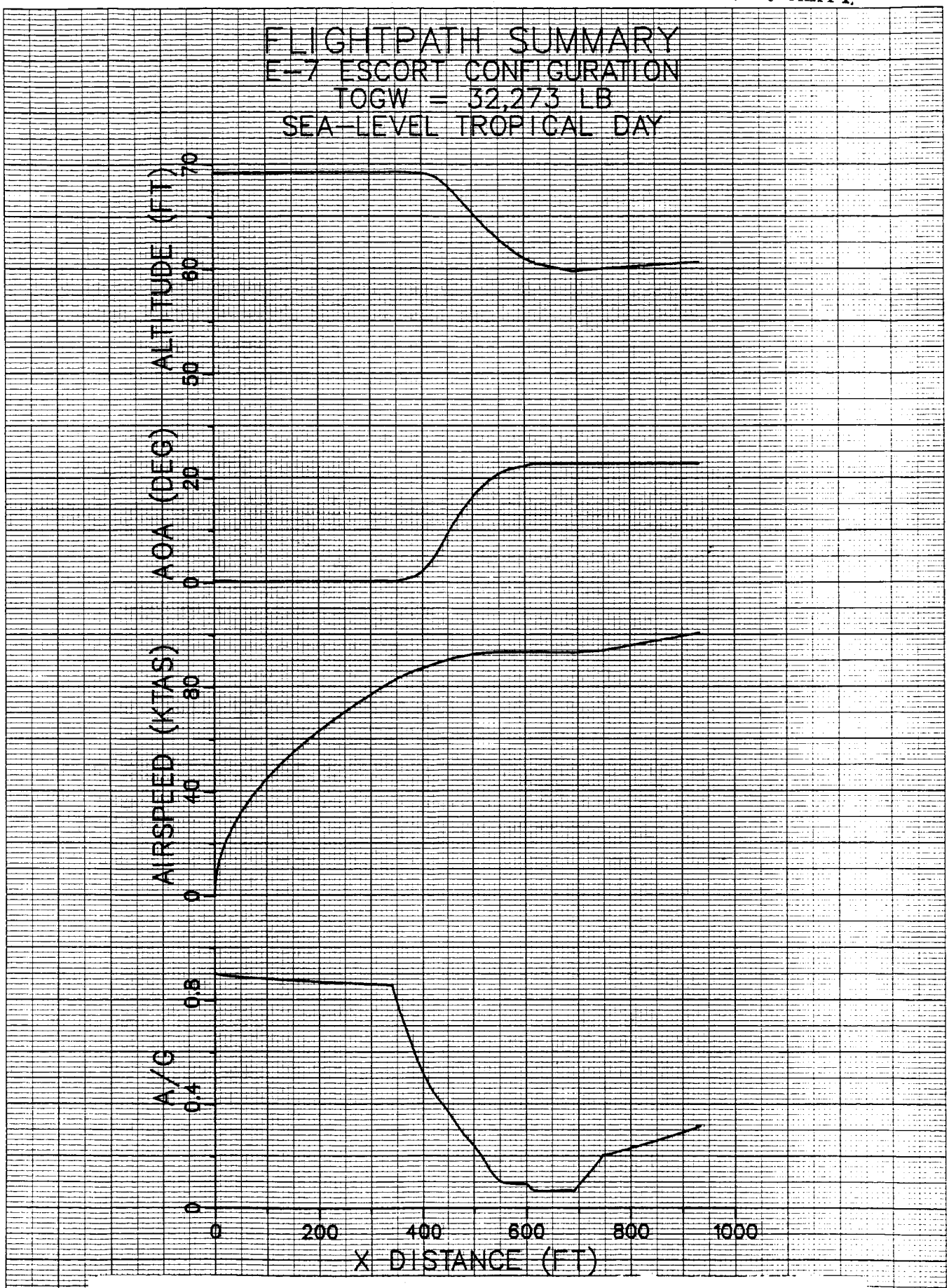

Figure 8-2, Escort Weight Transition Flightpath Summary.

9. TRANSITION TO HOVER

Current operational procedures for the AV-8A, as shown in Reference 13, allow for several types of landings. Most operational landings do not require an actual hover phase, where the airplane is aloft with zero airspeed. The airplane more commonly performs conventional landings or slow landings in which the thrust is vectored to decrease the landing speed but the airplane still lands with positive airspeed. Historically, the performance of hover has been a hazard-prone flight regime and is the acid test of the low-speed characteristics of the airplane. It is beyond the scope of this study to analyze the detailed dynamics of the airplane in hover since this analysis requires detailed design of the flight-control and reaction-control systems. The primary interest of this analysis is to assess the lift and thrust that are required to guide the airplane successfully through transition to hover.

This analysis considers two transition schemes: a current operational procedure and an optimum procedure that minimizes expended fuel.

The current operational procedure for decelerating transition (transition to hover) of the AV-8A is structured about a key position approximately one nautical mile from the touchdown point at an altitude of 200 ft above ground level (AGL) in level or slightly descending flight. The sequence proceeds as follows:

Approaching key

1. Nozzles are set to 40 deg for visual-flight rules or at 20 deg for instrument-flight rules.

2. Angle of attack (AOA) is held to about eight degrees.

3. Throttle is set to maintain level or slightly descending flight.

At key

4. Nozzles are set to hover stop.

Departing key

5. Attitude is maintained.

6. Throttle is maintained to descend to about 50 feet AGL.

At approximately 50 knots

7. The aircraft is flared slightly to stop.

The objective of optimizing the decelerating transition is to minimize the expended fuel. The basic purpose of transition, when thought of in terms of aircraft energy, is to reduce the kinetic energy of the airplane to zero. Theoretically, this could be acheived by converting all of the kinetic energy to potential energy. Operationally, this option is unattractive because it requires the aircraft to pull up from level flight, trade velocity for altitude, and then be able to hover over a landing pad 500 ft above the original flight path. It is desirable to begin the transition with as little energy as possible, at nominally 200 ft AGL at minimum non-accelerating level-flight speed. This condition naturally dictates that the transition be performed in level flight throughout the sequence. To further optimize the transition the airplane should stay in the configuration that minimizes the specific excess power times the fuel-flow. However, during the majority of the transition, the engines are operating at intermediate rated thrust (IRT) to decelerate the airplane and to maintain level flight. Therefore, to minimize the fuel flow, the transition time must be minimized. The optimum transition sequence is similiar to the current operational procedure.

1. The transition begins at about 24 deg AOA, which is the minimum level-flight condition for wing-borne flight.

2. Rather than vectoring the thrust to an intermediate position, the core thrust vector is deflected to the maximum 110 deg and the ejector is used to maintain the AOA.

3. As airspeed decreases, engine power setting is increased to maintain level flight. This condition is maintained until the engine power setting reaches IRT.

4. The core vector is set to 90 deg (hover stop) and full ejector is used.

5. The AOA is reduced at about 2 deg/sec such that the velocity is zero when pitch is zero. Power setting is used to maintain level flight and the reaction-control system is used to control pitch.

Figure 9-1 shows time histories of airspeed and pitch. Note that the airspeed quickly reduces and is down to 50 knots in four seconds. It can be seen that when the pitch angle reaches zero the airspeed is also zero. Time histories of pertinent state variables are included in Appendix H.

This sequence has several advantages over the current procedures: transition takes only 15 sec, the distance traveled is less than 1000 ft, and transition only requires about 50 lb of fuel. These capabilities, though, have an undesirable side effect. In order to decrease the transition time, the aircraft must decelerate very rapidly. At about three seconds into

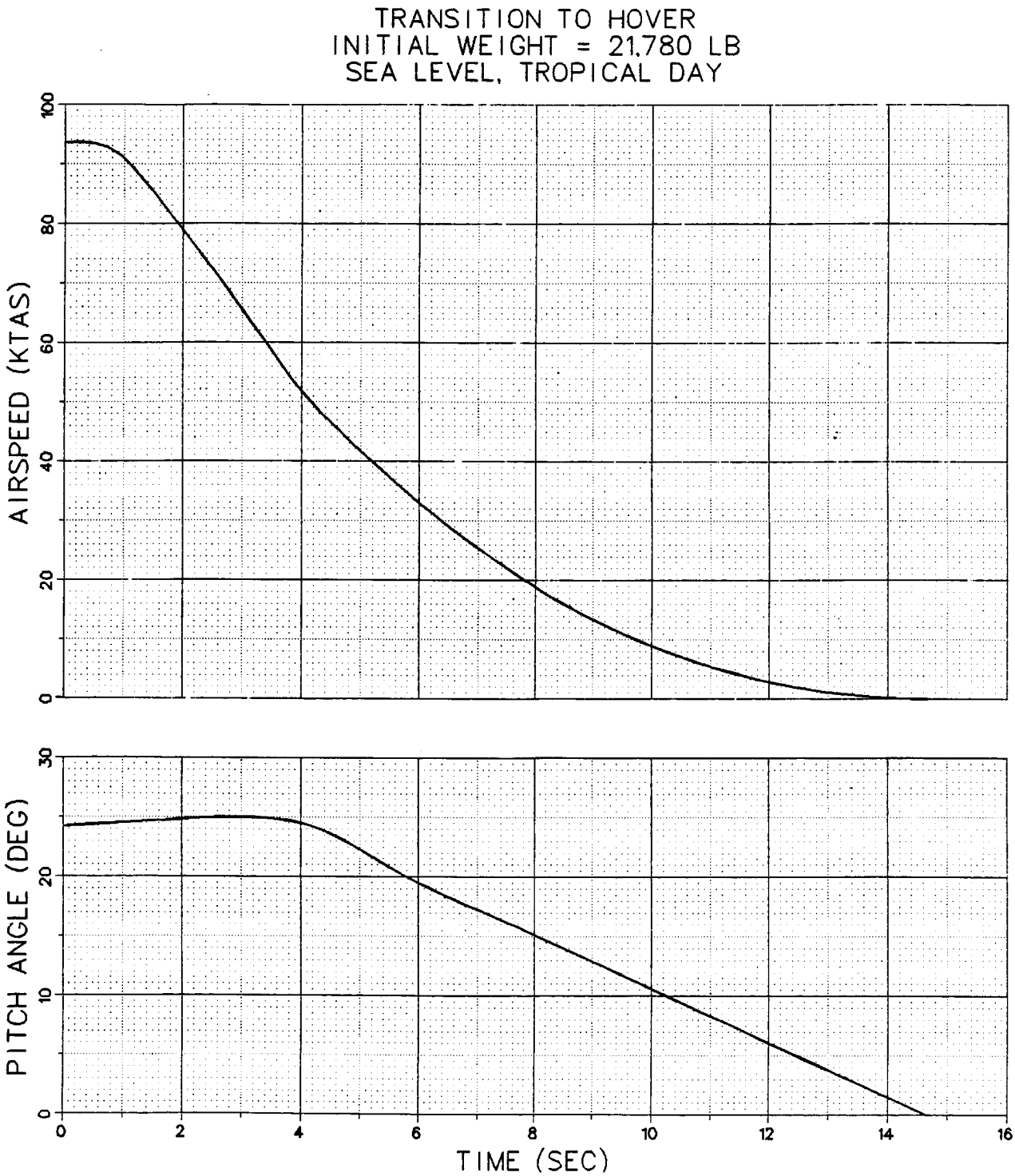

Figure 9-1, Transition to Hover - Airspeed and Pitch.

transition, the flight-path acceleration is about -23 ft/sec . The pilot feels this force as a 0.3-g increment in normal load factor and a 0.7-g decrement in horizontal acceleration. In a conventional airplane, these forces would be similar to slapping the throttle to idle and deploying full flaps and speed brakes. The forces are not unreasonable, but may not be desirable in most landings. If the operational situation does not require maximum performance, the E-7 transition capability is adequate to deviate from the optimum path by activating the ejector at a slower rate and still keep the expended fuel within acceptable limits.

10. EJECTOR PERFORMANCE

The performance of propulsive lift is sometimes considered a high-risk item that can determine the viability of a vertical-landing aircraft configuration. In the E-7 configuration, a slight risk is possible because of uncertainty in the ejector augmentation ratio, ϕ. The ejector performance severely impacts the ability of the airplane to hover (e.g., if ϕ is reduced by 0.1, the useful load decreases by about 1500 lb, which nearly eliminates the fuel available for hover). The vertical thrust determines the useful load (fuel and retained weapons) that can be carried during hover. The ejector performance also impacts the takeoff performance, but to a lesser degree. This study investigates the effects of changes in ejector performance on STO weight. The approximate error distribution on ejector performance at this time has a 90% confidence interval from -5%ϕ to +5%ϕ. To adequately investigate this interval, dispersions in were investigated from -0.1 to +0.1.

Similiar to the analysis described in Section 3, the minimum level-flight speed, V_{MIN}, was calculated over a range of gross weights for ϕ values of 1.53, 1.63, and 1.73. As can be seen in Figure 10-1, the change in ϕ affects V_{MIN} only slightly. For any given weight, a 0.1 change in ϕ changes V_{MIN} by less than one knot. When the ejector performance decreases, the optimum ejector setting increases to compensate for the loss in vertical thrust. Because the ejector ram drag is a function of the amount of flow that is entrained, the ram drag decreases when ϕ decreases.

Because V_{MIN} is insensitive to ϕ, so is the STO weight. STO weight varies about 400 lb for a 0.1 variation in ϕ, as shown in Figure 10-2. Summaries of the carrier-takeoff sequences for ϕ =1.53 and ϕ =1.73 are shown in Figures 10-3 and 10-4 respectively. Time histories of pertinent variables are shown in Appendix I.

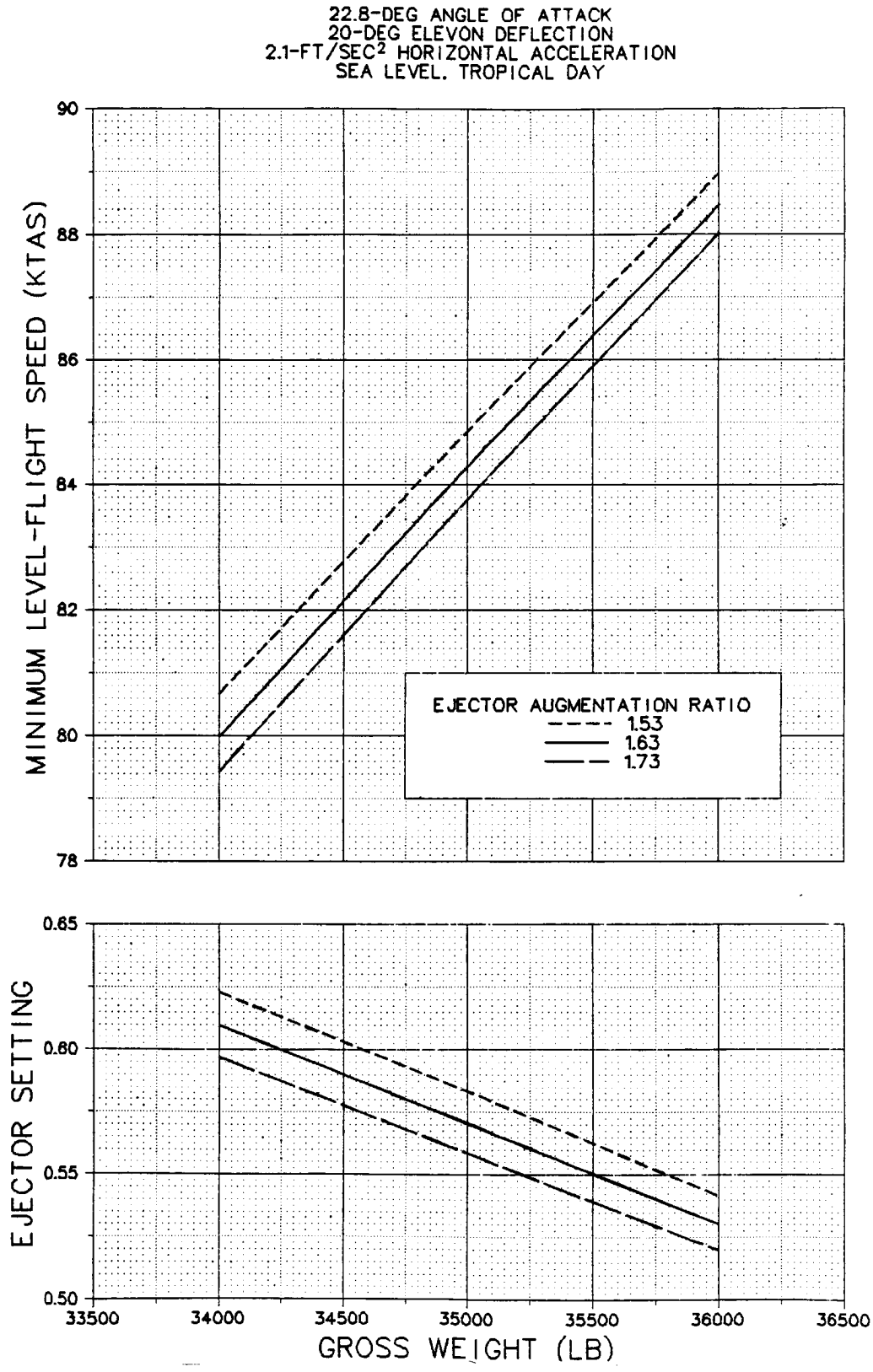

Figure 10-1, V_{MIN} Sensitivity to ϕ.

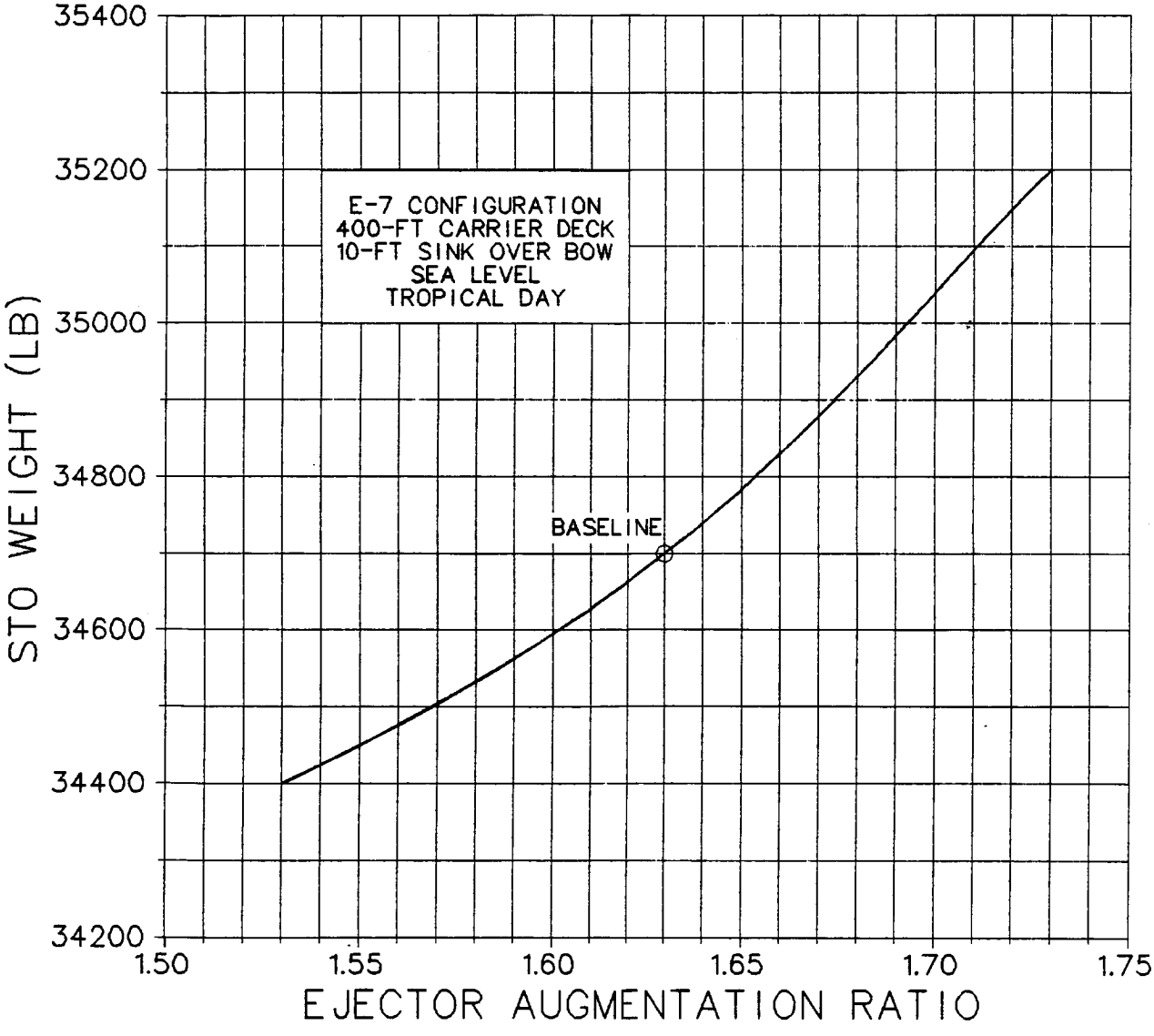

Figure 10-2, STO Weight Sensitivity to ϕ.

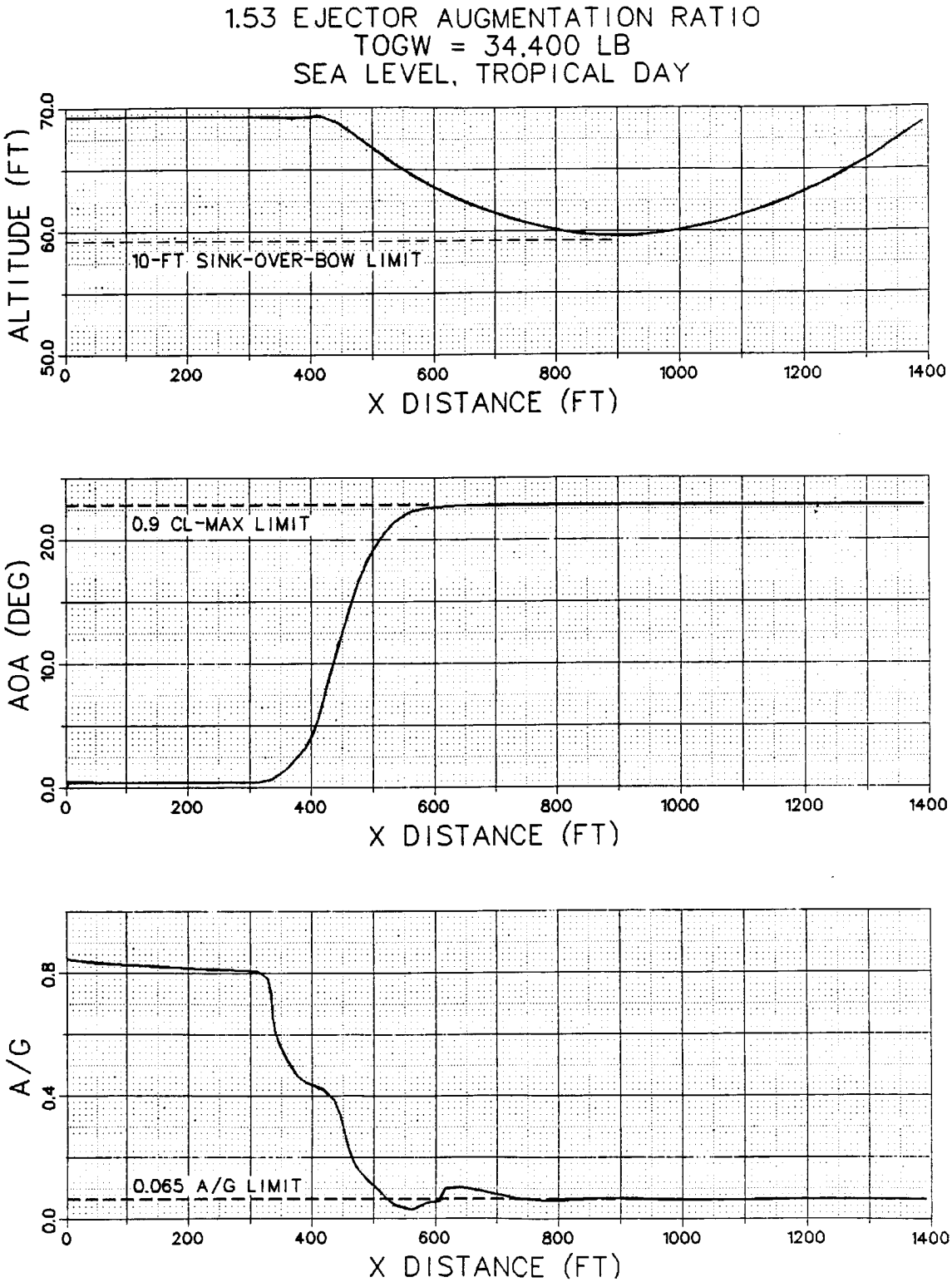

Figure 10-3, Takeoff Flight-Path Summary for ϕ=1.53.

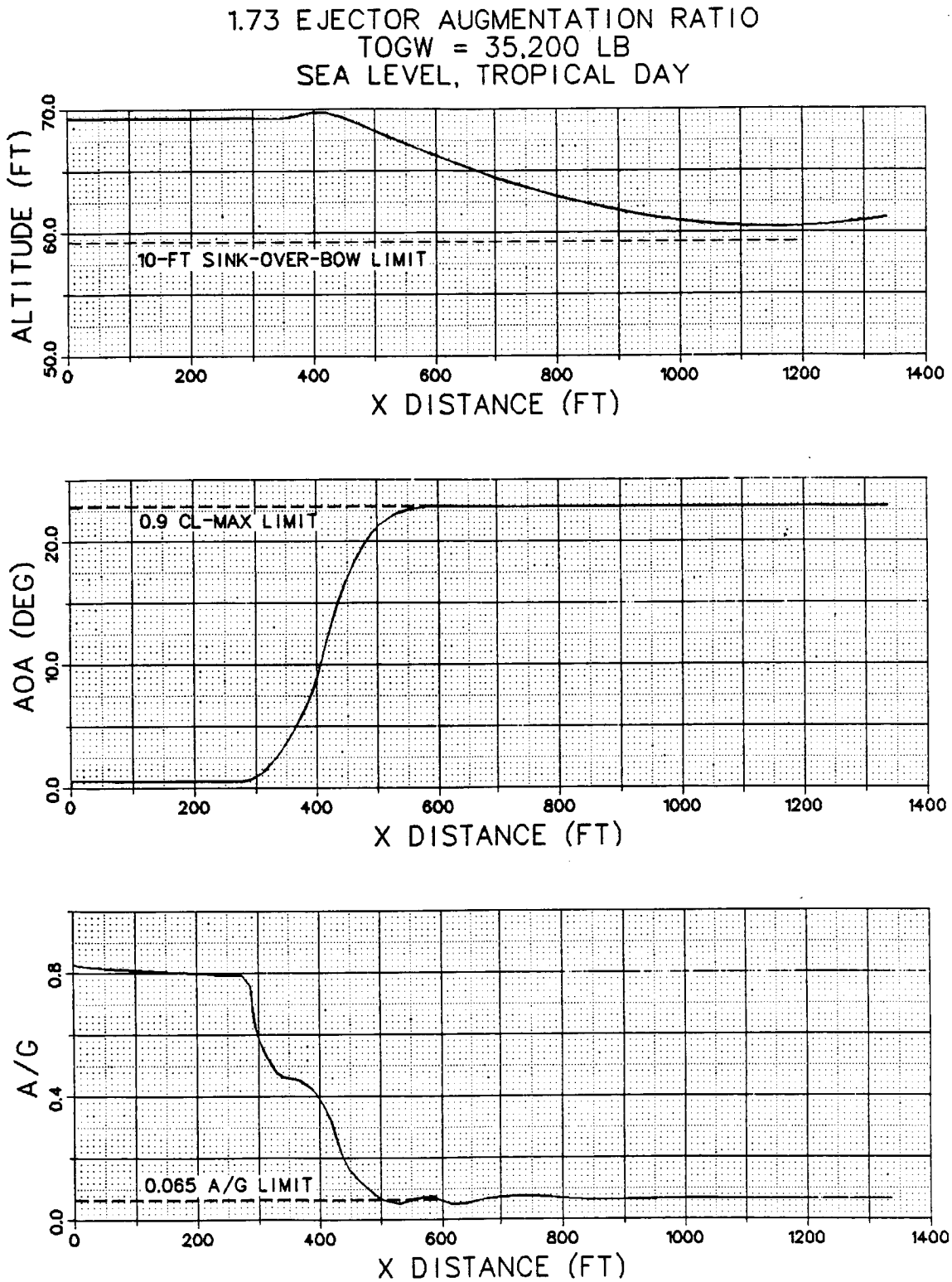

Figure 10-4, Takeoff Flight-Path Summary for ϕ=1.73.

11. NON-AFTERBURNING TAKEOFF

Damage to takeoff and landing areas by routine aircraft traffic is a concern in many operational scenarios. Sod fields are especially susceptable to damage from landing gear and engine exhaust plumes. Aircraft that use afterburned vectored thrust can easily damage many surfaces. Hot and high-velocity jet streams can also create a bad environment for following aircraft. Other aircraft can be damaged or degraded by injestion of hot gasses, foreign objects, and debris that are generated by previous aircraft. For all these reasons, it is sometimes desirable to takeoff and land without afterburning thrust. The E-7 is designed to hover in intermediate rated thrust (which helps to maintain a cool hover footprint), but field takeoff performance is usually based on afterburning the flow wherever possible. This study investigates the field takeoff performance of the baseline E-7 for non-afterburning operations. The analysis is based on a loading of (4)MK-83 + (2)AIM-9 to represent a typical loading for ground-based operations.

Takeoff ground-roll distance, Sg, was calculated for four combinations of afterburning thrust (A/B). These combinations are (1) the baseline (both aft- and core-thrust afterburning), (2) aft A/B only, (3) core A/B only, and (4) no A/B. When the aft thrust is afterburned, it is only utilized for ground-roll acceleration. It is not feasible to afterburn the aft flow when part of the fan flow is directed to the ejectors. Therefore, the takeoff speed is affected by the core afterburner but not the aft afterburner. At a takeoff gross weight of 35,544 lb, the takeoff speed is set by 1.1 times the minimum level-flight speed, V_{MIN}, that has a climb-gradient potential of 0.5%. In calculating the V_{MIN} of the E-7 with core A/B, maximum allowable angle of attack (AOA) is optimum, as shown in Section 3. However, it is not obvious that maximum AOA is optimum when core A/B is not used. Figure 11-1 shows a carpet plot of V_{MIN} as a function of AOA and ejector setting. The slope of the 0.5%-climb-gradient constraint shows that the optimum AOA is indeed 27 deg. Therefore, the takeoff speed is 87.7 KTAS for afterburned core thrust and 114.6 KTAS for non-afterburned core thrust. A plot of airspeed vs. S_g, Figure 11-2, shows the acceleration characteristics of each case. In considering only acceleration capability, the aft afterburner is more critical than the core A/B. However, the core A/B affects the overall takeoff performance more because it affects the takeoff speed as well as the acceleration. When the core thrust is not afterburned, S_g approximately doubles to almost 1500 ft. This distance is much greater than the maximum-performance takeoff, but would be adequate for many land-based operations. Further state-variable comparisons between the four combinations of afterburner are shown in Appendix J.

This part of the study is concerned with the field-takeoff capabilities of the E-7 with the interdiction loading, whereas, the study described in Section 6 used the escort loading.

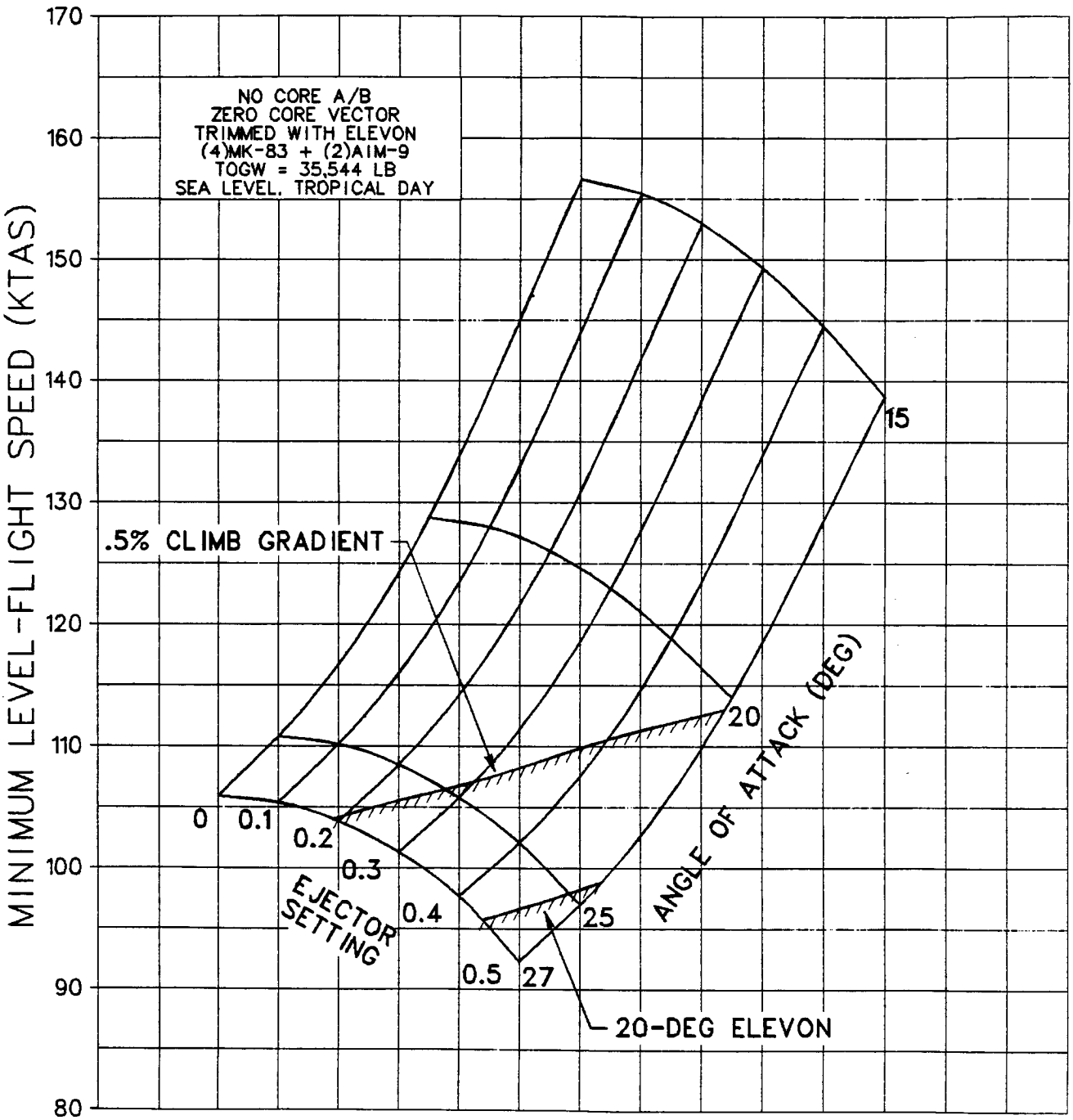

Figure 11-1, V_{MIN} Without Core Afterburner.

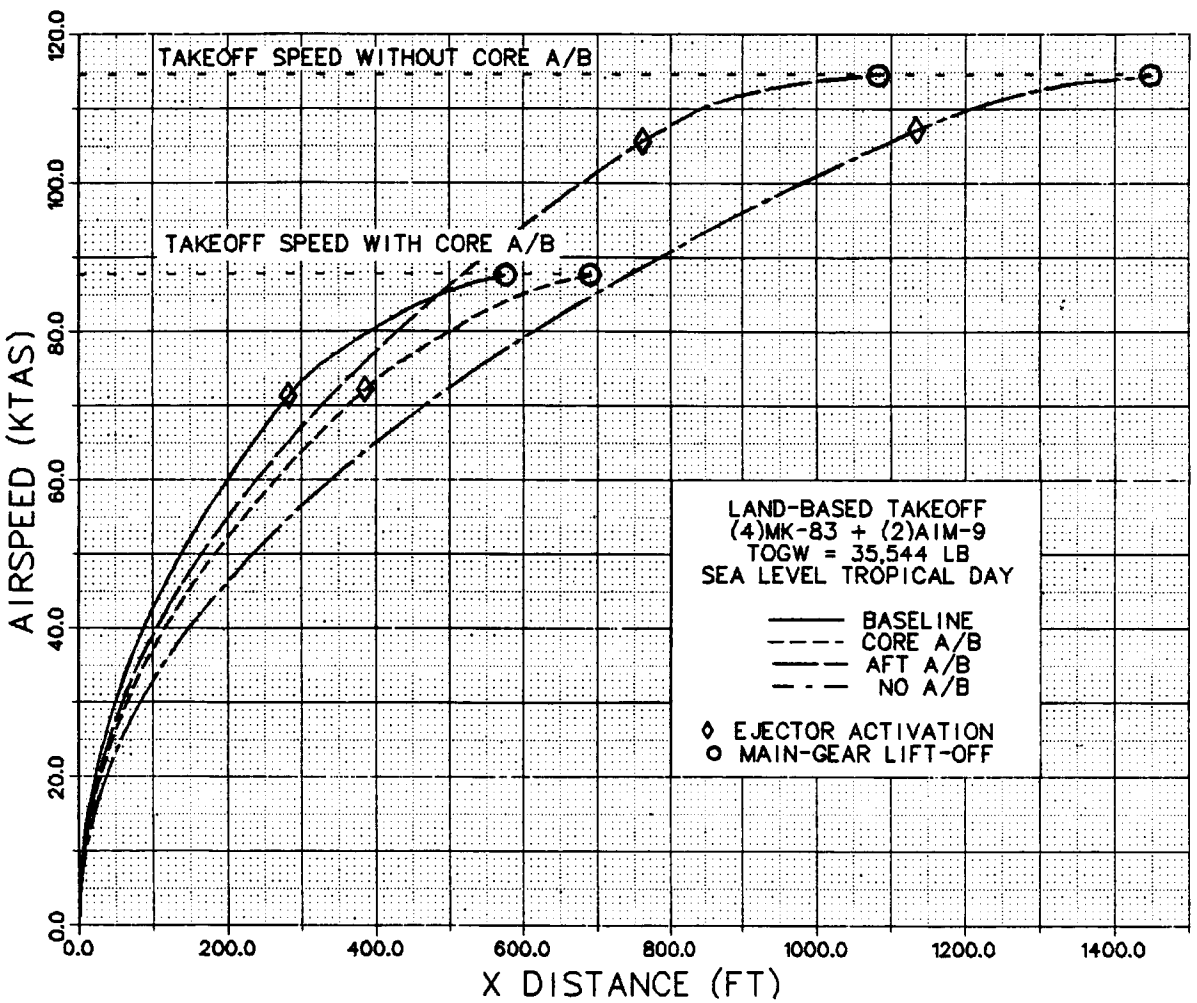

Figure 11-2, Non-Afterburner-Takeoff Comparison.

Between these two tasks, one can draw a relationship for ground-roll distance as a function of takeoff gross weight. These two points are shown in Figure 11-3. The theoretical trend on which the points lie is based on classical handbook methods that have been calibrated to the two detailed-analysis points. The trend was calibrated in two steps:

1. A takeoff velocity function was derived from handbook methods using an equivalent weight that is assumed linear with actual takeoff gross weight. The linear relationship is based on the two detailed points of weight and takeoff velocity. This method models the airspeed that is required to takeoff by setting the equivalent weight to approximately the aerodynamic lift.

2. The distance required to accelerate to takeoff speed is then calculated by classical methods but is based on actual weight, not equivalent weight. To account for differences in takeoff caused by store-drag differences, rotation losses, and thrust vectoring, the calculated S_g is corrected to the detailed S_g by adding an error term that is linear with calculated S_g.

The theoretical trend is probably accurate to within 50 ft (an airplane length) over the range of gross weights shown in Figure 11-3.

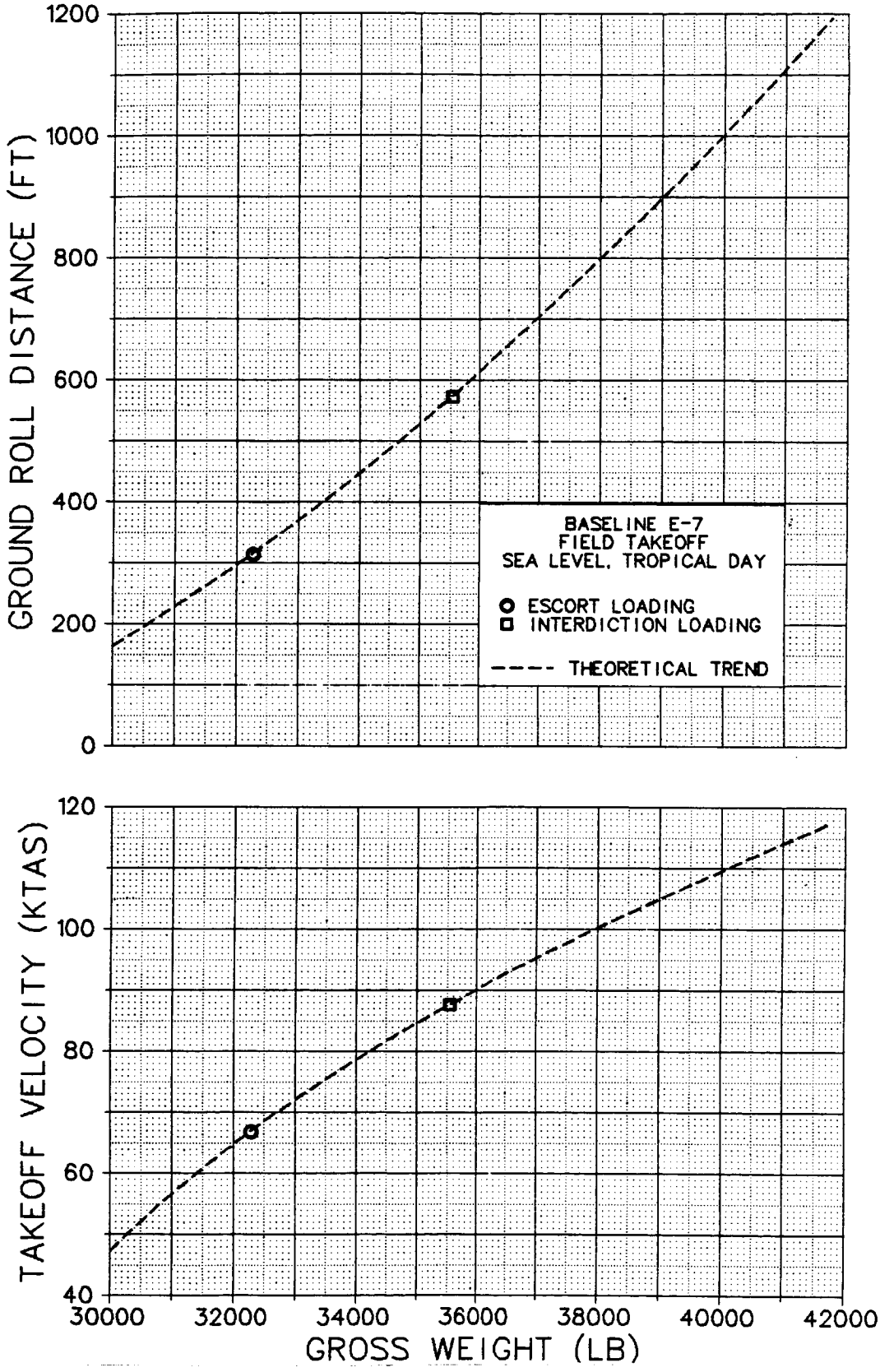

Figure 11-3, Ground-Roll Distance vs. Gross Weight.

12. NON-EJECTOR TAKEOFF

The results presented in Section 6 suggest that if the E-7 were equipped with a vectorable aft nozzle it would be possible to achieve non-ejector field-takeoff performance that is similar to that of the baseline E-7. This result then raised interest in calculating the non-ejector STO weight. The analysis procedure is similar to that used in Section 4; however, for this investigation, the ejector doors will be closed and the ejector not activated.

As usual, the first step in the analysis is to optimize the control deflections while calculating the minimum level-flight speed, V_{MIN}. A carpet plot of V_{MIN} as a function of core-thrust vector angle and gross weight is shown in Figure 12-1. For this optimization, the elevon deflection is set to 20 deg and the angle of attack (AOA) is set to 22.8 deg. The aft vector is used to trim the moments to zero. The aft-nozzle-deflection limit of -20 deg is plotted on the carpet as a constraint. Typically, V_{MIN} is constrained by horizontal acceleration, but this is not the case without the ejector activated. The nozzle-deflection limit does not significantly constrain V_{MIN}. At any particular weight, the intersection of the constraint is very close to the unconstrained V_{MIN}. The benefit of non-ejector takeoff is evident when Figure 12-1 is compared to Figure 3-3. At gross weights less than 34,800 lb, the baseline V_{MIN} is less than the non-ejector V_{MIN}, but at greater than this weight the converse is true. At 37,000 lb the non-ejector V_{MIN} is about four knots less than that of the baseline E-7. The lower V_{MIN} is attained by the ability to afterburn the aft-thrust, which yields a lifting component as well as an accelerating component. The occurance of the trade-off point at 34,800 lb gross weight is caused by a reduction in ejector effectiveness because ejector ram drag becomes a larger penalty at higher airspeeds.

When the carrier-takeoff sequence is simulated, the resulting STO weight is about 37,400 lb, which is significantly greater than the baseline STO weight. This increased performance is possible because of reduced V_{MIN} and the ability to afterburn the aft thrust throughout the entire carrier-takeoff sequence. A summary of key parameters in the takeoff are shown in Figure 12-2. Installation of the vectorable aft nozzle and the use of this procedure yields three benefits:

1. The useful load (fuel and weapons) at takeoff increases by 2500 lb, which does not include 200 lb of dry weight increase attributable to the vectorable aft nozzle. This increase is greater than the weight of (2)MK-83LDGP.

2. The horizontal acceleration does not drop to the 0.065-a/g limit as it does on the baseline takeoff. This feature translates into increased safety on takeoff.

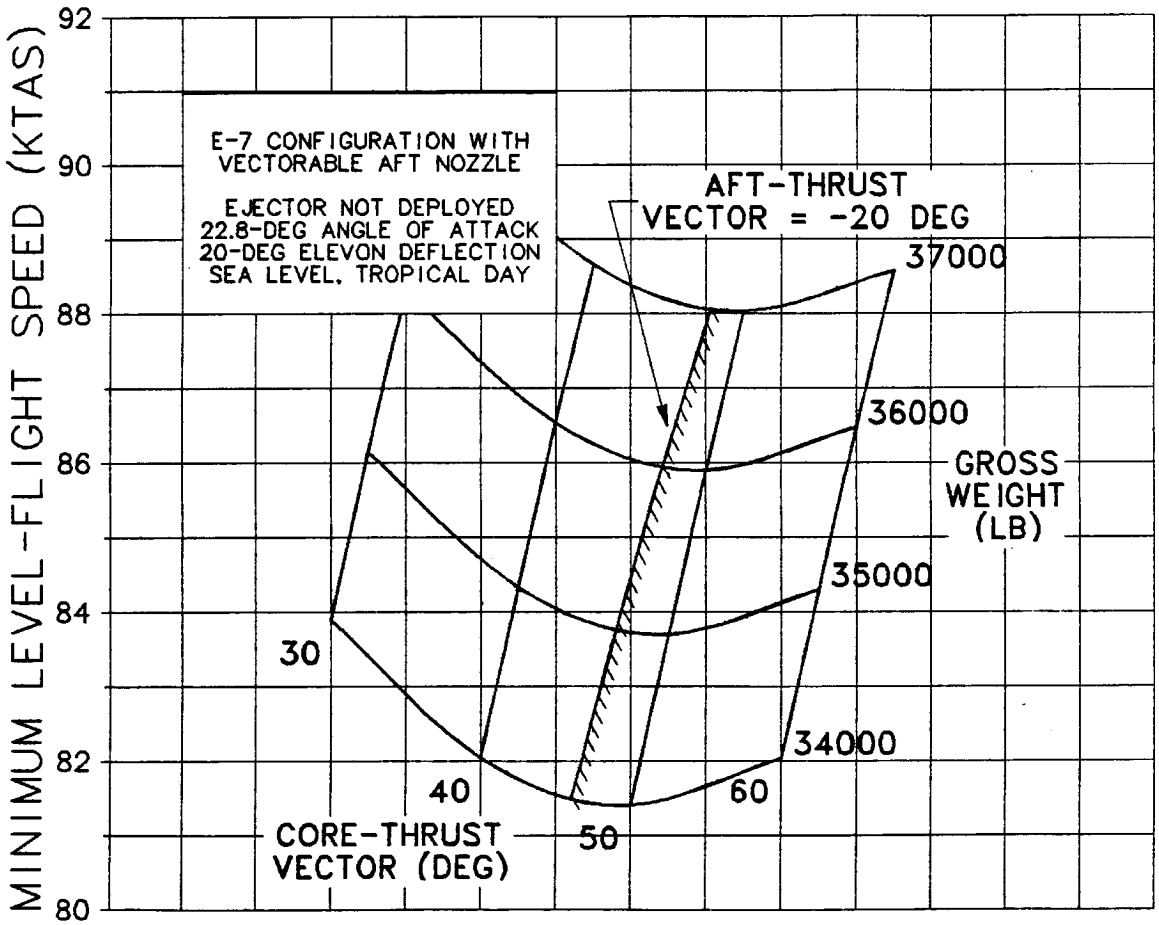

Figure 12-1, Non-Ejector V_{MIN} With Vectorable Aft Nozzle.

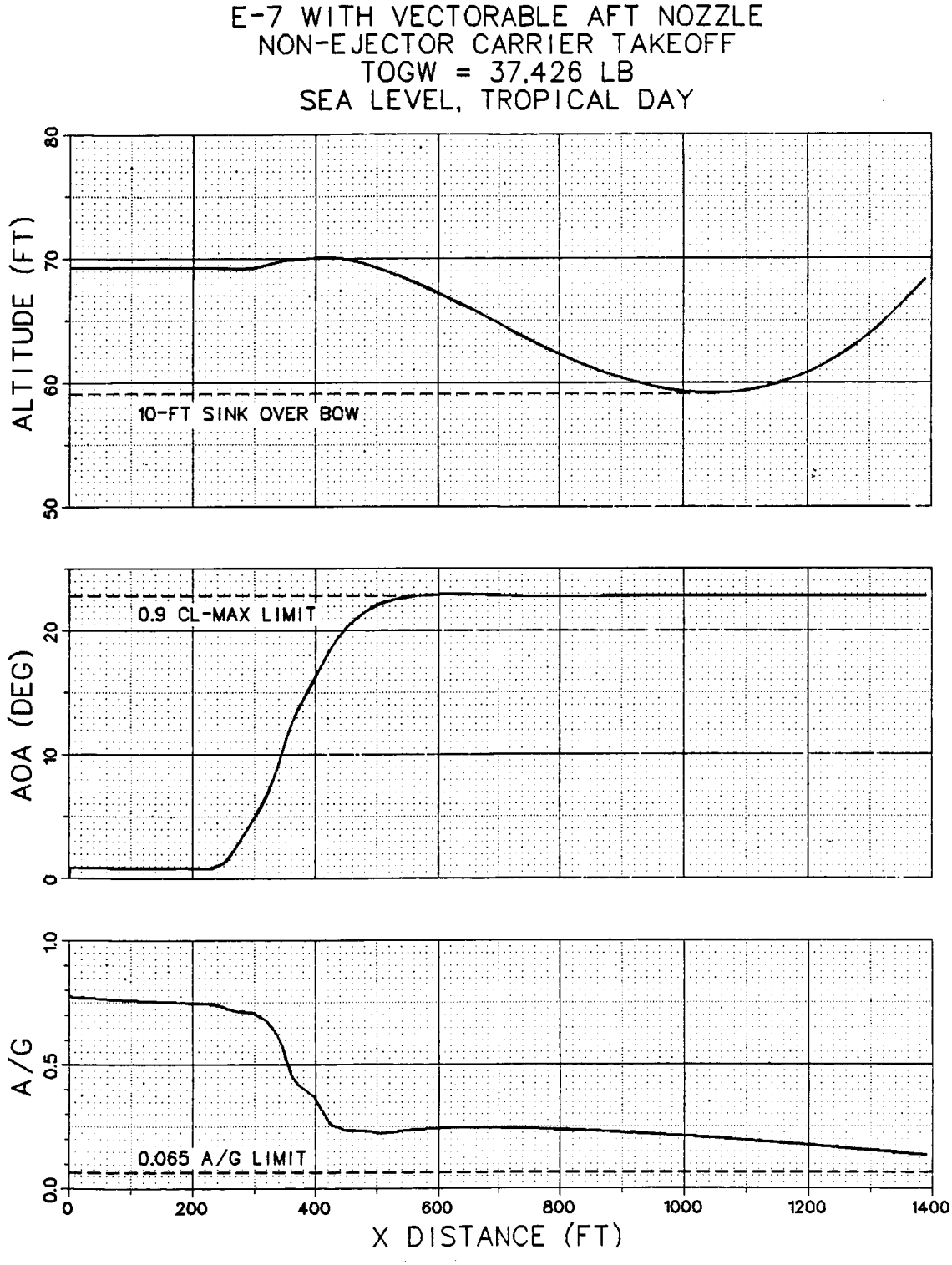

Figure 12-2, Non-Ejector-Takeoff Summary.

3. The sequence of control deflections required for optimum takeoff are less complicated than those required for the baseline. The control system can be restricted to fairly simple pitch-controlling elements.

Non-ejector STO weight was also calculated for the E-7 with 10-inch and 20-inch nose-gear-strut extensions as well as a vectorable aft nozzle. The STO weights are 37,600 and 37,200 lb respectively. Summaries of the carrier-takeoff sequences are shown in Figures 12-3 and 12-4. The variations in STO weight are small relative to inaccuracies in the calculation procedure. These results show less benefit in adding strut extensions than those shown in Section 5. The baseline benefits from increased static pitch because it allows the airplane to initiate rotation later to delay the large decrease in acceleration caused by the ejector. When the ejector is not used, the horizontal acceleration remains large at the beginning of rotation and decreases as AOA increases; therefore, delaying rotation has less benefit. Time histories of non-ejector carrier takeoffs are shown in Appendix K for nose-gear-strut extensions of 0, 10, and 20 inches.

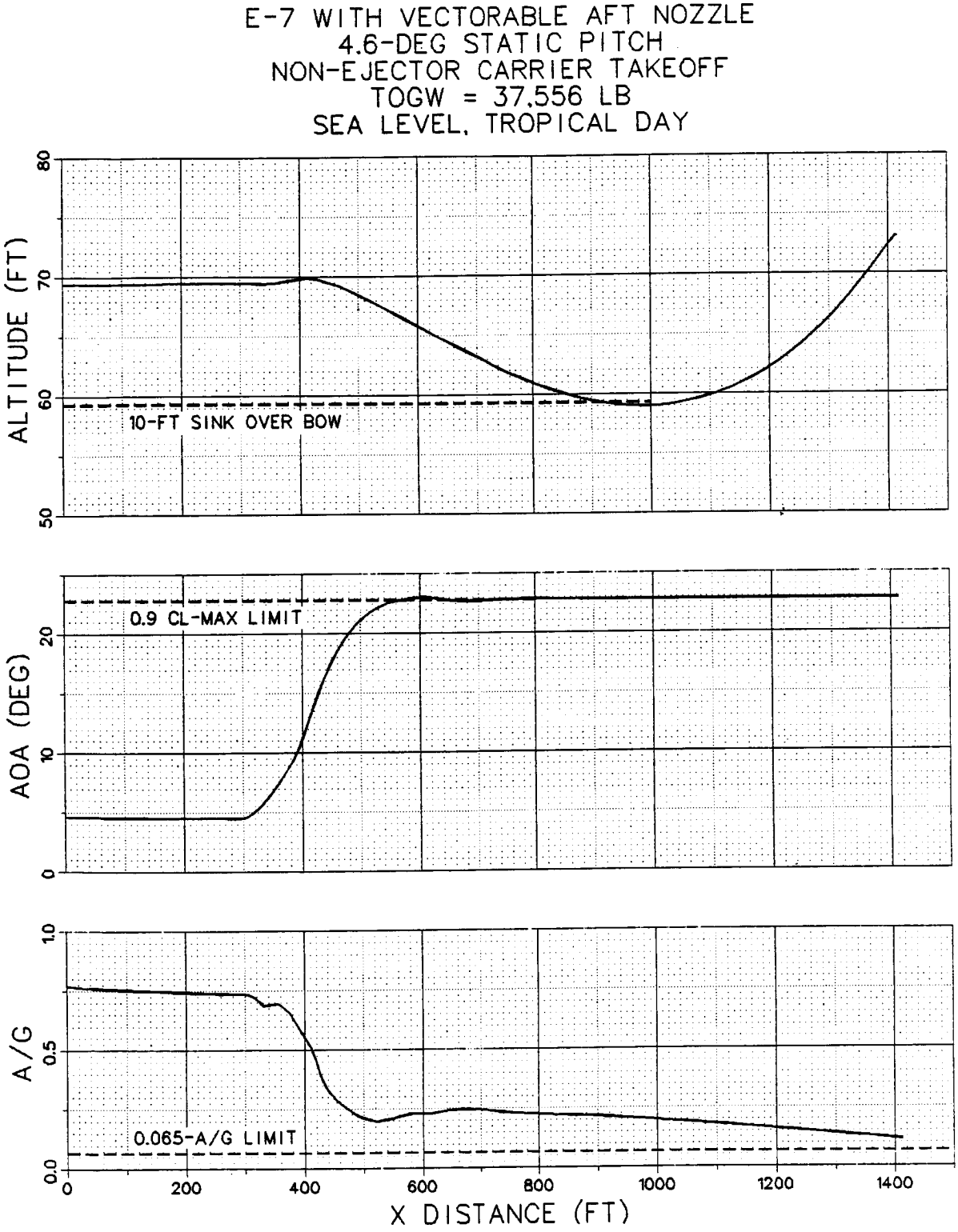

Figure 12-3, Non-Ejector-Takeoff Summary for 4.6-Deg Static Pitch.

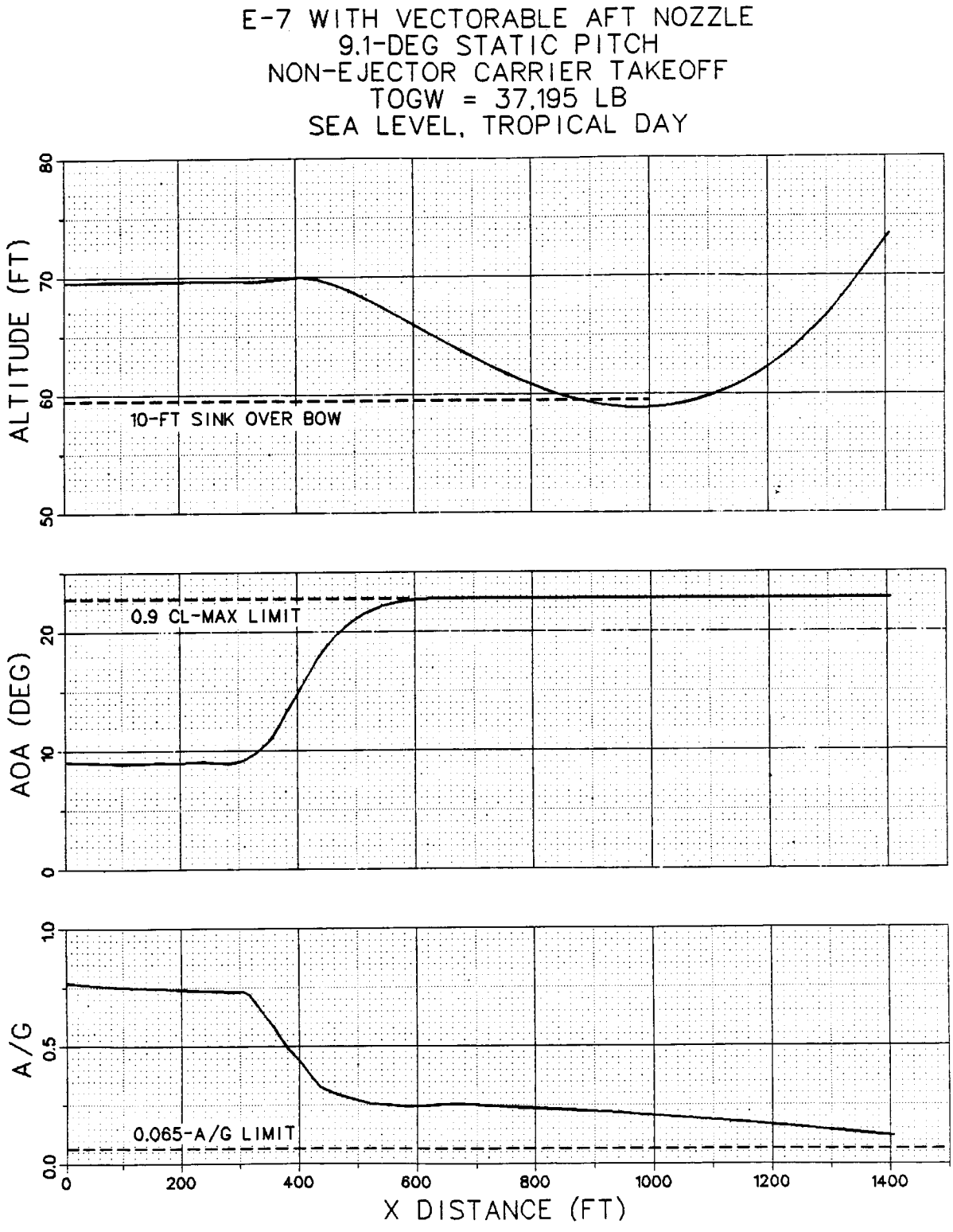

Figure 12-4, Non-Ejector-Takeoff Summary for 9.1-Deg Static Pitch.

13. BOUNDARY-LAYER-CONTROL BLOWING

In improving the takeoff characteristics of an airplane, one must consider the possibility of increasing the lift coefficient, C_L. A large variety of techniques are available to increase the C_L at takeoff. Depending on the specific configuration, it could be necessary to increase the $C_{L_{MAX}}$ or increase the C_L at a fixed angle of attack (AOA). The C_L of the E-7 configuration is constrained by an AOA limit. One method to increase the C_L at a fixed AOA is to install boundary-layer-control (BLC) blowing. On the E-7, one could conceptually install BLC blowing on the upper surface of the elevon. Although detailed design is beyond the scope of this study, lift and moment coefficient increments can be estimated. Under the assumption that the supplied blowing is sufficient to keep the flow over the elevon attached, the lift and moment coefficient increments are plotted in Figure 13-1. A drag increment is not added directly, but an increase in induced drag is accounted for because of an increase in C_L. Besides the effect on the aerodynamics, certain penalties are associated with the installation of BLC blowing. A 200-lb increase in dry weight is assumed to account for the addition of ducts to direct engine-air flow to the elevon. Air flow taken from the engine reduces the thrust from the ejector and from the core and aft nozzles. The detailed assessment of how the bleed affects the engine is not within the program's scope and is assumed to be a five percent reduction in the total engine thrust. The above assumptions are not the result of detailed study but are intended to reasonably anticipate major impacts on the E-7 design. The benefits of BLC blowing were assessed by calculating the field-takeoff capabilities of the E-7 with a loading of (4)MK-83 + (2)AIM-9.

Minimum level-flight speed, V_{MIN}, was calculated for surveys of elevon deflection and ejector setting and is plotted in Figure 13-2. In the case of field-takeoff speed, V_{LO} (A detailed definition of V_{LO} is given in Section 6.), the E-7 is limited by the 0.5%-climb-gradient-potential requirement. This constraint limits V_{MIN} to about 88 KTAS, which is higher than that of the baseline E-7. The penalties of adding the BLC blowing outweigh the increased aerodynamic lift.

To further define this phenomenon, V_{MIN} was calculated for each effect of the BLC blowing and is summarized in Figure 13-3. The first bar in the figure shows V_{LO} of the baseline E-7. V_{MIN} for the baseline is 79.7 KTAS which correspond to a V_{LO} of 87.7 KTAS. When the effect of aerodynamic lift is incorporated, the C_L increases from 1.38 to 1.692. However, V_{LO} decreases only 0.3 KTAS. In this case, the increase in aerodynamic lift is partially negated by a decrease in propulsive lift. The increase in C_L causes the drag coefficient, C_D, to increase from .6894 to 1.1260. Because the takeoff is constrained by the climb-gradient potential, the ejector setting must be reduced to allow

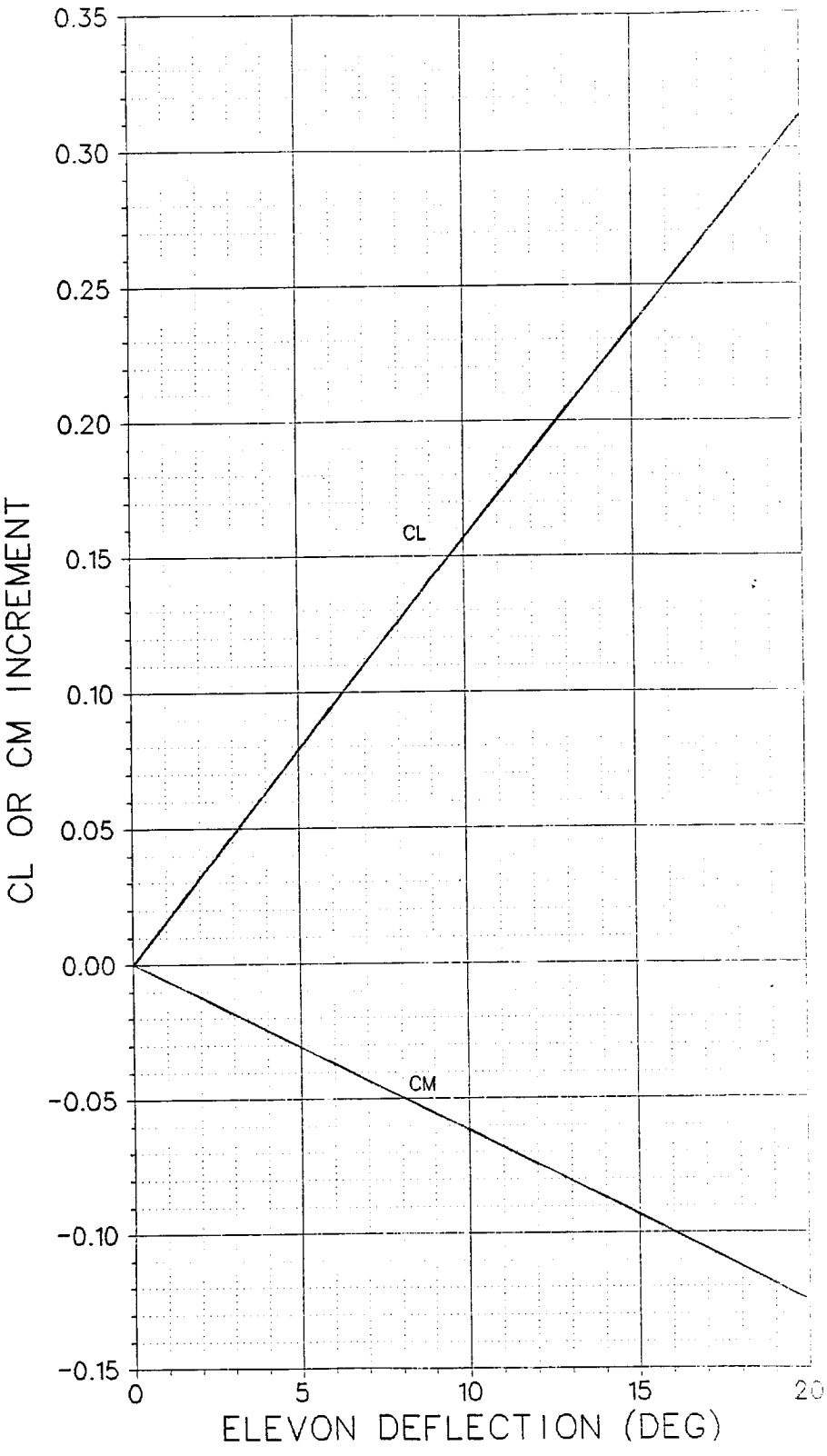

Figure 13-1, Aerodynamic Increments for BLC Blowing.

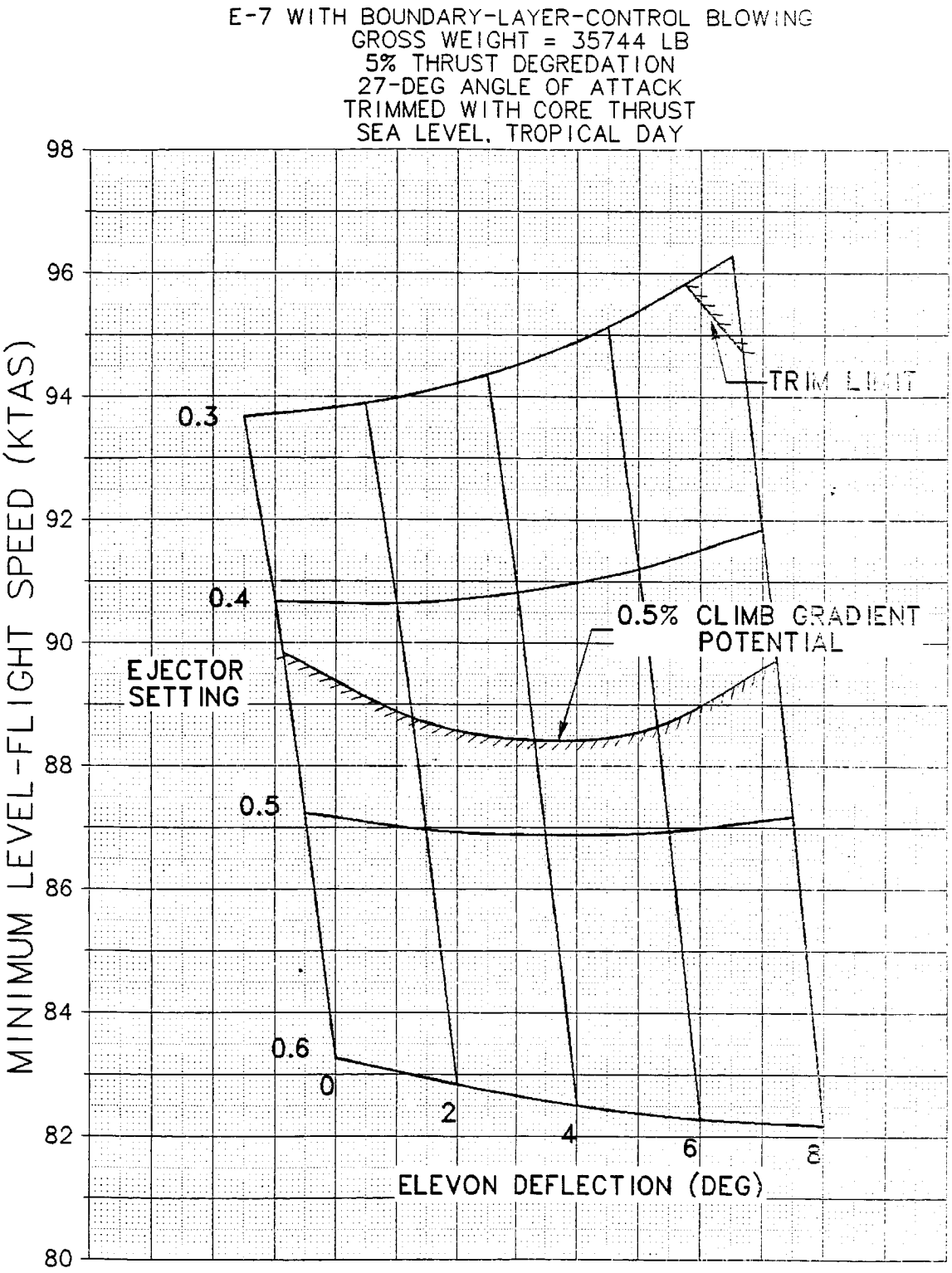

Figure 13-2, V_{MIN} With BLC Blowing.

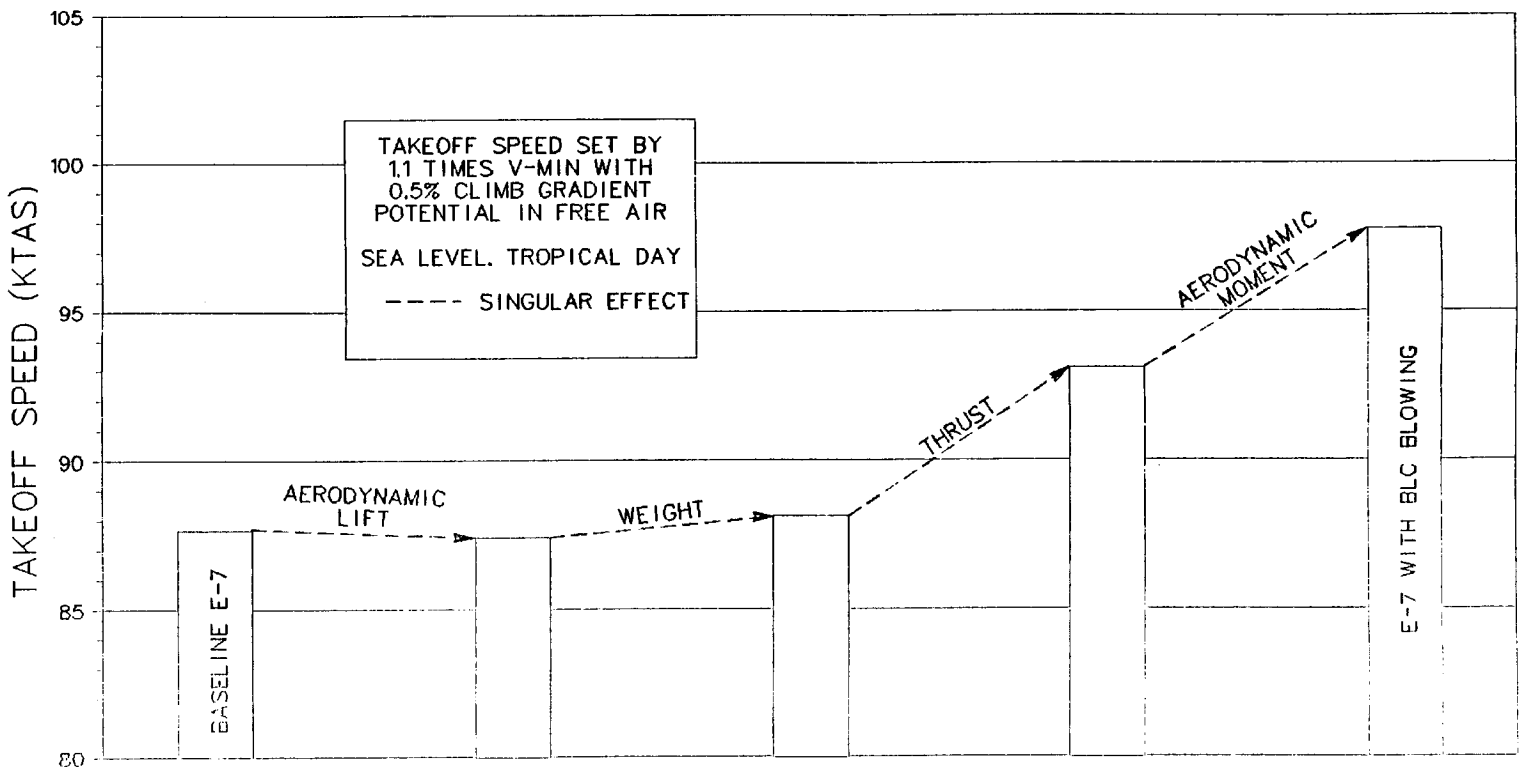

Figure 13-3, Takeoff Speed Increments for Singular Effects of BLC Blowing.

sufficient forward thrust to counter the increased drag. When the effect of increased weight is incorporated in the V_{MIN} analysis, V_{LO} increases to 88.1 KTAS, which is higher than the baseline V_{LO}. But, the 200-lb increase in weight is the least harmful of the degrading effects. Because the BLC blowing would require bleed from the engine, the engine thrust is reduced by five percent. Thrust reduction increases V_{MIN} because the loss in propulsive lift must be replaced by aerodynamic lift. Increasing V_{MIN} then increases V_{LO} to 93.1 KTAS. The largest detrimental factor is the effect of the aerodynamic moment caused by the elevon. When the effectivness of the elevon is increased, the optimum elevon deflection shifts. The optimum deflection for the baseline is the maximum allowable, 20 deg. One can see in Figure 13-2 that the optimum elevon deflection is about four degrees. Reducing the elevon deflection also reduces the C_L of the wing. In doing so, more propulsive lift must be provided by the ejectors and V_{MIN} increases. The resulting V_{LO} is 97.8 KTAS, 10 knots greater than the baseline V_{LO}.

The overriding disadvantage of installing the BLC blowing is the difficulty in trimming the large increase in nose-down pitching moment. Overall, the configuration is not sensitive to increases in C_L. This trend is visible in the angle-of-attack optimization that is shown in Figure 3-2. The small slope of the constraint line indicates that the configuration can trade off between propulsive lift and aerodynamic lift. As gross weight increases, aerodynamic lift becomes more efficient than propulsive lift. Even when no additional moment is associated with an increase in C_L, the benefit to V_{LO} is slight.

14. SUMMARY

The primary goal of this study was to identify ways to improve the STO weight capability of the E-7 configuration as an indicator of those methods that could be applied to STOVL aircraft in general.

The first method studied was the addition of vectoring capability to the aft nozzle. Results show very little improvement over the baseline configuration because use of the ejector decreases the aft thrust. This result, though, is only true over a narrow range of gross weights. Surveys of minimum level-flight speed, V_{MIN}, show improvement in performance at weights either greater or less than the baseline STO weight. The aft vector is probably more effective on other STOVL configurations or on the E-7 operating in other situations, e.g., from longer decks or with heavier loadings from land-based operations. The vectoring aft nozzle gains other advantages such as increased combat versatility and better short-landing performance. Besides the increased complexity and cost, one must not underestimate the effect of increasing the dry weight by 200 lb. The weight increase is compensated by improved takeoff performance and would have little effect on high-speed performance, but any dry-weight increase affects hover performance. When 200 lb is added to the dry weight, the hover fuel available is reduced by about 10%. Overall, the benefits of the aft vector do not offset the degradation in the hover performance of the E-7 configuration. However, vectoring capability is probably an asset on most STOVL configurations.

Increasing the static pitch of the airplane was investigated to reduce the time required to rotate. The increase in pitch was achieved by lenthening the nose gear strut. This modification has a slight positive effect by increasing the STO weight by 700 lb. The gear extension would weigh about 50 lb and may decrease the fuel volume just slightly. Overall, the modification gains a slight benefit at little cost.

As a third method to improve the STO weight, the addition of a close-coupled canard to the airplane was investigated. For all practical purposes, this addition is not possible on the E-7 because of problems with structural attachment and pilot visibility. That does not mean, however, that it cannot be successfully employed on other STOVL configurations. This method was investigated by theoretically attaching a canard to the E-7. The canard increases the STO weight by 1800 lb, much of which may be simply due to a 10% increase in lifting surface. The assumed canard weighs about 700 lb. For the specific E-7 configuration, 700 lb of ballast would be required to maintain balance in hover. This much increase in dry weight would nearly eliminate the fuel available for hover. The canard has little effect on the combat performance. Sustained turn load factor increases slightly due to the higher L/D of the close-coupled canard. The acceleration

time increases slightly because of degraded wave drag characteristics, which may be corrected by minor redesign. This study indicates that the improved takeoff perormance is marginally worth the increase in dry weight caused by the canard. However, the benefit of a canard is much more dependent upon integration into a specific configuration. Though it does not apply well to the E-7 as currently designed, many STOVL designs could benefit from a wing/canard arrangement if the canard can be properly integrated.

The intent of the task detailed in Section 6 was to identify areas of propulsive lift that have high leverage on STO weight. Every combination of three propulsive components was investigated: ejector, core-thrust vector, and aft-thrust vector. The takeoff ground-roll distance for the escort mission loading was used as a figure of merit. The ability to reduce the nose-gear-unstick speed is a key factor in the capability of the single-components cases. The ejector is useful in achieving rotation but is inferior to the vectorable aft nozzle because of the inability to afterburn the fan flow when using the ejector. Clearly, substantial performance improvements could be gained at higher gross weights if the aft thrust could be afterburned at partial ejector thrust. The best combination of two components arises with the high synergism between the ejector and the core nozzle. This result indicates high leverage in the thrusts and locations of these two components; however, the hover requirement imposes a severe constraint on both of these parameters.

Previous analysis of the E-7 takeoff and transition for the escort loading showed successful transition within about 20 sec from brake release to wing-borne flight. This study optimized the transition time by maximizing specific excess power to reach wing-borne flight as soon as possible. The results proved to be impressive. At STO weight, the weight at which the airplane can barely attain thrust-borne flight, the transition to wing-borne flight was complete at 16 sec after brake release. At the escort mission weight, the weight assumed in previous analysis, wing-borne flight was achieved in nine seconds. Transition of STOVL aircraft appears to be no problem provided that (1) positive acceleration can be maintained at all times, (2) the thrust at takeoff is not significantly greater than the thrust required for wing-borne flight.

Transition to hover of the E-7 configuration had not been investigated until this study. Previously, it was assumed that the ejector would always have enough thrust to keep the airplane in level flight. The intent of this study was to assess the fuel that would be required for the transition phase. The optimum sequence is similar to the current AV-8A operational sequence. The entire transition is performed at essensially constant altitude. Basically, the ejector is activated to full thrust and the engine power setting maintains level flight. The E-7 can perform the transition in less than 15 seconds and uses about 50 lb of fuel. In doing so the pilot would experience rather

high decelerations that may be undesirable. It would be possible to transition the airplane over a longer period of time in order to decelerate slower. The fuel consumed would increase but would still be at an acceptable level.

The ejector augmentation ratio, ϕ, is a very important design parameter because it directly impacts the hover capability of the E-7. However, ϕ has little impact on takeoff performance. Since, in takeoff, the ejectors are operating at partial capacity anyway, the loss in augmentation can be countered by an increase in ejector setting. For a five percent increase in ϕ, the STO weight increases by about 400 lb.

Some operational considerations tend to penalize the use of afterburning thrust (A/B) on takeoff. In previous analyses, the takeoff performance of the E-7 has taken advantage of A/B. The takeoff performance of the E-7 is substantialy degraded when no afterburner is used. For a typical air-to-ground loading, the takeoff ground-roll distance doubles when no A/B is used. The difference is caused primarily by an increase in takeoff speed because the core A/B contributes to propulsive lift. Ground-roll acceleration is also decreased when the aft and core A/B are not used. Though the performance is greatly degraded relative to the maximum performance takeoff, the operational performance is still very good: the E-7 can takeoff with (4)MK-83 + (2)AIM-9 in less than 1500 ft. This performance is sufficient to meet most operational requirements.

One of the results of the study detailed in Section 6 showed that when the E-7 is equipped with a vectorable aft nozzle it can achieve, without activating the ejectors, takeoff performance similar to that of the baseline. To futher investigate this method, the STO weight was calculated for a non-ejector carrier takeoff. The resulting STO weight is 2700 lb greater than the baseline STO weight. Once again, this study indicates that the afterburning thrust of the aft nozzle is a very important consideration in takeoff performance. When the non-ejector takeoff was combined with the technique of increasing the static pitch, the STO weight did not significantly increase. Because of the effectiveness of the vectorable nozzle in controlling pitch, reducing the overall rotation has less benefit.

Increasing the lift coefficient of the baseline has little leverage on the E-7 takeoff performance in general. Specifically, increasing the lift by using boundary-layer-control blowing on the elevon actually degrades the performance. The primary difficulty occurs in the moment that is generated by the increased lift on the elevon. The moment is so large that the elevon deflection must be reduced so that the ejector can trim it. Decreasing the elevon deflection decreases the lift of the overall wing; therefore, the modification increases the minimum level-flight speed. Even if the aerodynamic lift were increased without affecting the aerodynamic moment, the benefit would be marginal. Increasing the aerodynamic lift also increases the

aerodynamic drag and thereby decreases the horizontal acceleration. To maintain the required acceleration, the ejector thrust must be reduced and the core vectored farther aft, which reduces the propulsive lift. This trend is similar to that encountered in optimizing the takeoff angle of attack.

15. RECOMMENDATIONS

The configuration variations investigated in this study show promise in improving STOVL configurations in general, but some are not specifically suited to the E-7.

Extending the nose gear appears to yield advantages in improving STO weight and would be simple to implement on the E-7. This idea could be improved further by installing a jump strut, a nose gear assembly that has a spring-loaded strut that can initiate rotation of the airplane by applying direct upward force to the nose. The advantage of the increased static pitch is that it reduces the required rotation, whereas the jump strut decreases the rotation time by greatly increasing the pitch acceleration at the beginning of rotation. (Much of the rotation time of the baseline configuration occurs before reaching a 5-deg pitch.) Further investigation is warranted in preliminary consideration of the jump strut and in further study of the full design implications of incorporating the extended nose-gear strut.

A vectorable aft nozzle was advantageous on the E-7 predecessors, though benefits identified early in this study did not warrant the additional dry weight. However, the study of non-ejector takeoff, which is only possible through the use of the vectorable aft nozzle, identified the means for significantly increasing the takeoff performance of the E-7 as well as improving the simplicity of the takeoff sequence. If the E-7 is redesigned, installation of an aft vectorable nozzle should be considered.

It is not recommended that a canard be installed on the E-7. Since the canard did show some promise, though, one should consider preliminary design of an ejector configuration using a canard/delta. This concept would probably be very challenging to effectively integrate.

Current analysis indicates that the E-7 has extensive capability in transition to wing-borne flight and transition to hover. To further define this flight regime, it would be necessary to design the flight-control system in detail. When this task is complete, analysis of hover and transition would best be handled by man-in-loop digital simulation.

The field takeoff capability of the E-7 without afterburning thrust is adequate for most operational situations. It may be plausible to use intermediate rated thrust on takeoff as the standard operating procedure and only use the afterburner for carrier takeoffs and emergency situations. Because the core afterburner strongly affects the minimum level-flight speed, it is recommended to model the result of critical failure of the afterburner during carrier takeoff.

Overall, the low-speed analysis of the current E-7 design is quite complete. The recommendations above should be considered during any redesign of the basic concept or similar concept. As the E-7 design is further defined, more low-speed analysis will be required.

APPENDIX A

Baseline Data Libraries

The ground-effect parameter sigma, which is used to interpolate the aerodynamics data, is defined and plotted in Figure A-1.

Untrimmed aerodynamic data are plotted in Figures A-2 through A-7. Data are presented as functions of elevon deflection for free air and in ground effect. Drag coefficient data do not include increments for landing gear and ejector doors, which are 0.0198 and 0.0149, respectively. C_{m_q} is -0.101 and $C_{m_{\dot{\alpha}}}$ is -0.851. Minimum drag and aerodynamic limits are shown in Figures 2-1 and 2-2, respectively.

The propulsion data plotted in Figures A-8 through A-12 are presented on a per-engine basis. Data used for takeoff and mission analysis have a 1.09 engine-scale factor applied. The reaction control system applies a net thrust of 600 lb to the center of gravity.

Mass properties are presented in Figures A-13 and A-14.

The reaction force of each gear is modeled as

$R = K + \xi \dot{z}\ \mathrm{abs}(\dot{z})$ where

R = gear reaction force,

K = static force as a function of gear deflection,

ξ = damping coefficient as a function of gear deflection, and

$\dot{z}$ = gear deflection rate.

The parameters K and ξ for each gear are plotted in Figure A-15. Main-gear parameters are plotted for just one gear.

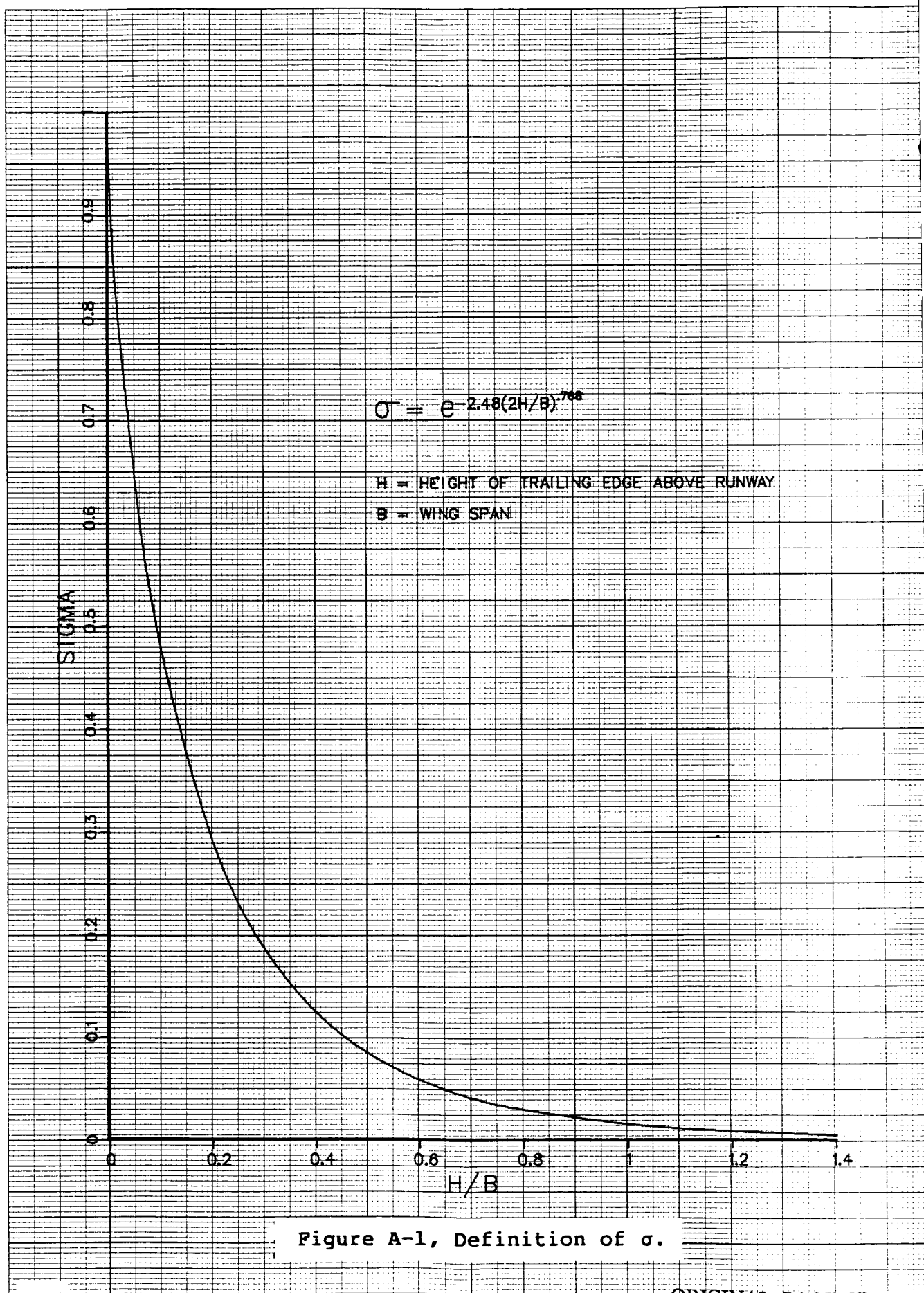

Figure A-1, Definition of σ.

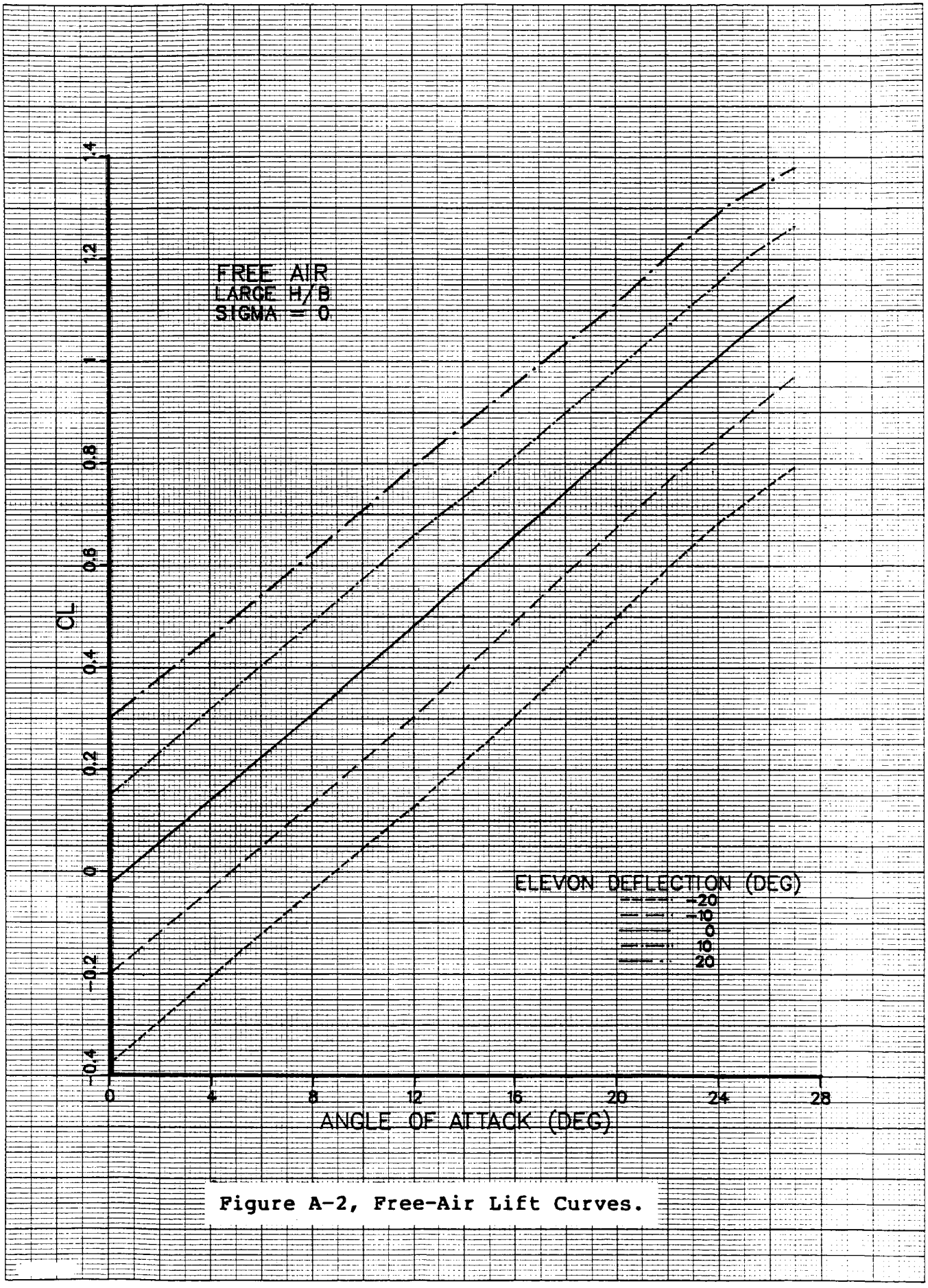

Figure A-2, Free-Air Lift Curves.

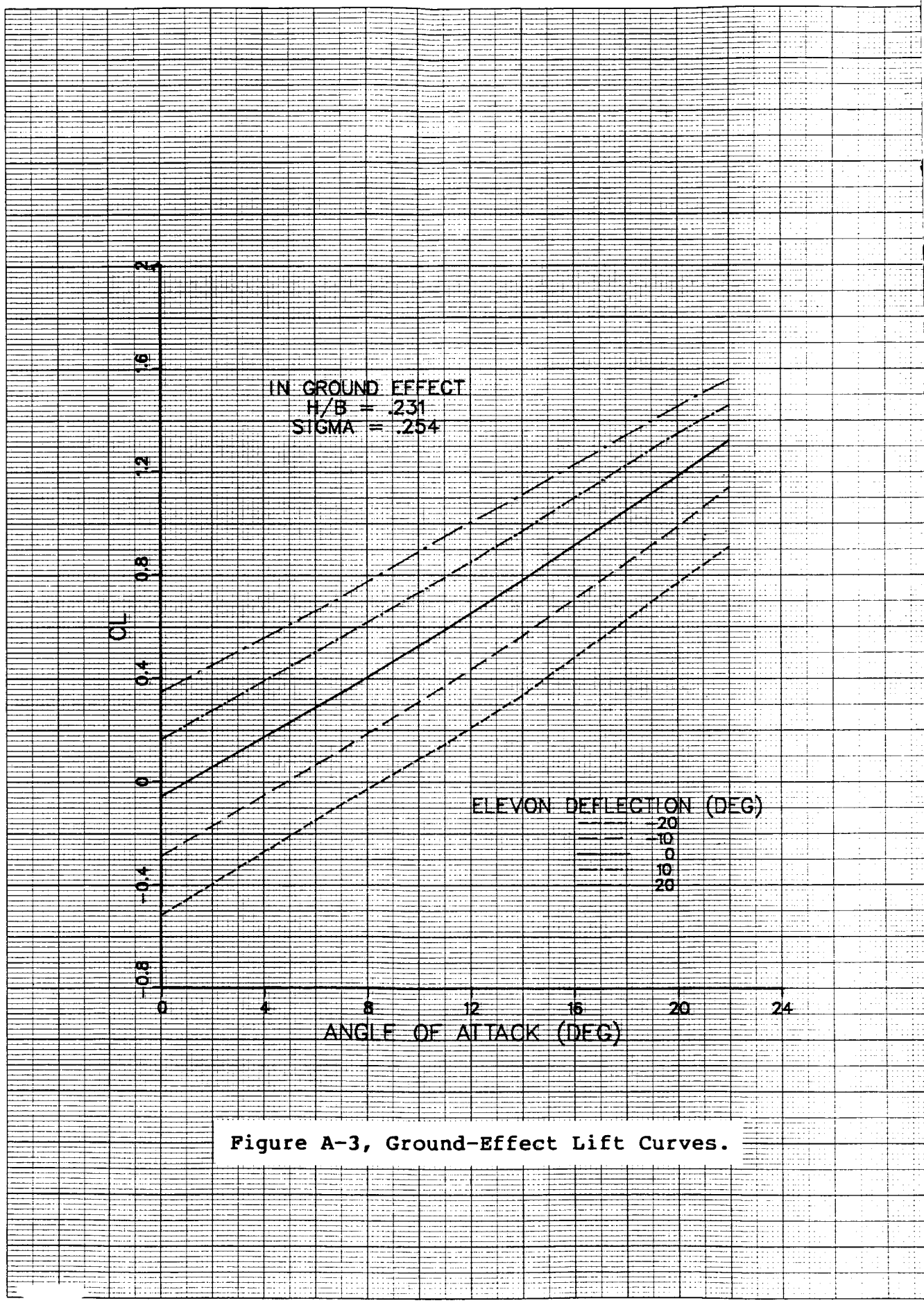

Figure A-3, Ground-Effect Lift Curves.

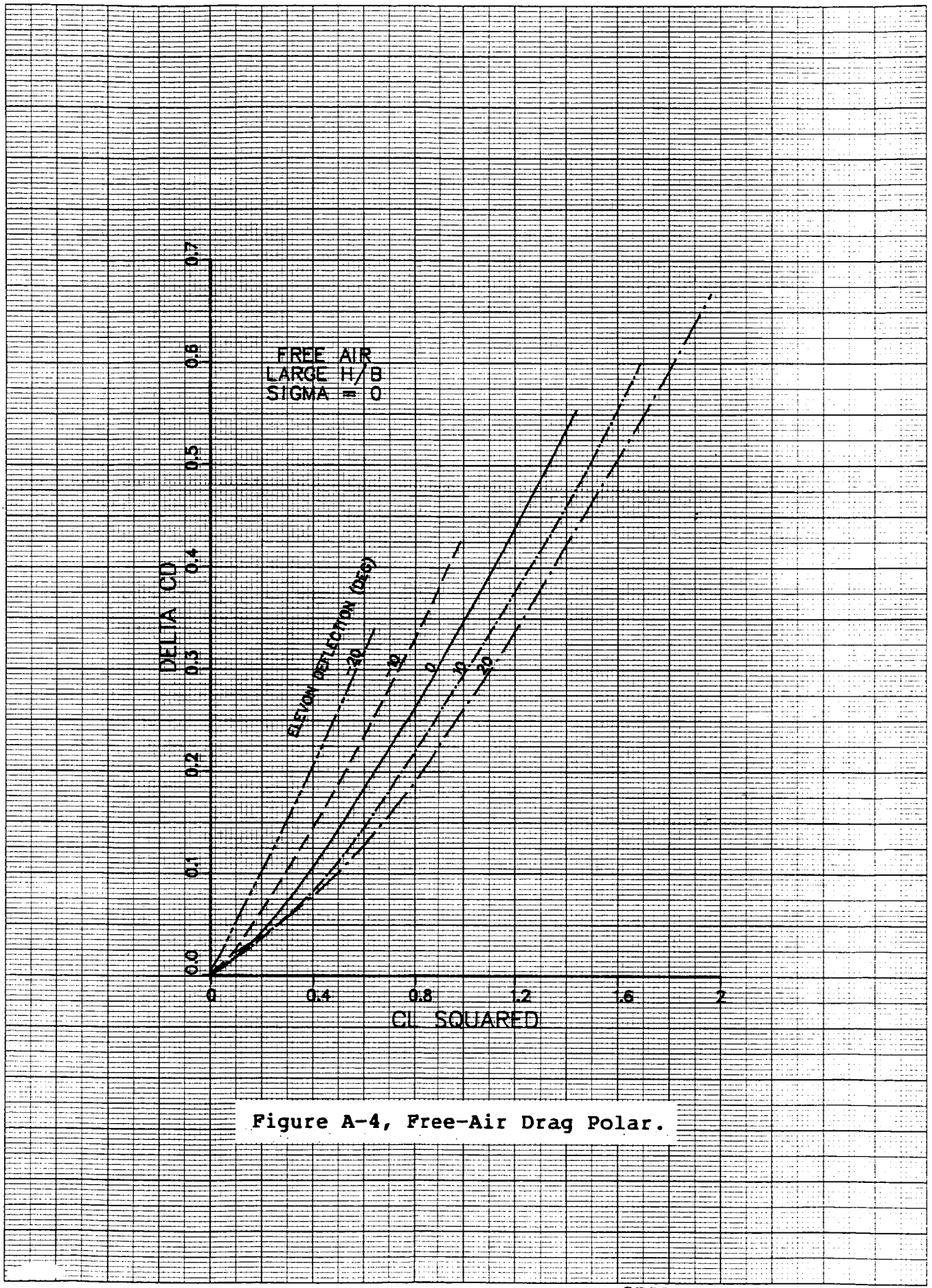

Figure A-4, Free-Air Drag Polar.

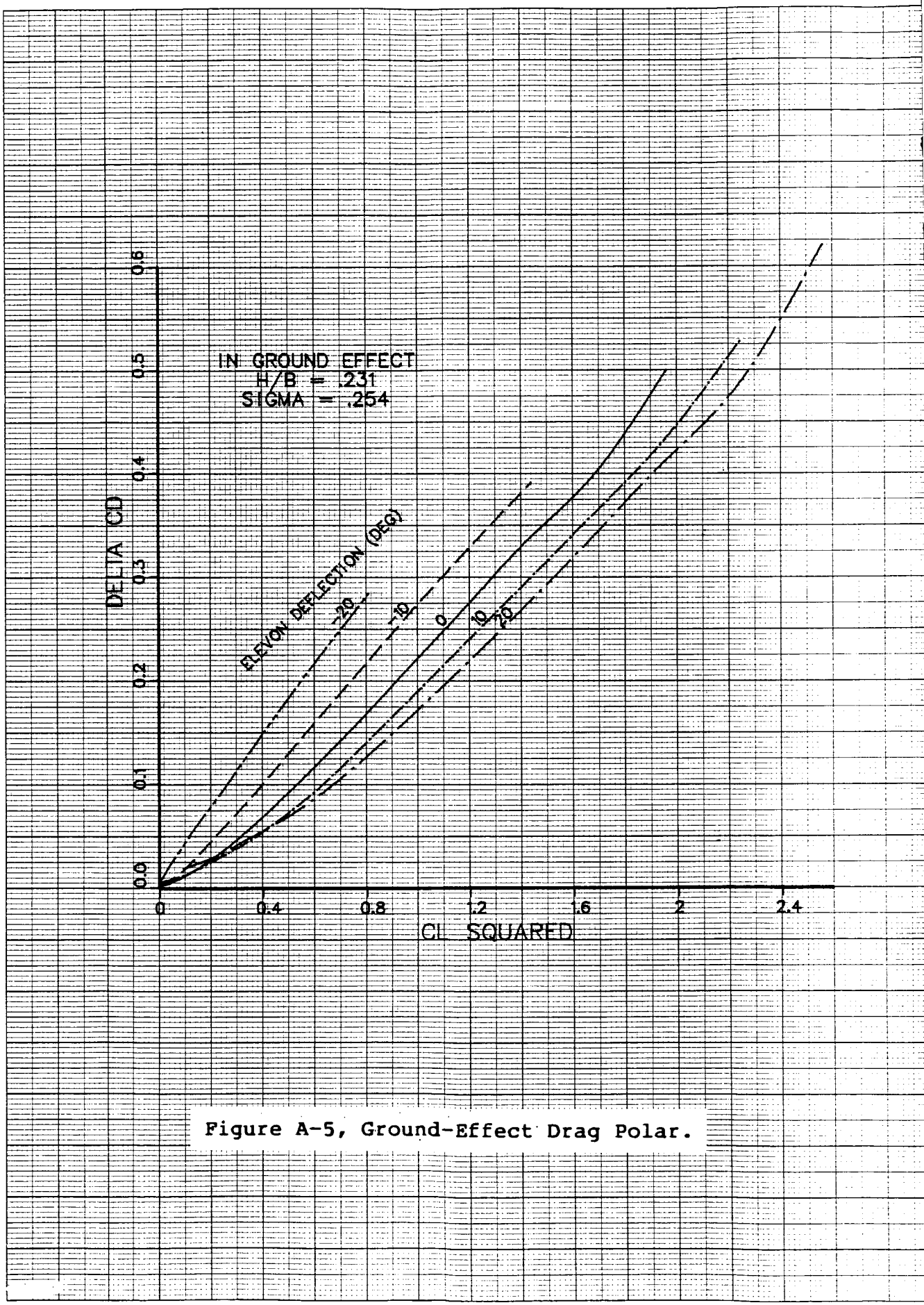

Figure A-5, Ground-Effect Drag Polar.

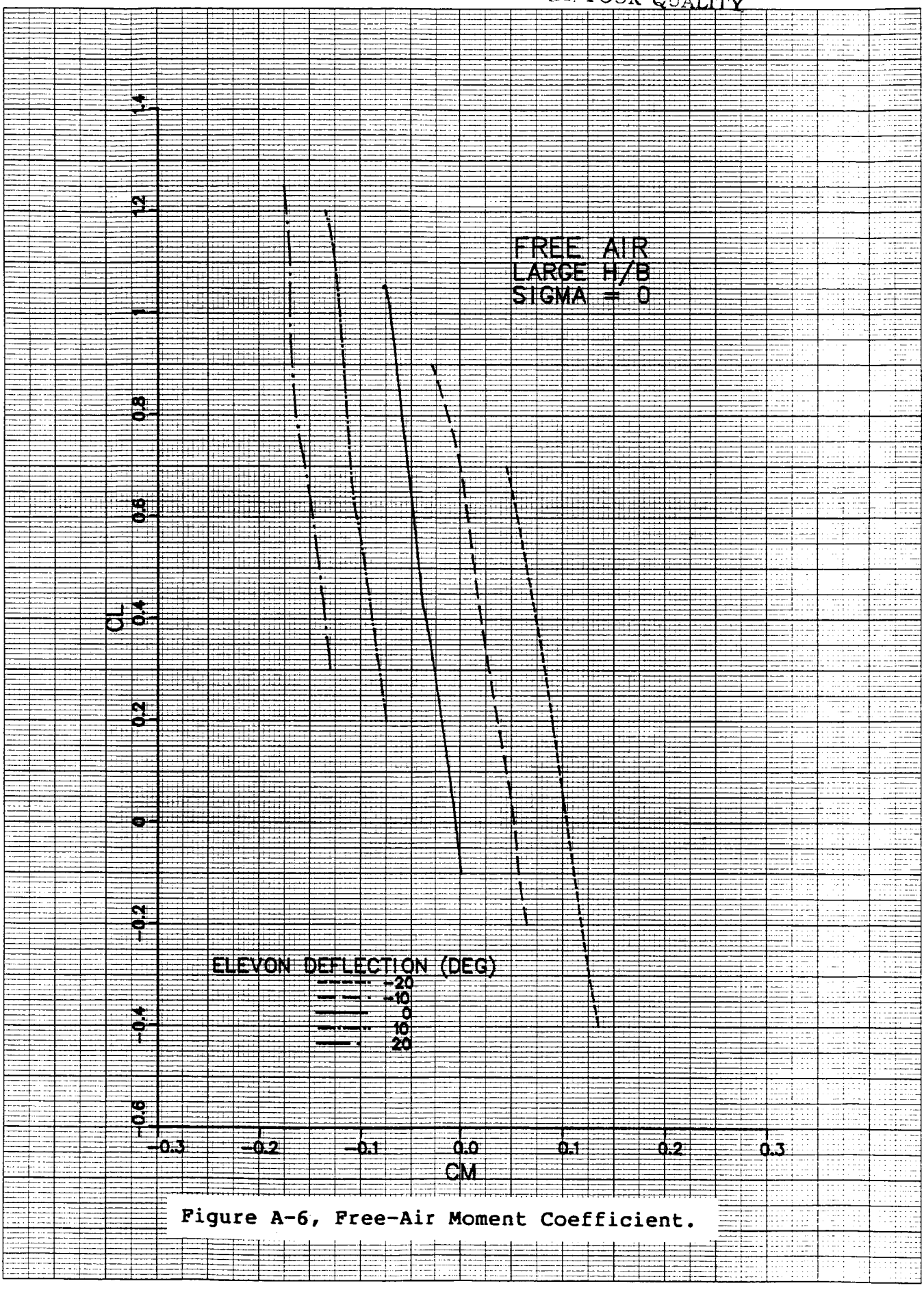

Figure A-6, Free-Air Moment Coefficient.

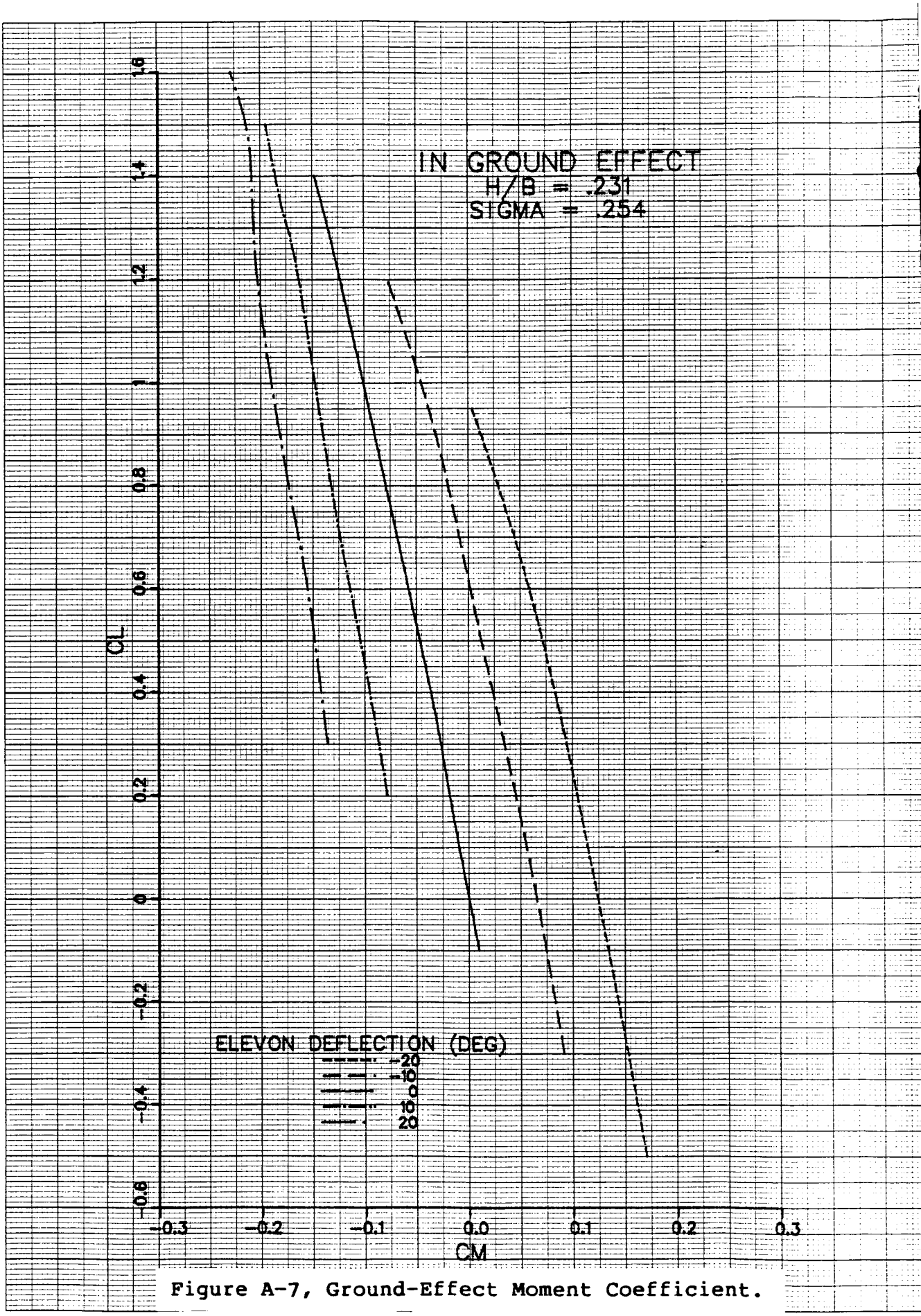

Figure A-7, Ground-Effect Moment Coefficient.

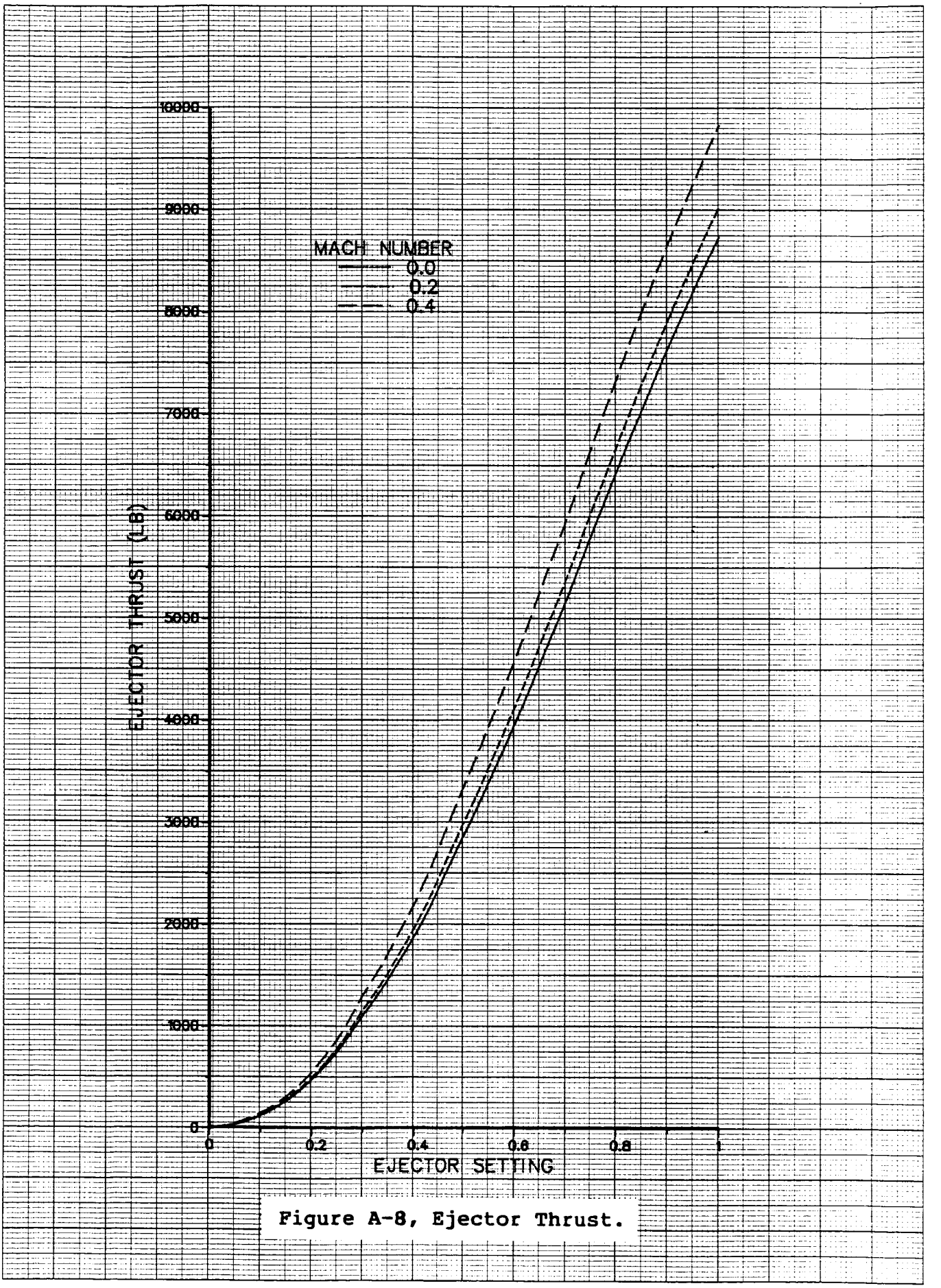

Figure A-8, Ejector Thrust.

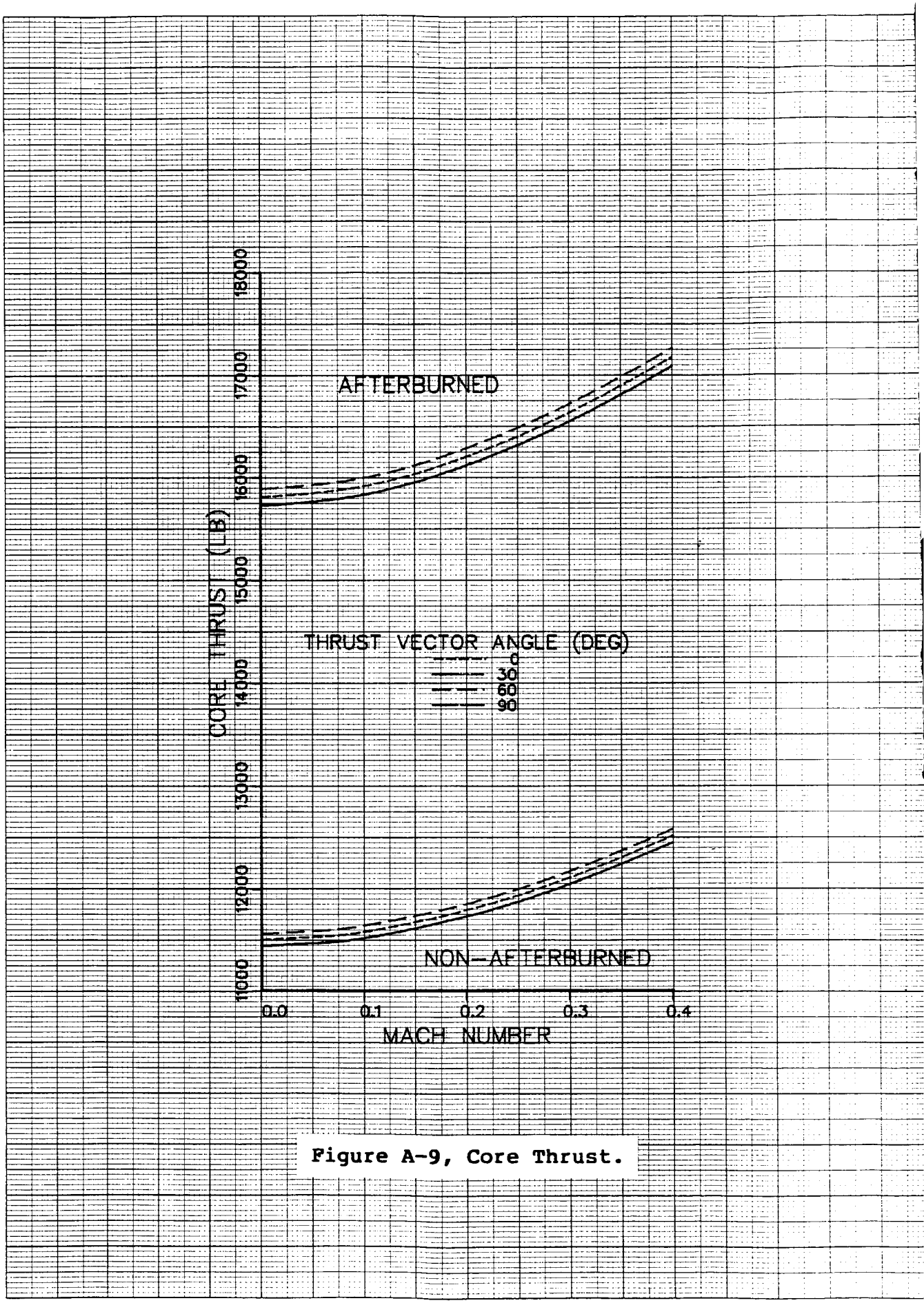

Figure A-9, Core Thrust.

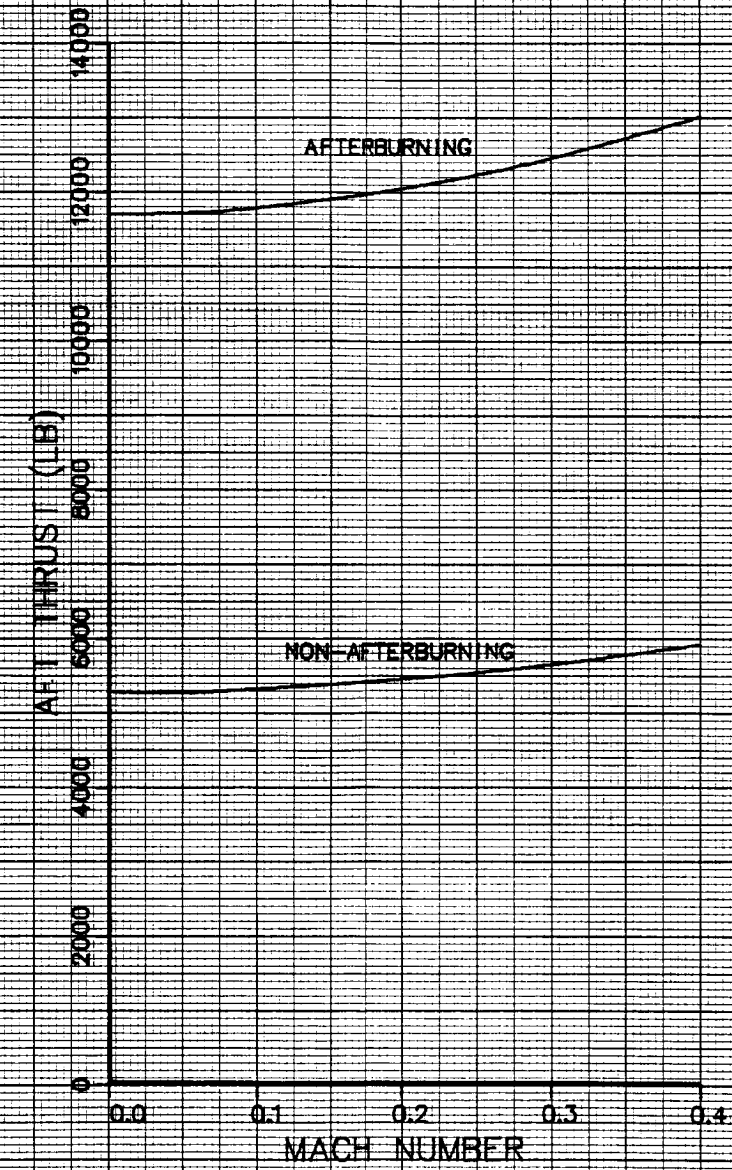

Figure A-10, Aft Thrust.

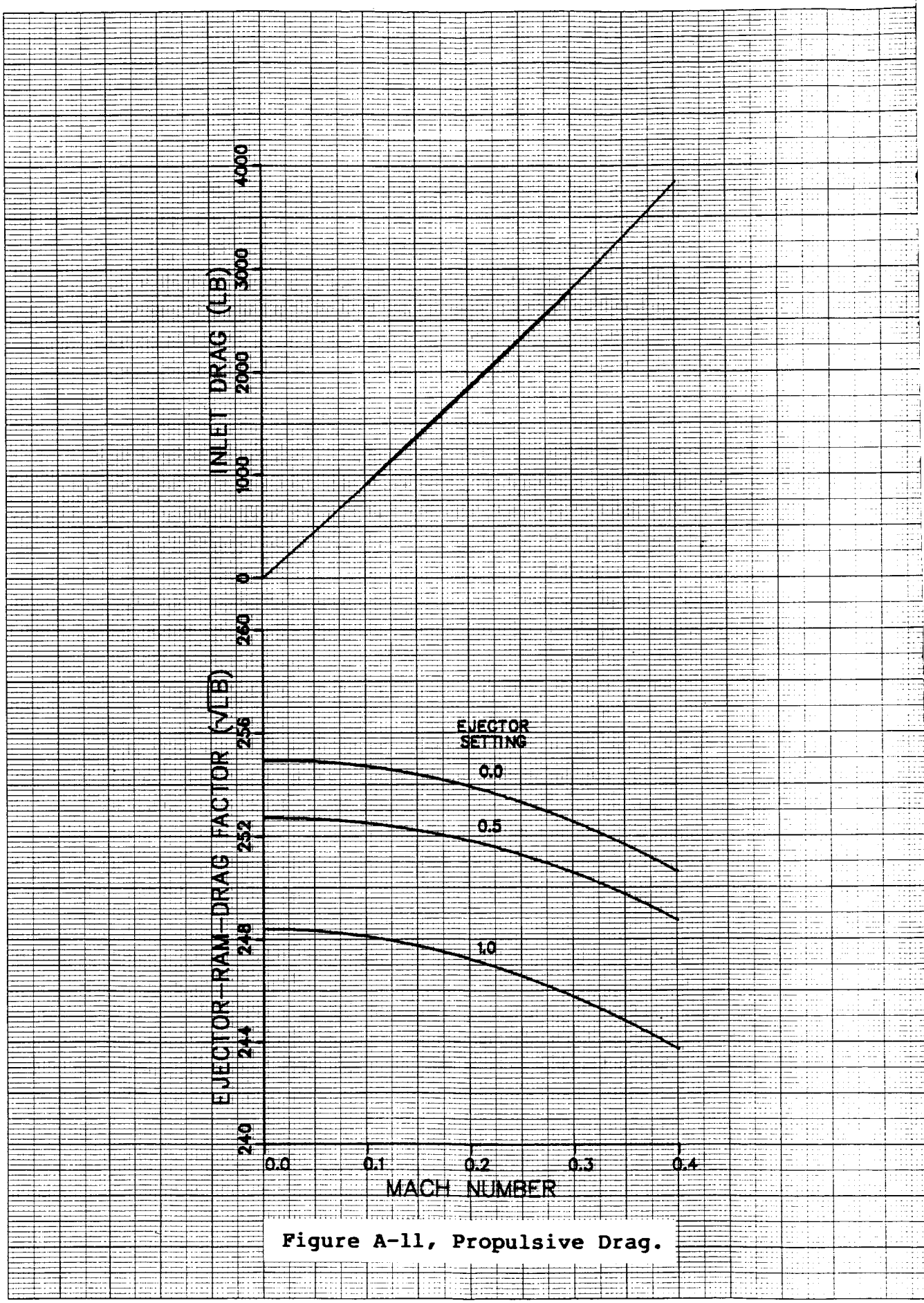

Figure A-11, Propulsive Drag.

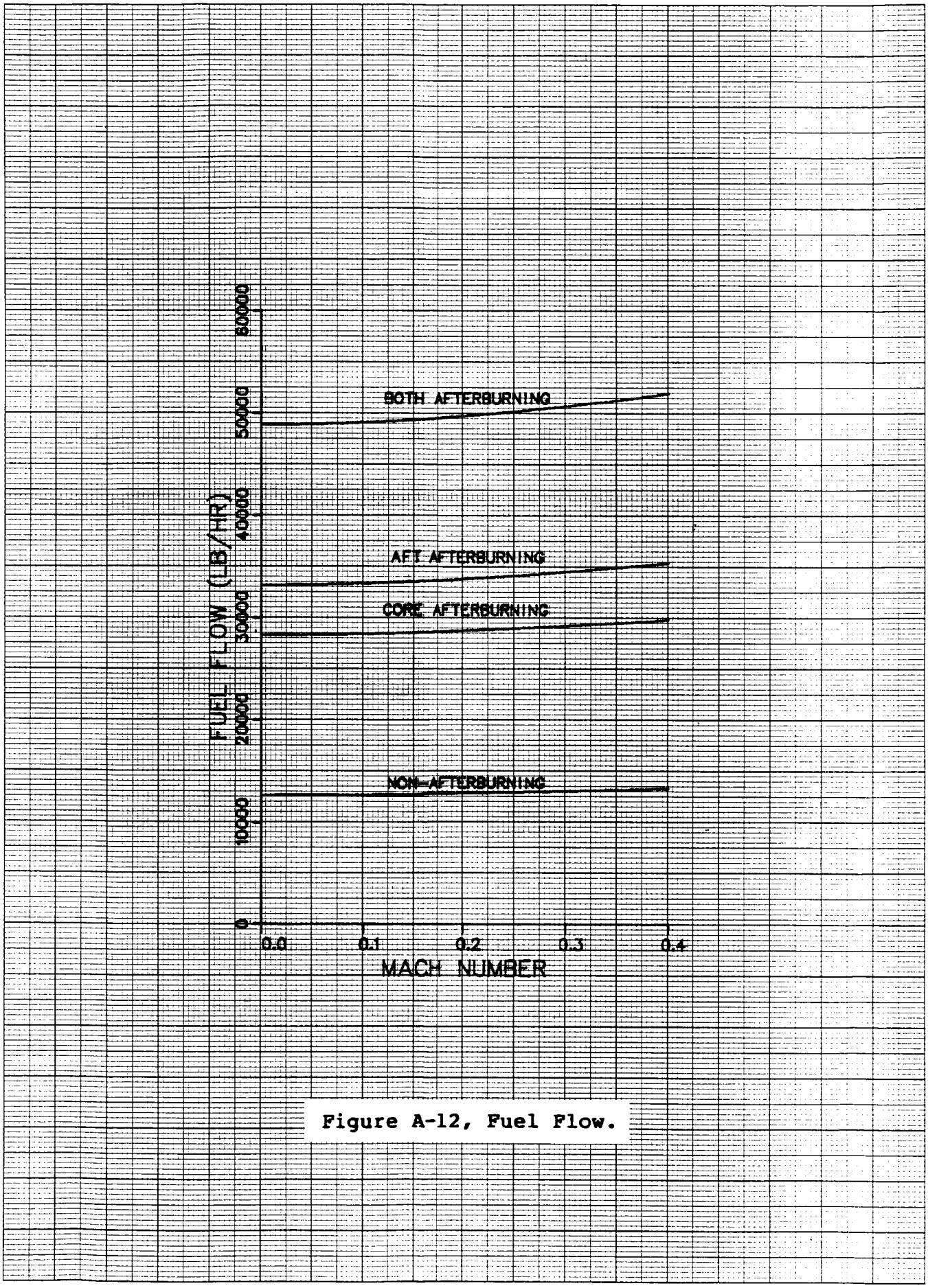

Figure A-12, Fuel Flow.

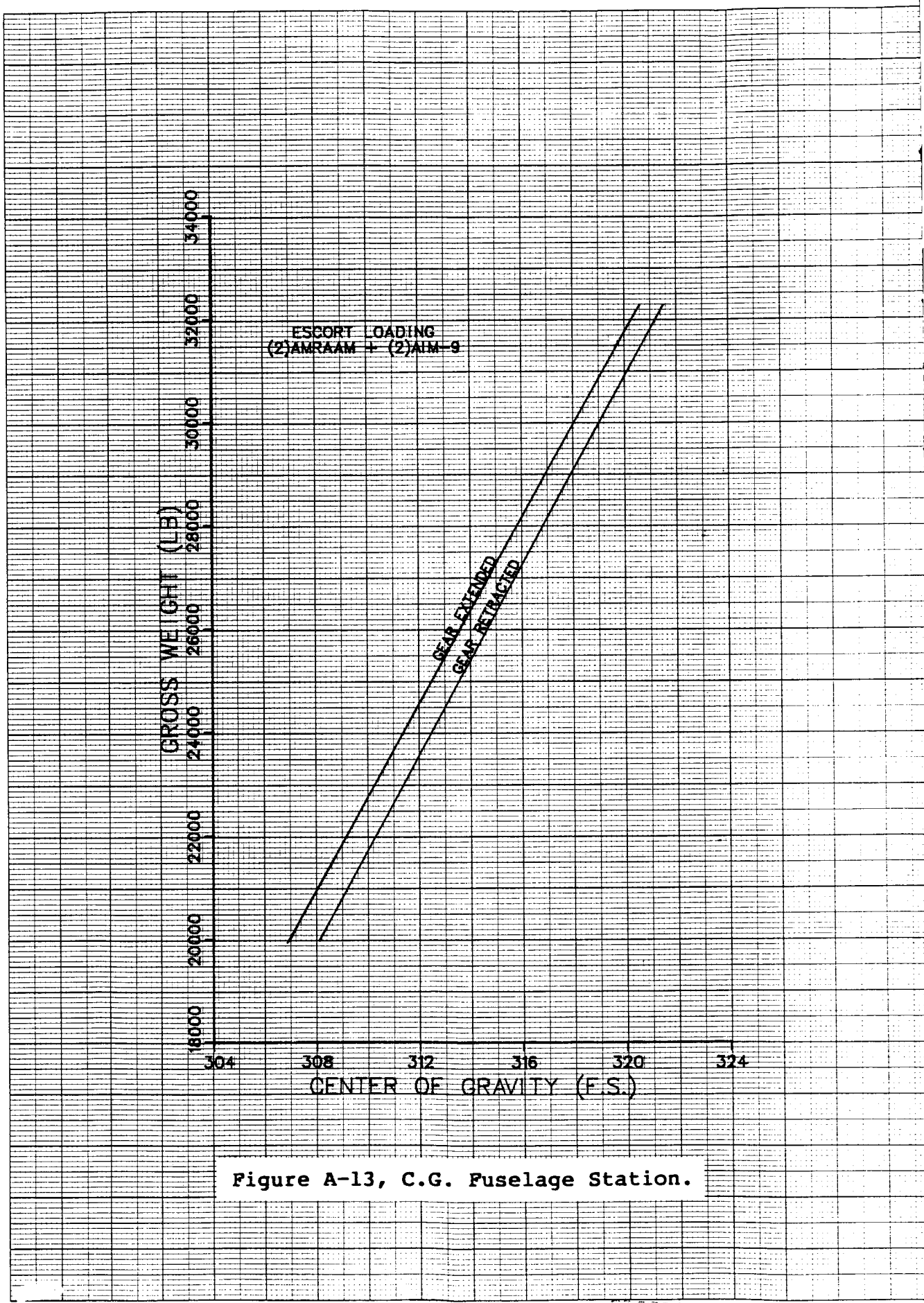

Figure A-13, C.G. Fuselage Station.

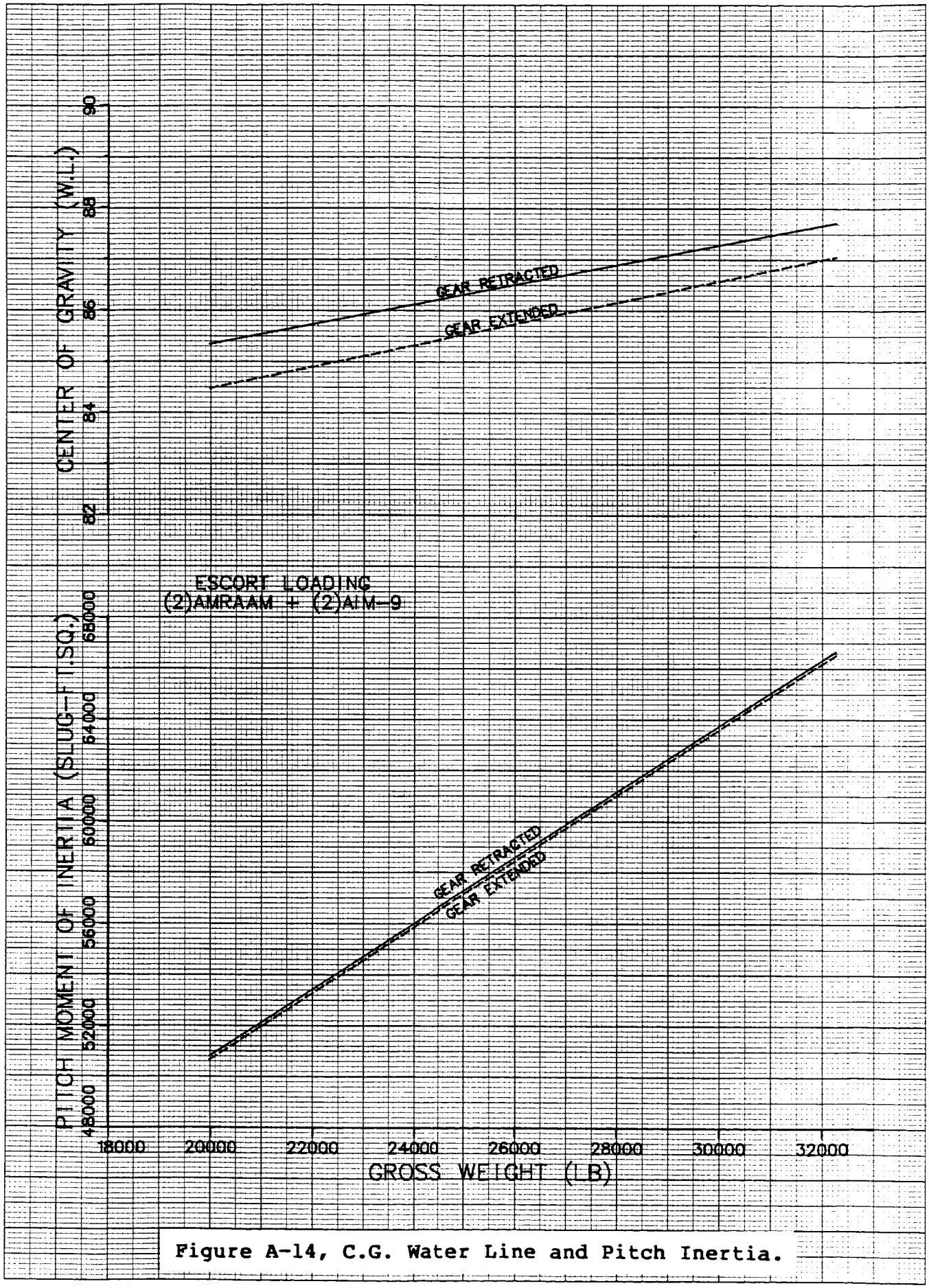

Figure A-14, C.G. Water Line and Pitch Inertia.

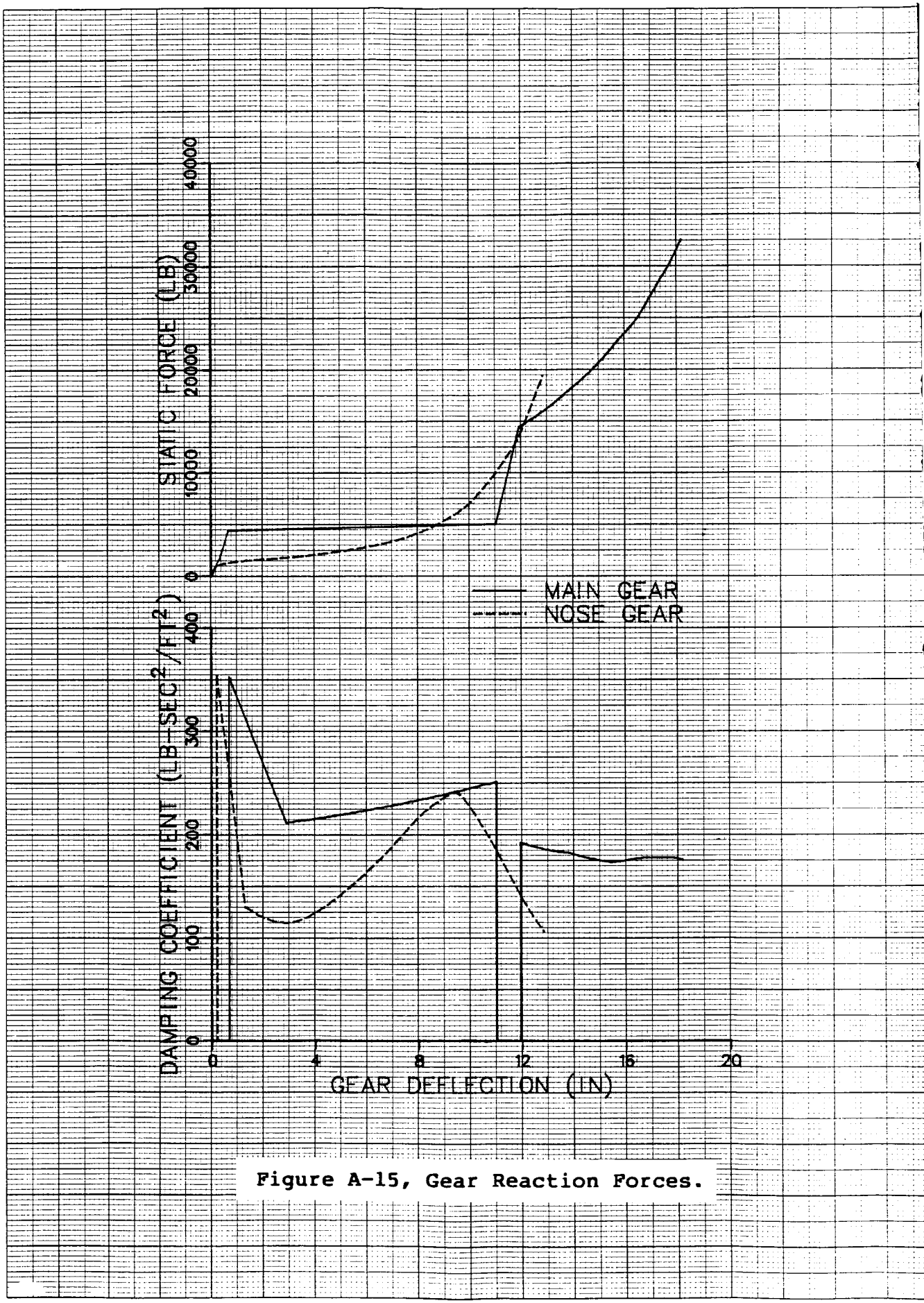

Figure A-15, Gear Reaction Forces.

APPENDIX B

Aft-Thrust-Vectoring Takeoff Histories

Figure B-1 shows time-history plots of pertinent parameters for the takeoff of the aft-vectoring configuration operating at STO weight.

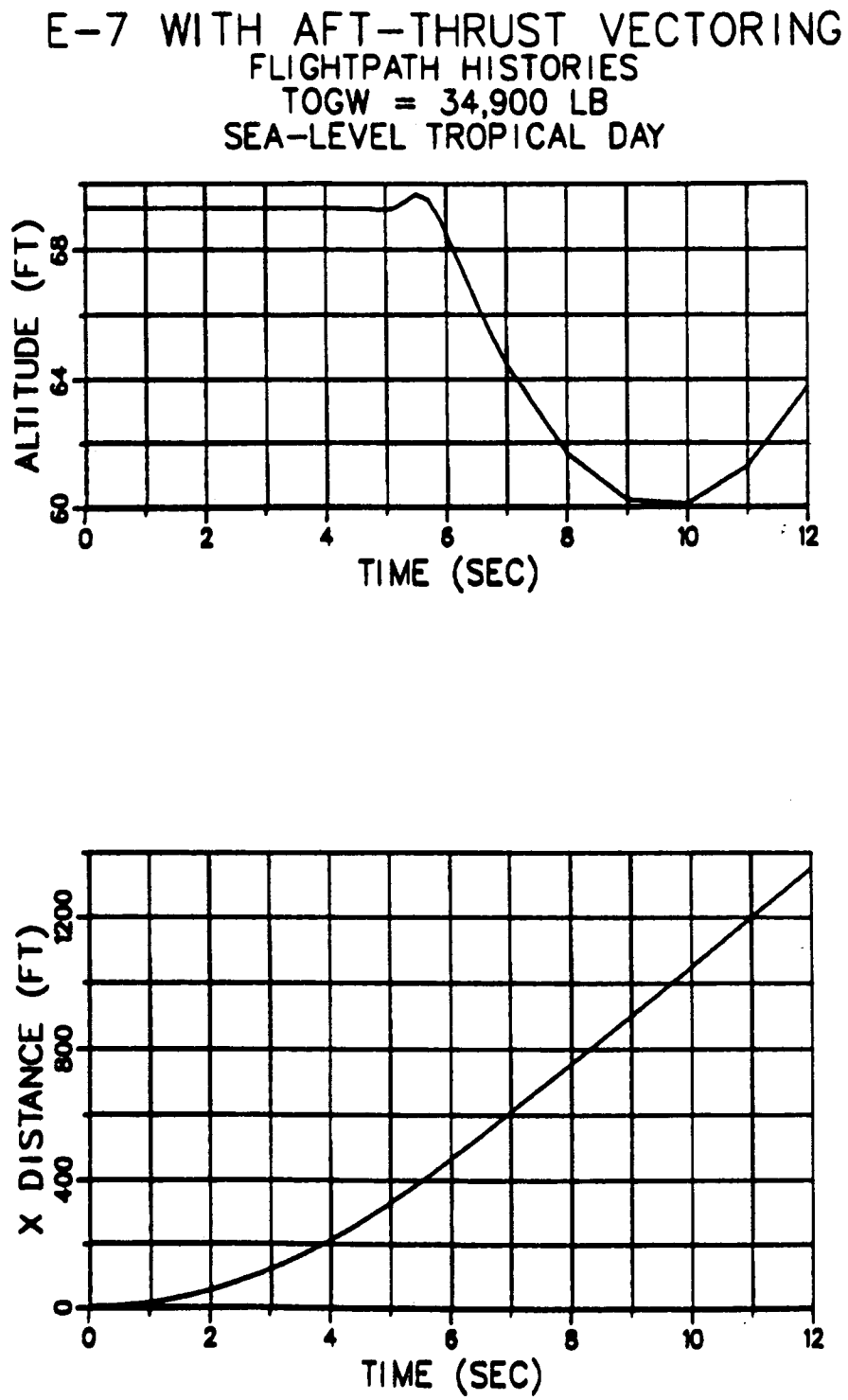

Figure B-1 Aft-Vectoring Configuration Time Histories

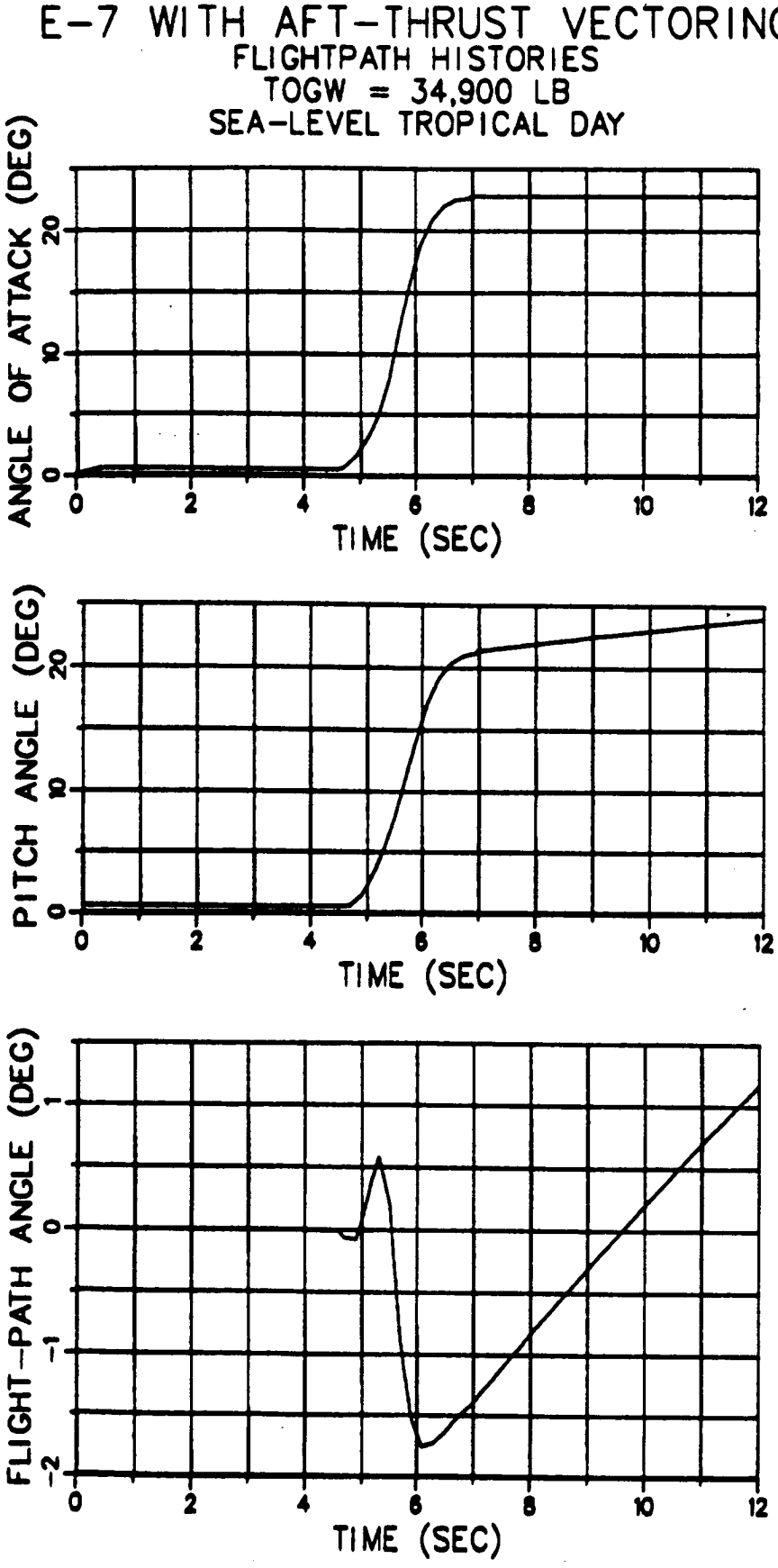

Figure B-1 Aft-Vectoring Configuration Time Histories (Continued)

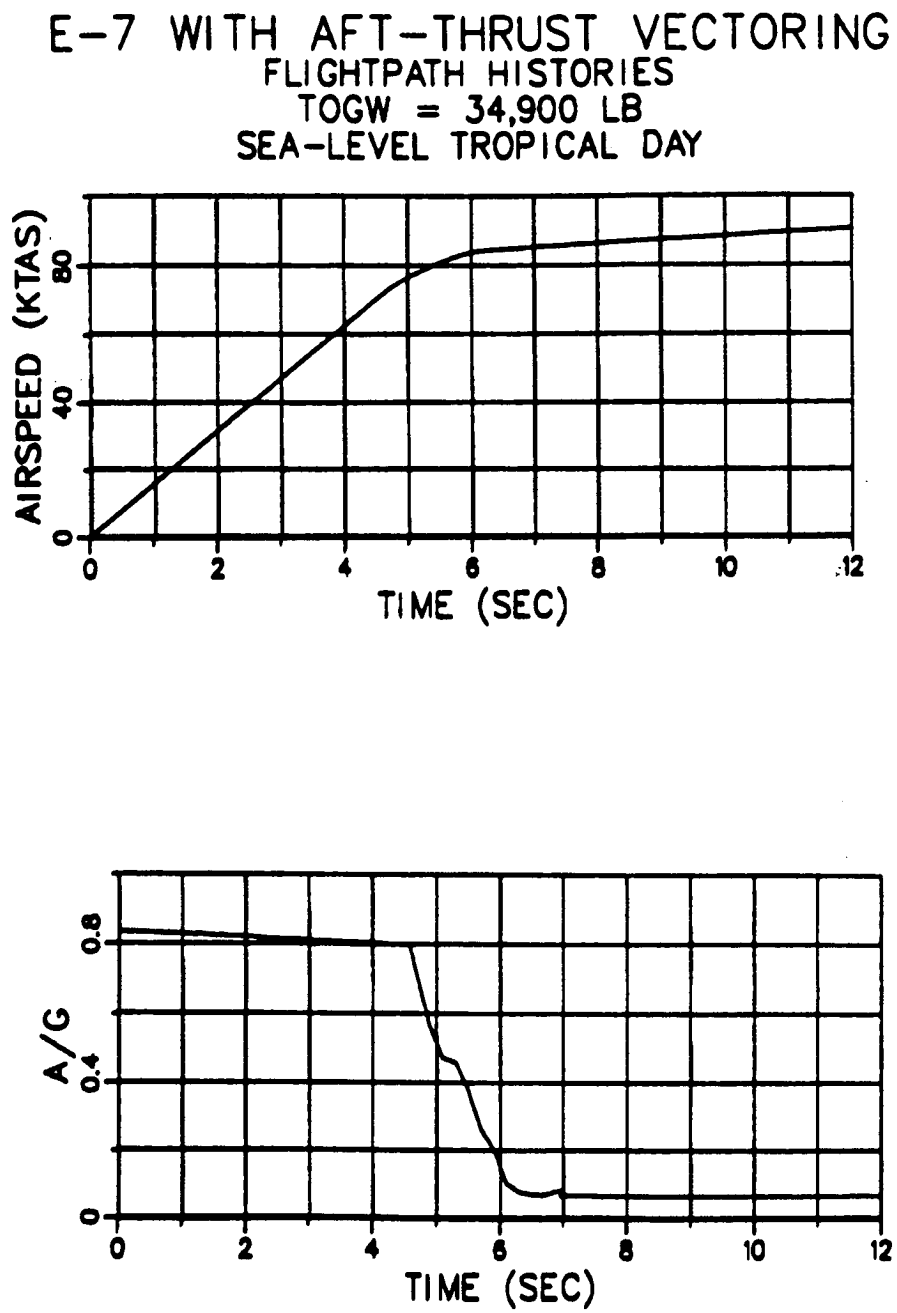

Figure B-1 Aft-Vectoring Configuration Time Histories (Continued)

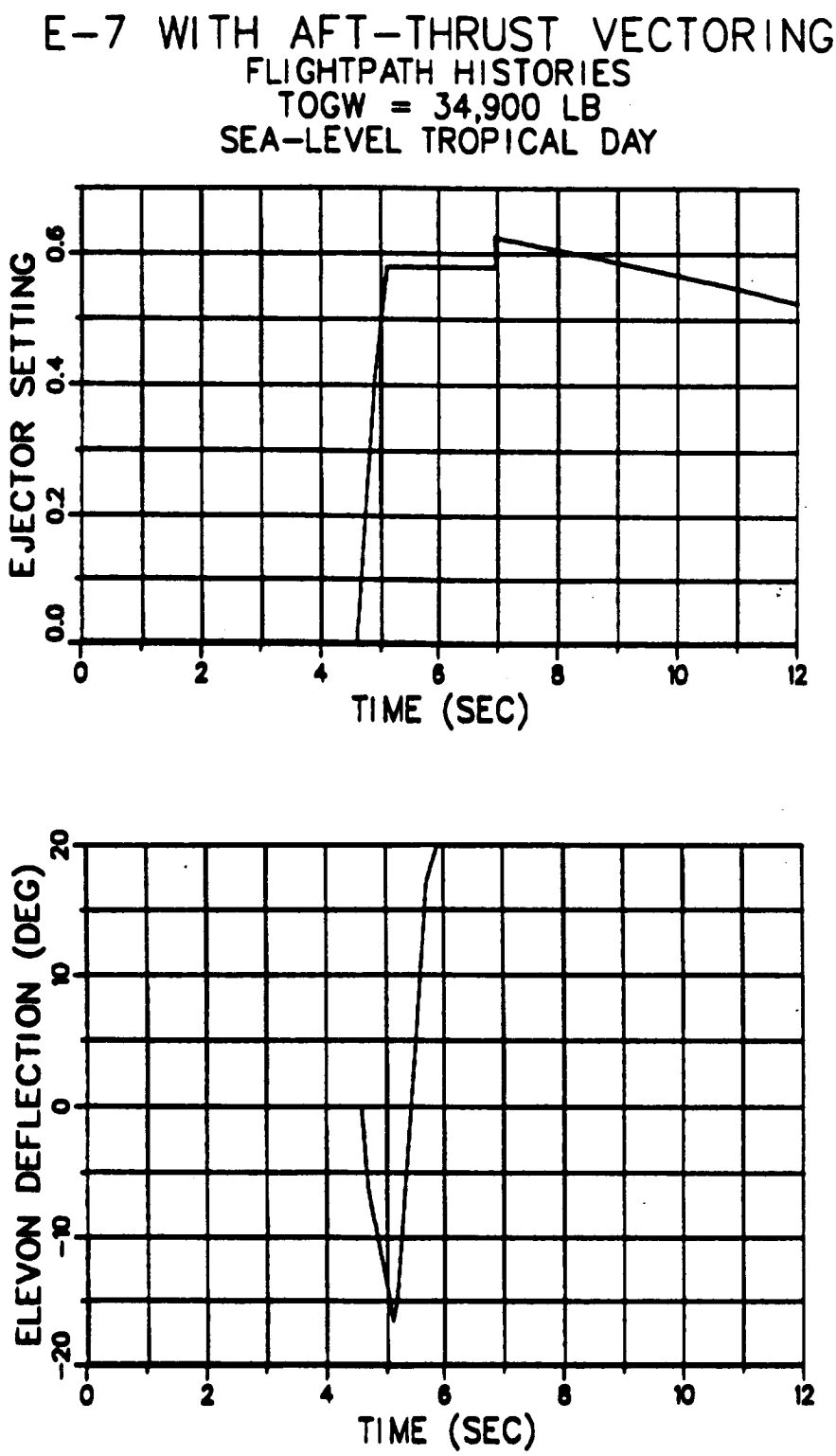

Figure B-1 Aft-Vectoring Configuration Time Histories (Continued)

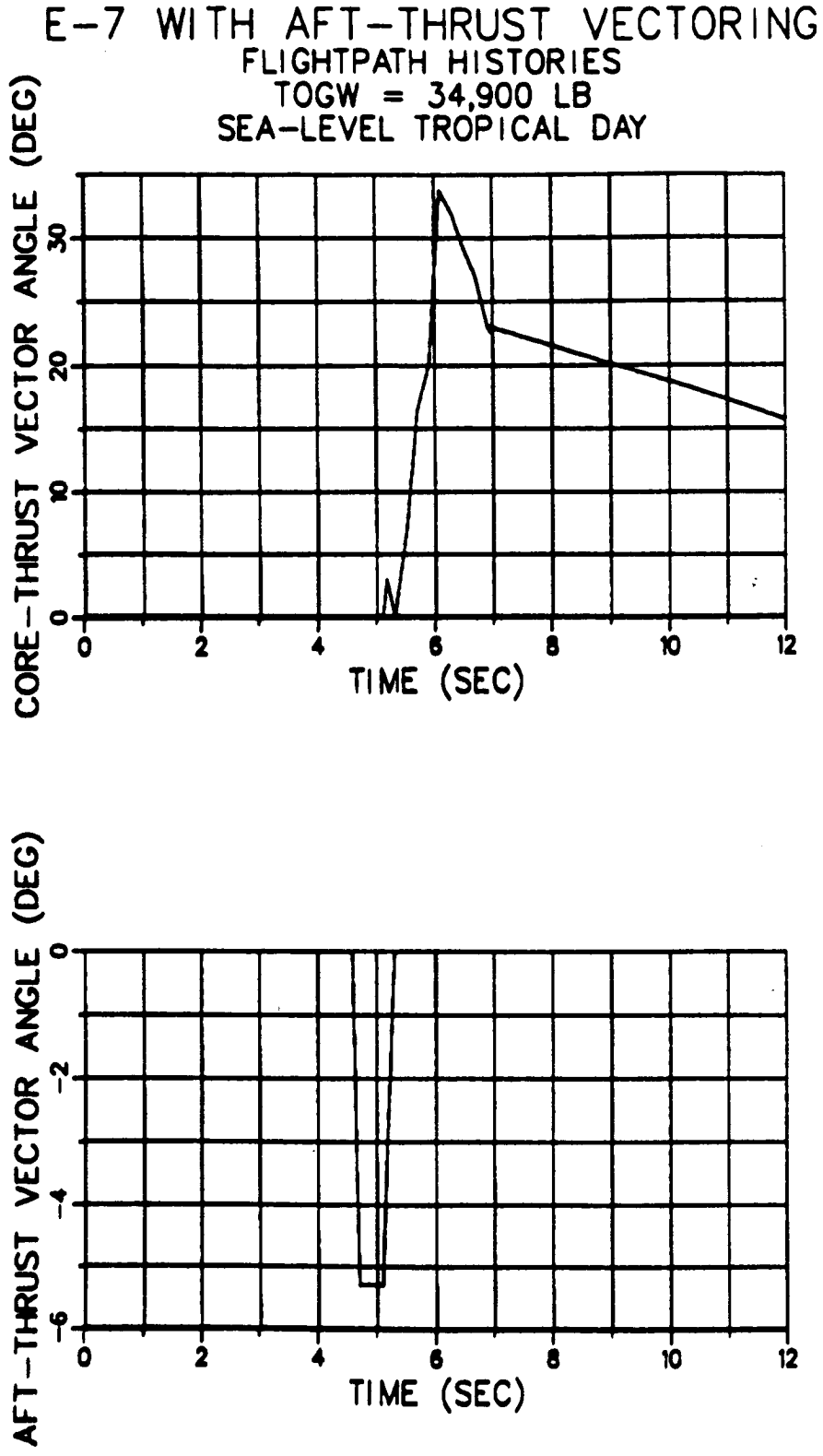

Figure B-1 Aft-Vectoring Configuration Time Histories (Continued)

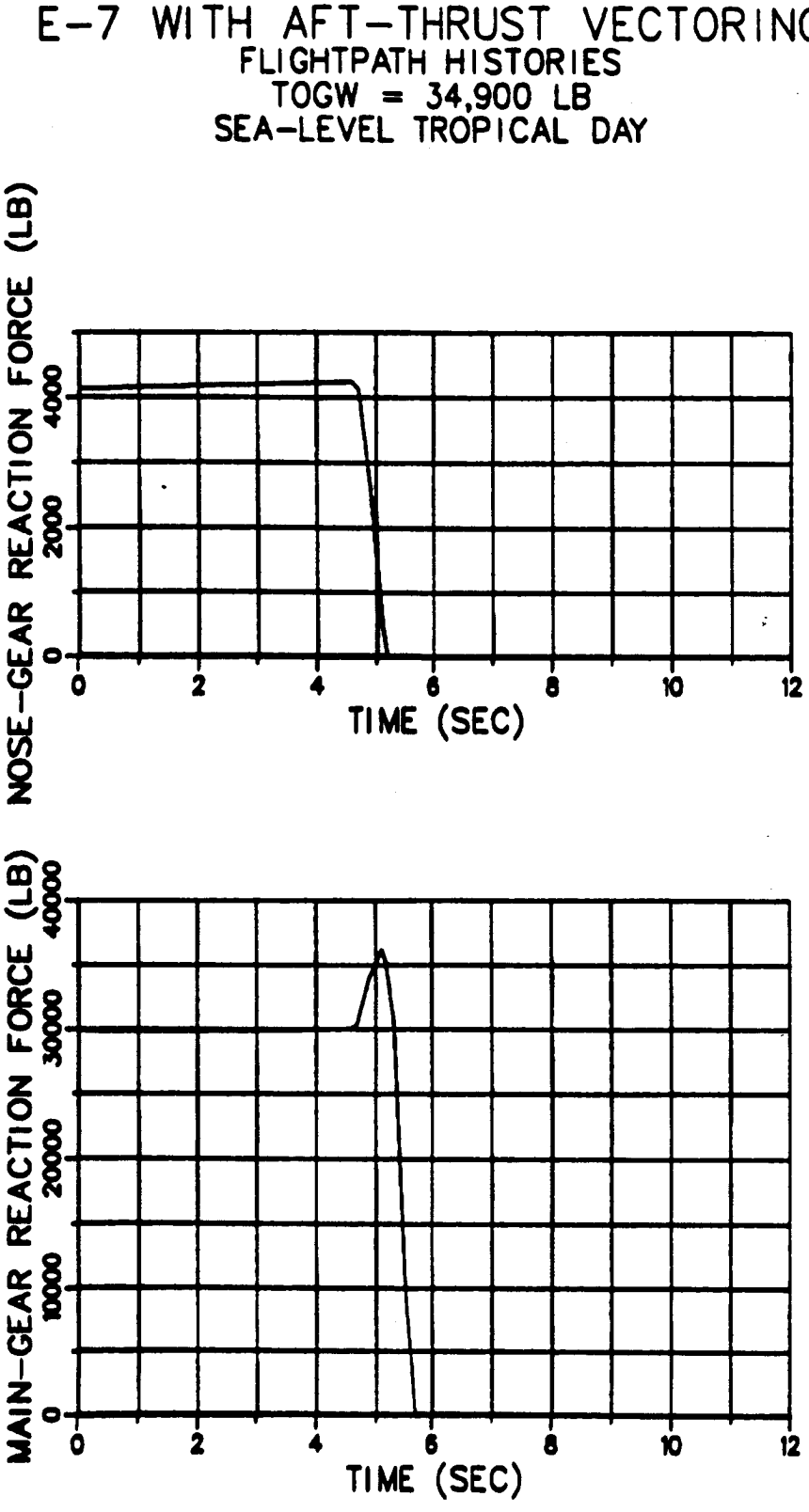

Figure B-1 Aft-Vectoring Configuration Time Histories (Concluded)

APPENDIX C

Increased-Static-Pitch Takeoff Histories

Figure C-1 shows time-history plots of pertinent parameters for E-7 with a 20-in nose-gear extension (8.5-deg static pitch) performing a carrier takeoff at STO weight.

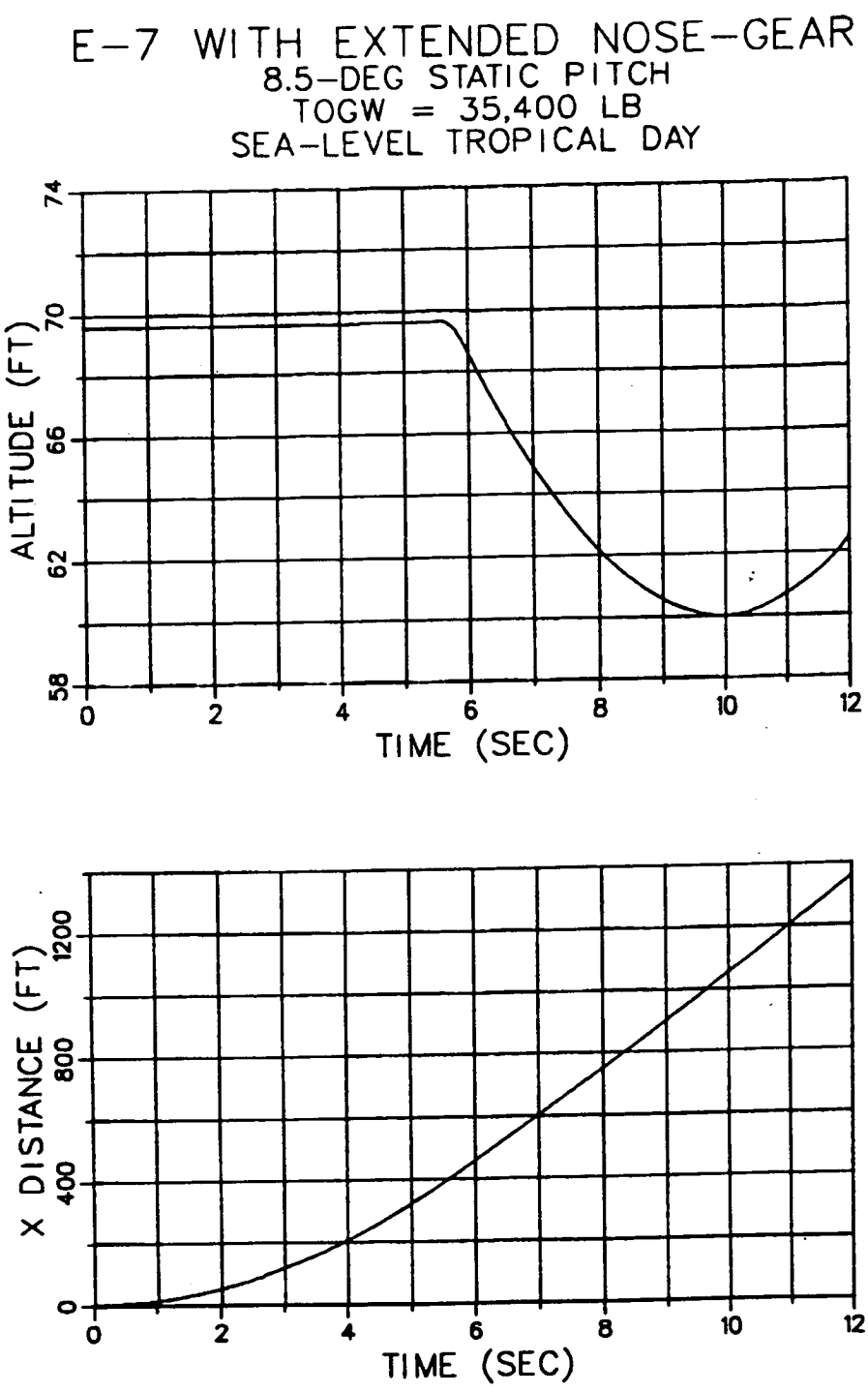

Figure C-1 Extended-Nose-Gear Configuration Time Histories

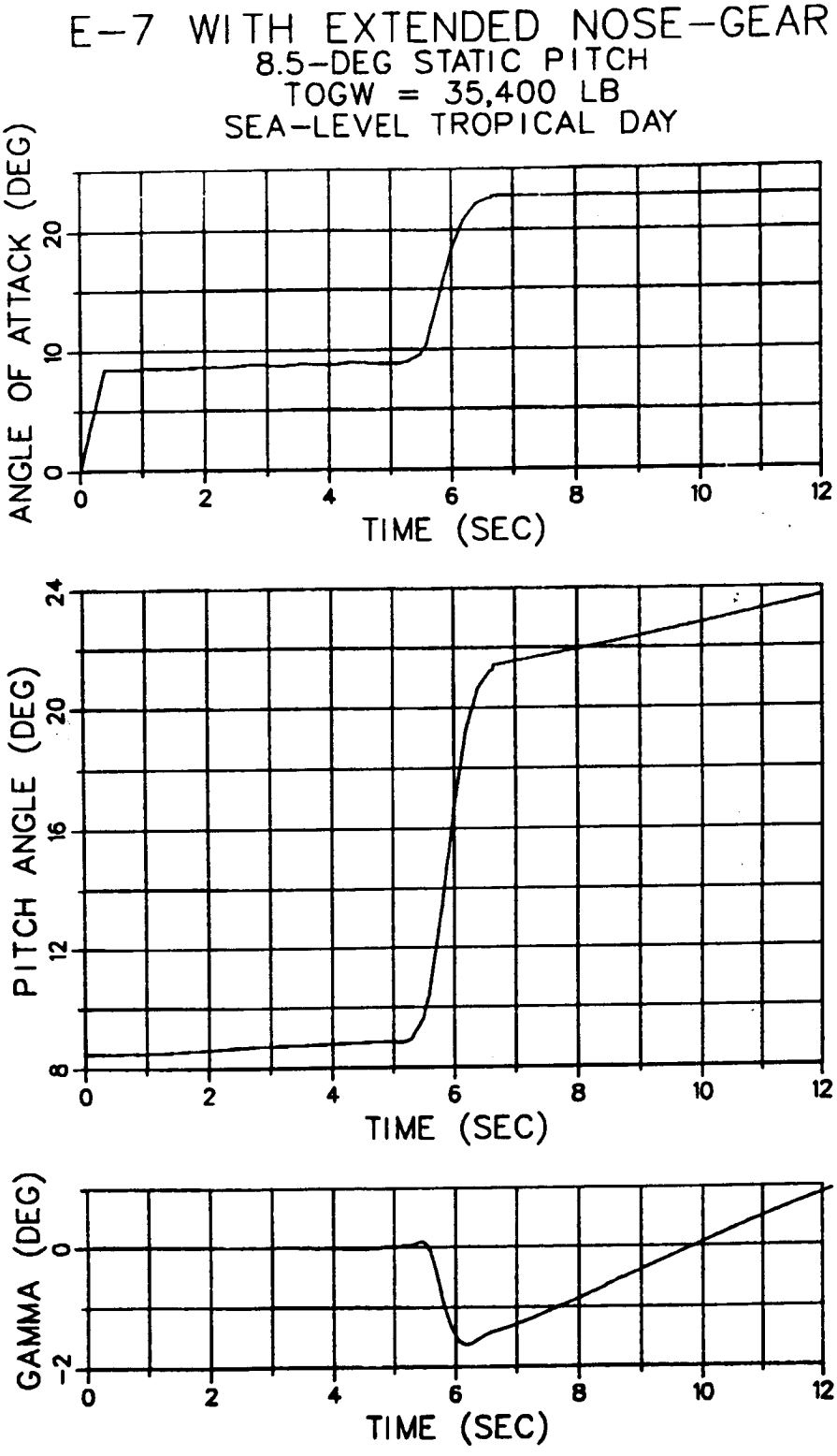

Figure C-1 Extended-Nose-Gear Configuration Time Histories (Continued)

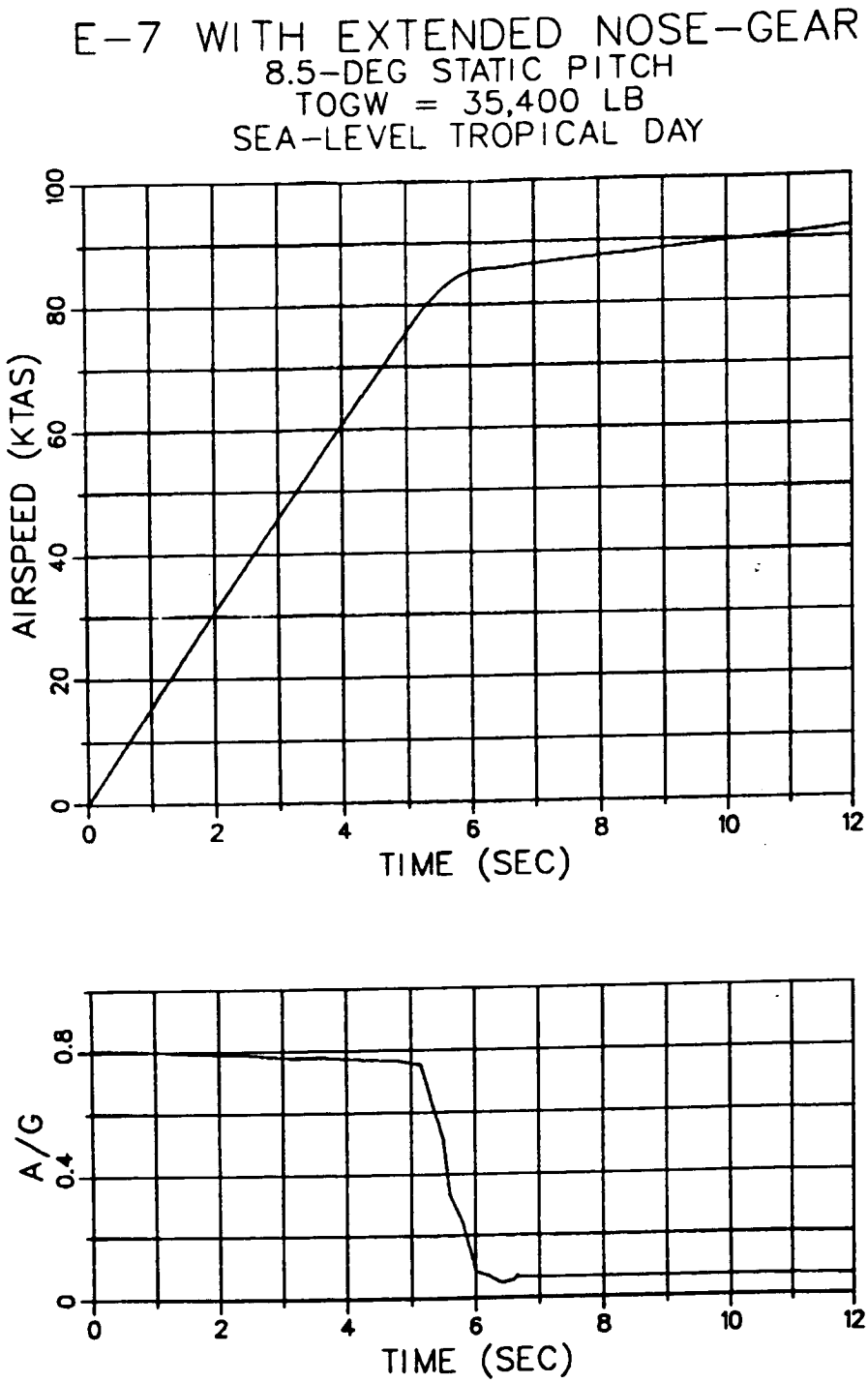

Figure C-1 Extended-Nose-Gear Configuration Time Histories (Continued)

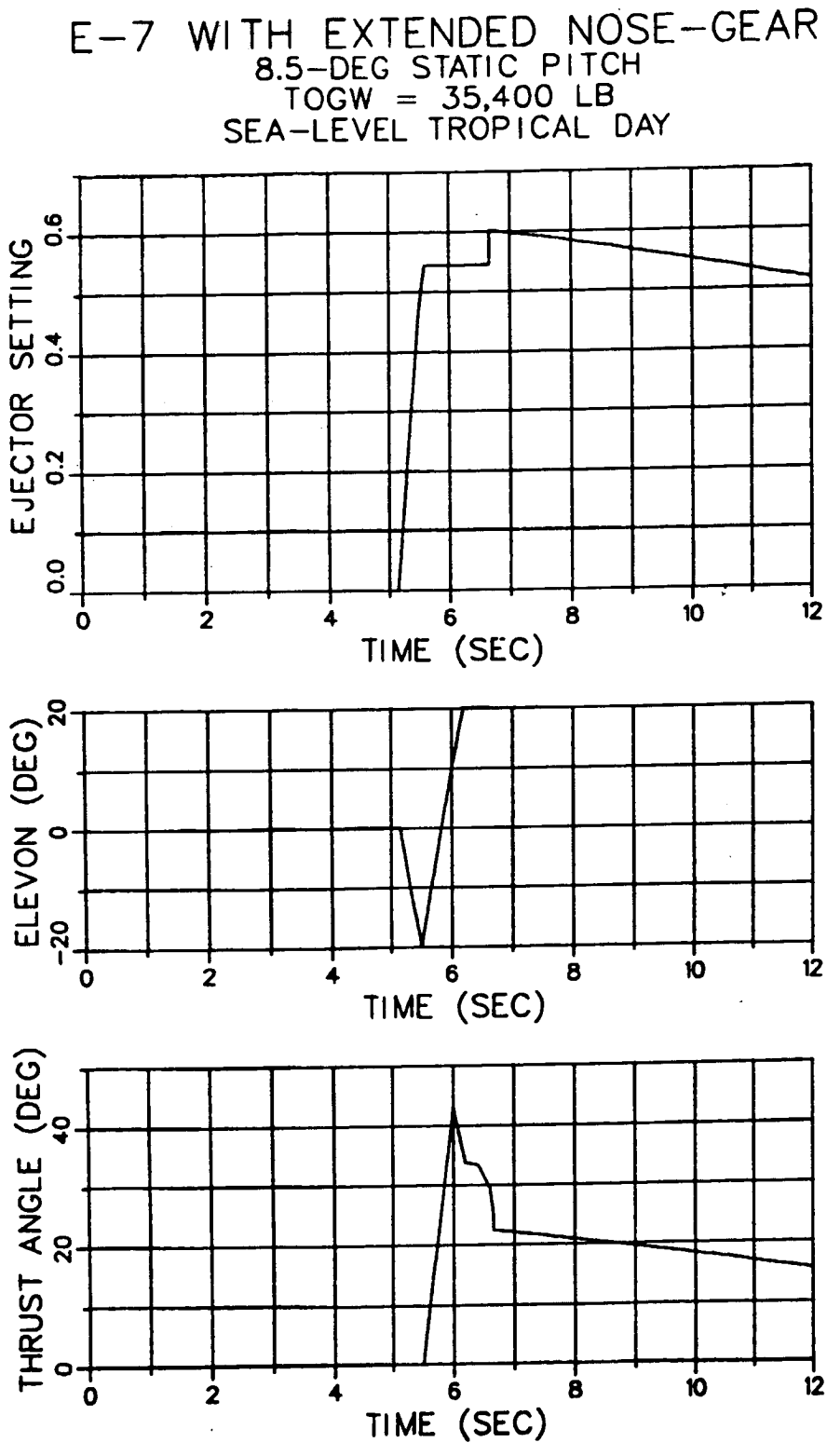

Figure C-1 Extended-Nose-Gear Configuration Time Histories (Continued)

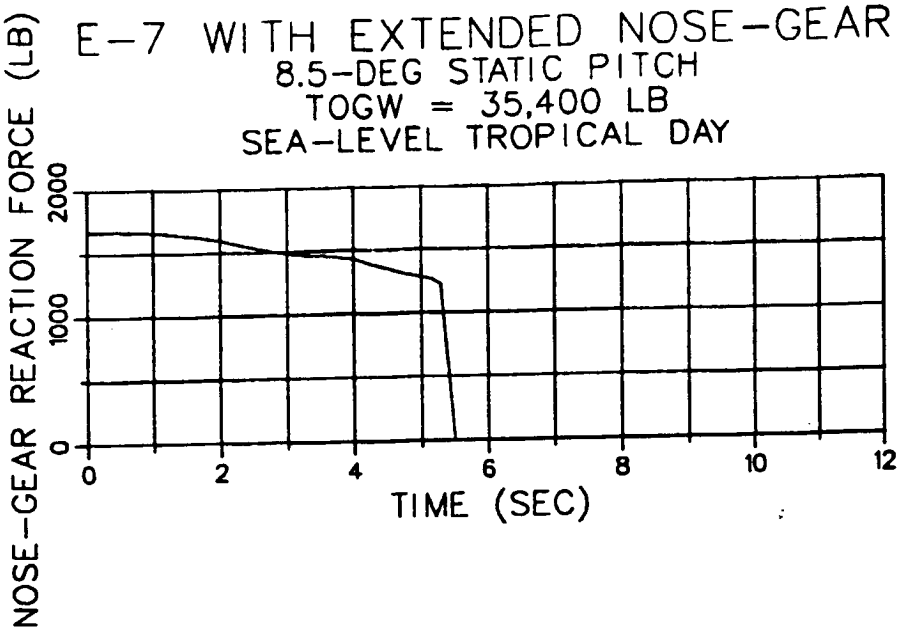

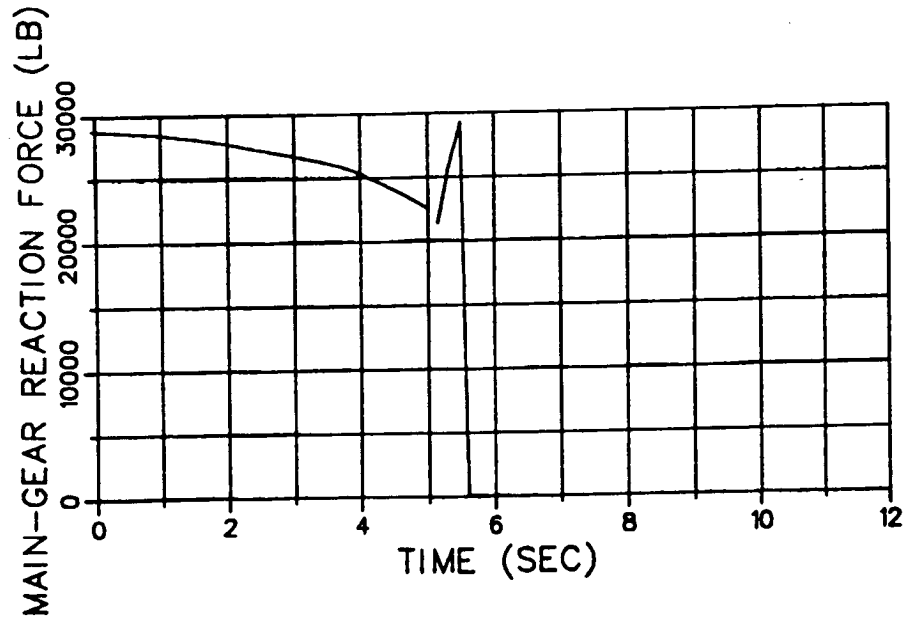

Figure C-1 Extended-Nose-Gear Configuration Time Histories (Concluded)

APPENDIX D

Incremental-Propulsive-Lift Takeoff Histories

Figures D-1 through D-8 show time-history plots of pertinent parameters for E-7 using all combinations of three propulsive-lift components (ejector, aft vector, and core vector) performing a takeoff at escort-mission weight.

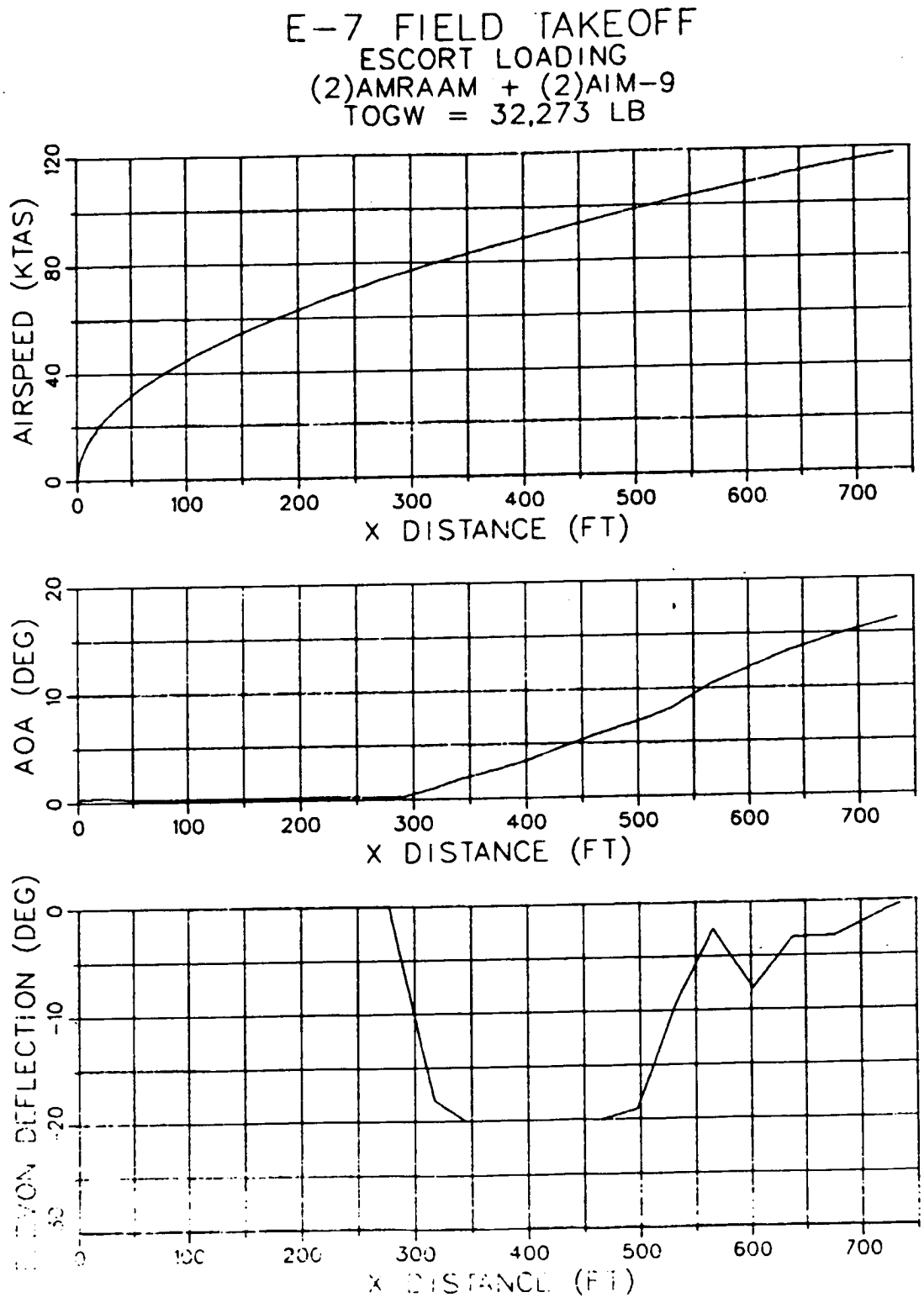

Figure D-1 No-Components Case Time Histories

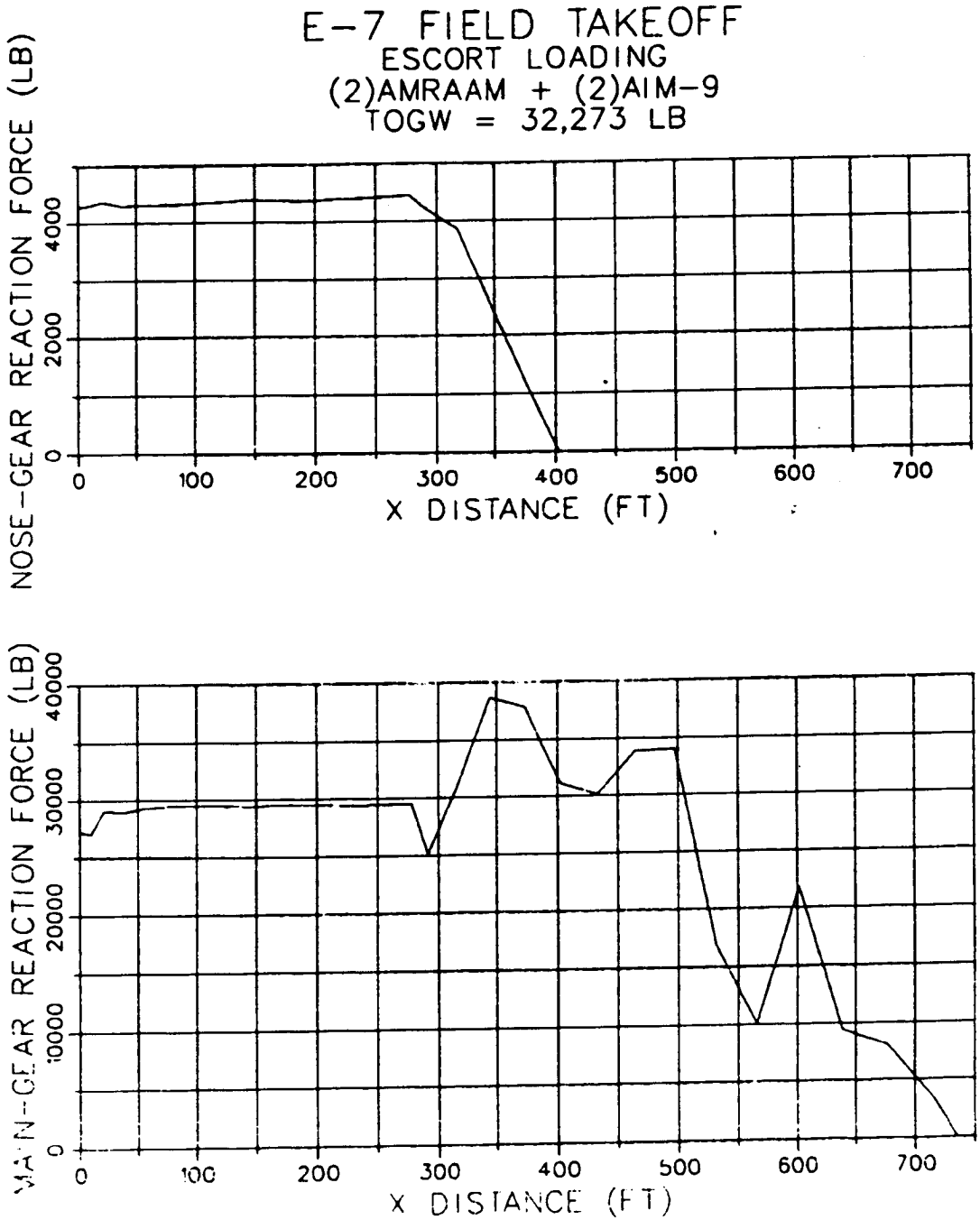

Figure D-1 No-Components Case Time Histories (Concluded)

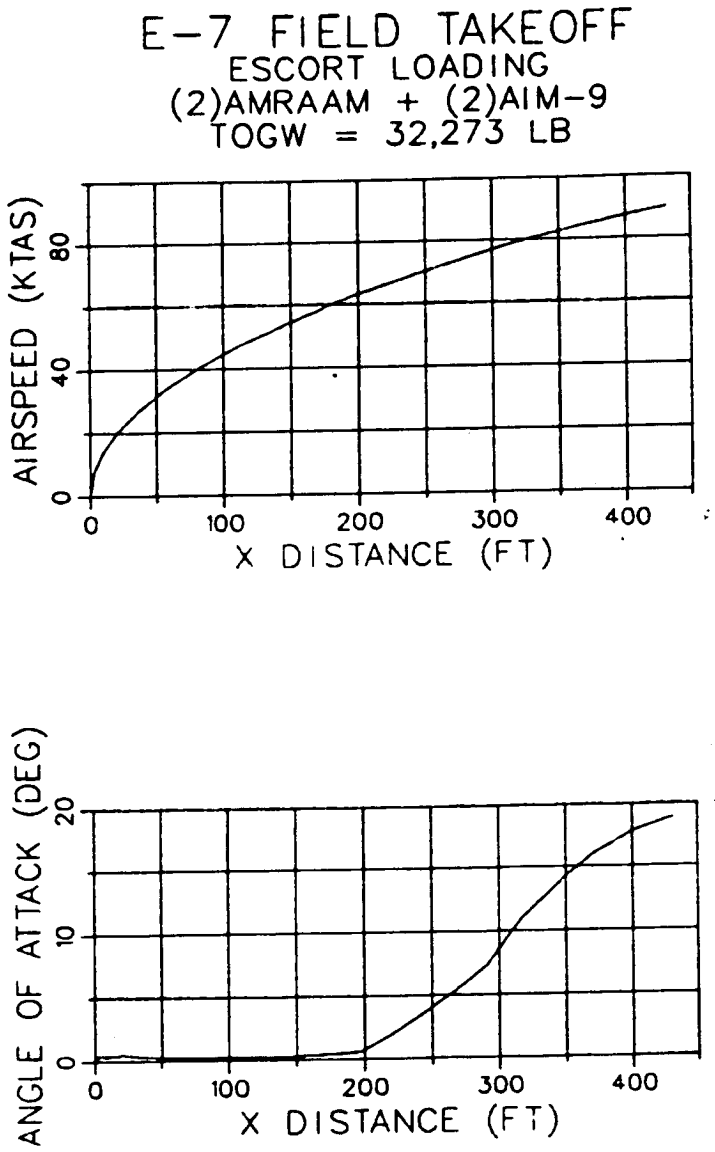

Figure D-2 Aft-Vector-Only Case Time Histories

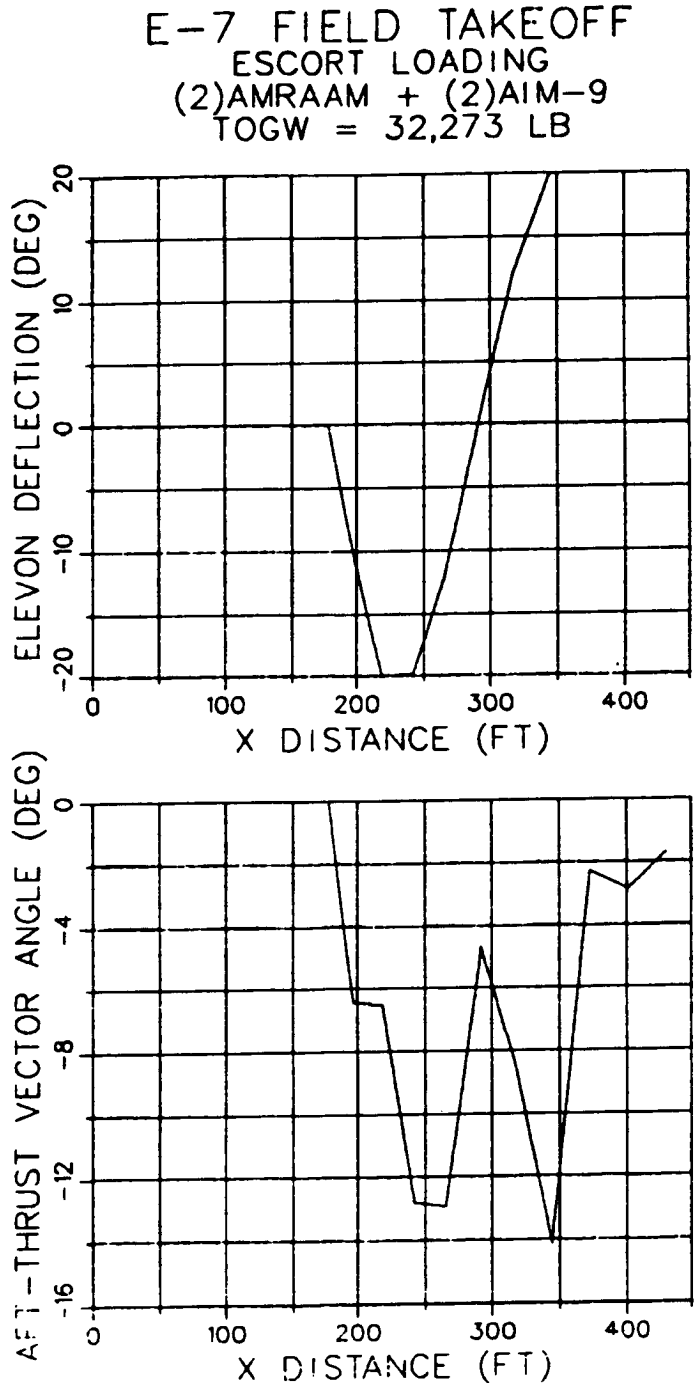

Figure D-2 Aft-Vector-Only Case Time Histories (Continued)

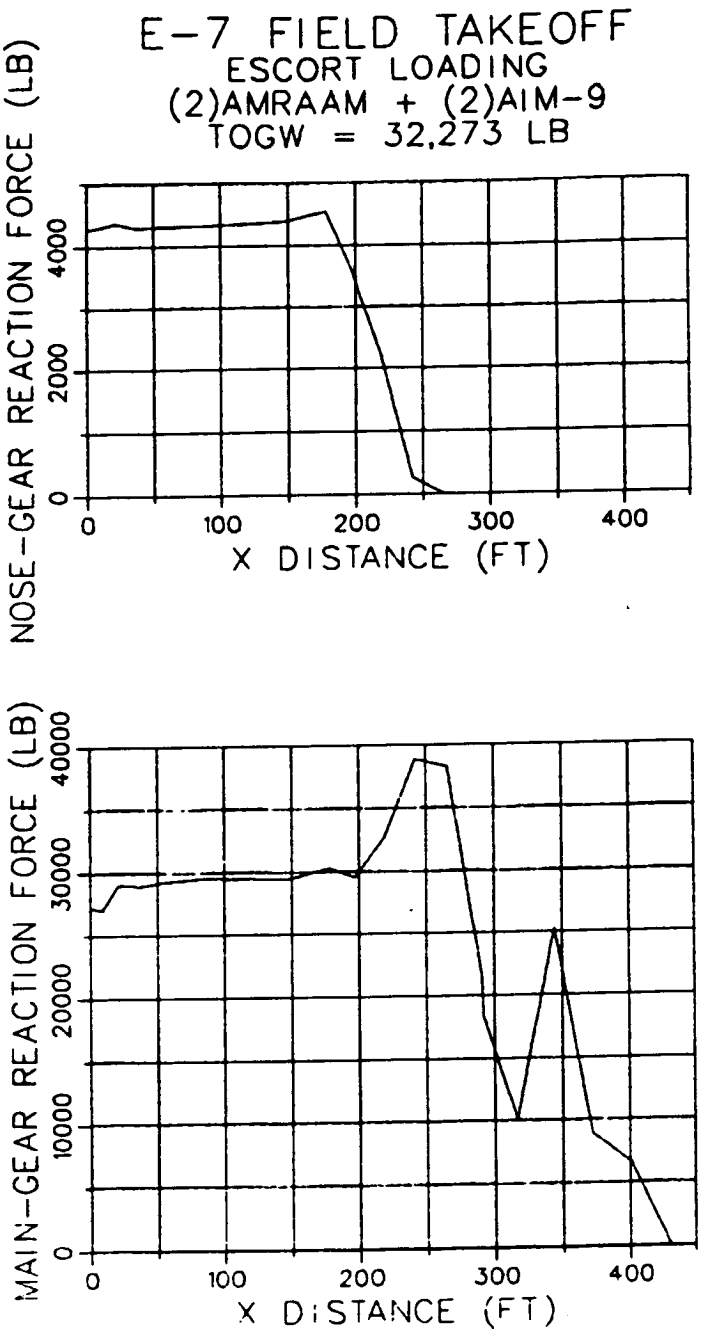

Figure D-2 Aft-Vector-Only Case Time Histories (Concluded)

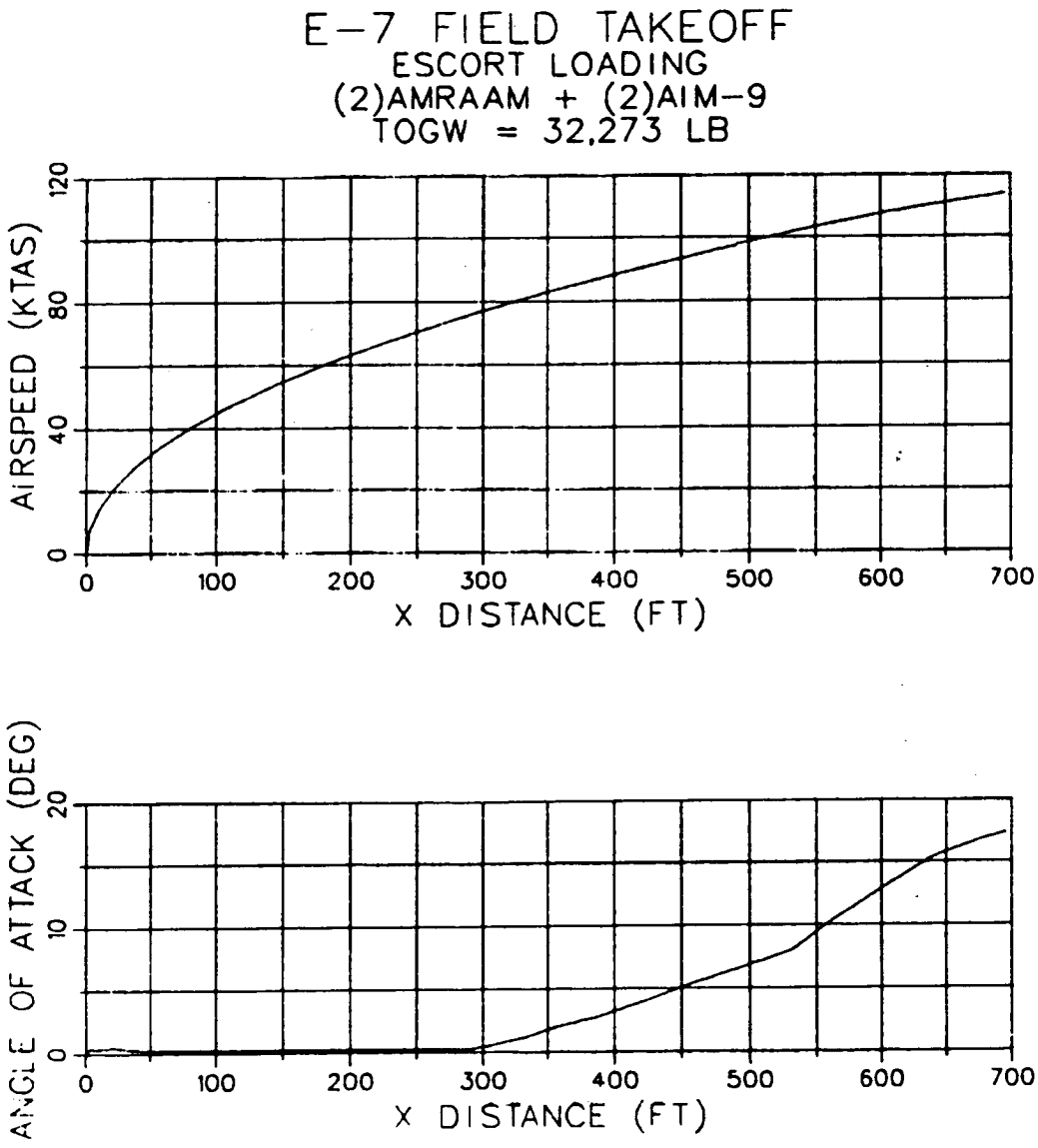

Figure D-3 Core-Vector-Only Case Time Histories

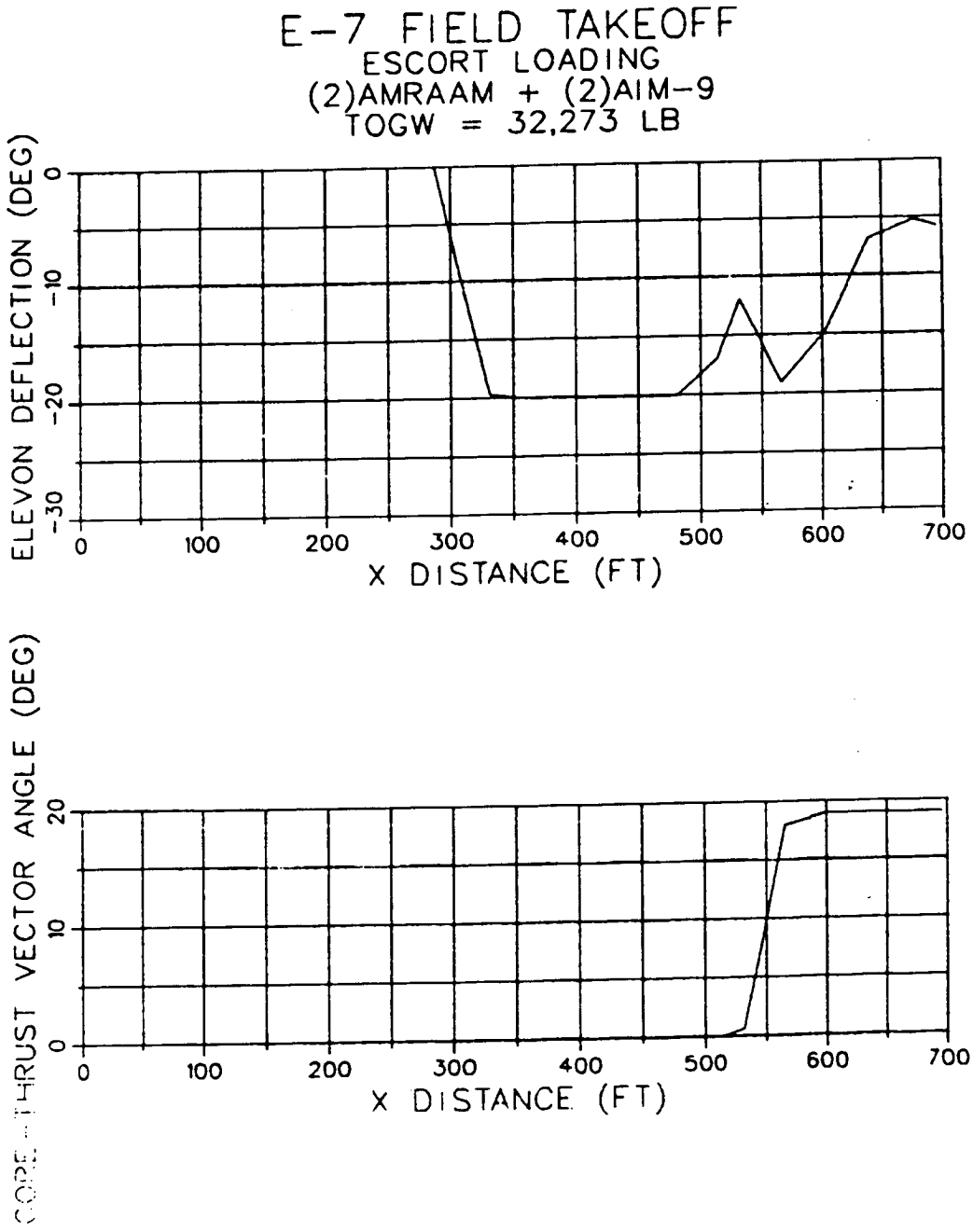

Figure D-3 Core-Vector-Only Case Time Histories (Continued)

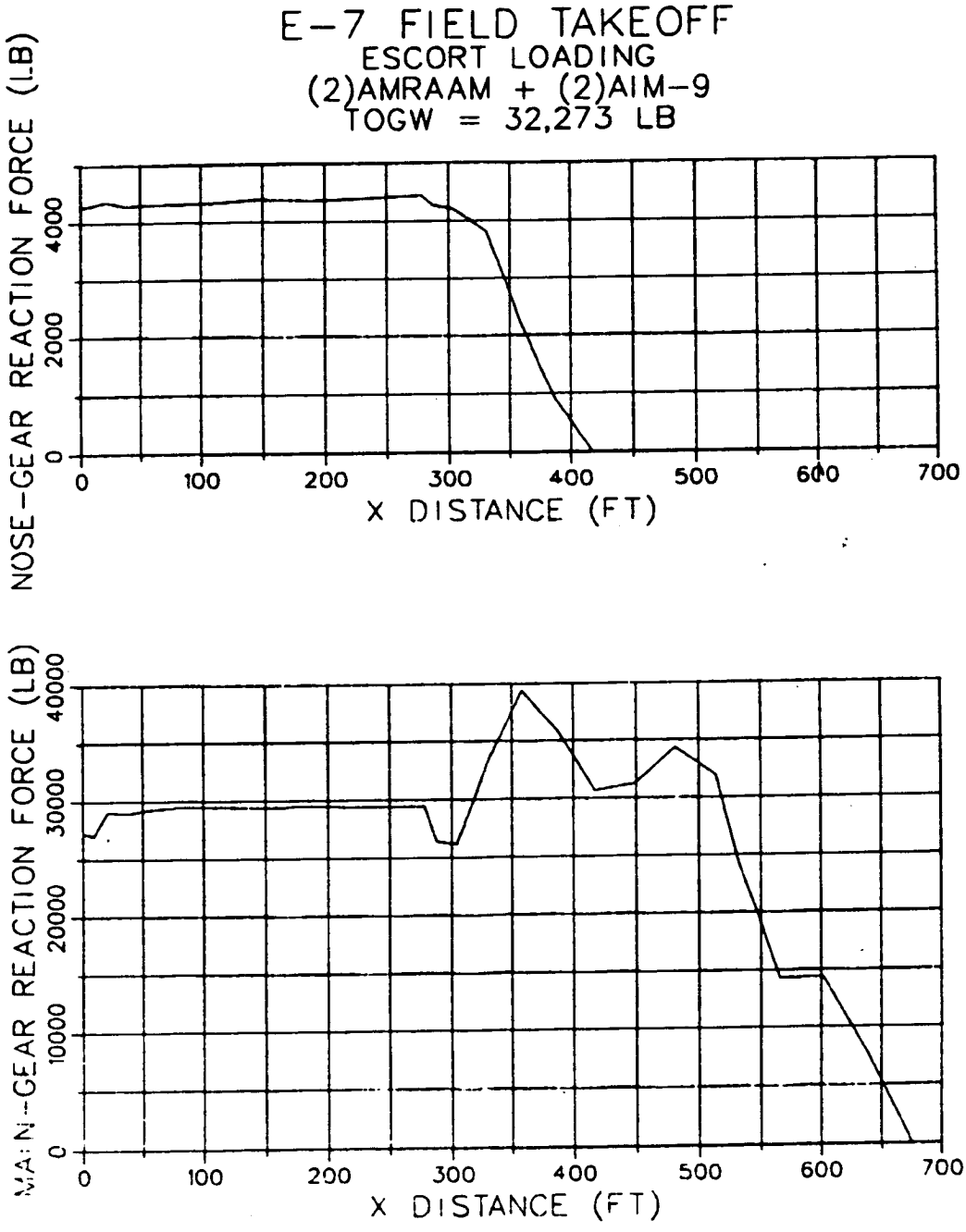

Figure D-3 Core-Vector-Only Case Time Histories (Concluded)

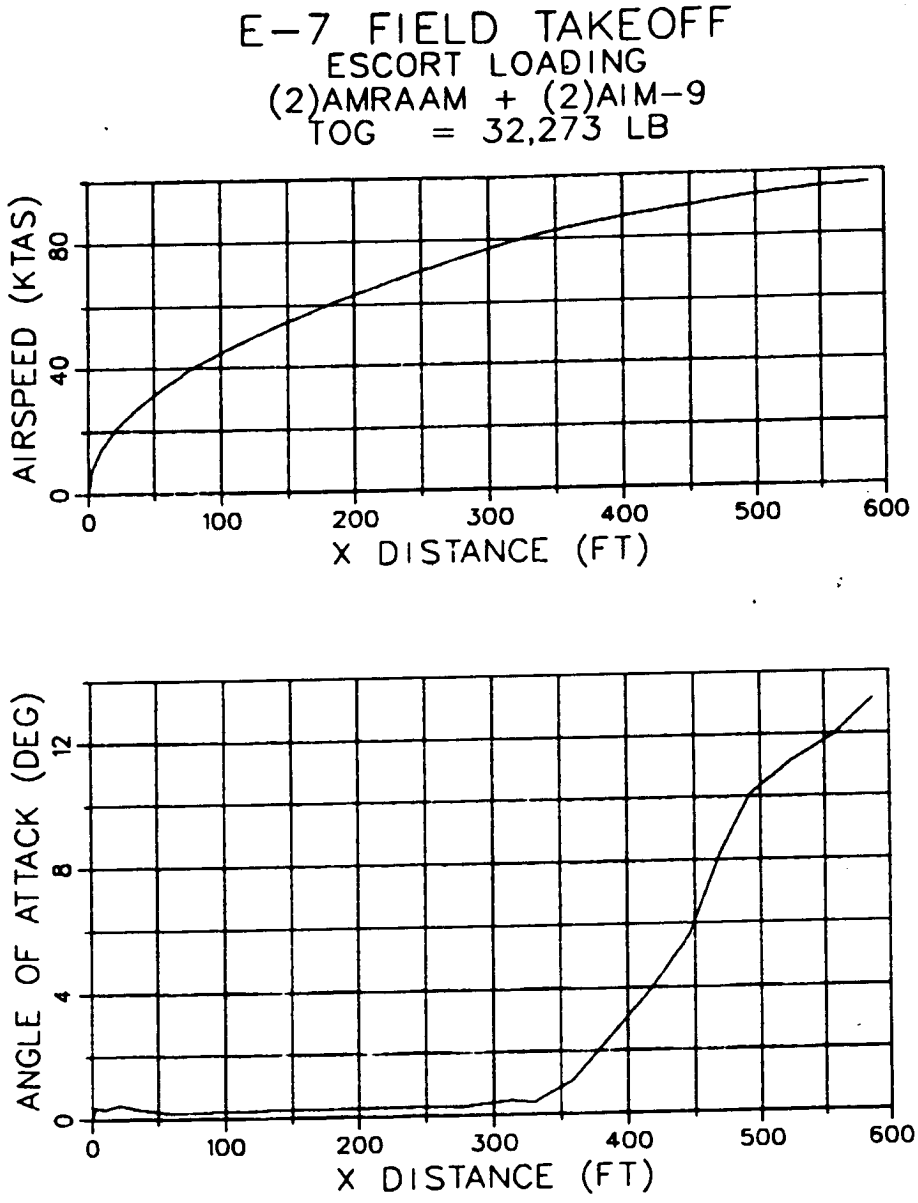

Figure D-4 Ejector-Only Case Time Histories

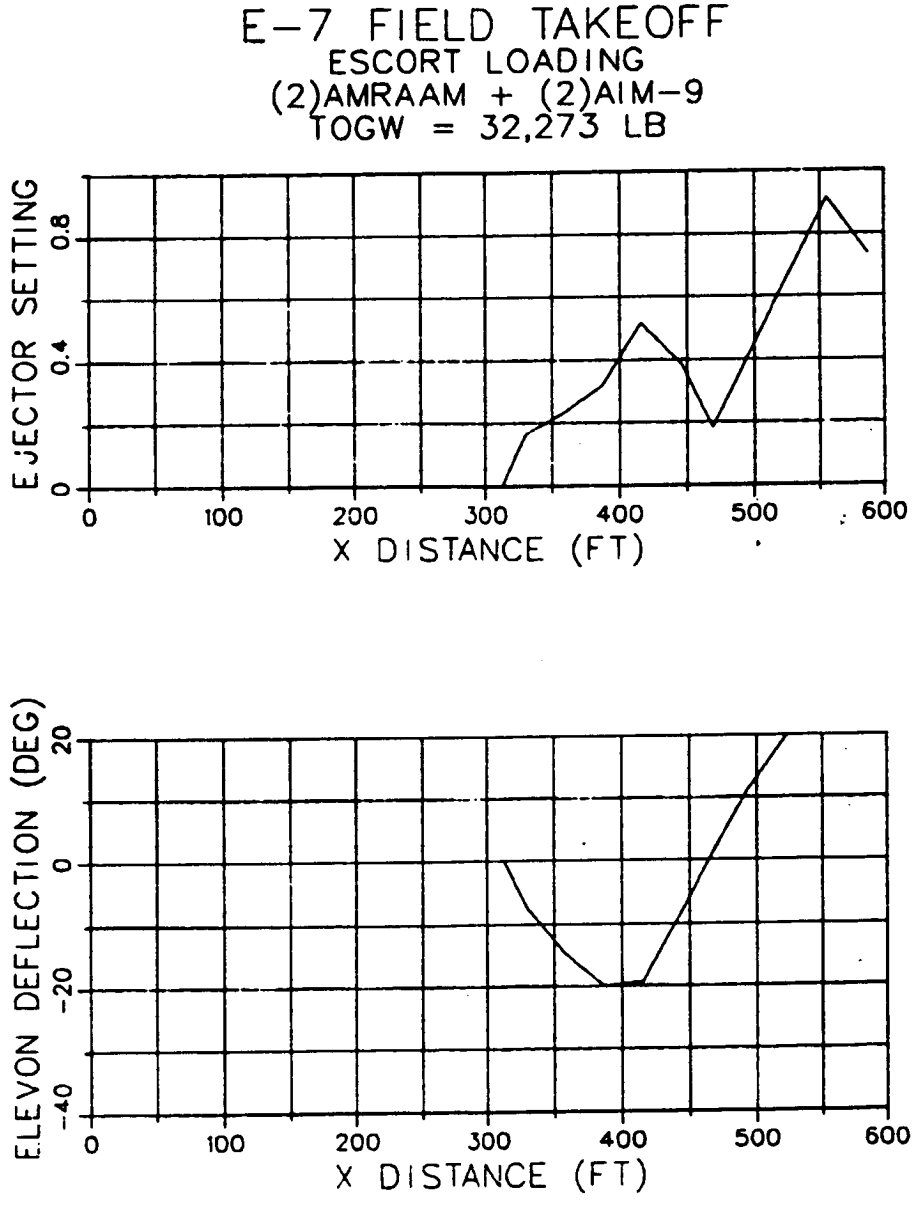

Figure D-4 Ejector-Only Case Time Histories (Continued)

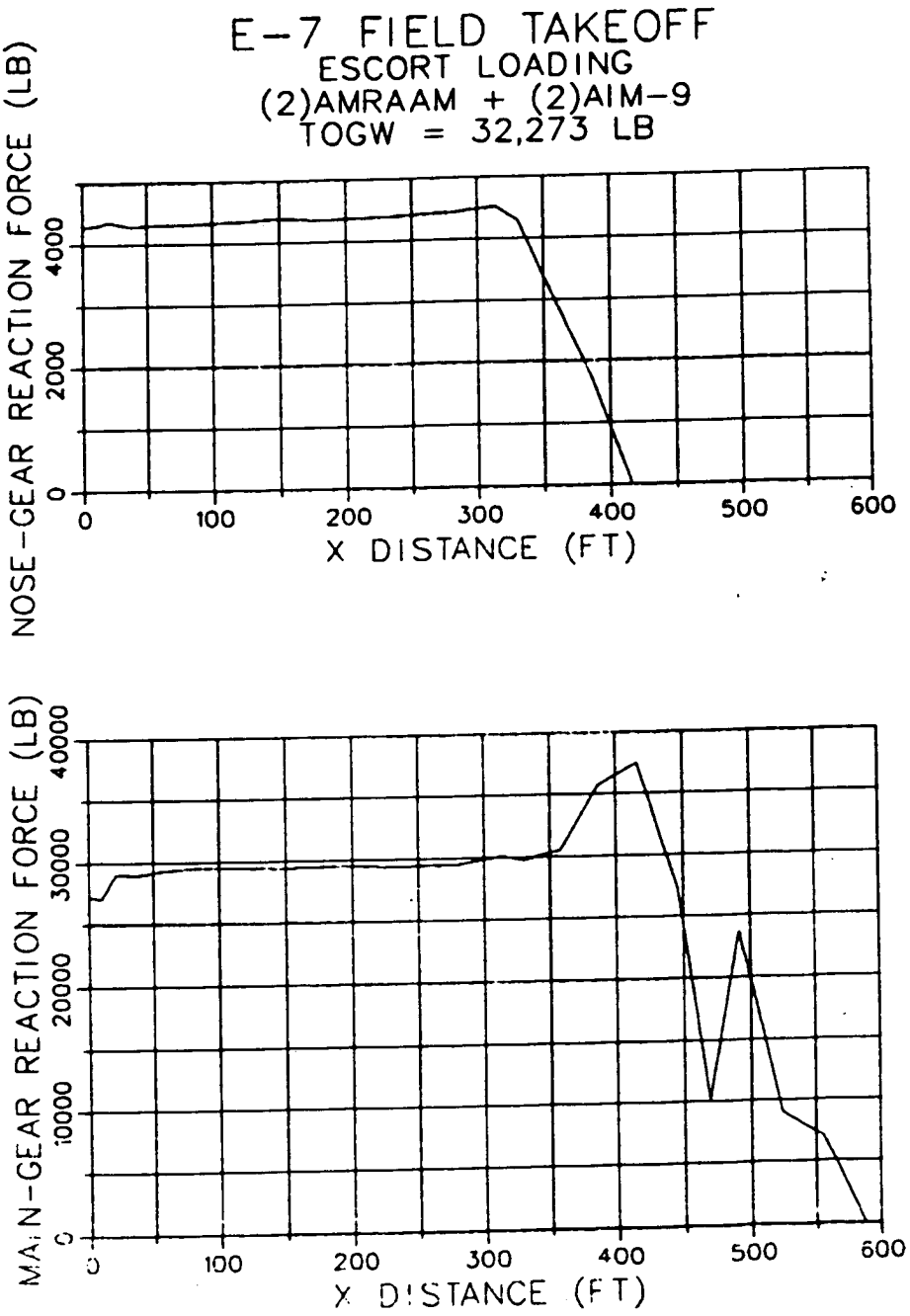

Figure D-4 Ejector-Only Case Time Histories (Concluded)

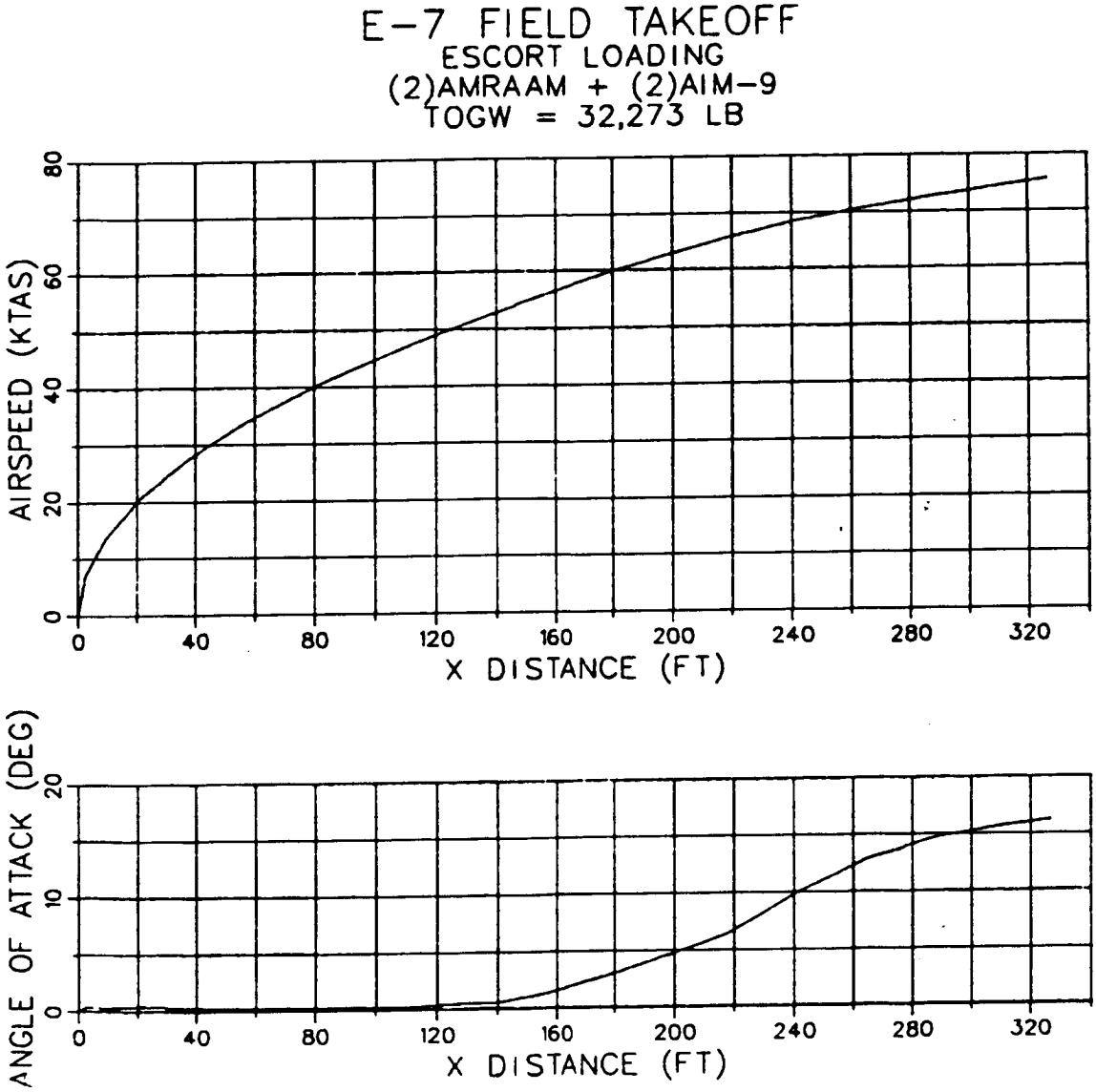

Figure D-5 Aft-and-Core-Vector Case Time Histories

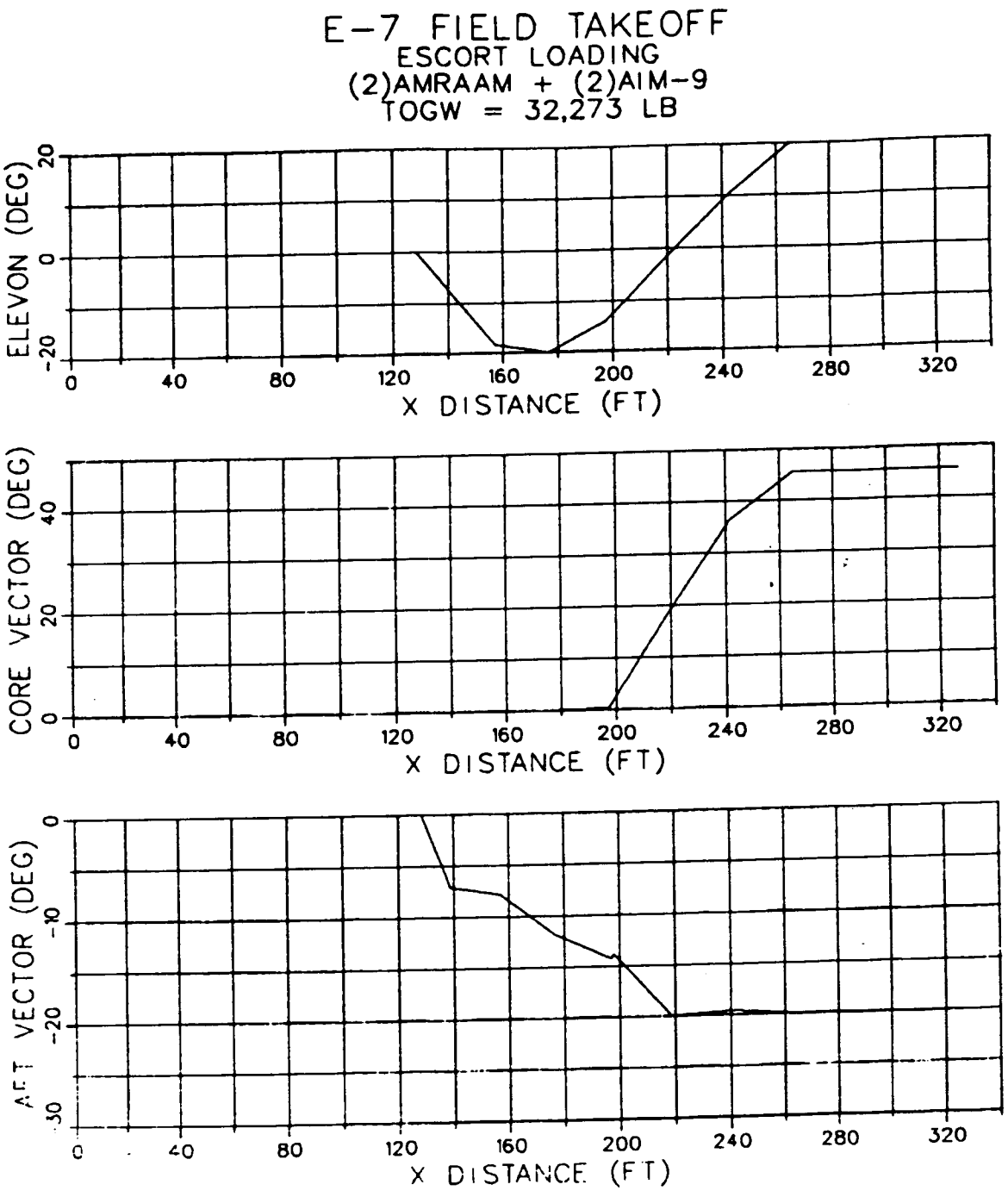

Figure D-5 Aft-and-Core-Vector Case Time Histories (Continued)

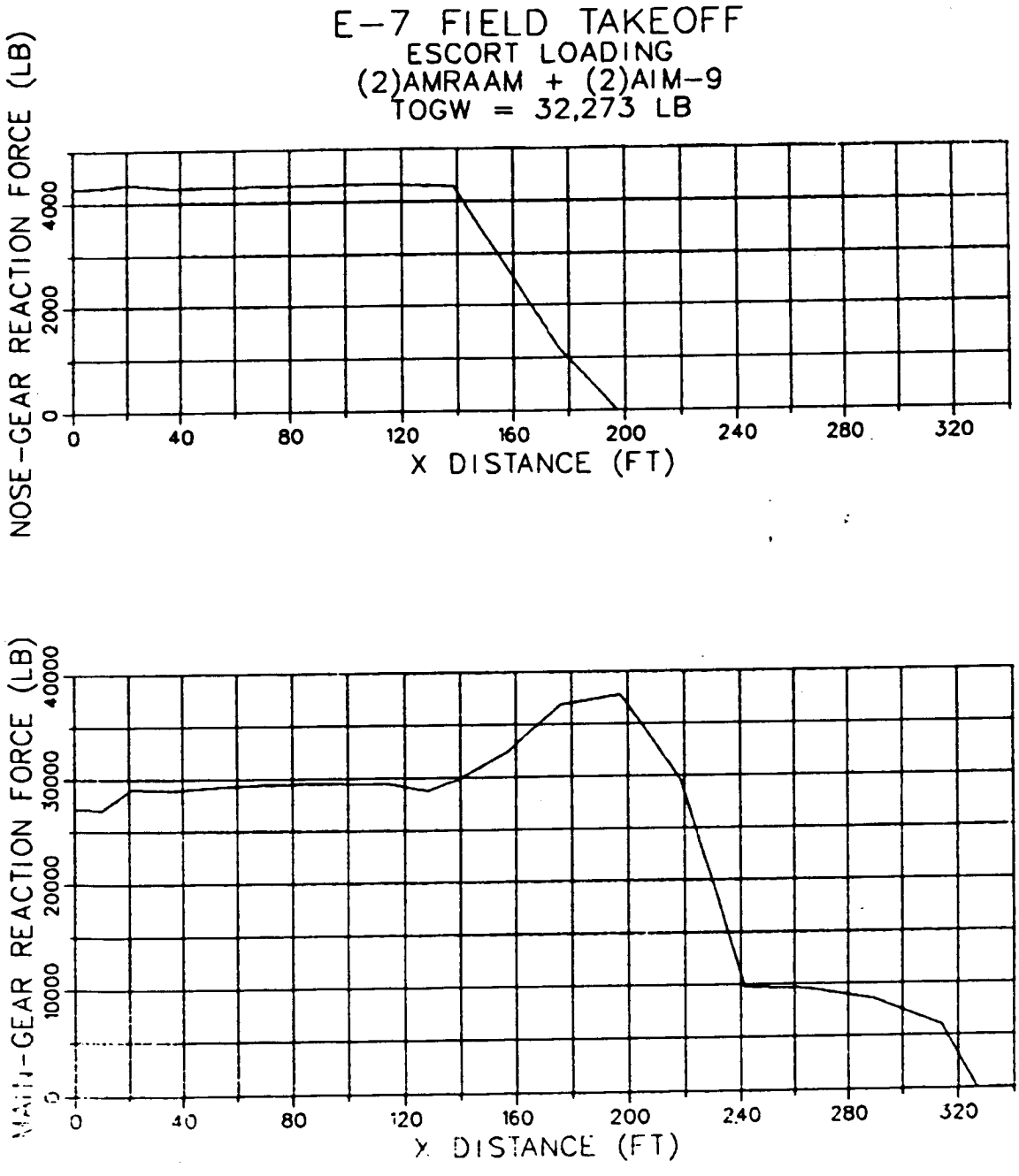

Figure D-5 Aft-and-Core-Vector Case Time Histories (Concluded)

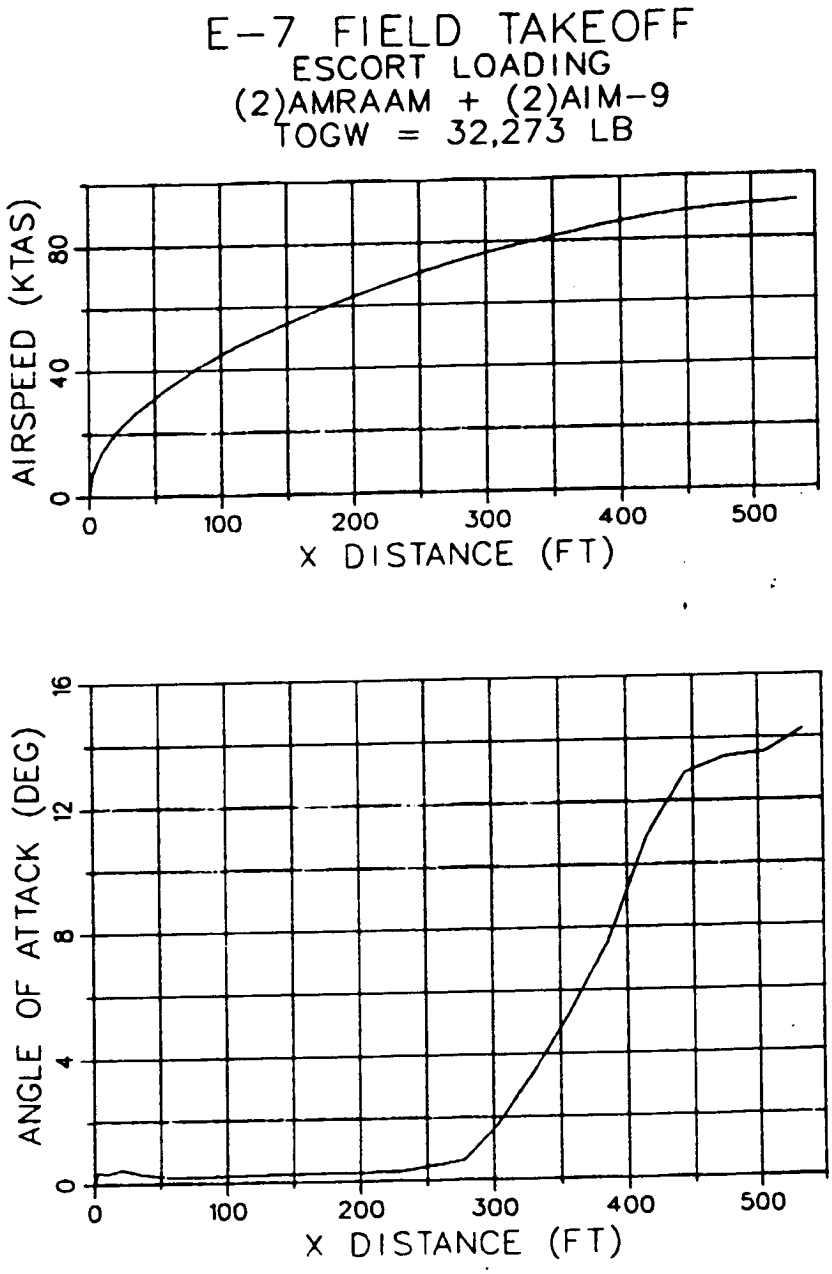

Figure D-6 Ejector-and-Aft-Vector Case Time Histories

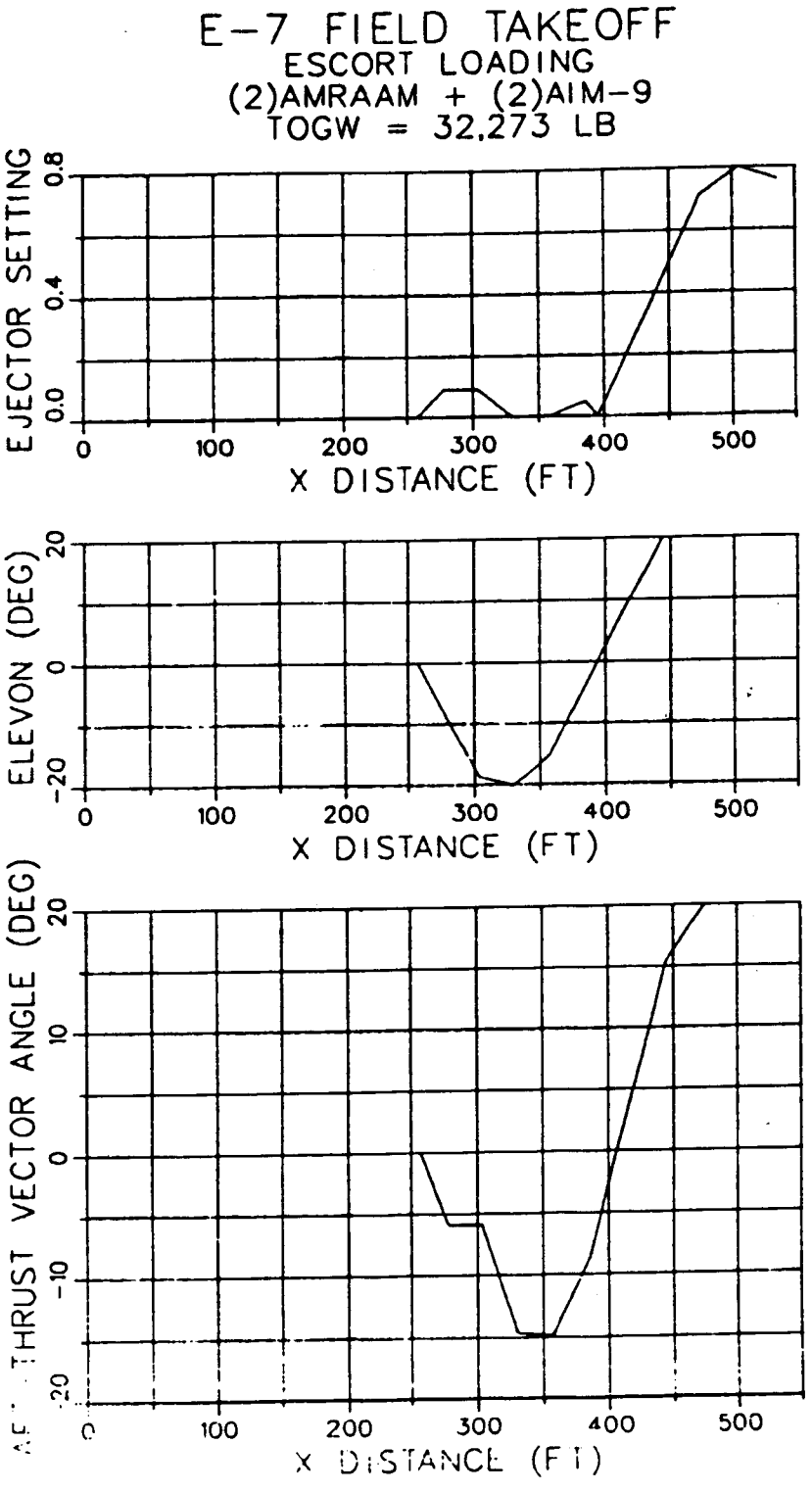

Figure D-6 Ejector-and-Aft-Vector Case Time Histories (Continued)

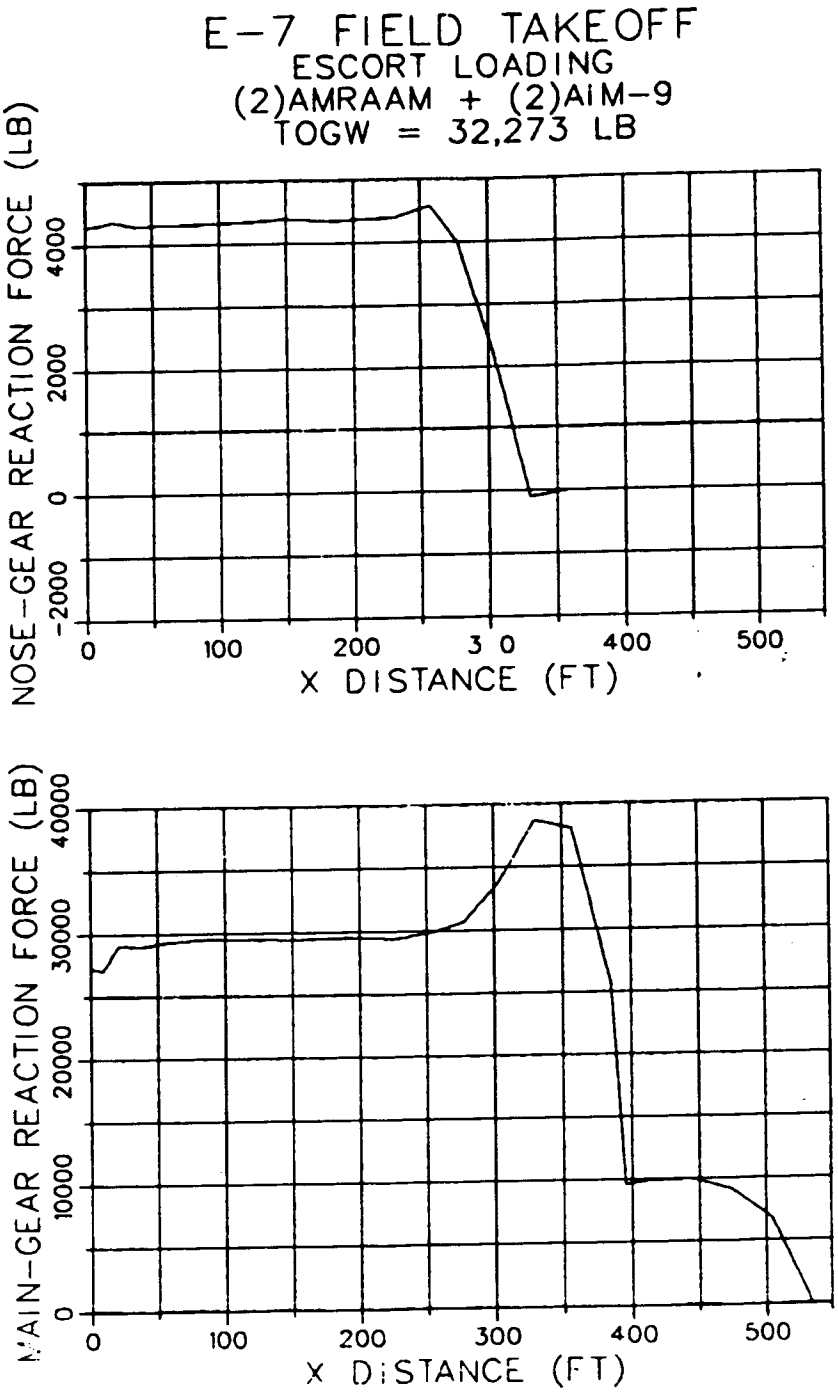

Figure D-6 Ejector-and-Aft-Vector Case Time Histories (Concluded)

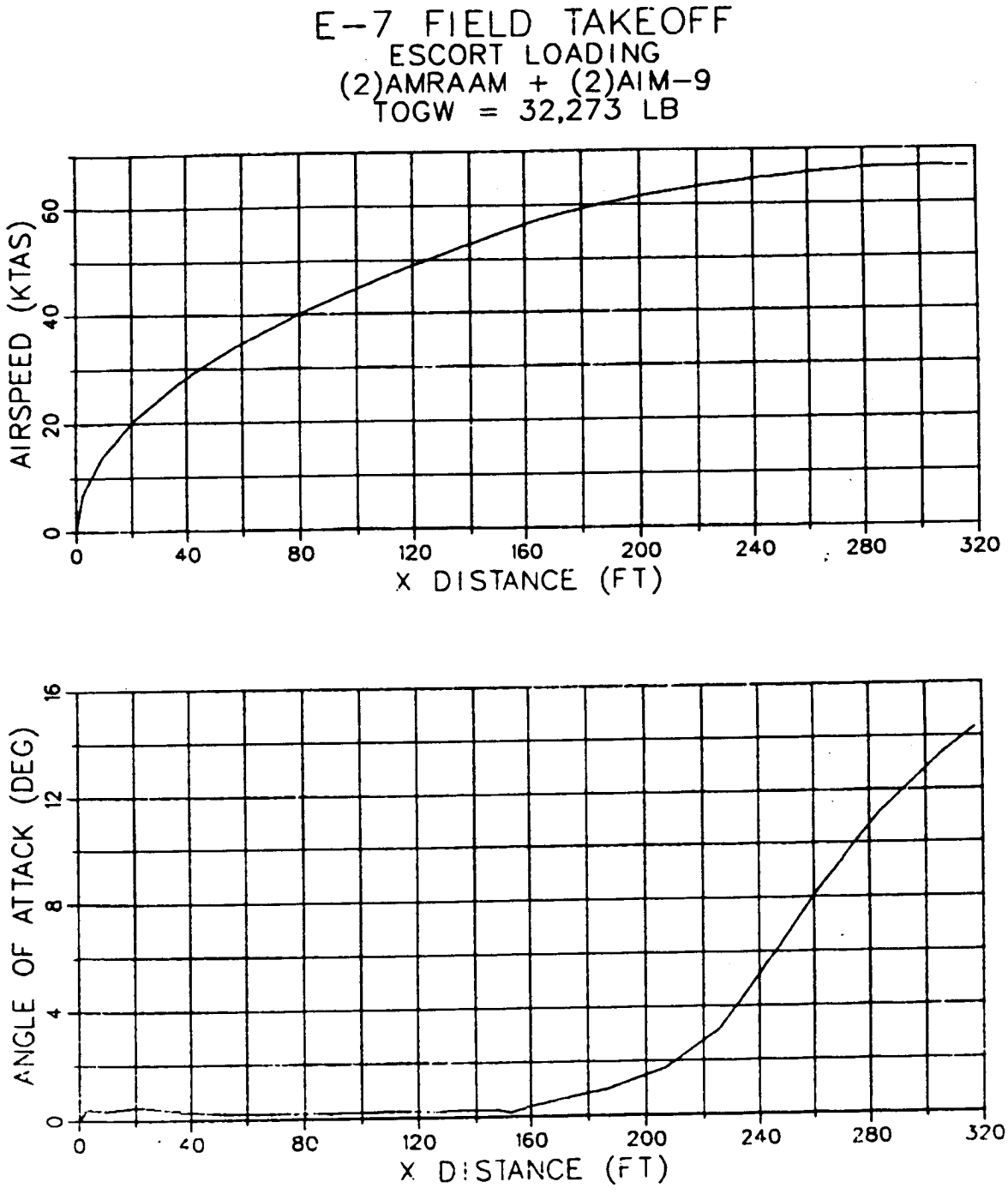

Figure D-7 Ejector-and-Core-Vector Case Time Histories

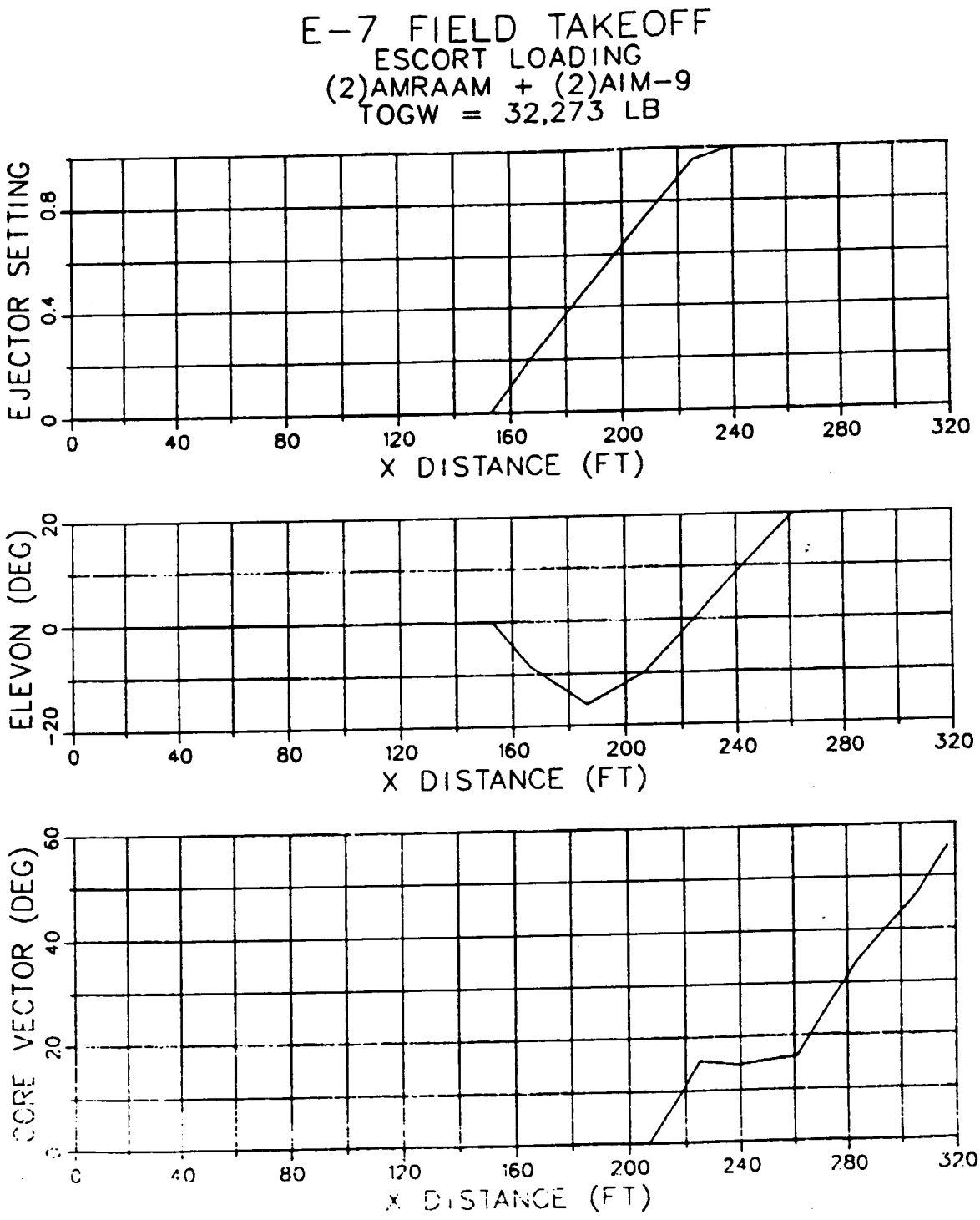

Figure D-7 Ejector-and-Core-Vector Case Time Histories (Continued)

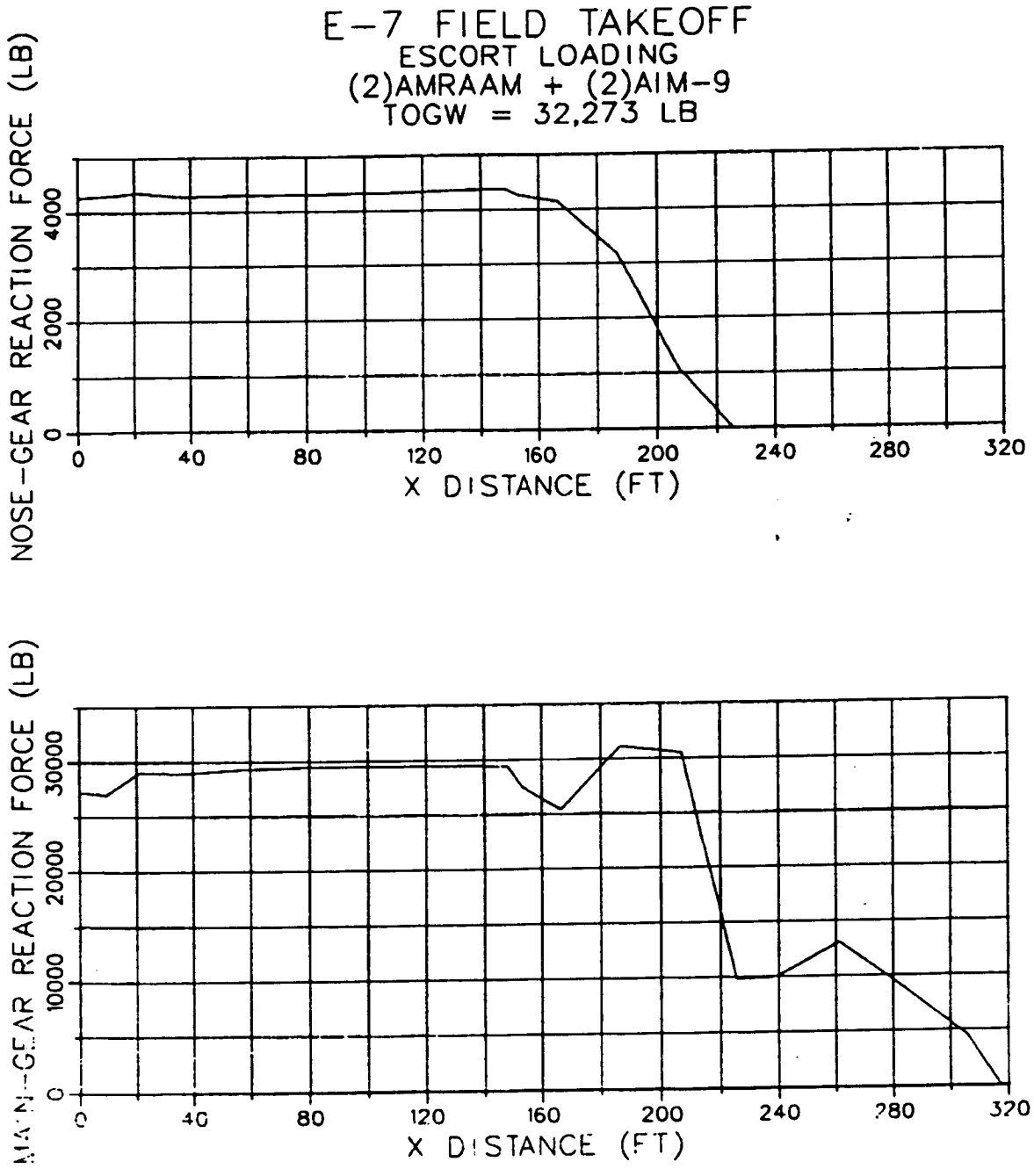

Figure D-7 Ejector-and-Core-Vector Case Time Histories (Concluded)

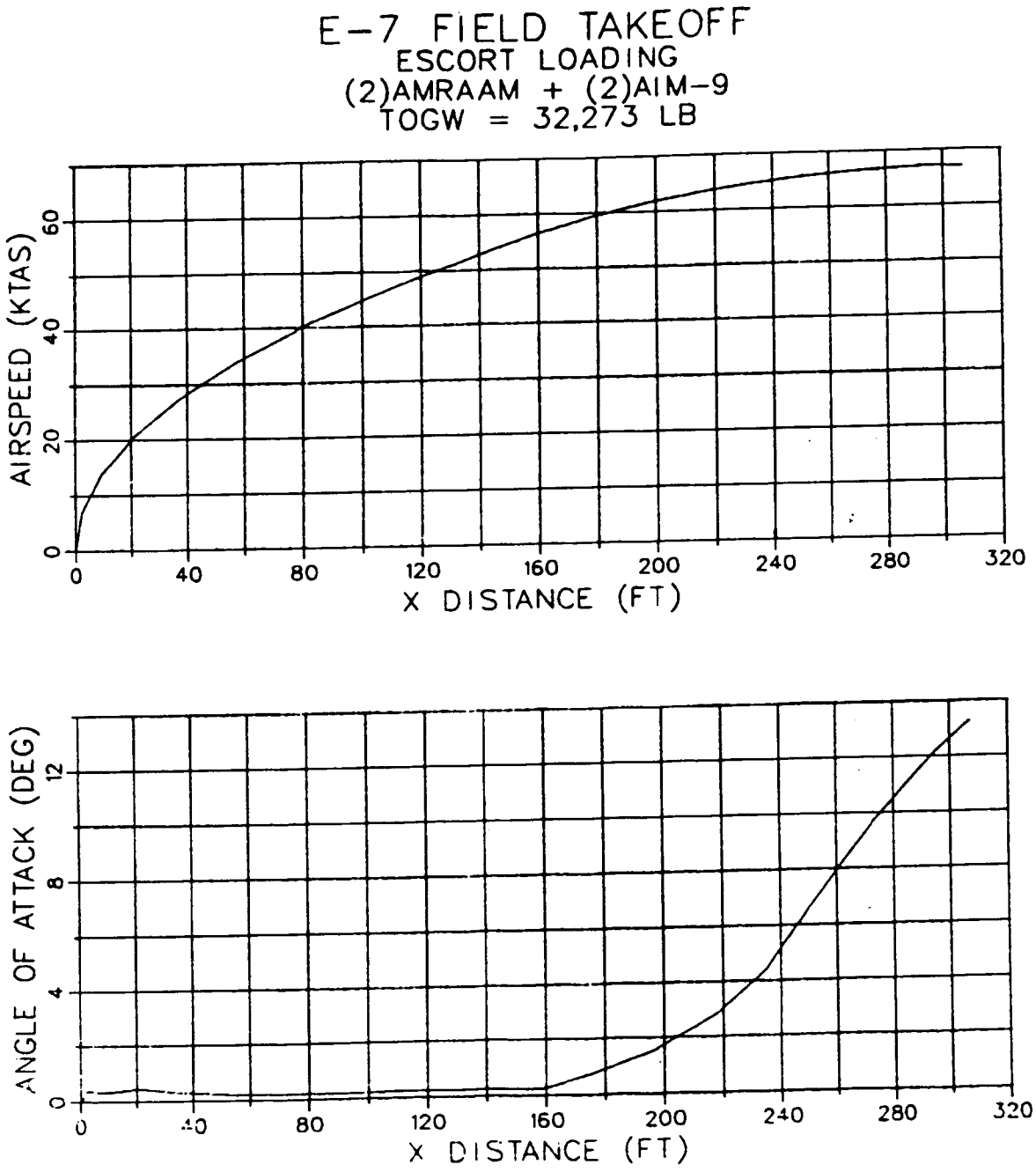

Figure D-8 All-Components Case Time Histories

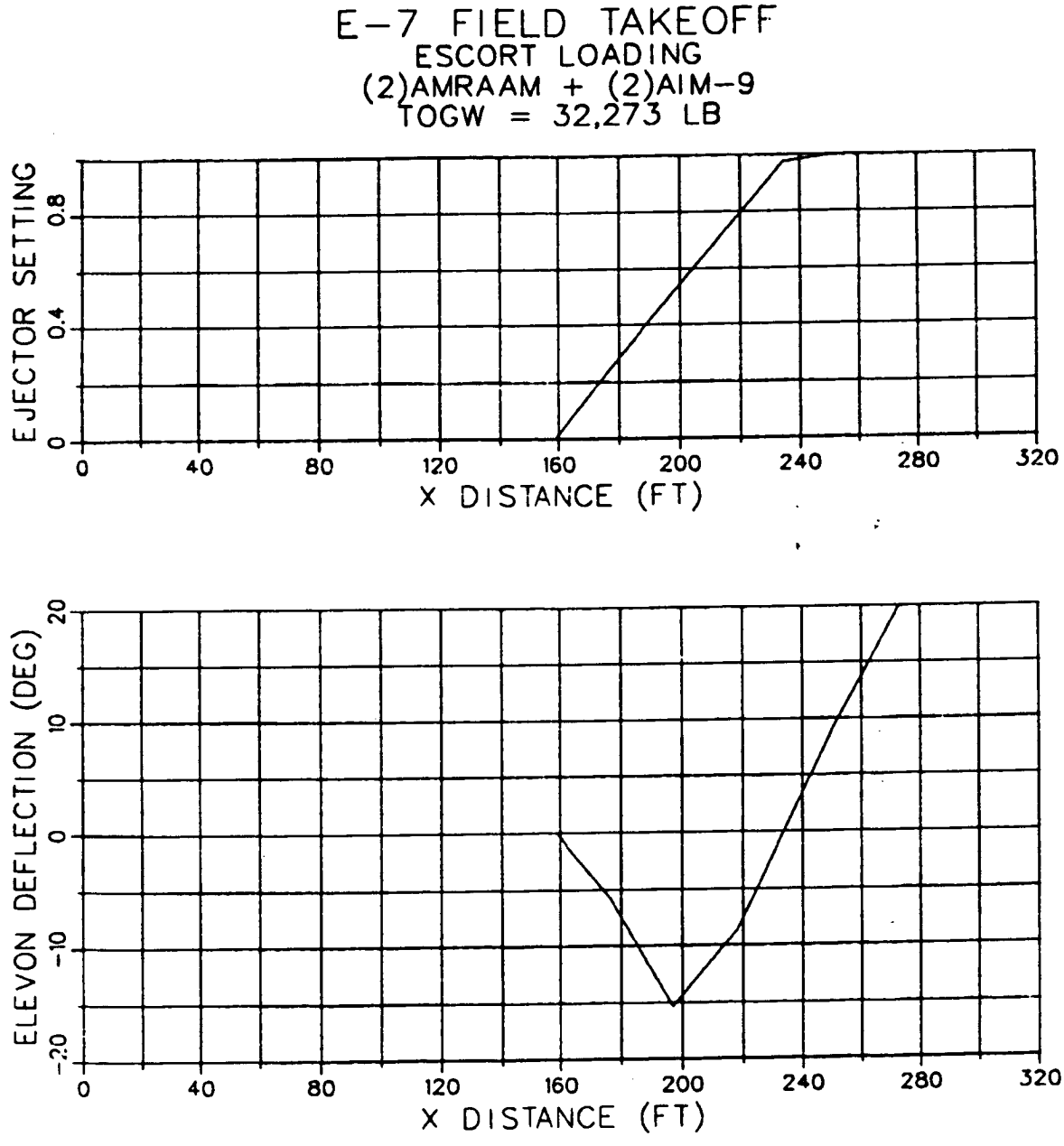

Figure D-8 All-Components Case Time Histories (Continued)

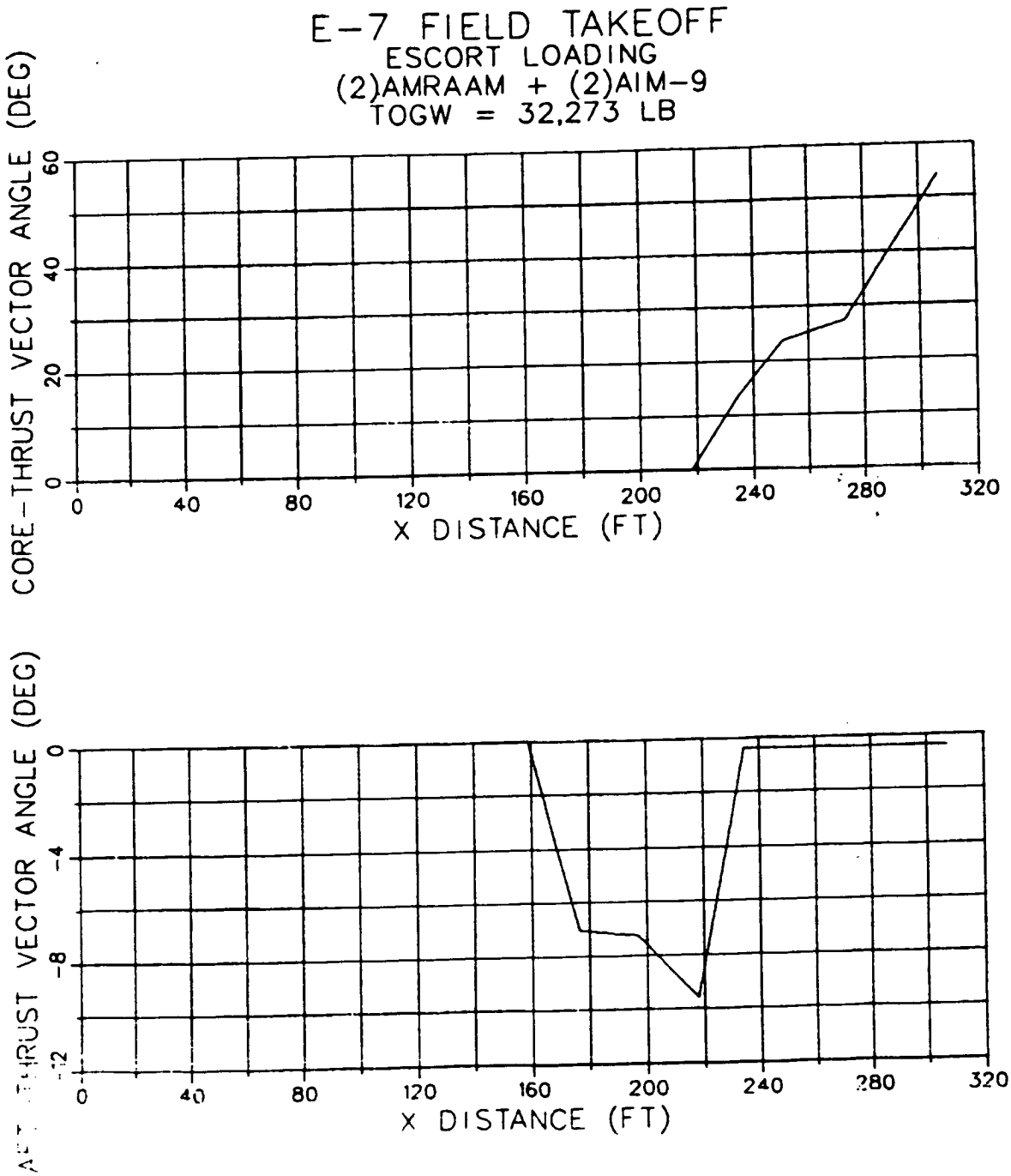

Figure D-8 All-Components Case Time Histories (Continued)

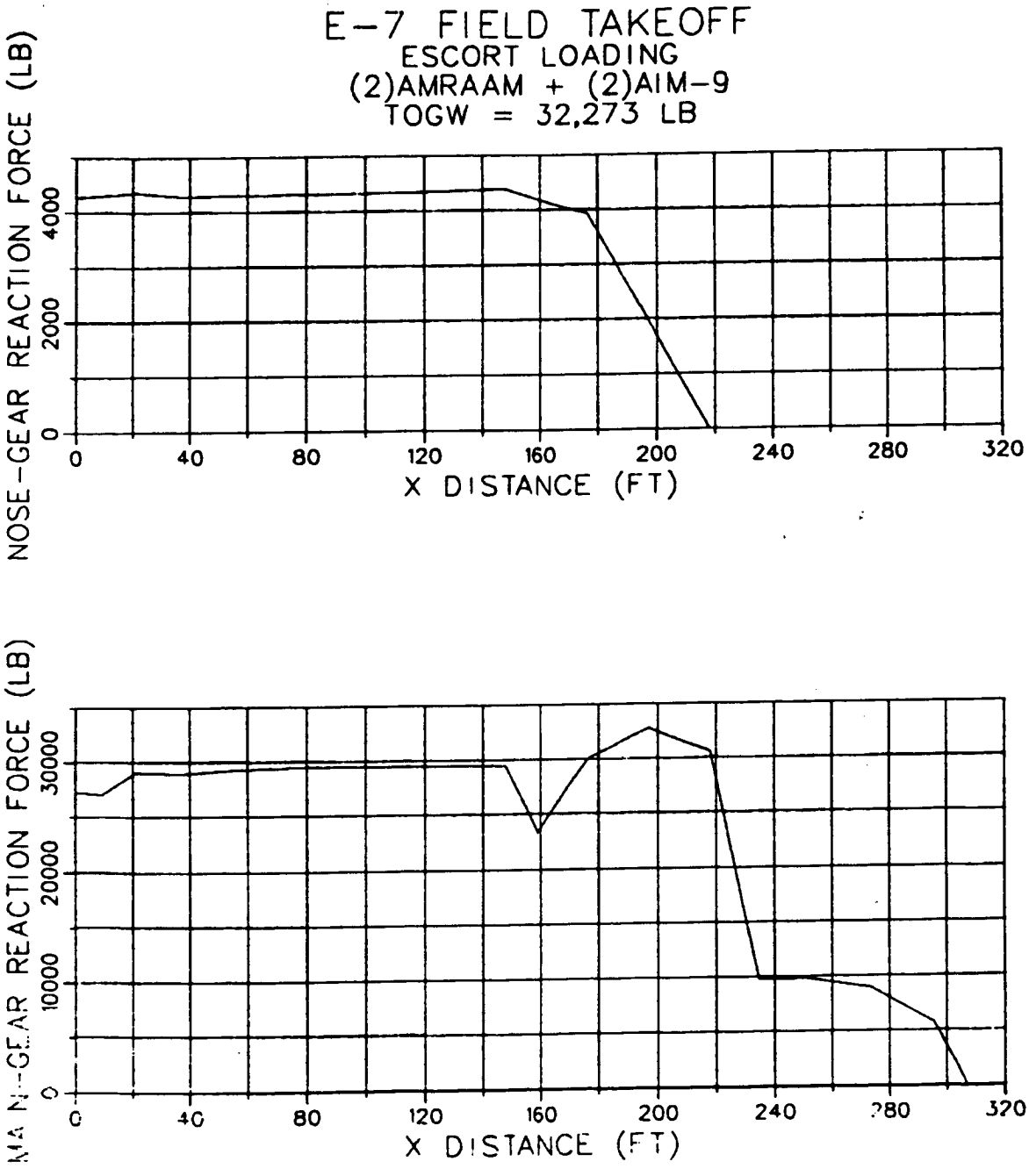

Figure D-8 All-Components Case Time Histories (Concluded)

APPENDIX E

Canard Database

Untrimmed lift coefficient is plotted in Figure E-1 as a function of angle of attack (AOA), elevon deflection, and canard deflection. Figure E-2 shows drag coefficient, including minimum drag, gear drag, and ejector-door drag, as a function of Cl, elevon, and canard. Moment coefficient is plotted as a function of Cl, elevon, and canard in Figure E-3. Ground-effect increments of all three coefficients at a sigma of 0.254 (h/b = 0.231) are plotted versus AOA in Figure E-4. Ground-effect data is interpolated on sigma as described in Section 2.

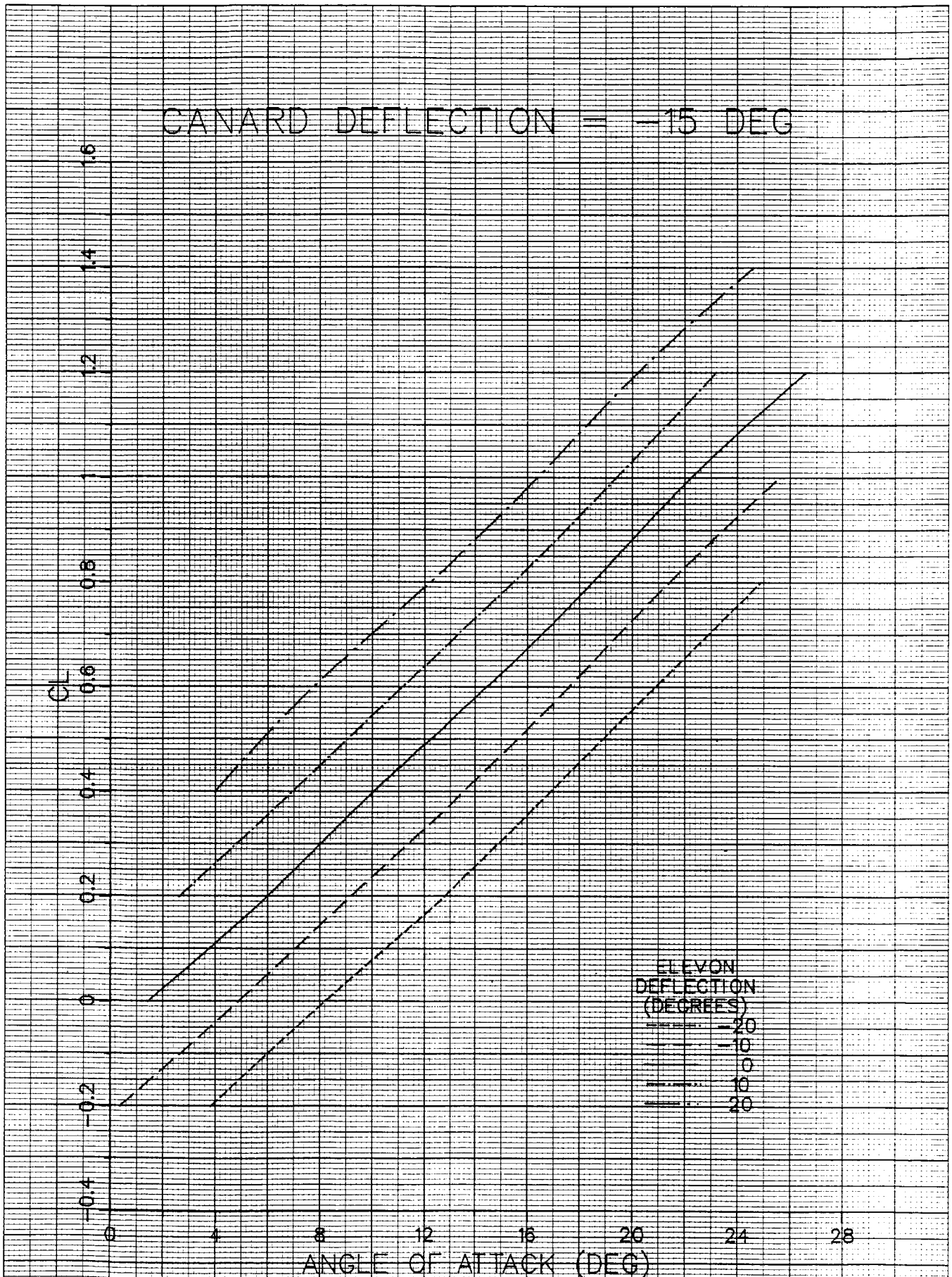

Figure E-1 Canard-Data Lift Curves

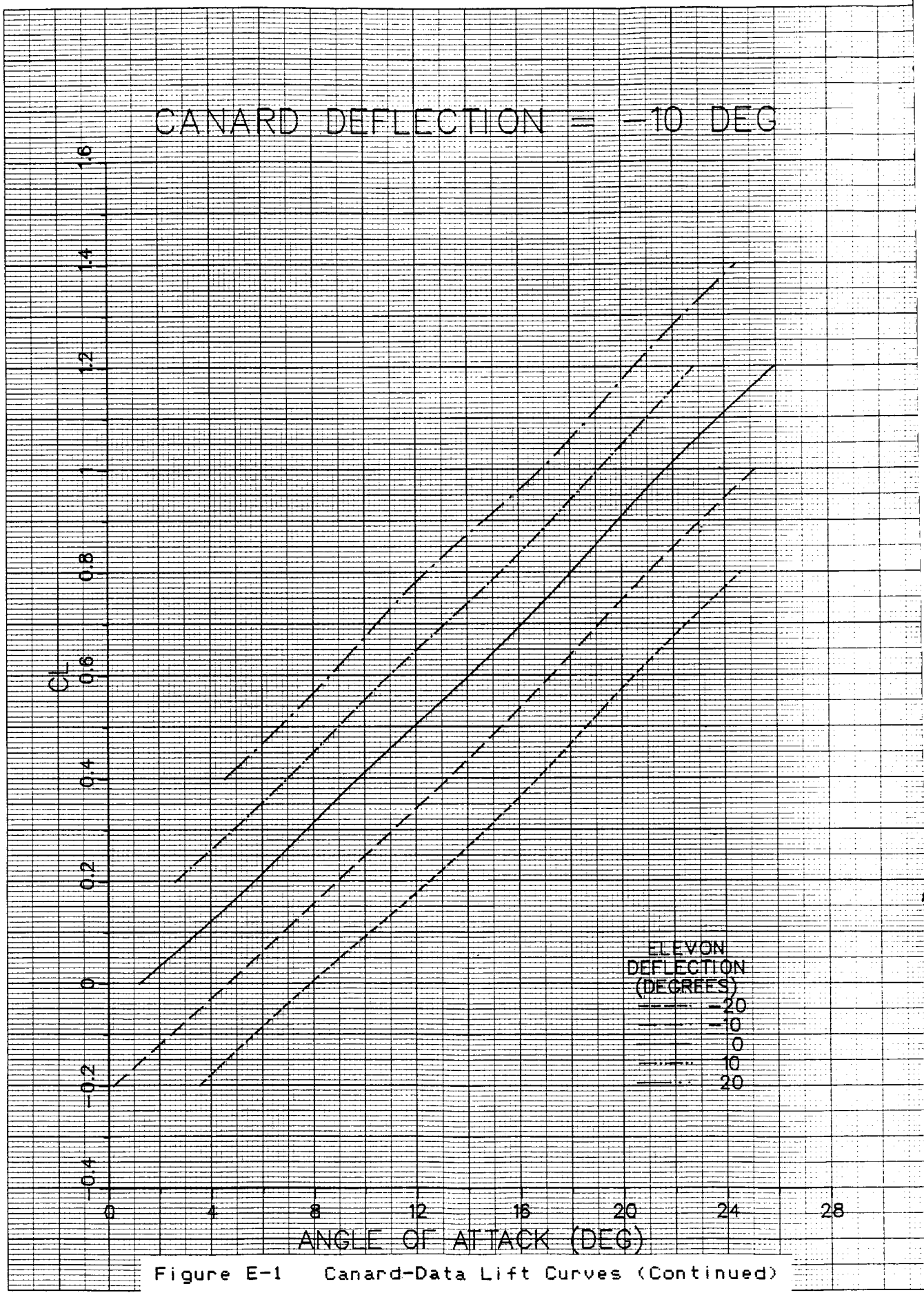

Figure E-1 Canard-Data Lift Curves (Continued)

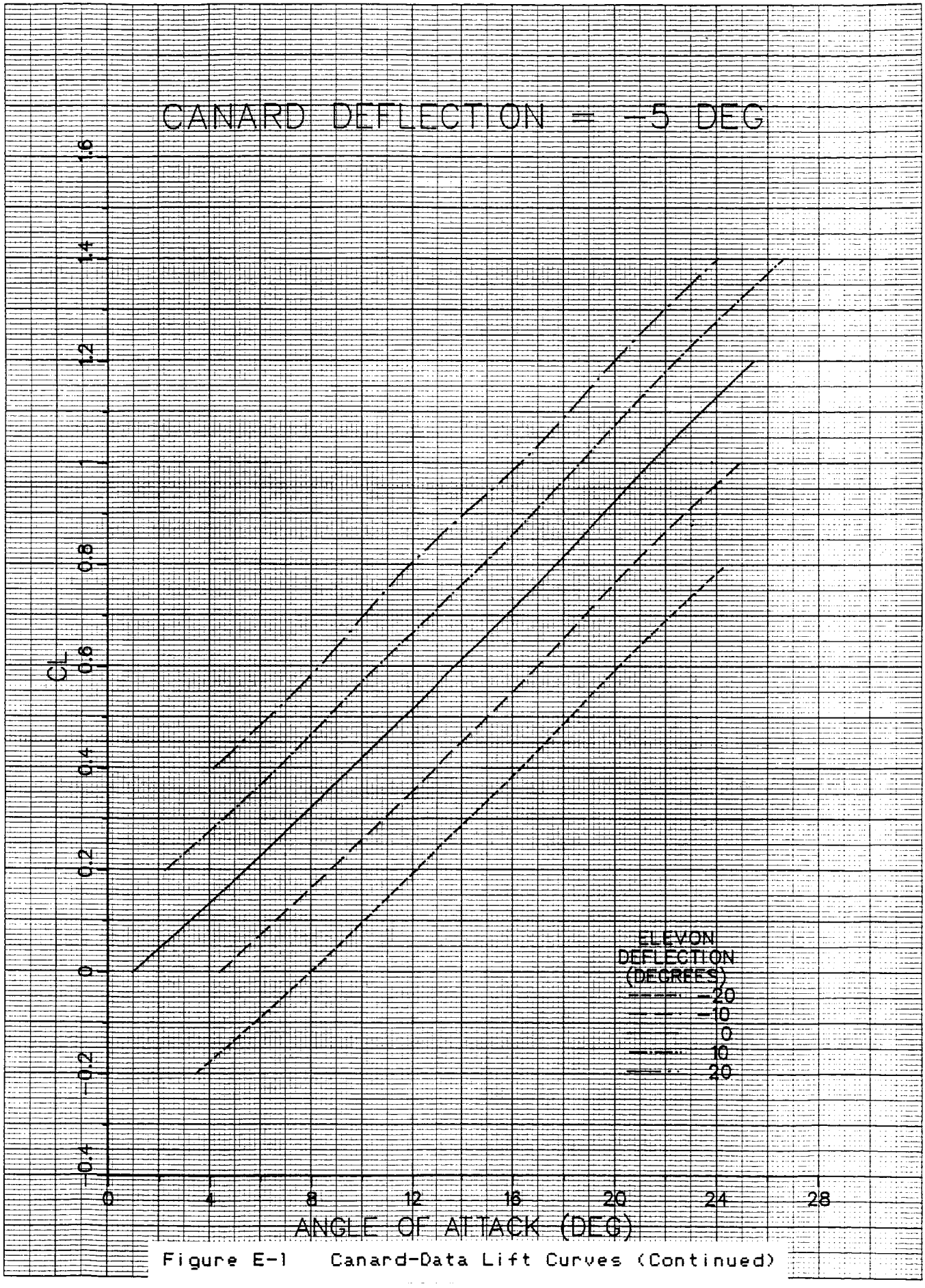

Figure E-1 Canard-Data Lift Curves (Continued)

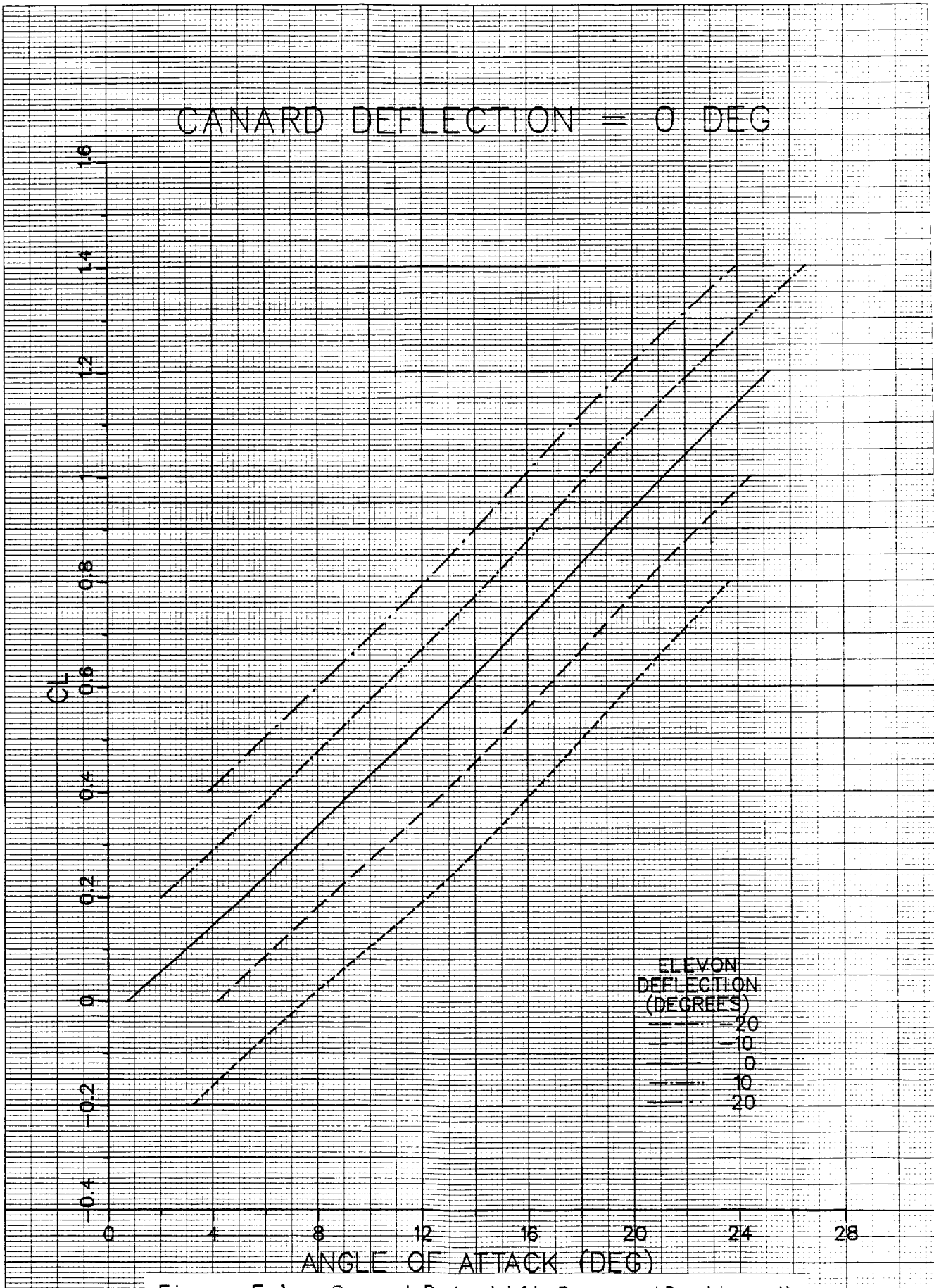

Figure E-1 Canard-Data Lift Curves (Continued)

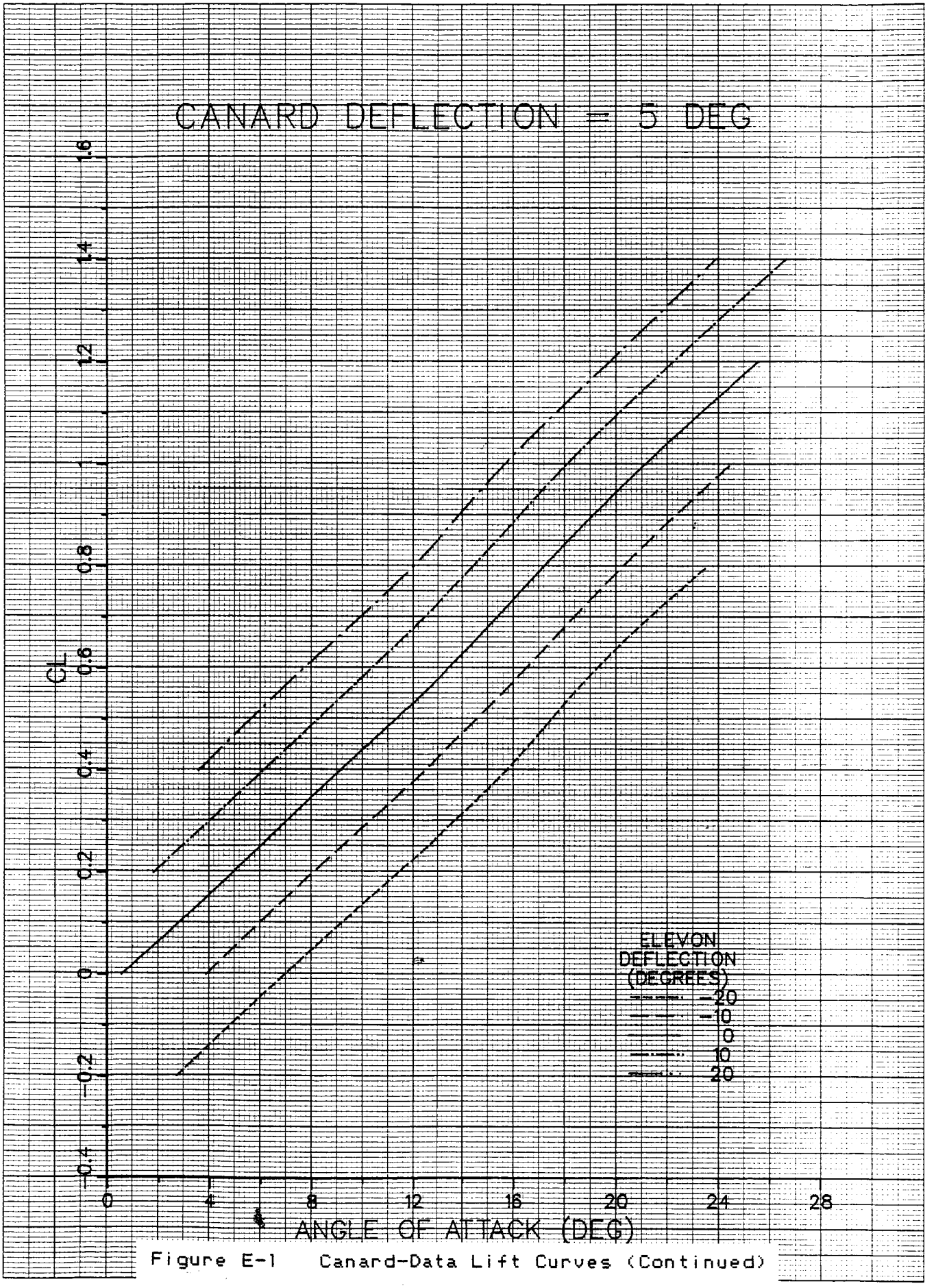

Figure E-1 Canard-Data Lift Curves (Continued)

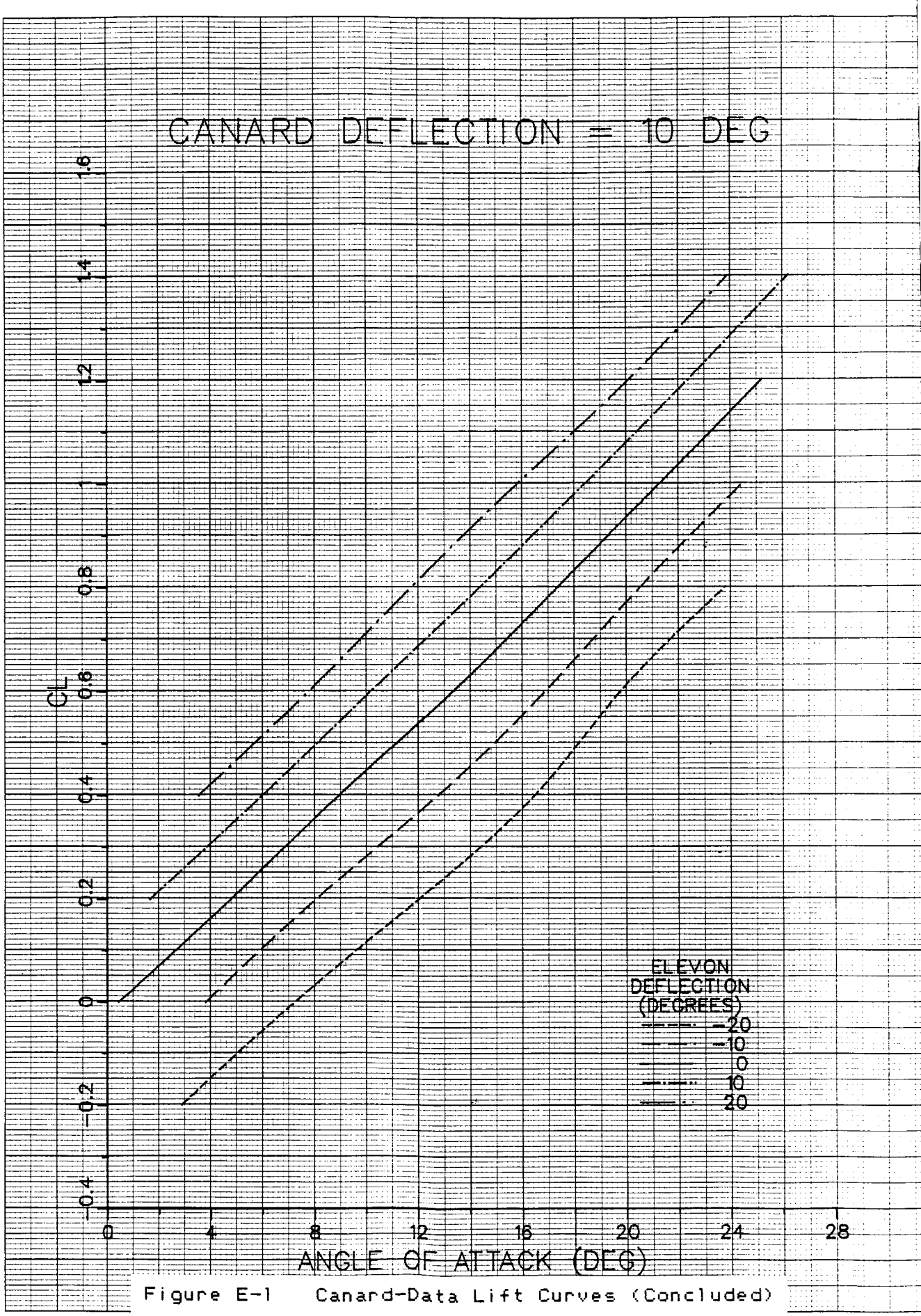

Figure E-1 Canard-Data Lift Curves (Concluded)

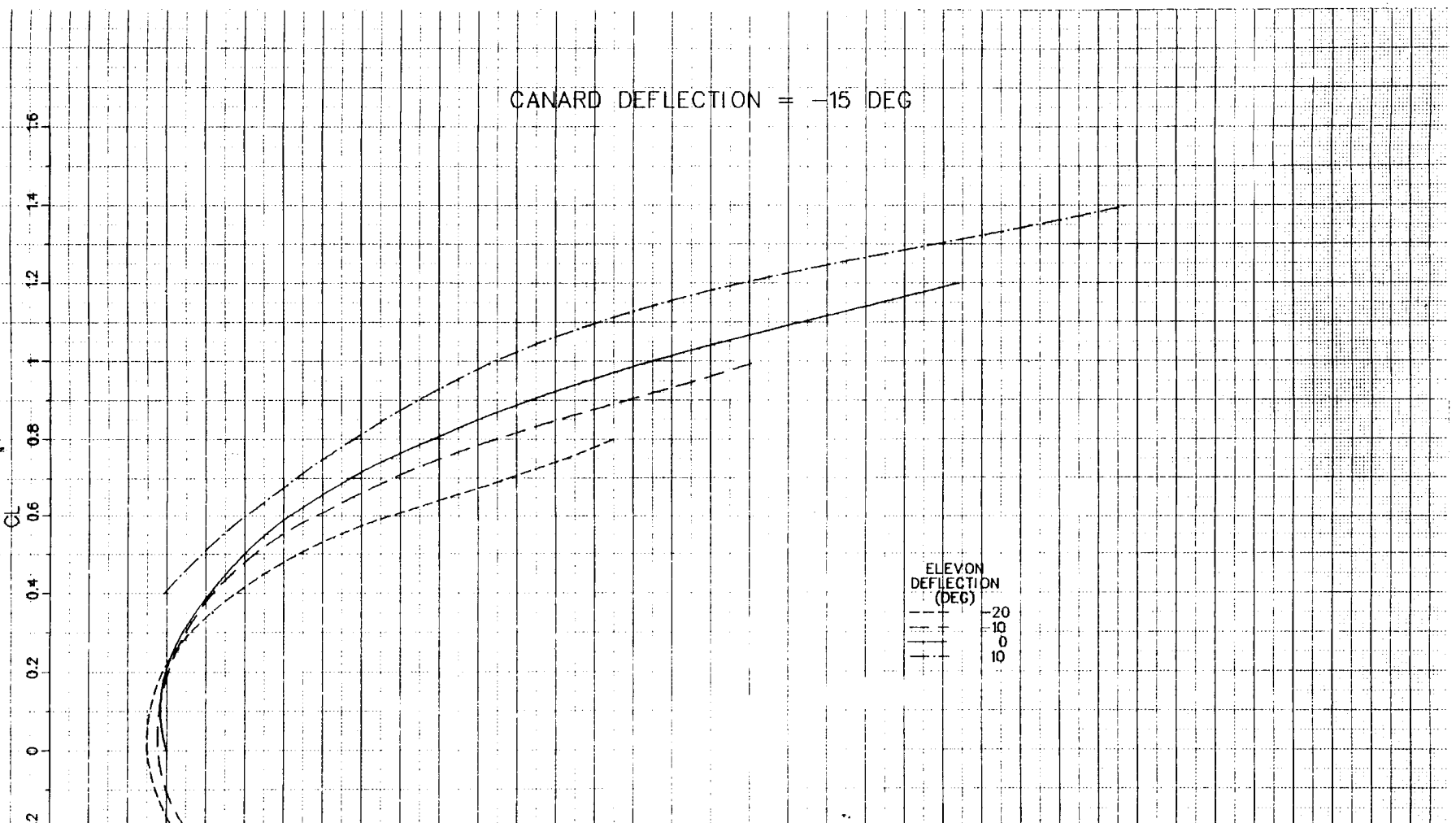

Figure E-2 Canard-Data Drag Polars

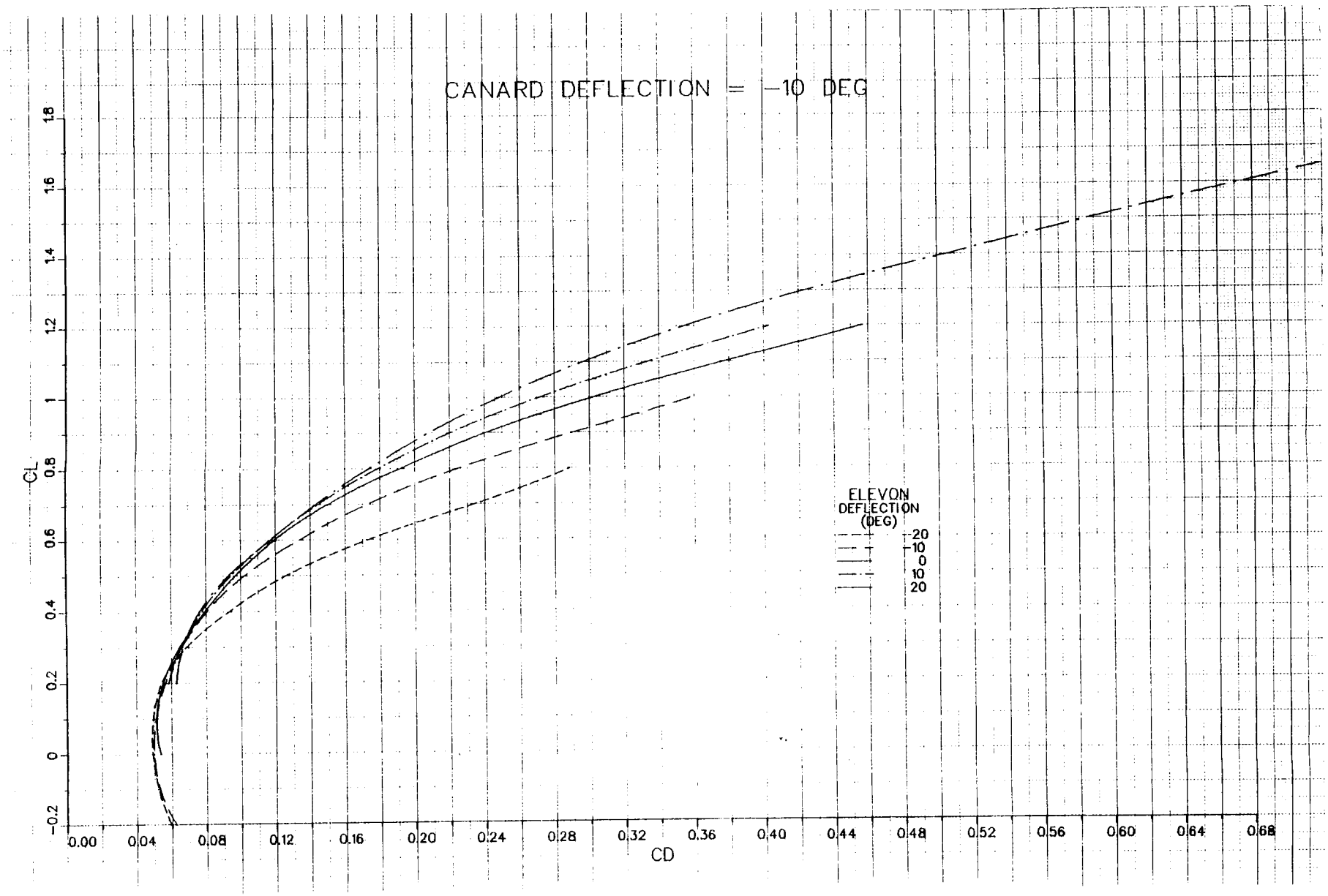

Figure E-2 Canard-Data Drag Polars (Continued)

Figure E-2 Canard-Data Drag Polars (Continued)

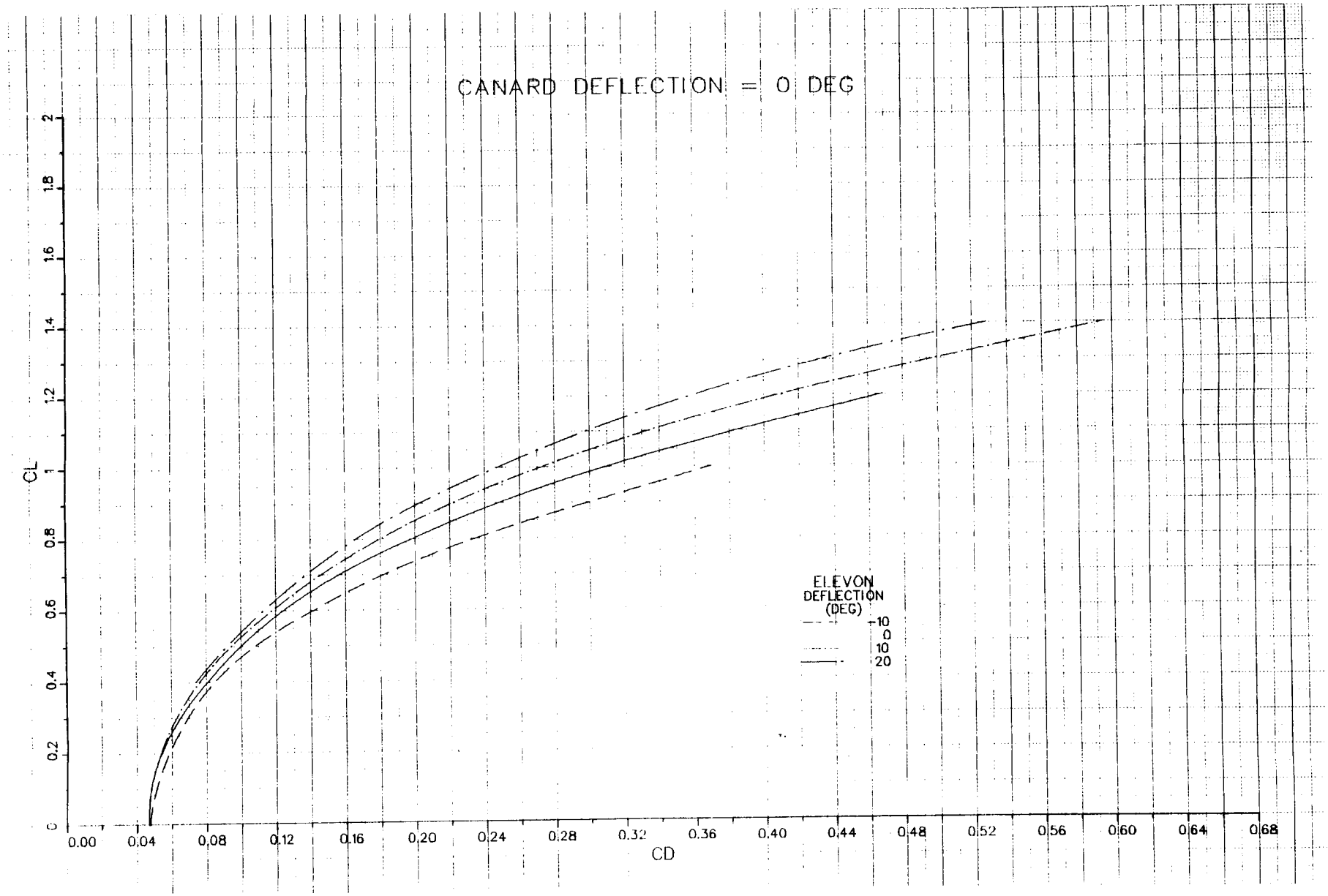

Figure E-2 Canard-Data Drag Polars (Continued)

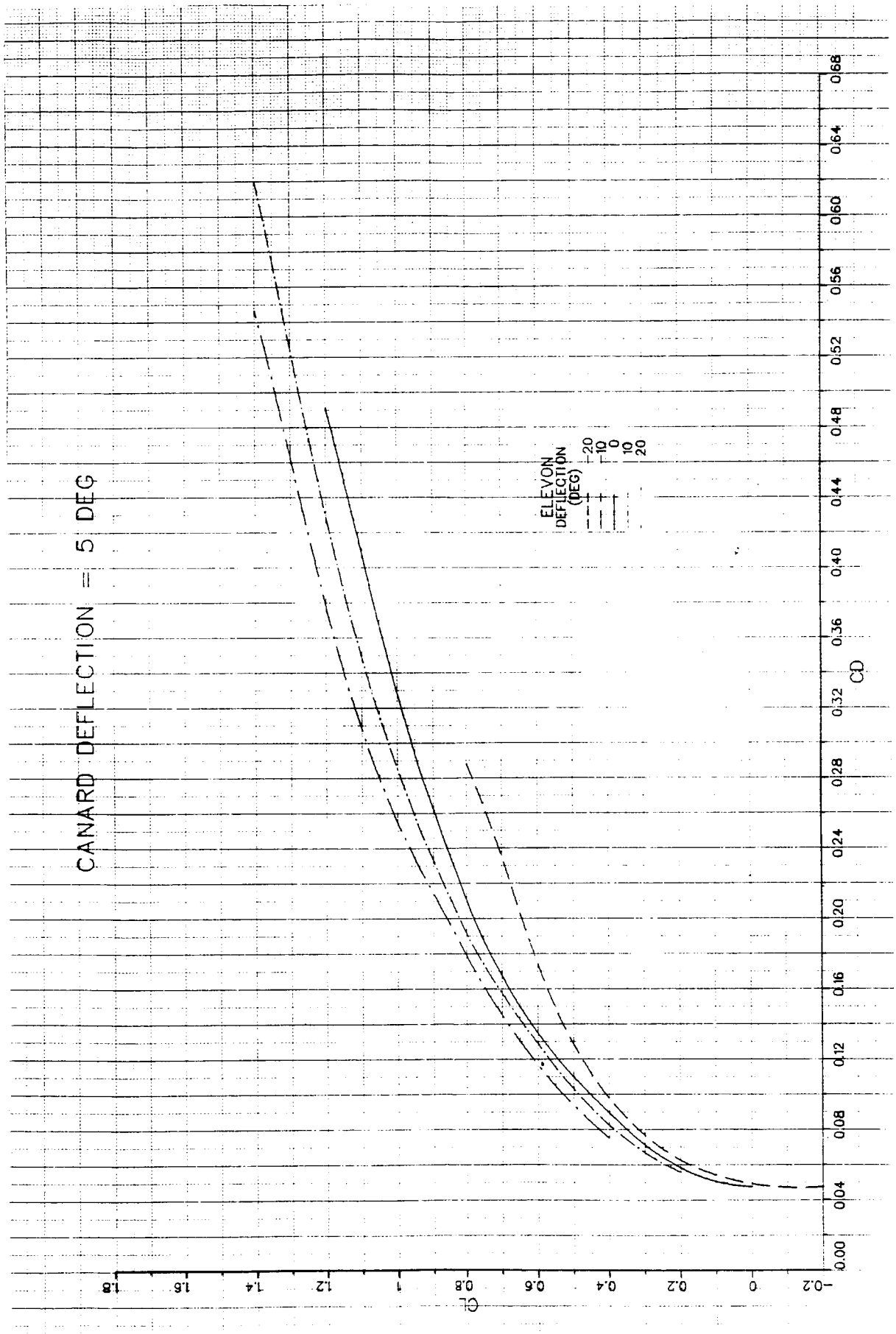

Figure E-2 Canard-Data Drag Polars (Continued)

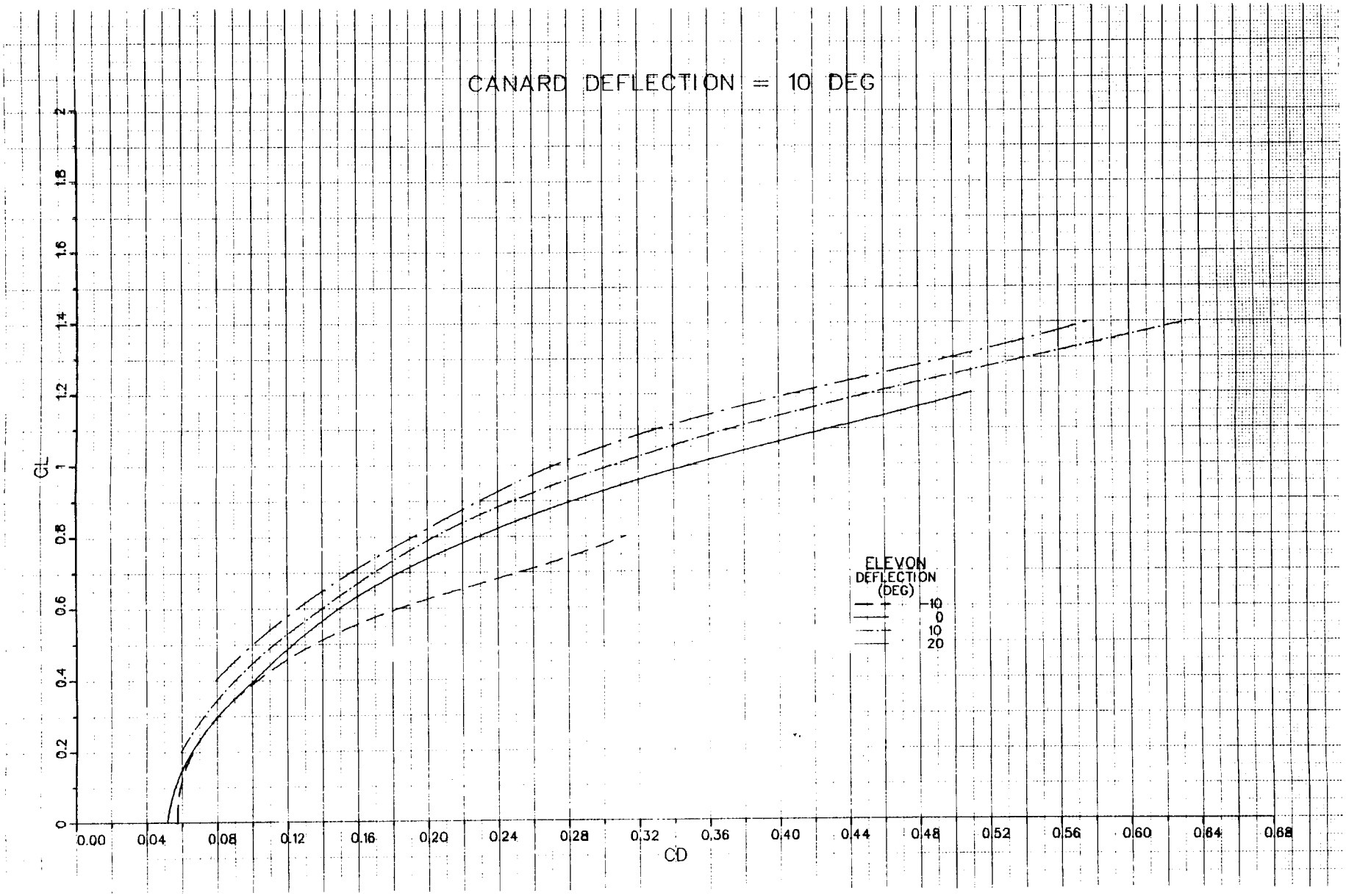

Figure E-2 Canard-Data Drag Polars (Concluded)

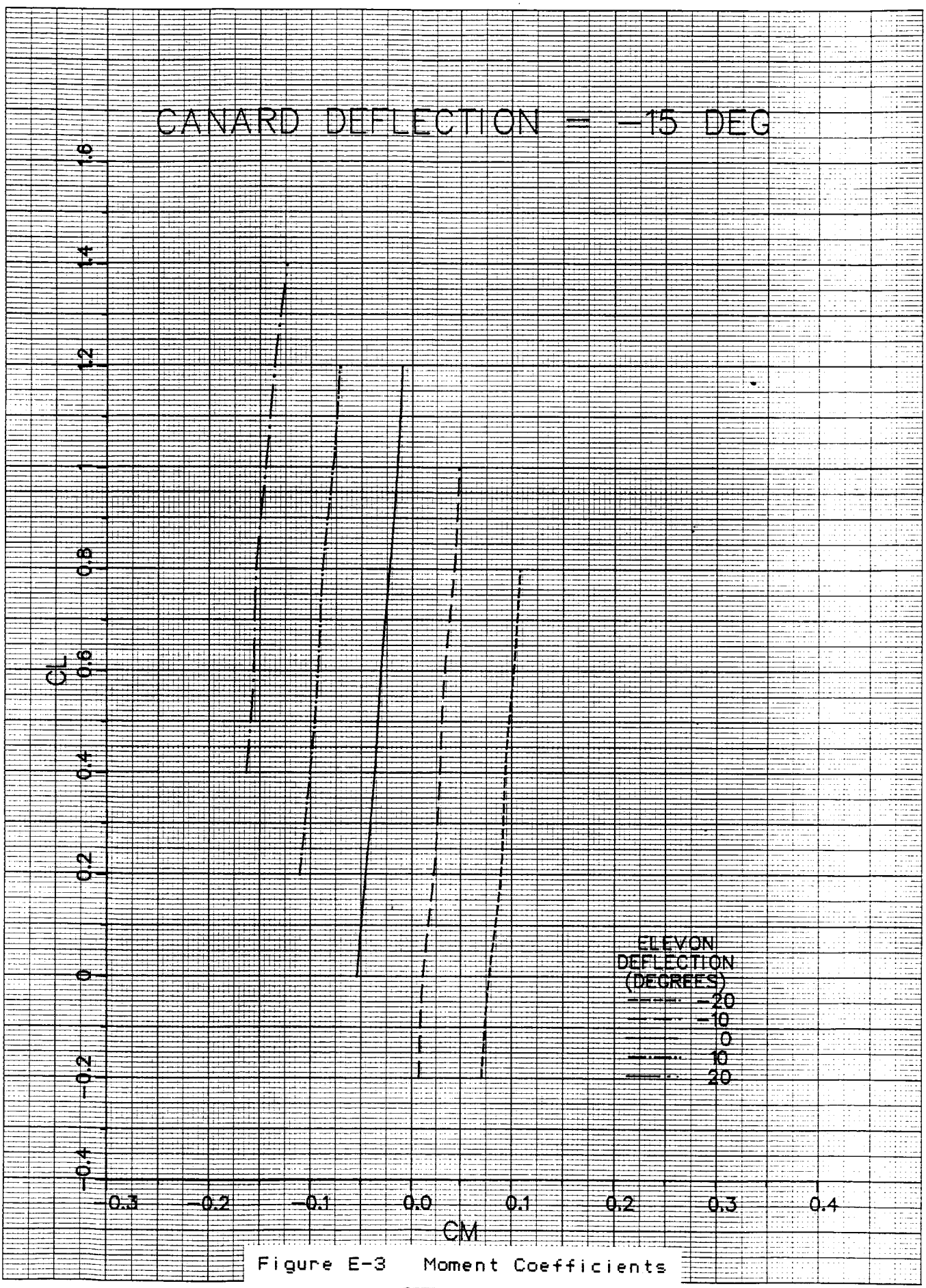

Figure E-3 Moment Coefficients

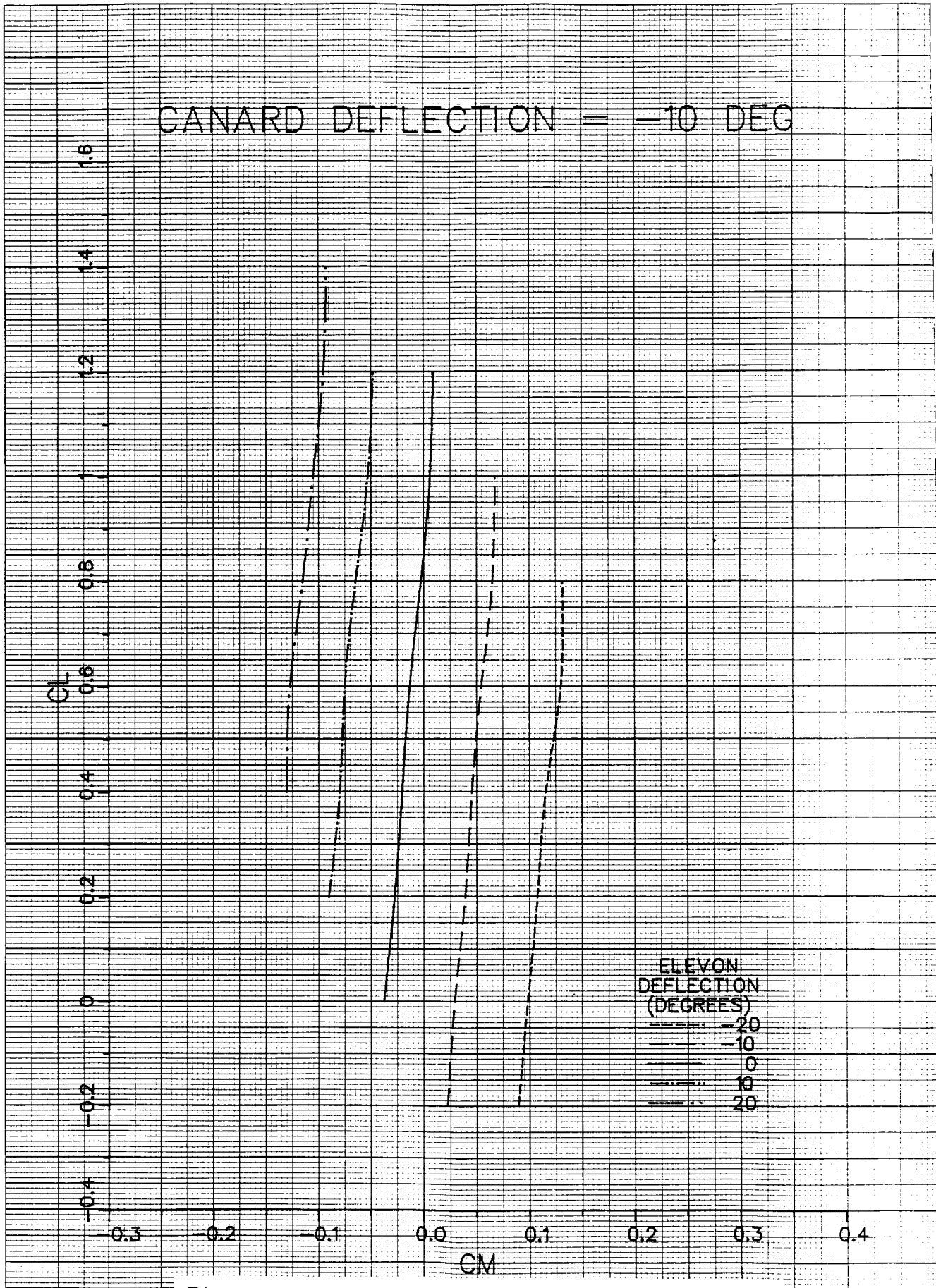

Figure E-3 Moment Coefficients (Continued)

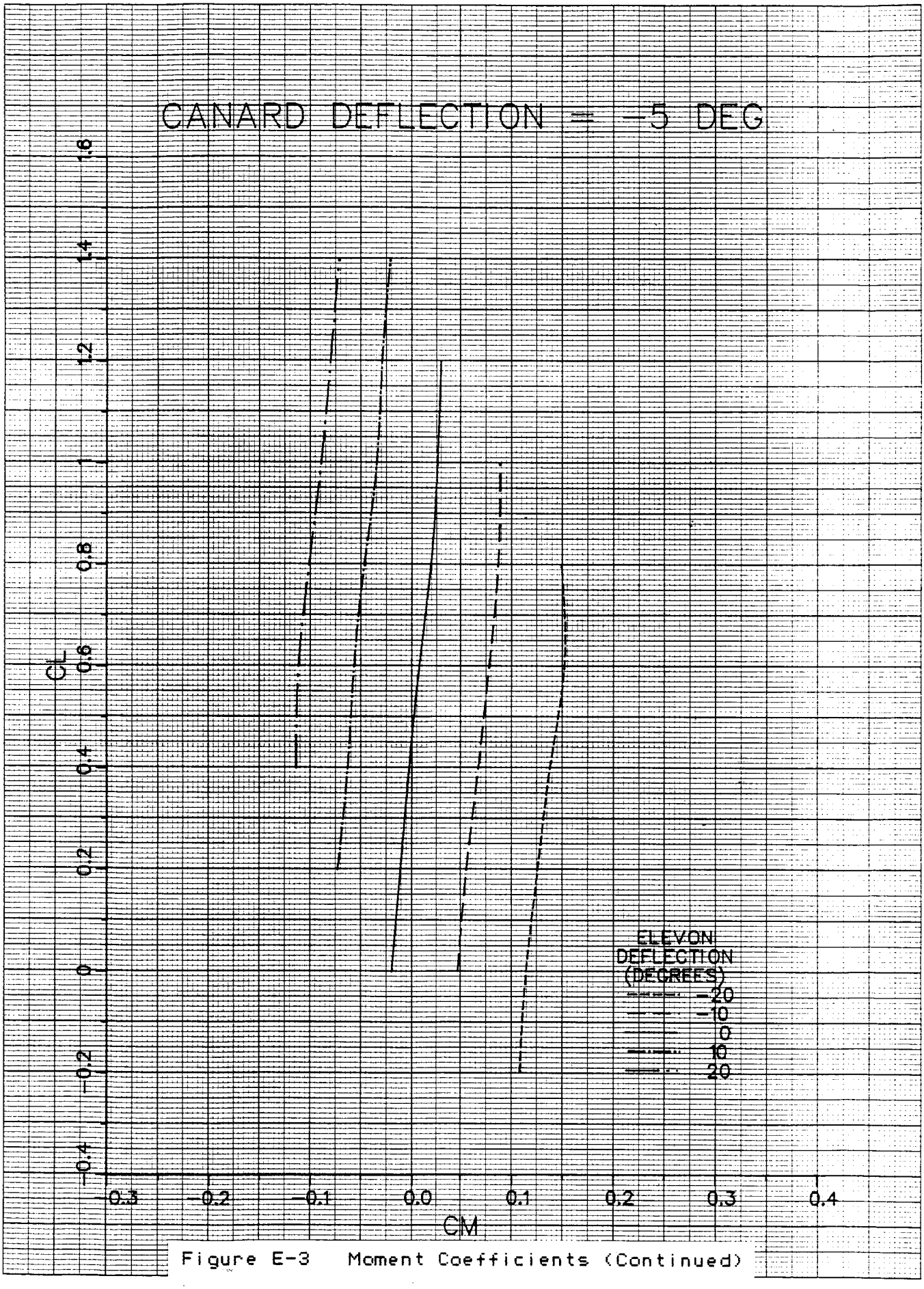

Figure E-3 Moment Coefficients (Continued)

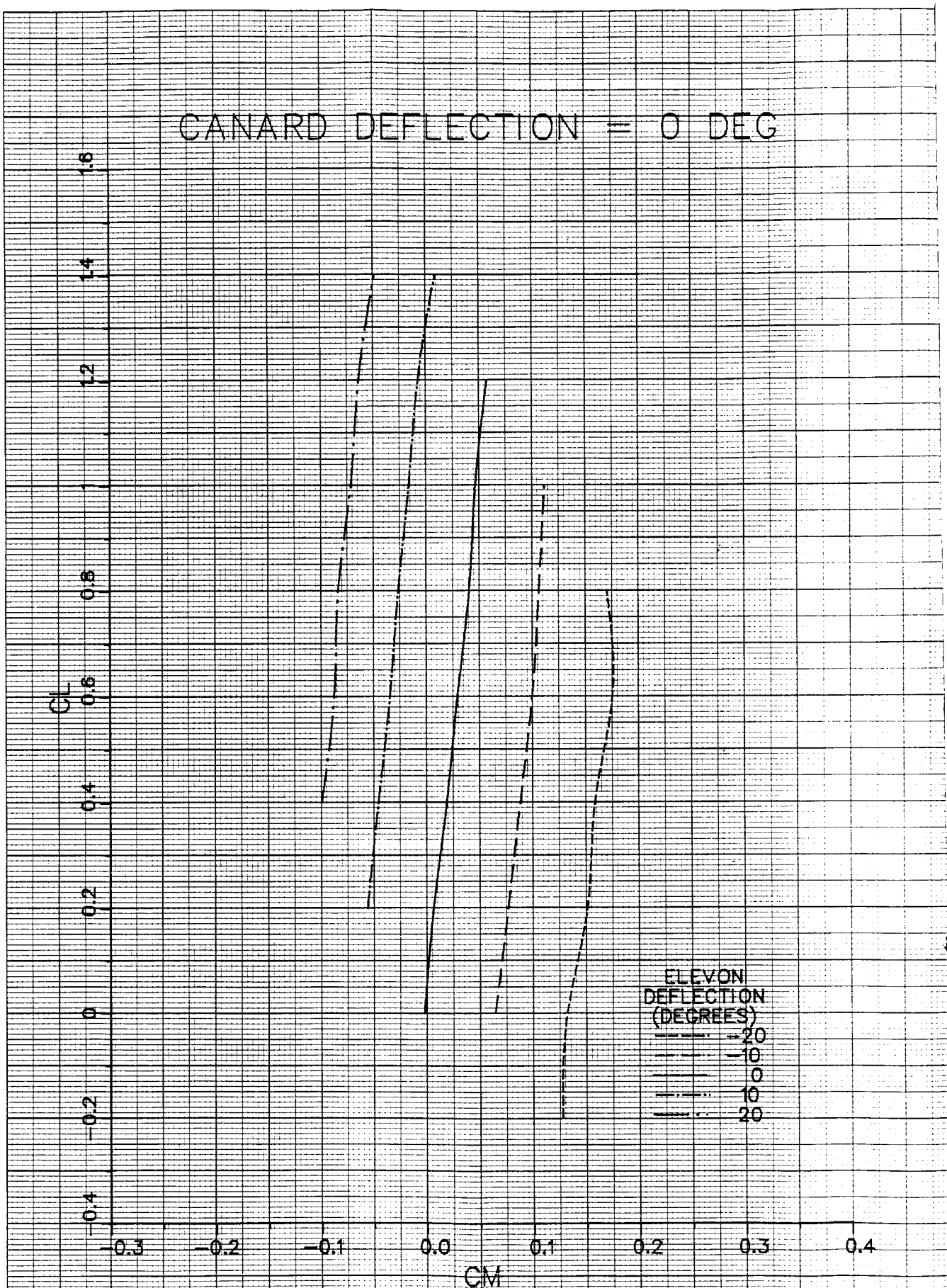

Figure E-3 Moment Coefficients (Continued)

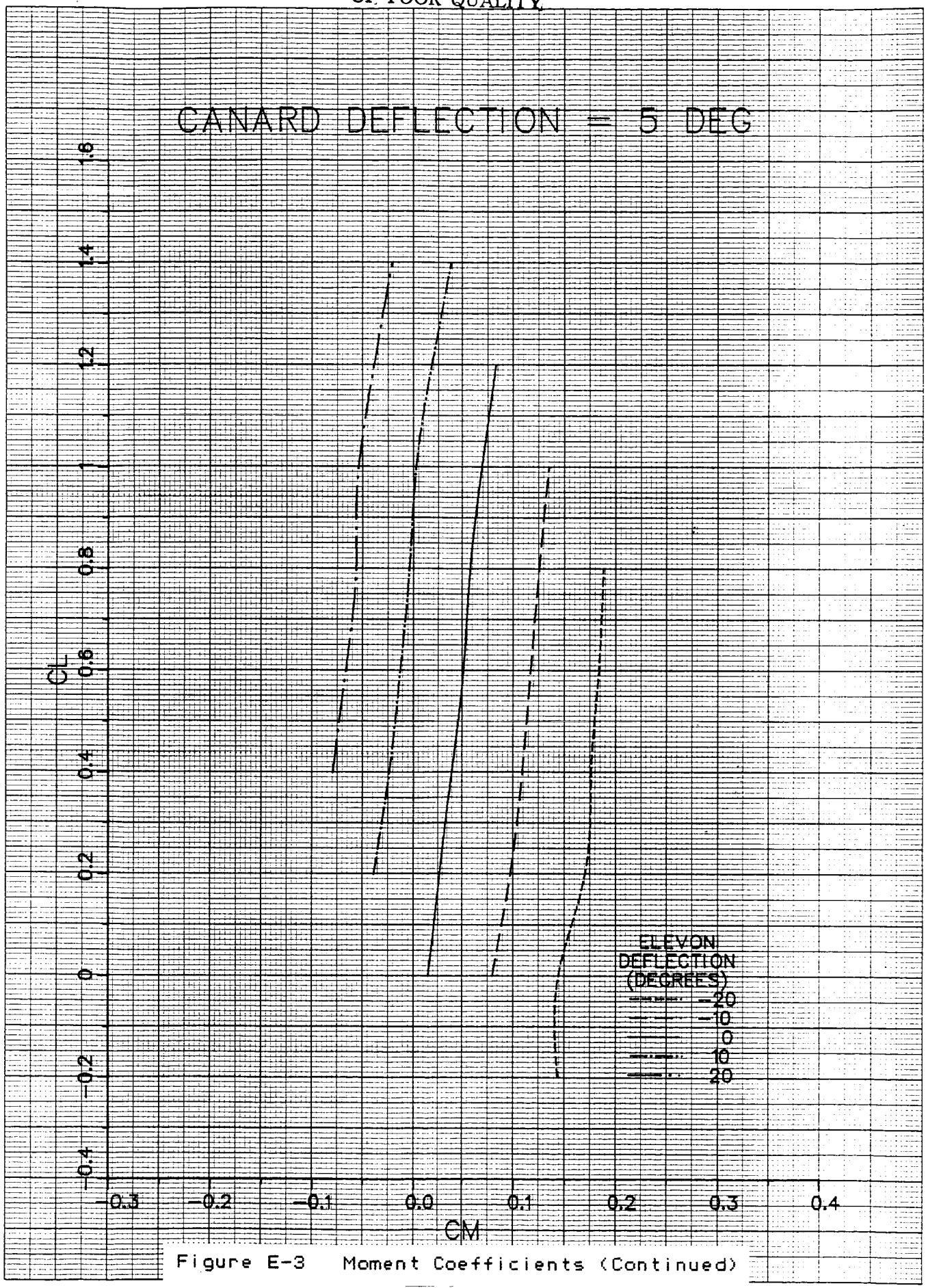

Figure E-3 Moment Coefficients (Continued)

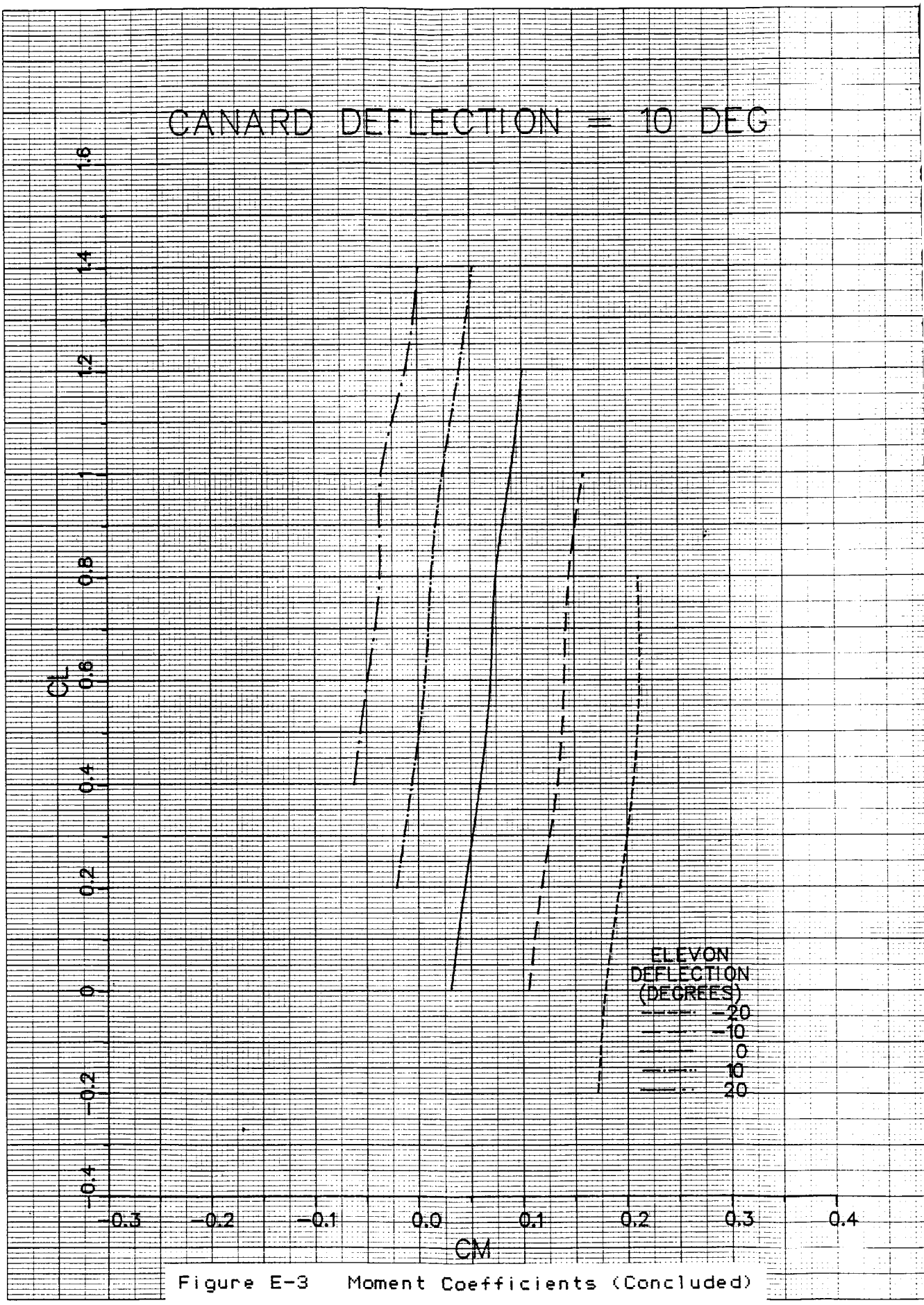

Figure E-3 Moment Coefficients (Concluded)

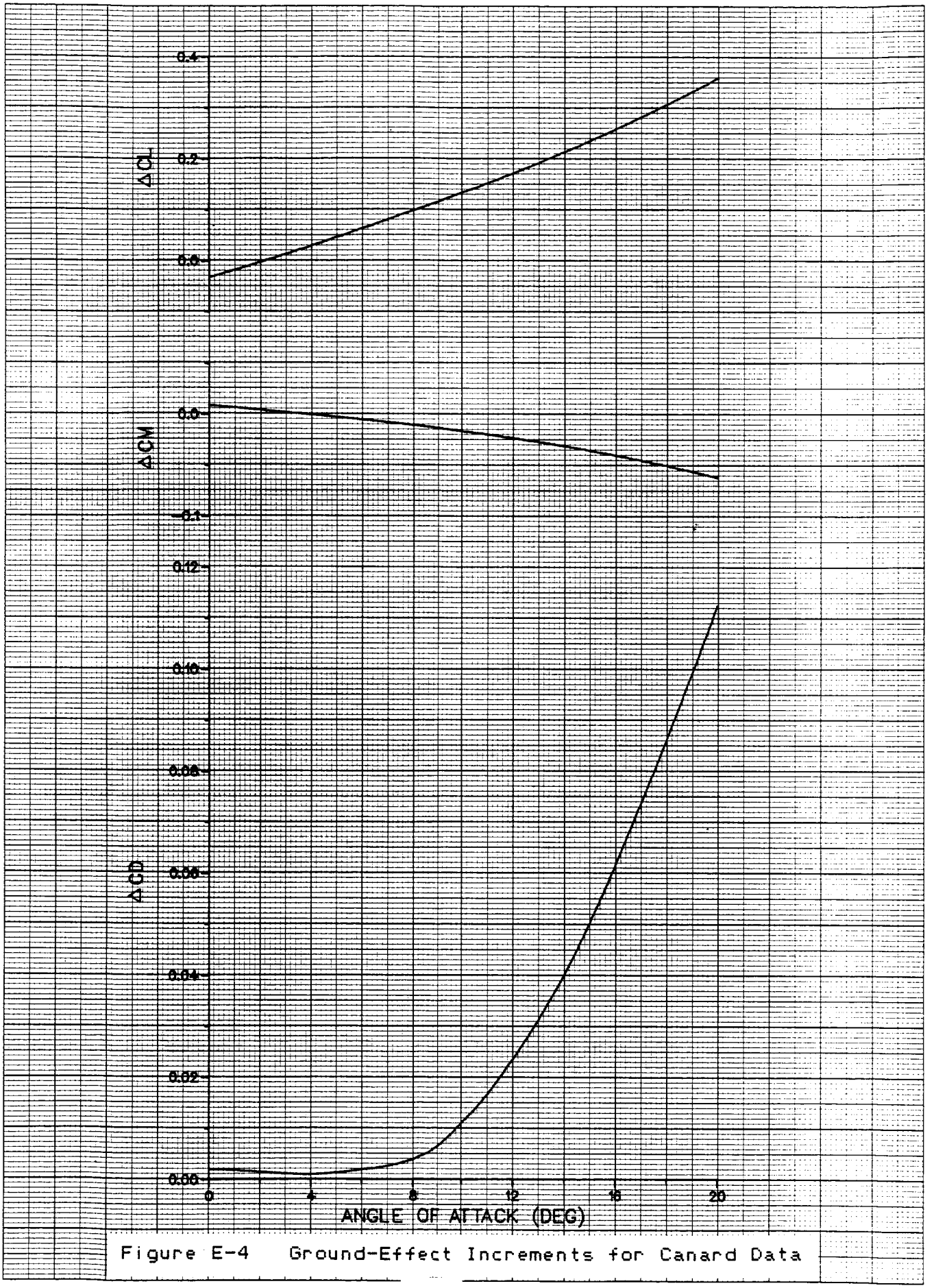

Figure E-4 Ground-Effect Increments for Canard Data

APPENDIX F

Canard Takeoff Histories

Figure F-1 shows time-history plots of pertinent parameters for E-7 with a close-coupled canard performing a carrier takeoff at STO weight.

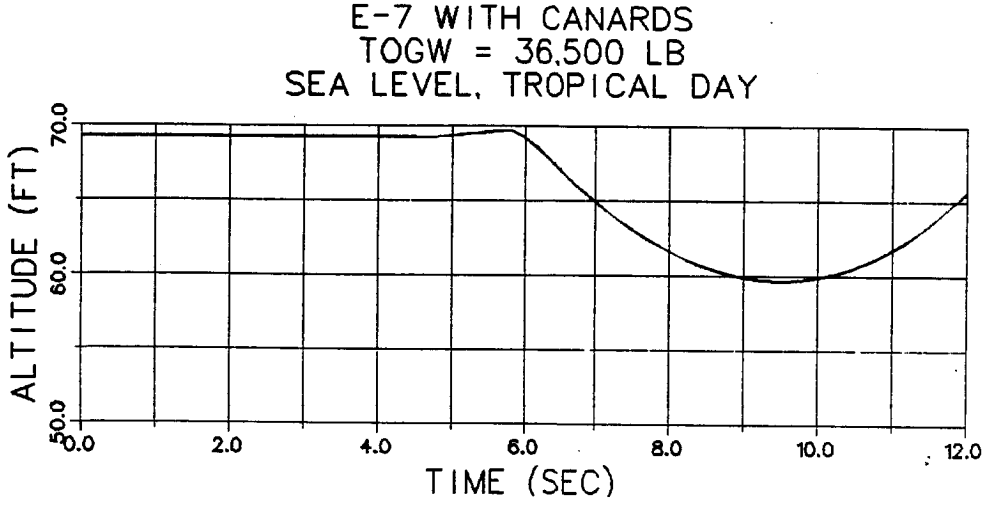

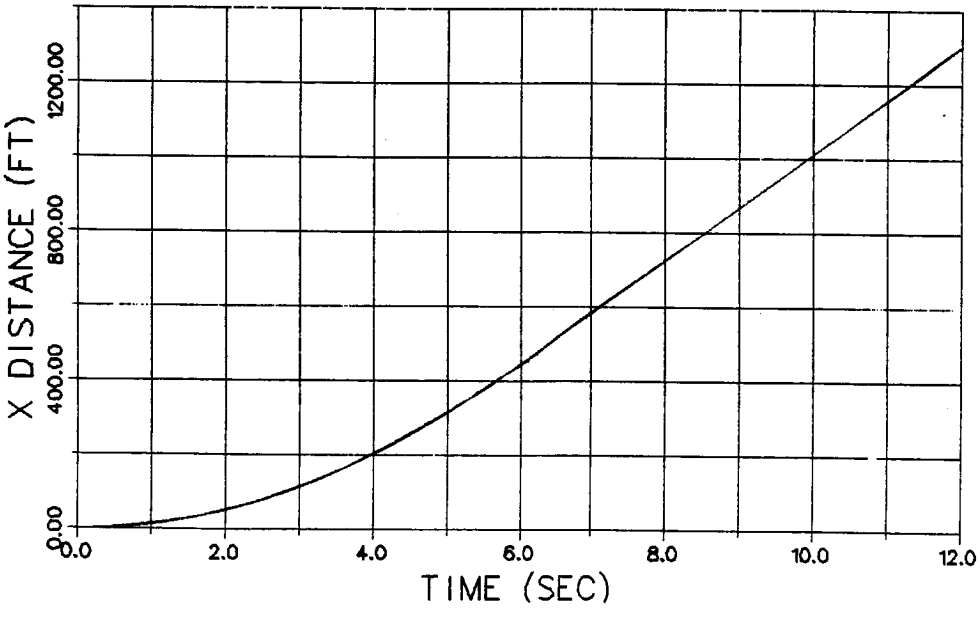

Figure F-1 Canard-Configuration Time History

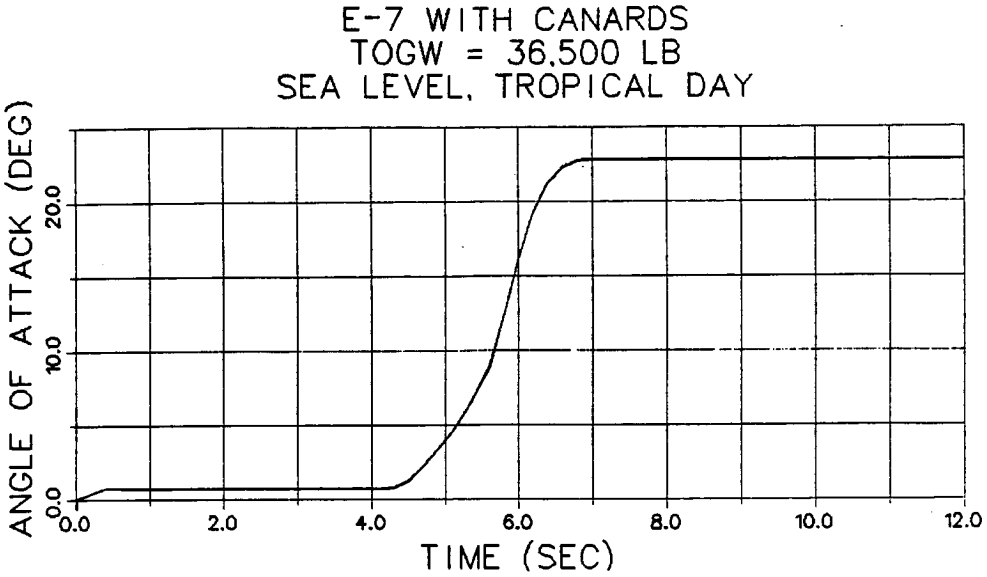

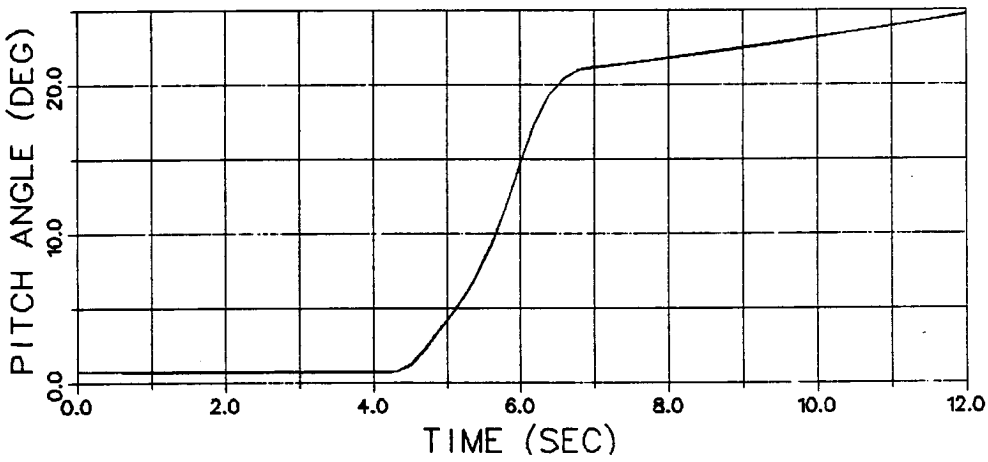

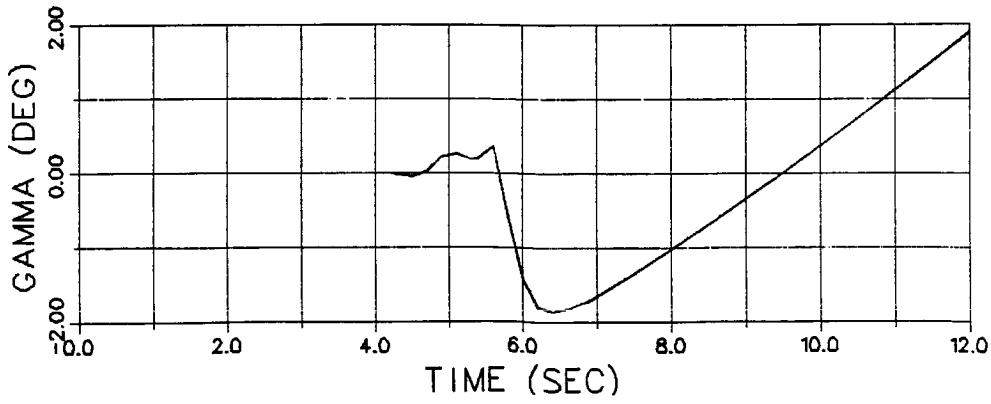

Figure F-1 Canard-Configuration Time History (Continued)

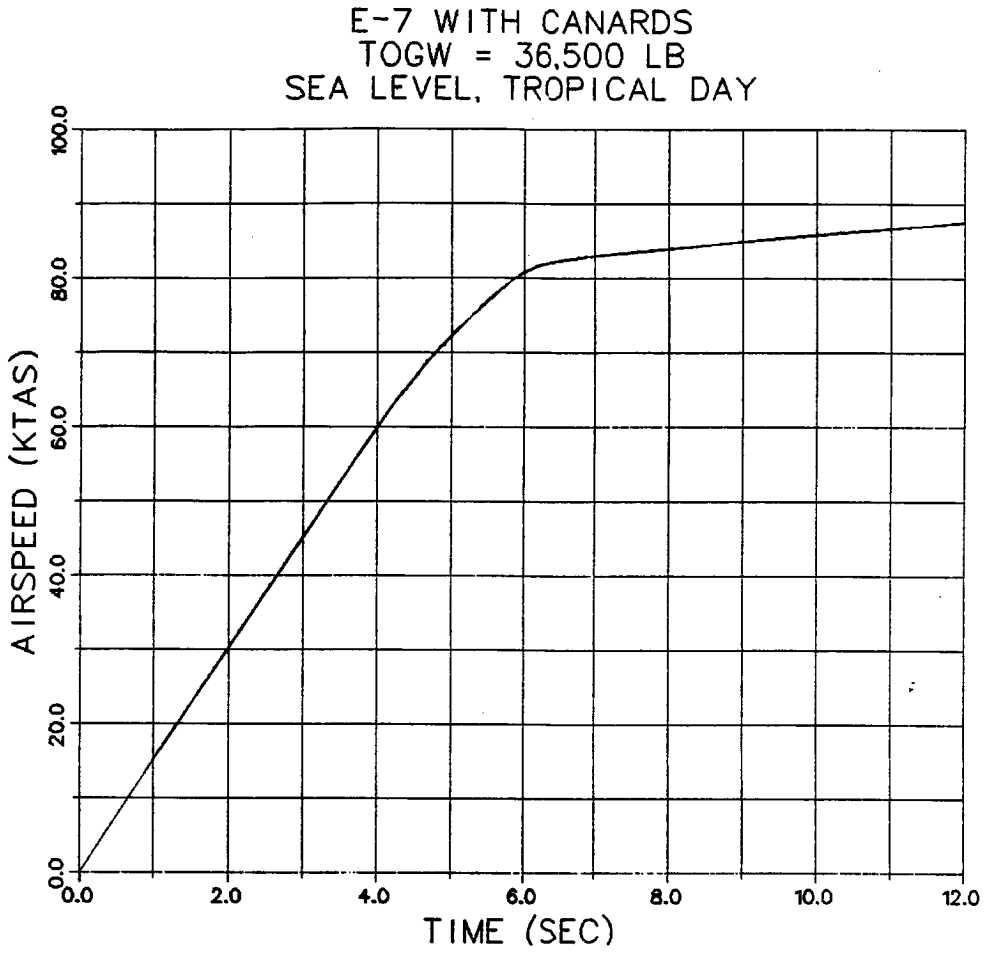

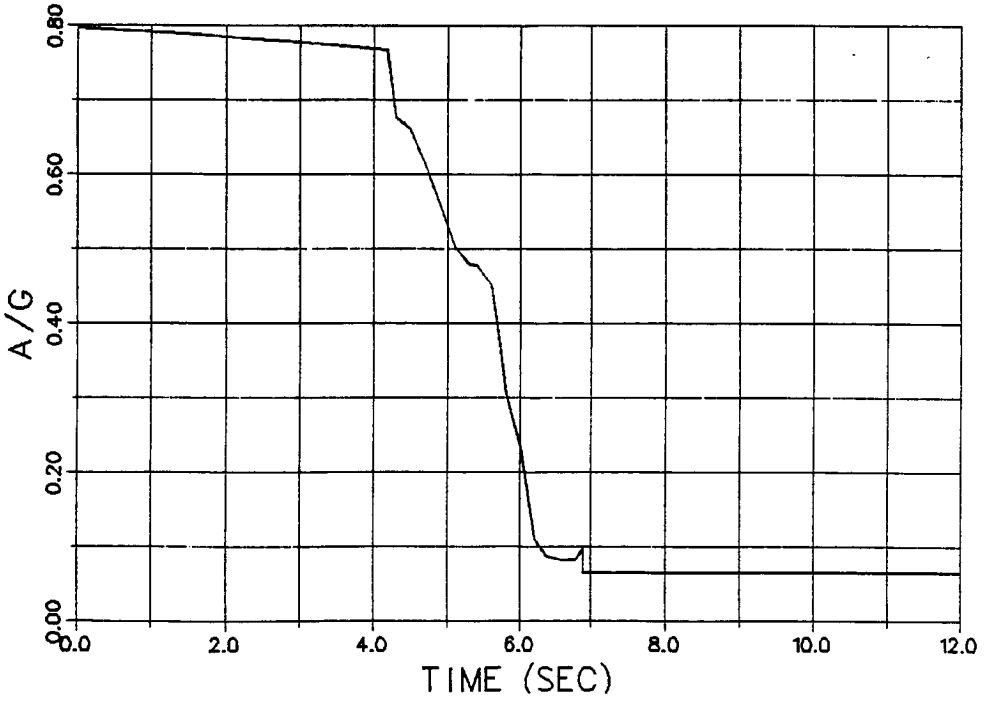

Figure F-1 Canard-Configuration Time History (Continued)

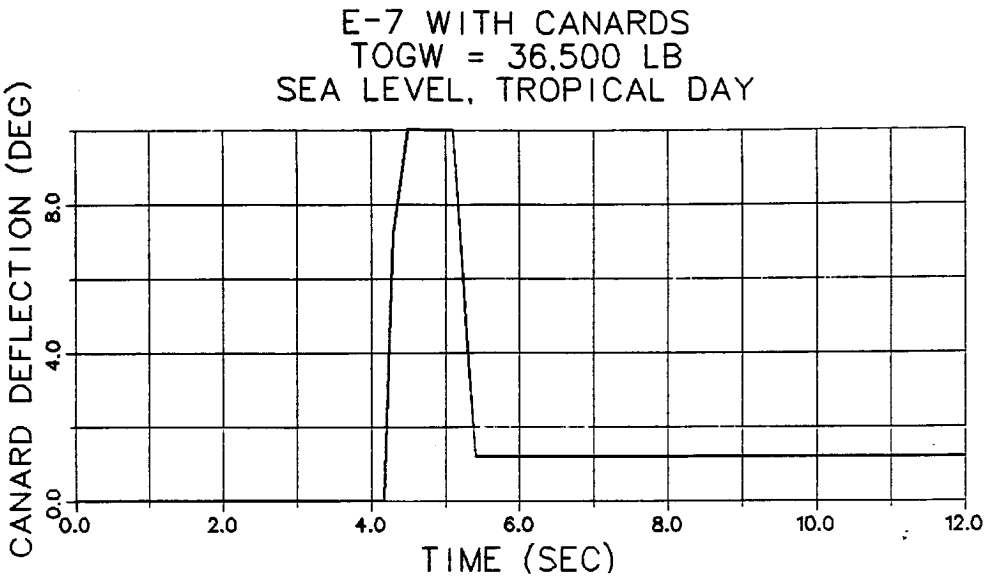

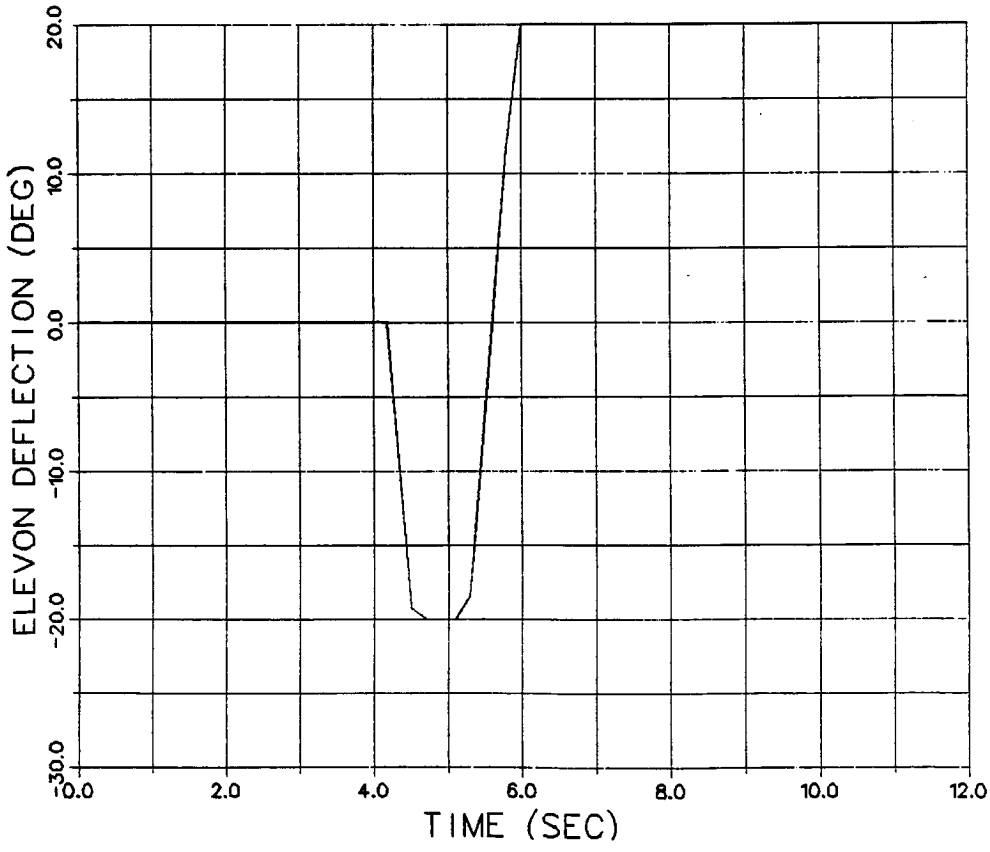

Figure F-1 Canard-Configuration Time History (Continued)

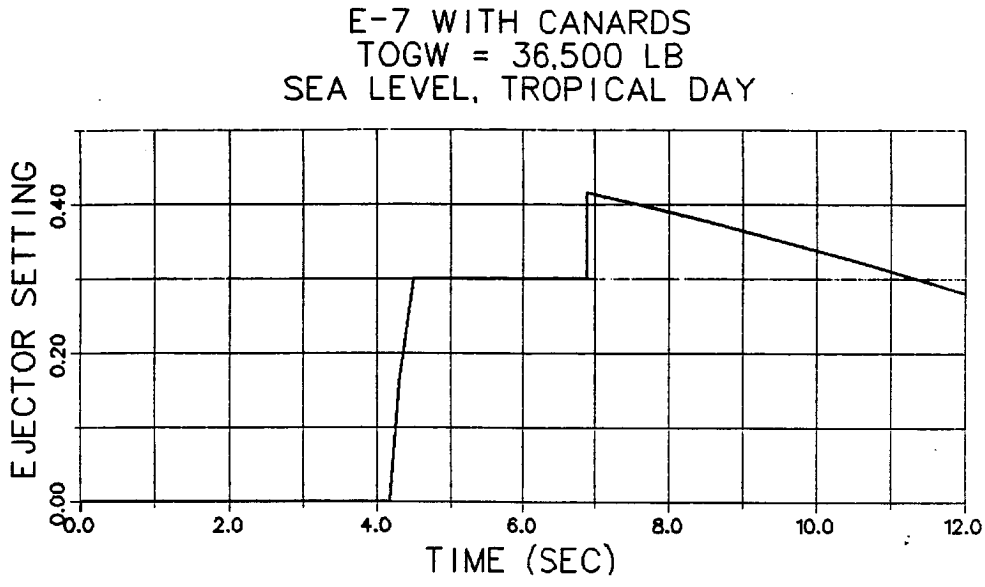

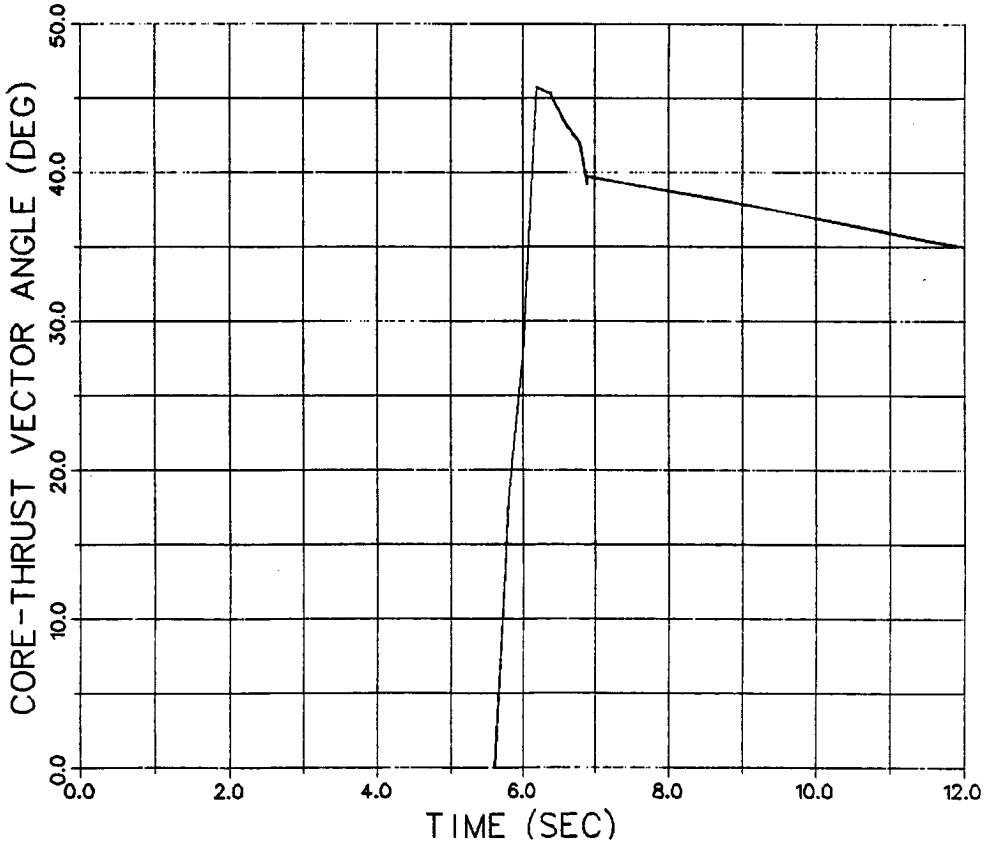

Figure F-1 Canard-Configuration Time History (Continued)

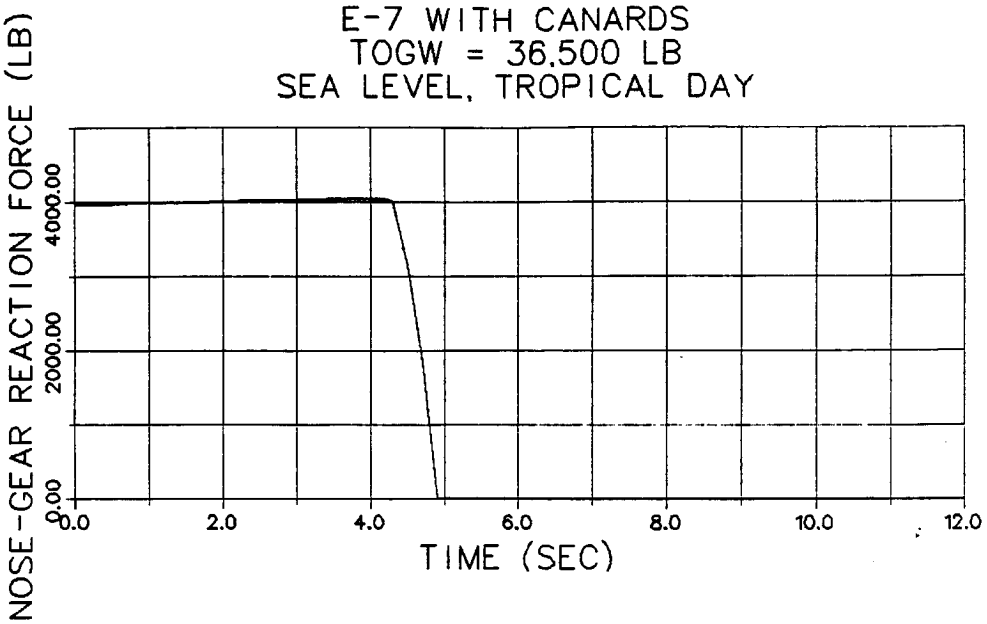

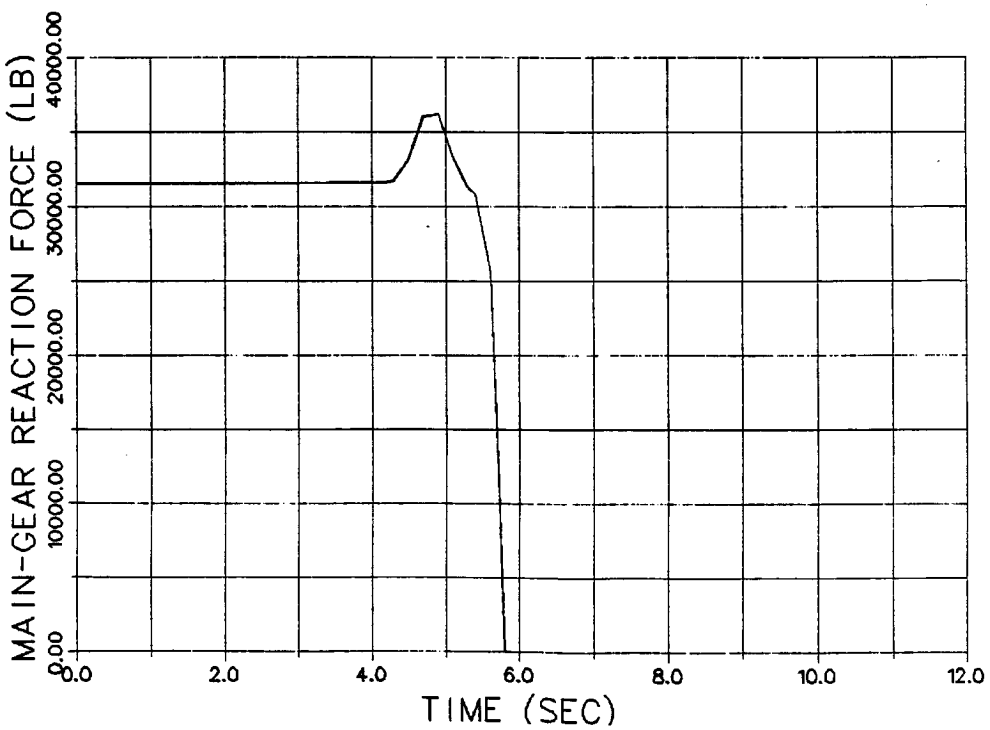

Figure F-1 Canard-Configuration Time History (Concluded)

APPENDIX G

Takeoff and Transition Histories

Time-history plots of pertinent parameters for the baseline E-7 performing a carrier takeoff at STO weight and escort-mission weight are shown in Figures G-1 and G-2, respectively.

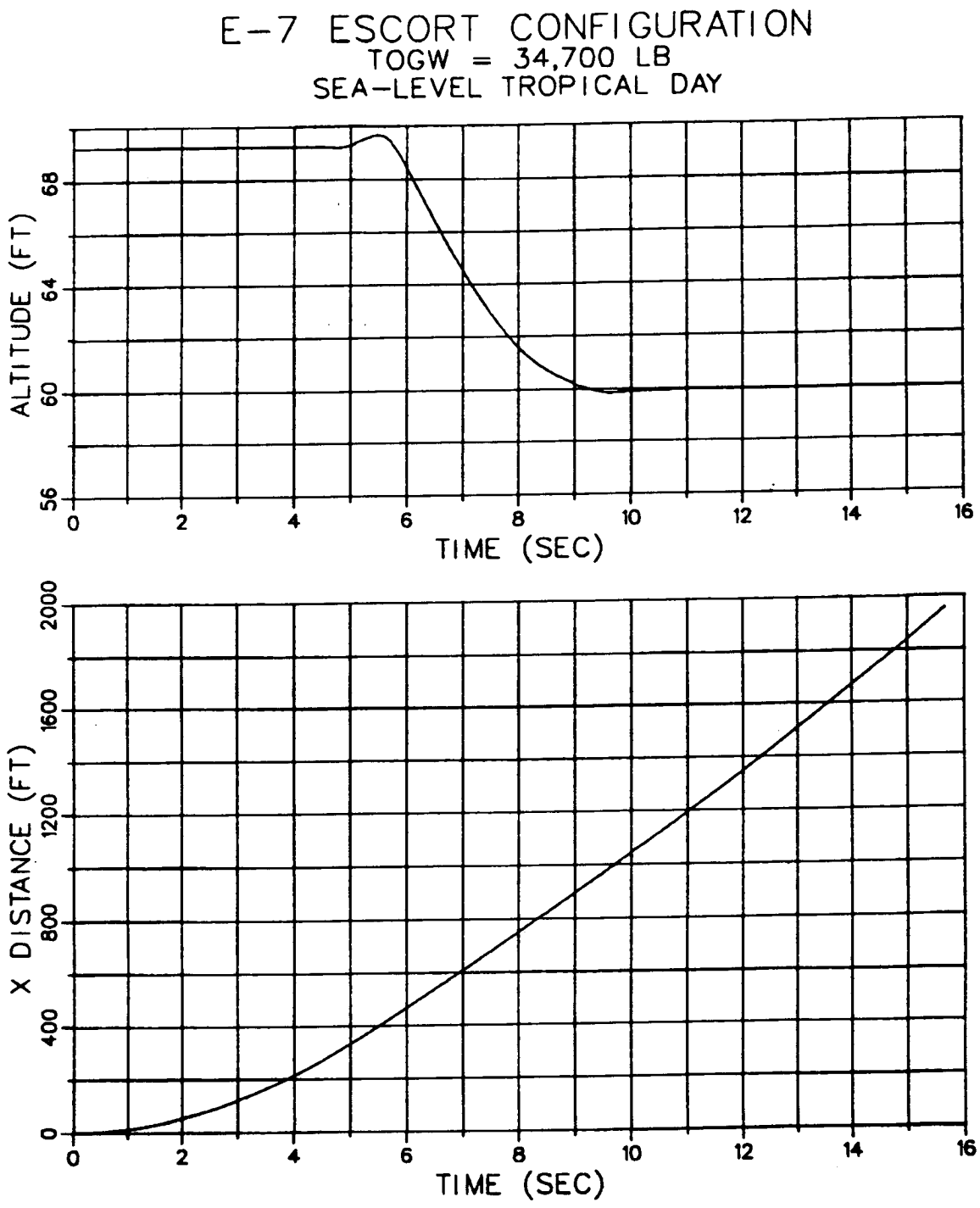

Figure G-1 STO-Weight Transition Time History

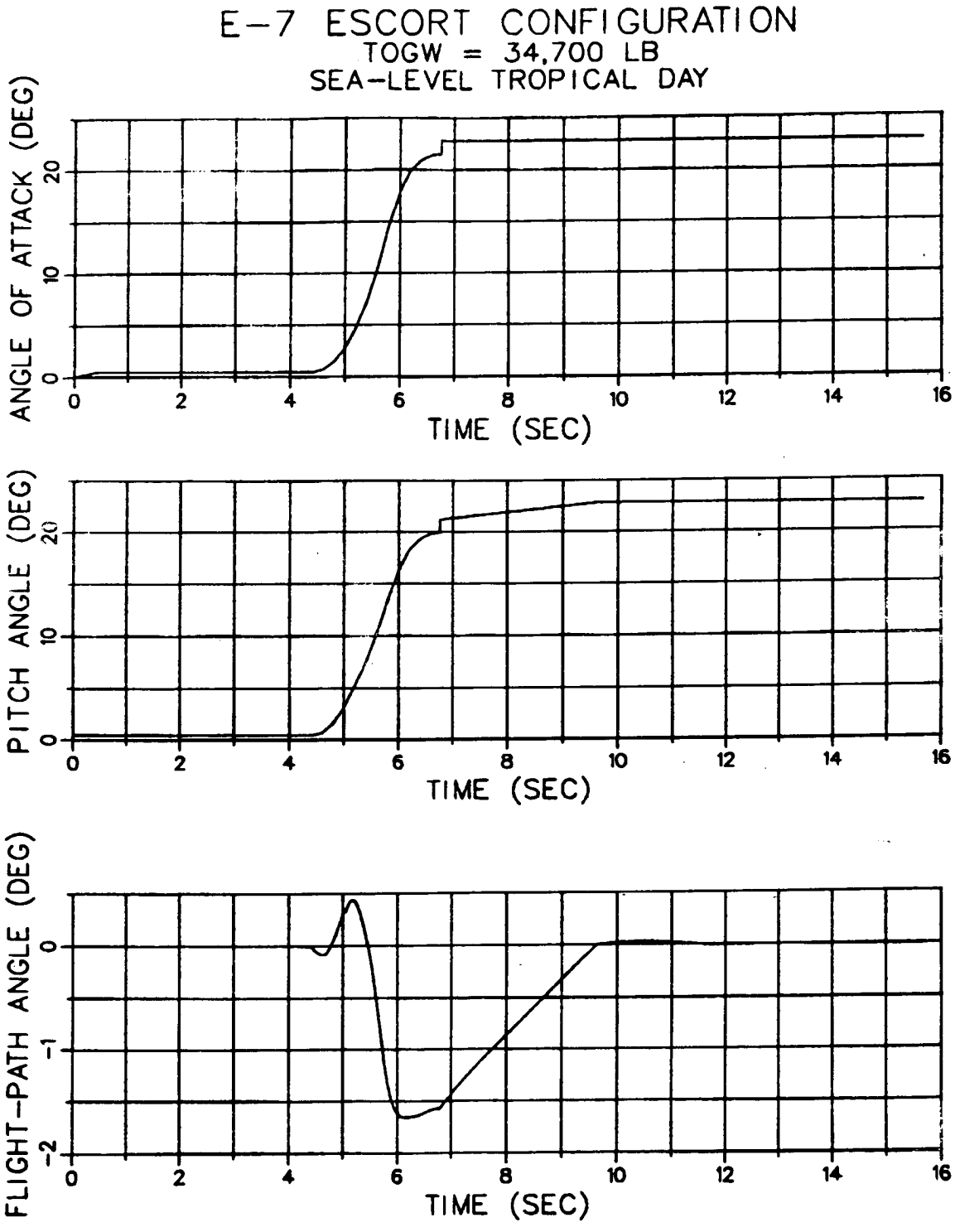

Figure G-1 STO-Weight Transition Time History (Continued)

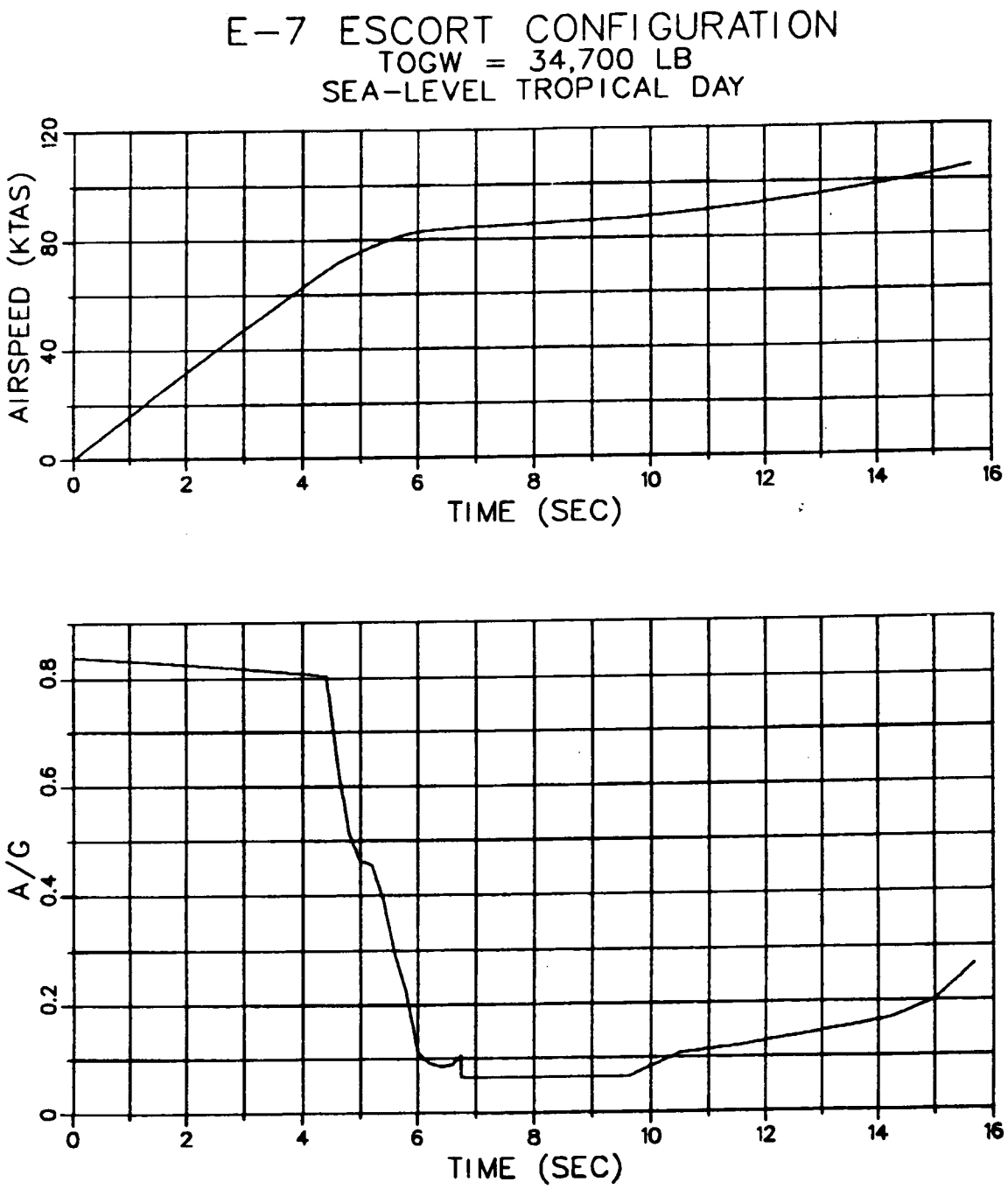

Figure G-1 STO-Weight Transition Time History (Continued)

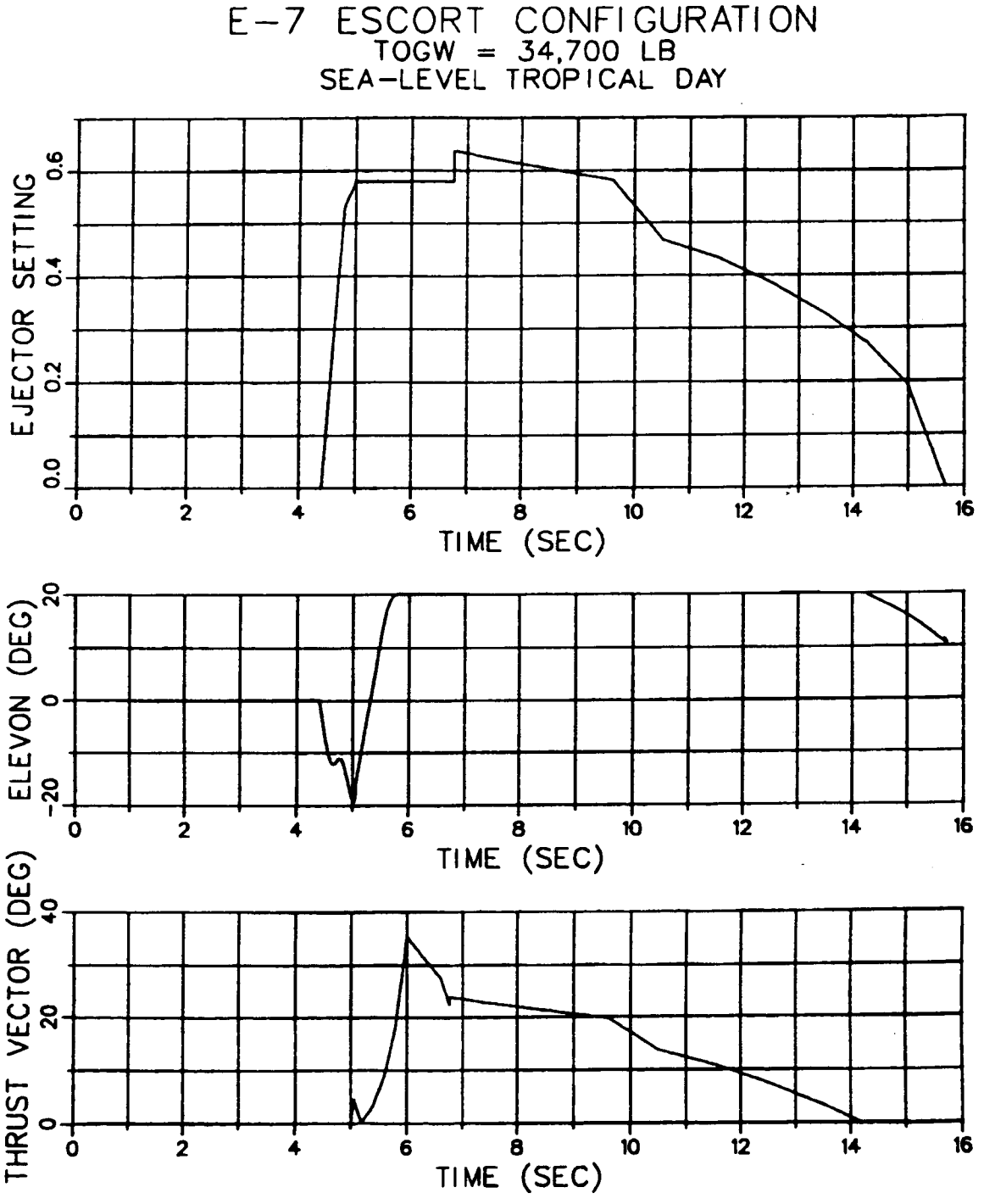

Figure G-1 STO-Weight Transition Time History (Continued)

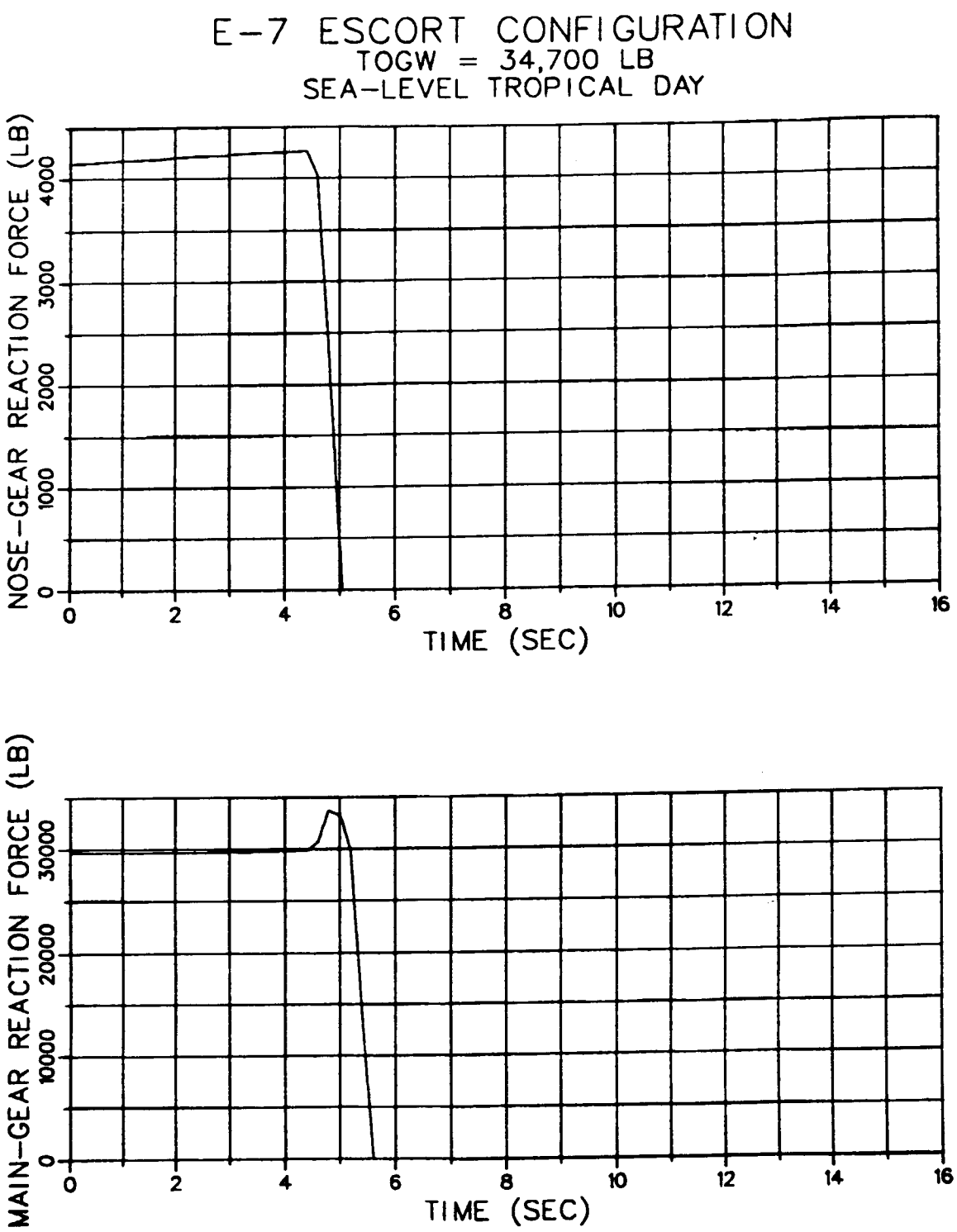

Figure G-1 STO-Weight Transition Time History (Concluded)

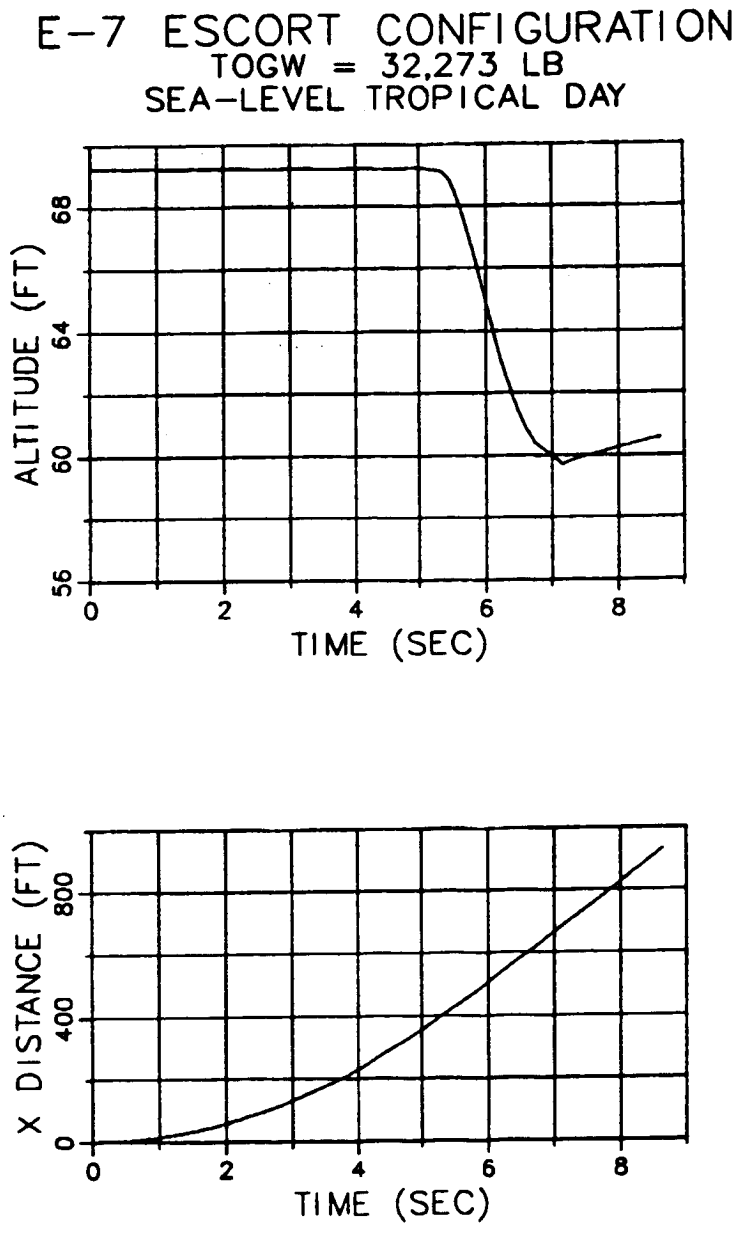

Figure G-2 Escort-Weight Transition Time History

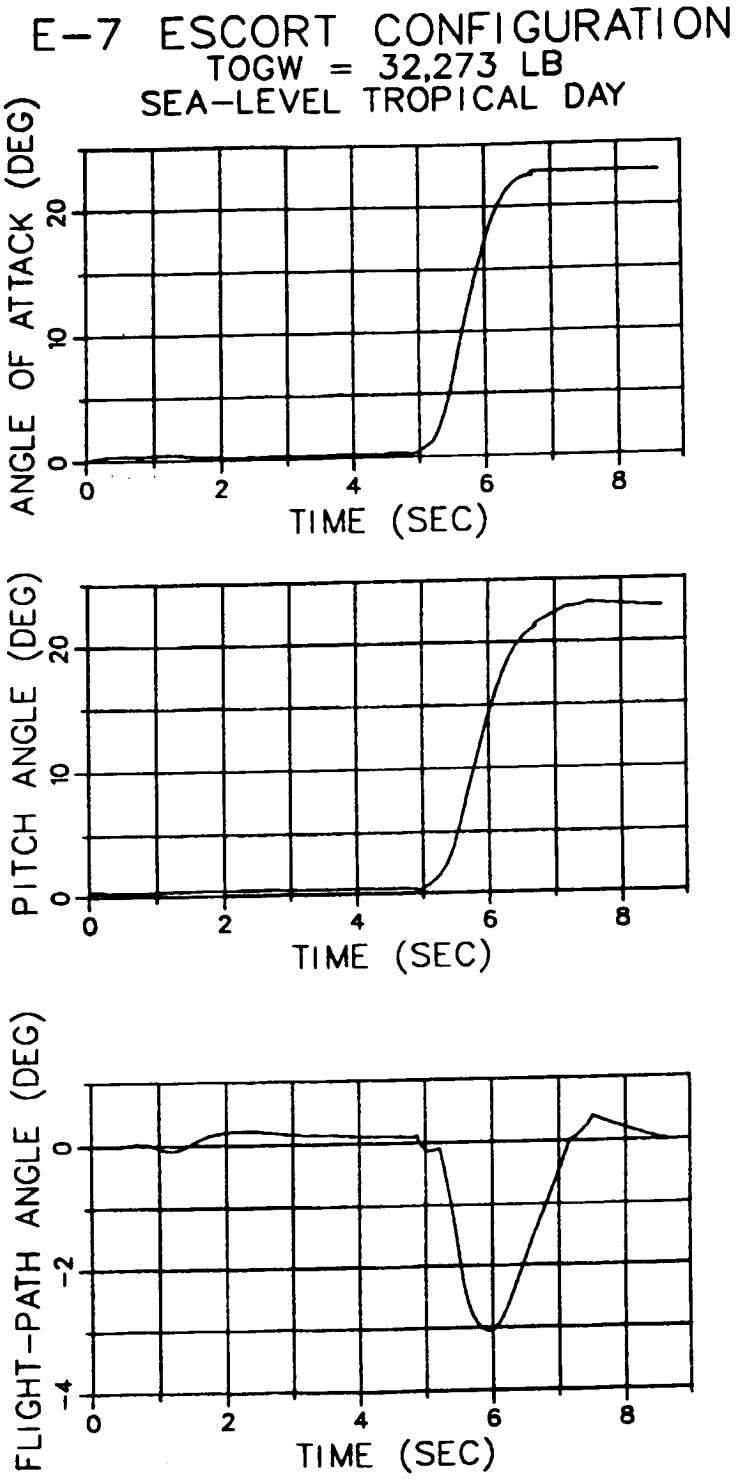

Figure G-2 Escort-Weight Transition Time History (Continued)

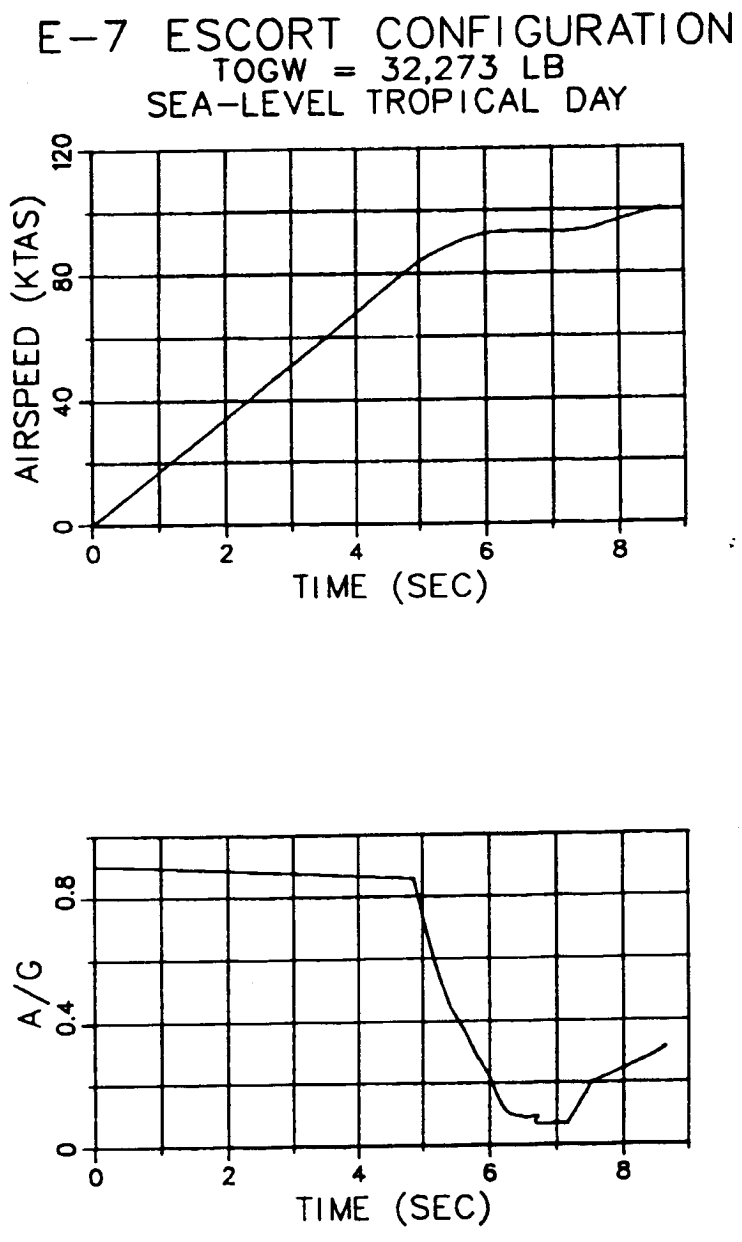

Figure G-2 Escort-Weight Transition Time History (Continued)

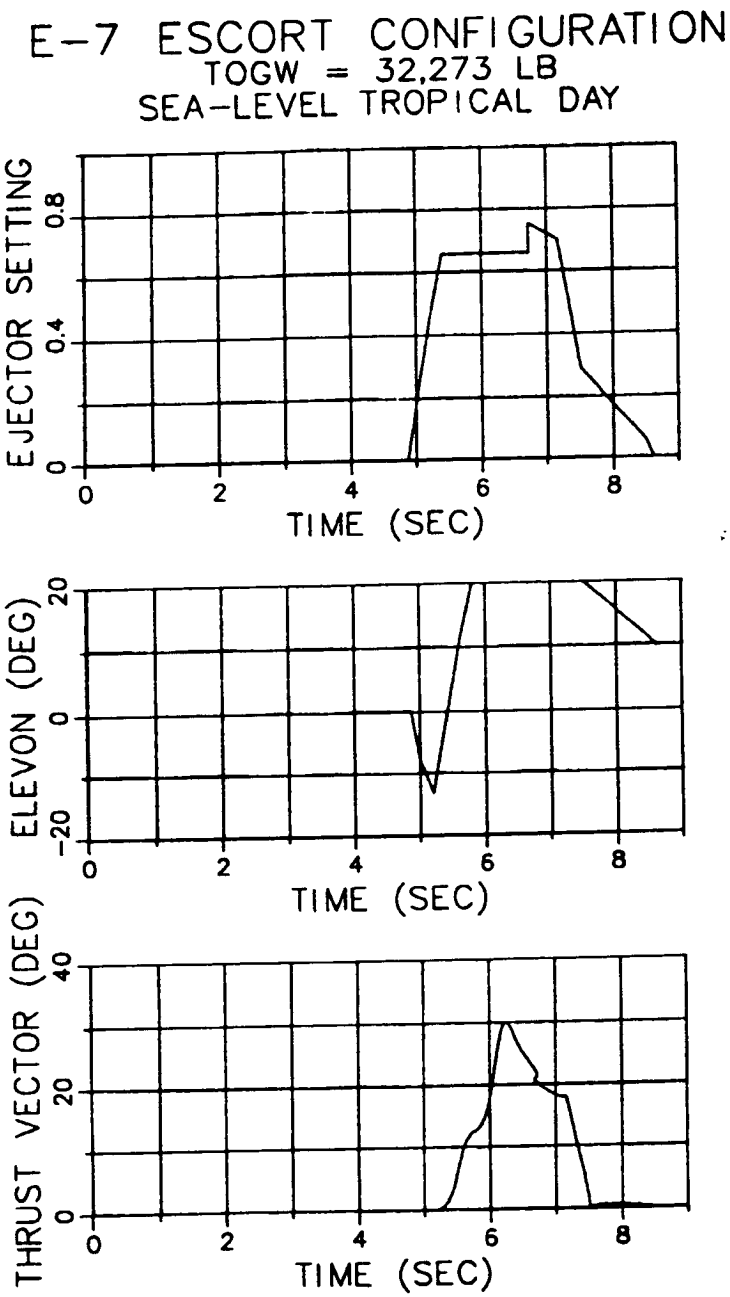

Figure G-2 Escort-Weight Transition Time History (Continued)

E-7 ESCORT CONFIGURATION
TOGW = 32,273 LB
SEA-LEVEL TROPICAL DAY

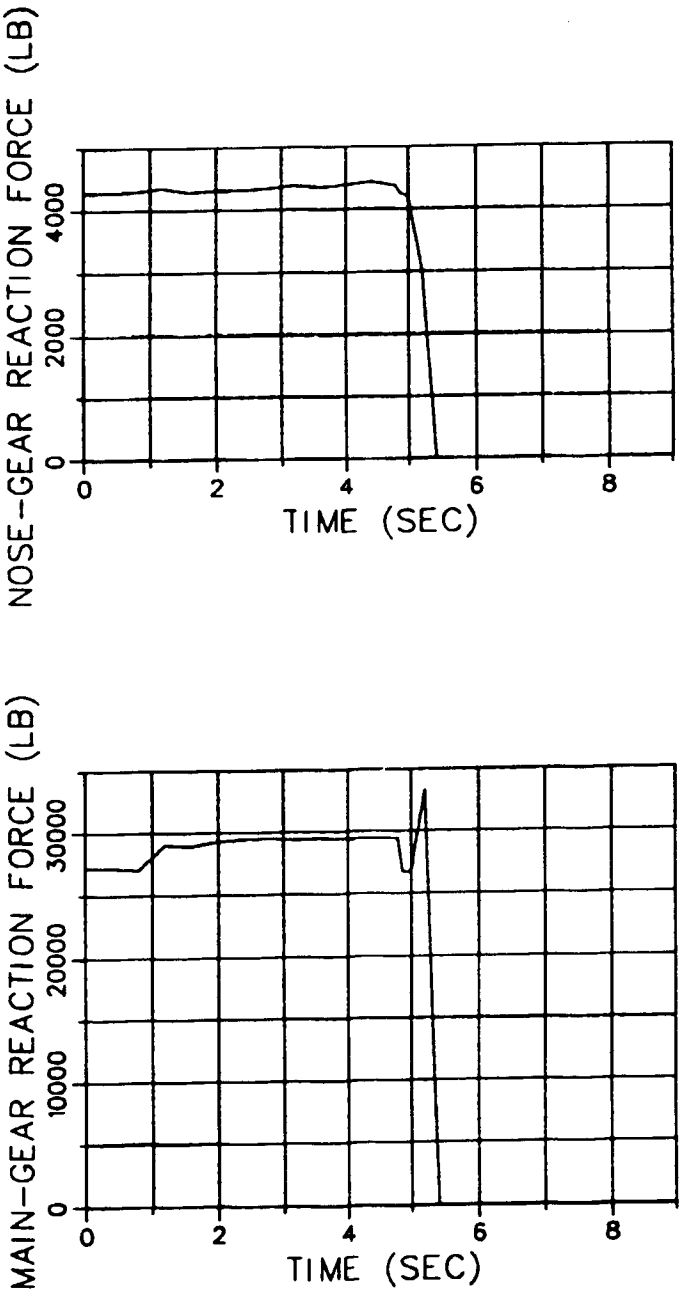

Figure G-2 Escort-Weight Transition Time History (Concluded)

APPENDIX H

Transition-to-Hover Histories

Time-history plots of pertinent parameters for the baseline E-7 performing a decelerating transition are shown in Figure H-1.

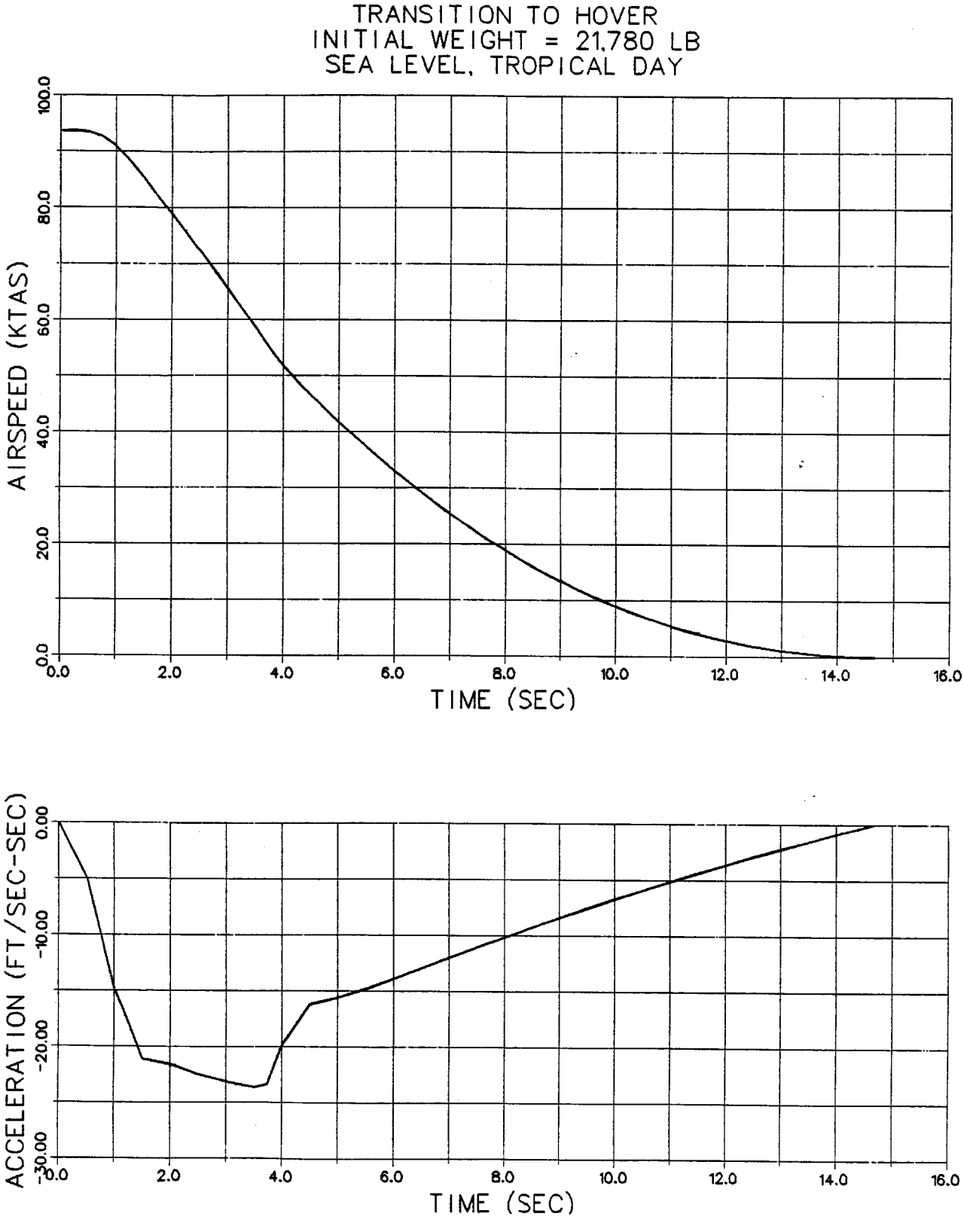

Figure H-1, Transition-to-Hover Time History.

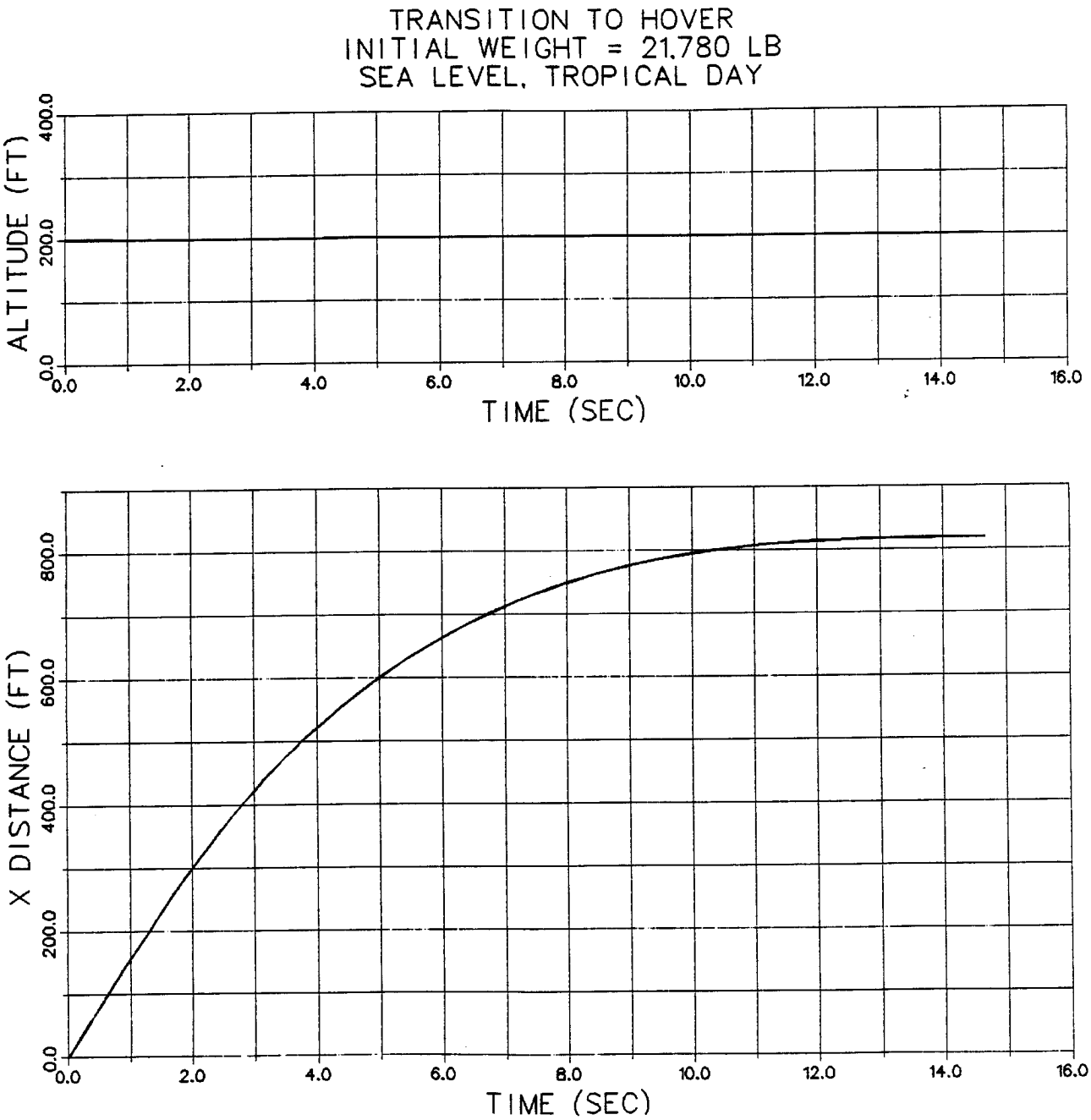

Figure H-1, Transition-to-Hover Time History (Continued).

C-

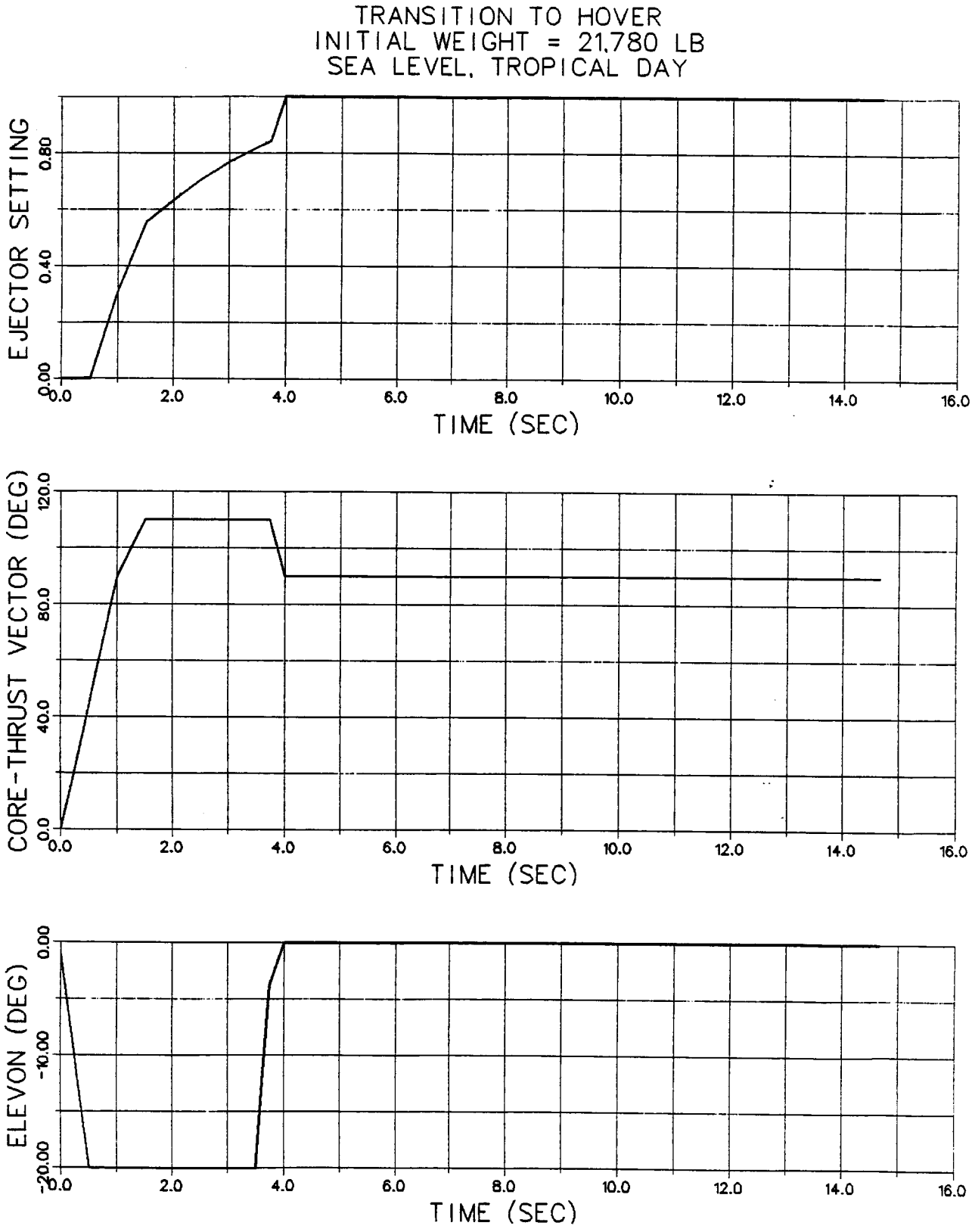

Figure H-1, Transition-to-Hover Time History (Concluded).

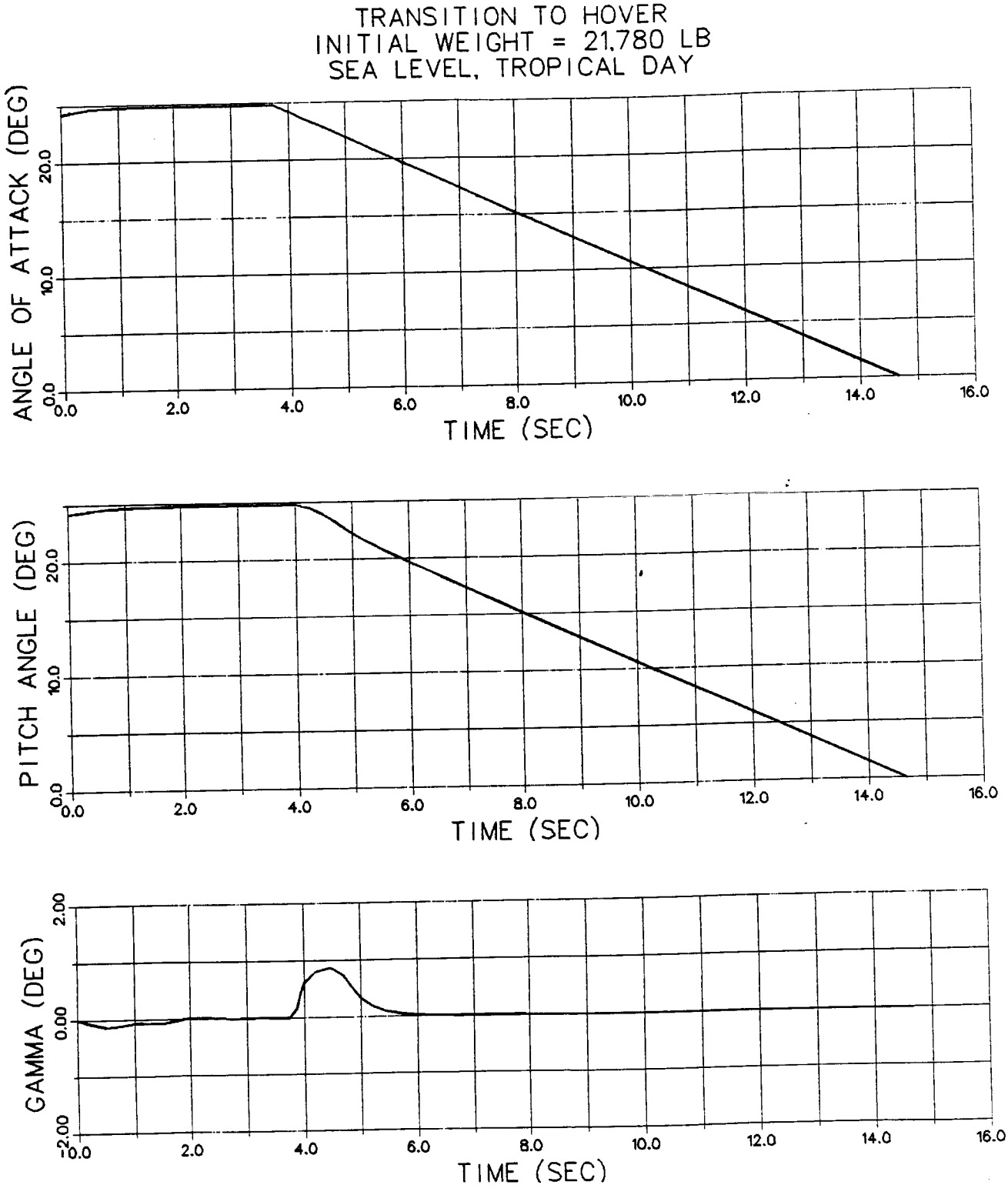

Figure H-1, Transition-to-Hover Time History (Continued).

APPENDIX I

Ejector-Performance-Sensitivity Takeoff Histories

Time-history plots of pertinent parameters for E-7 performing carrier takeoffs at STO weights for ejector-augmentation ratios of 1.53 and 1.73 are shown in Figures I-1 and I-2 respectively.

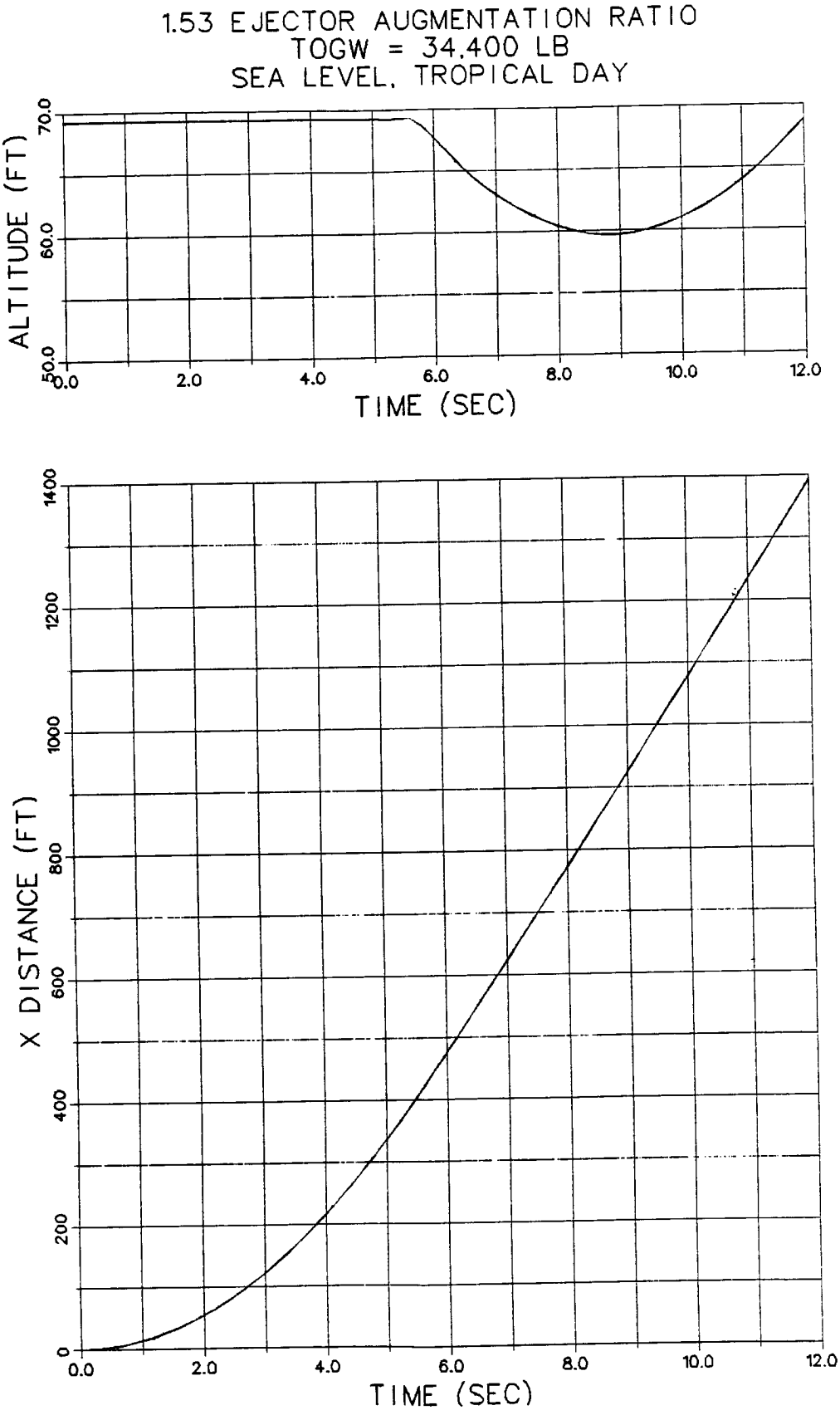

Figure I-1, Takeoff Time History for Φ=1.53.

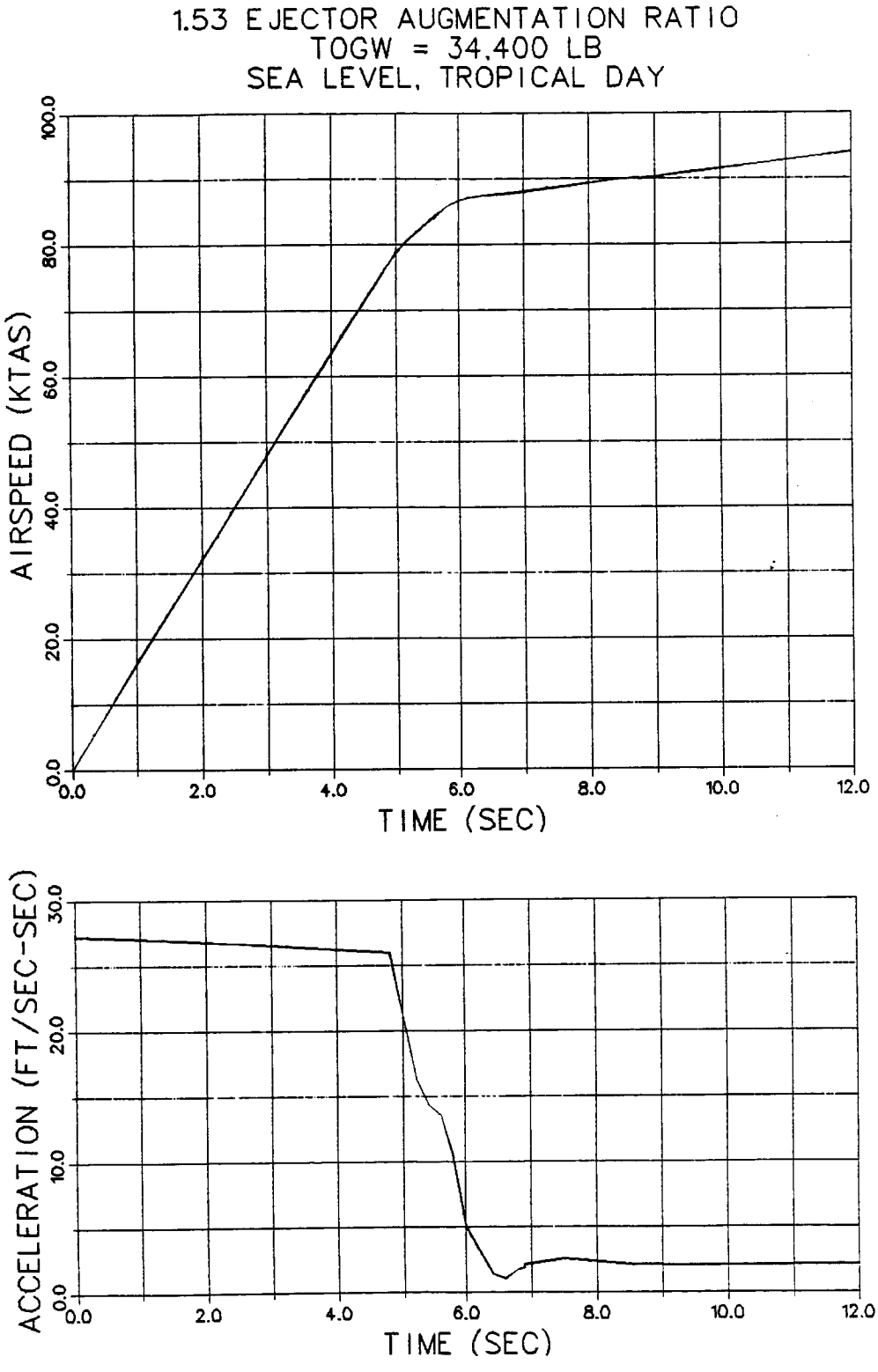

Figure I-1, Takeoff Time History for Φ=1.53 (Continued).

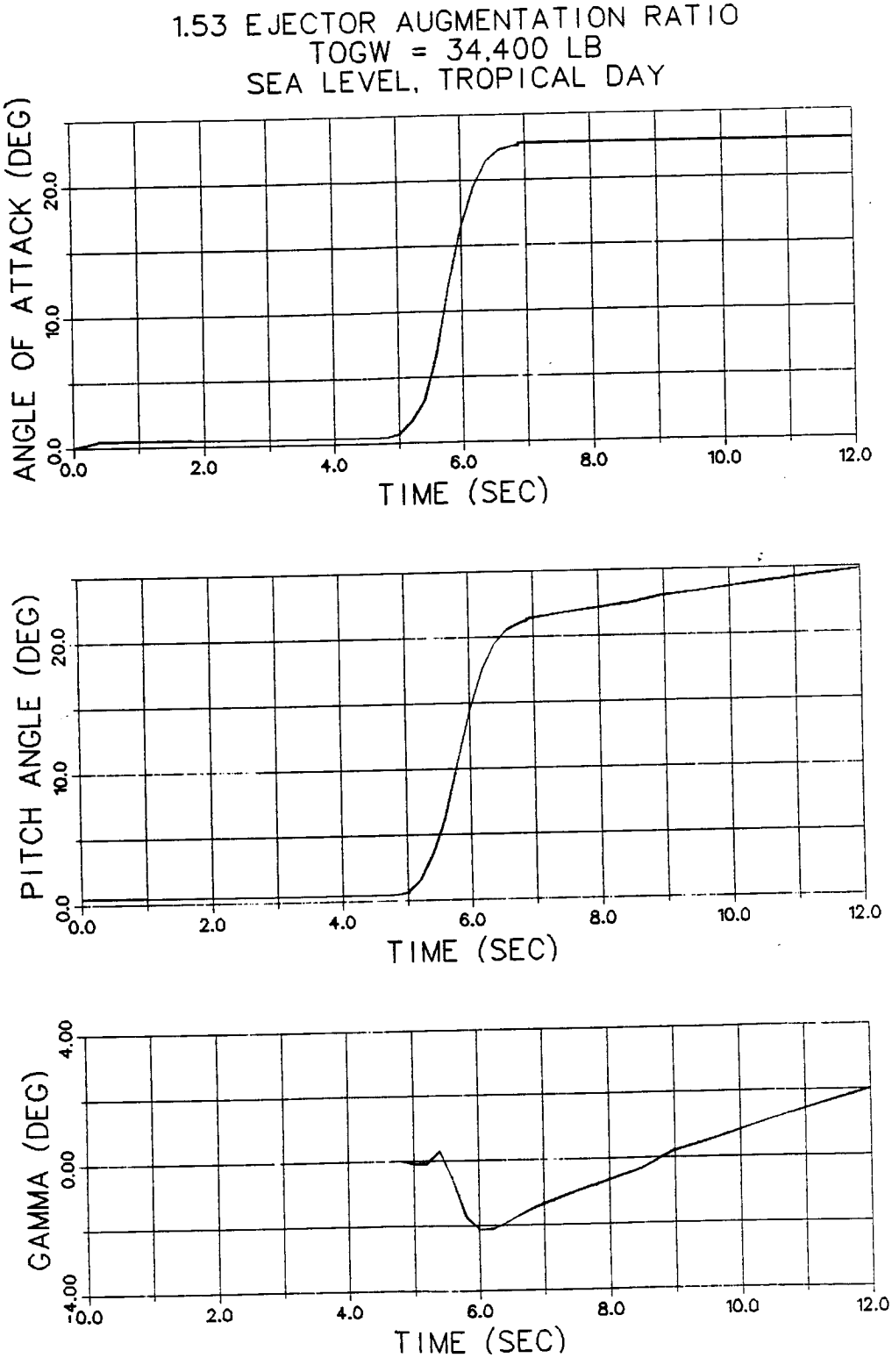

Figure I-1, Takeoff Time History for Φ=1.53 (Continued).

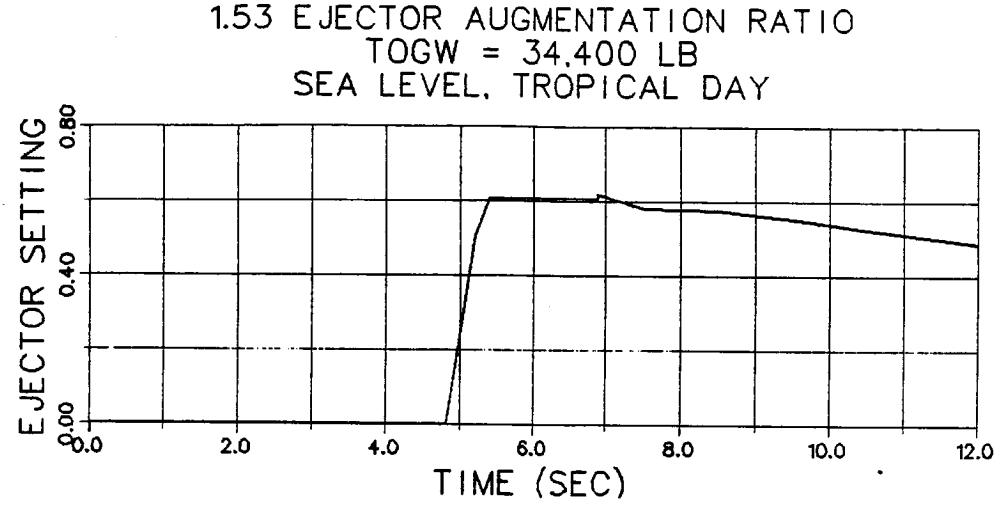

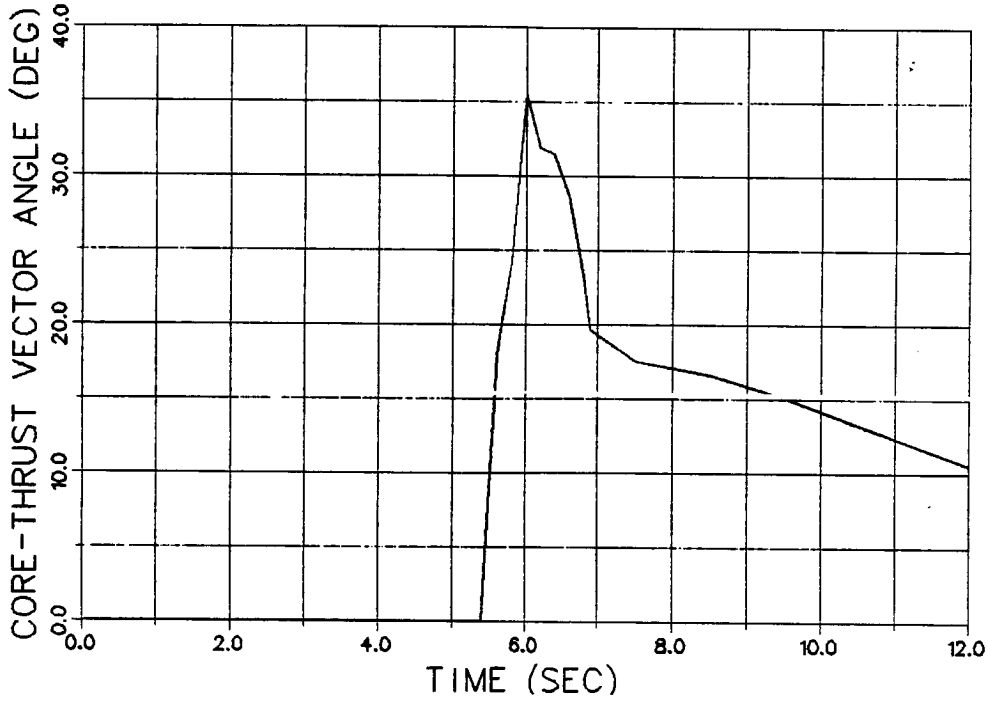

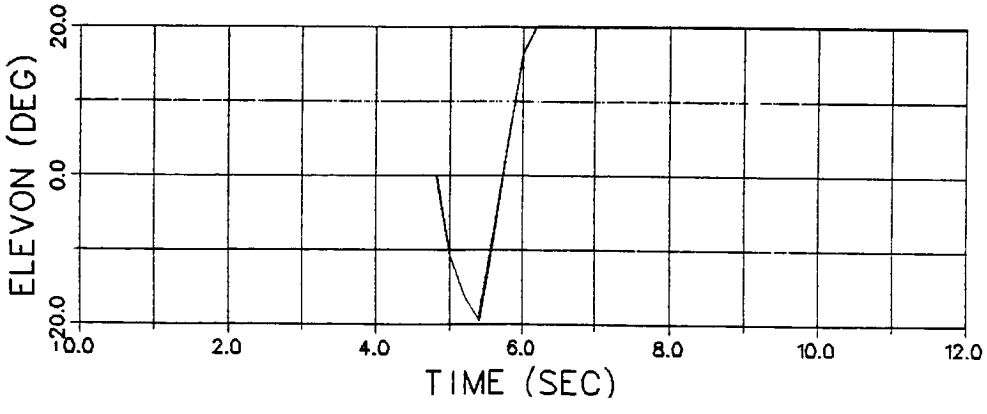

Figure I-1, Takeoff Time History for Φ=1.53 (Continued).

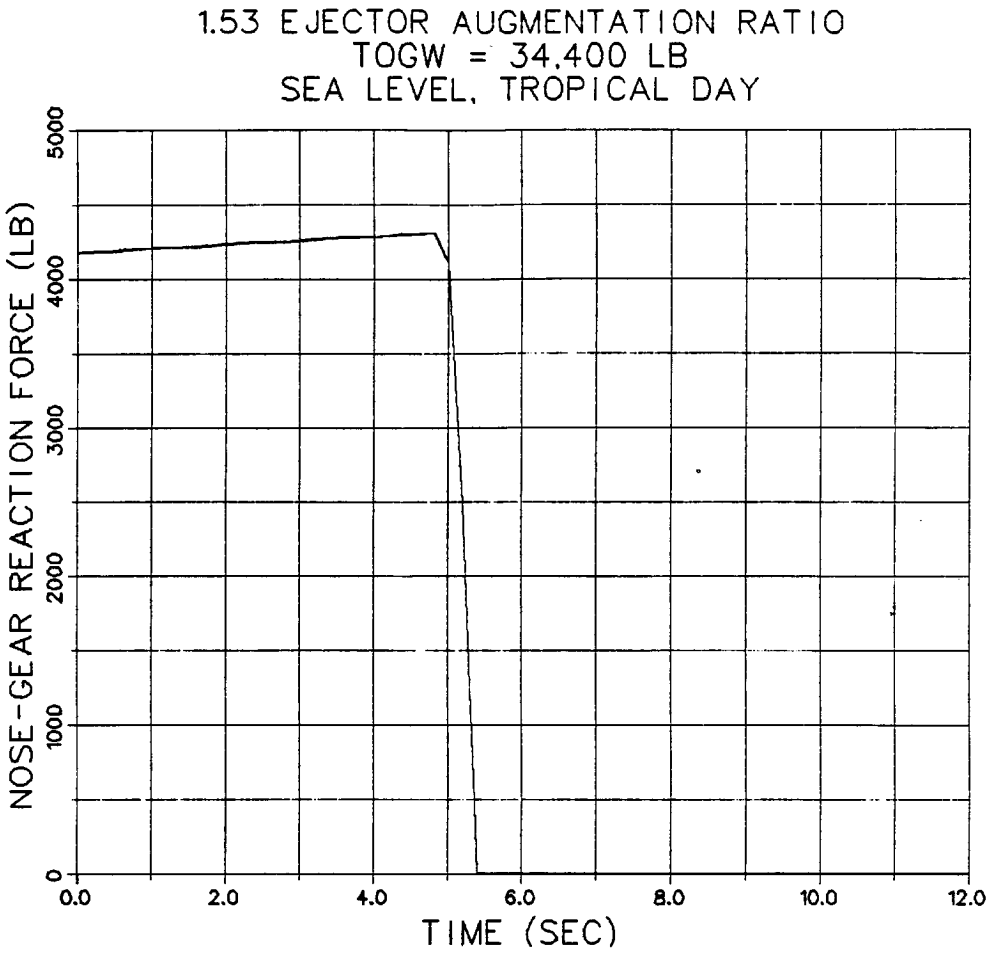

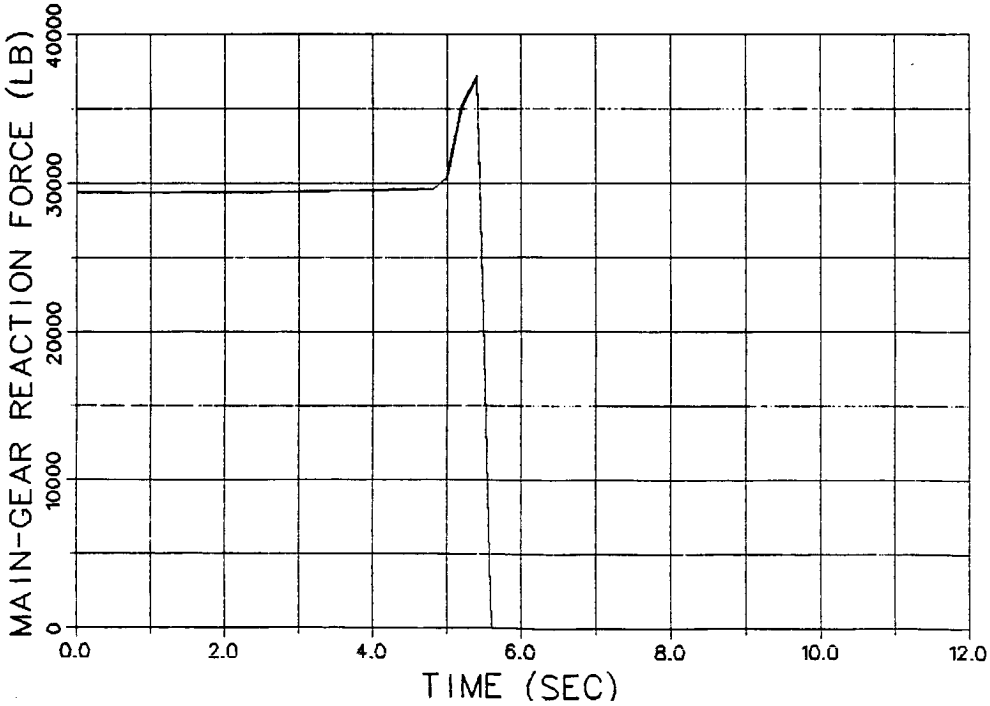

Figure I-1, Takeoff Time History for Φ=1.53 (Concluded).

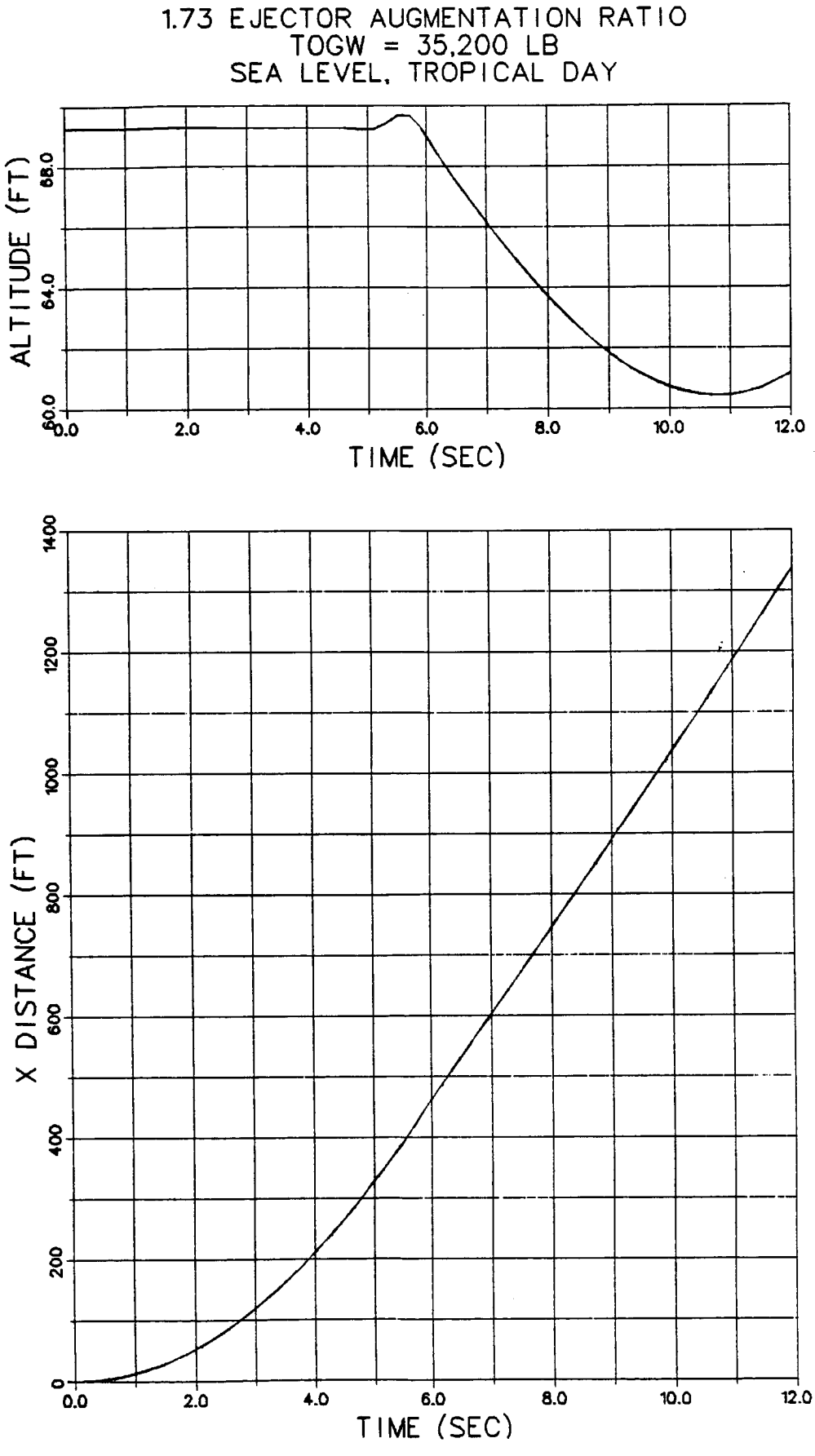

Figure I-2, Takeoff Time History for Φ=1.73.

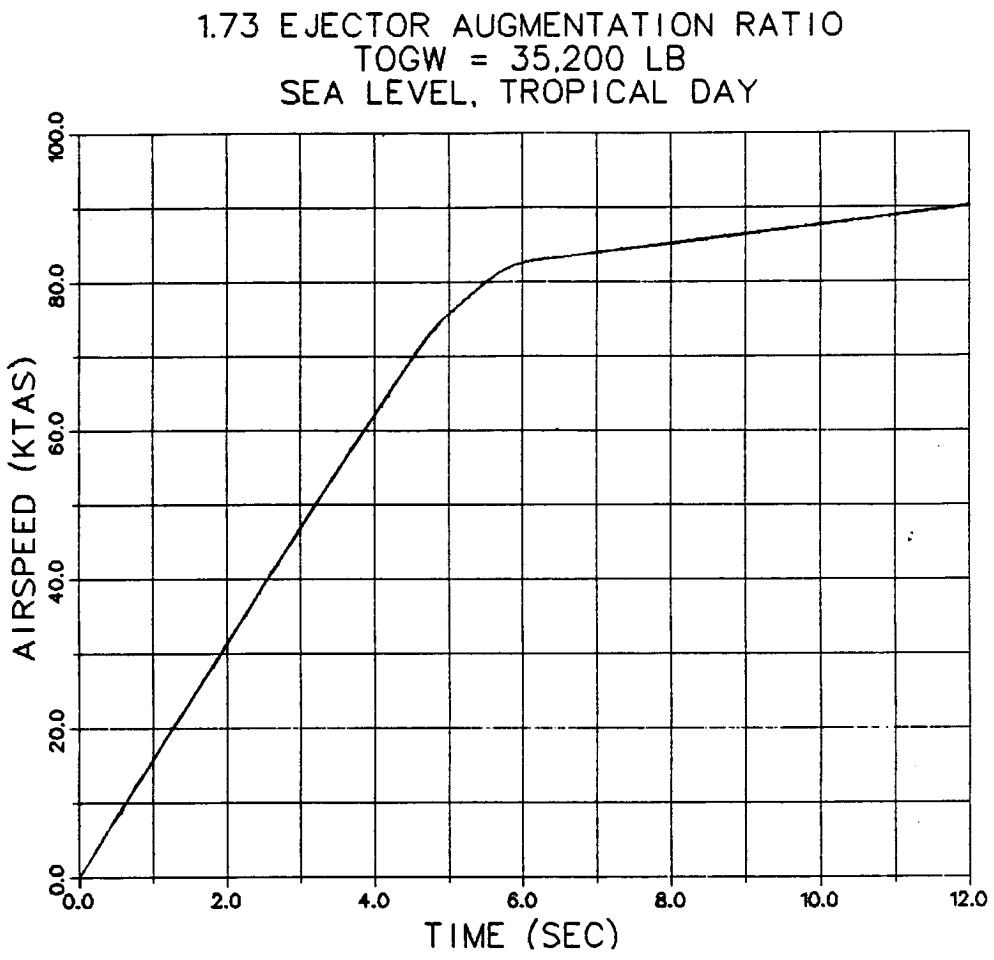

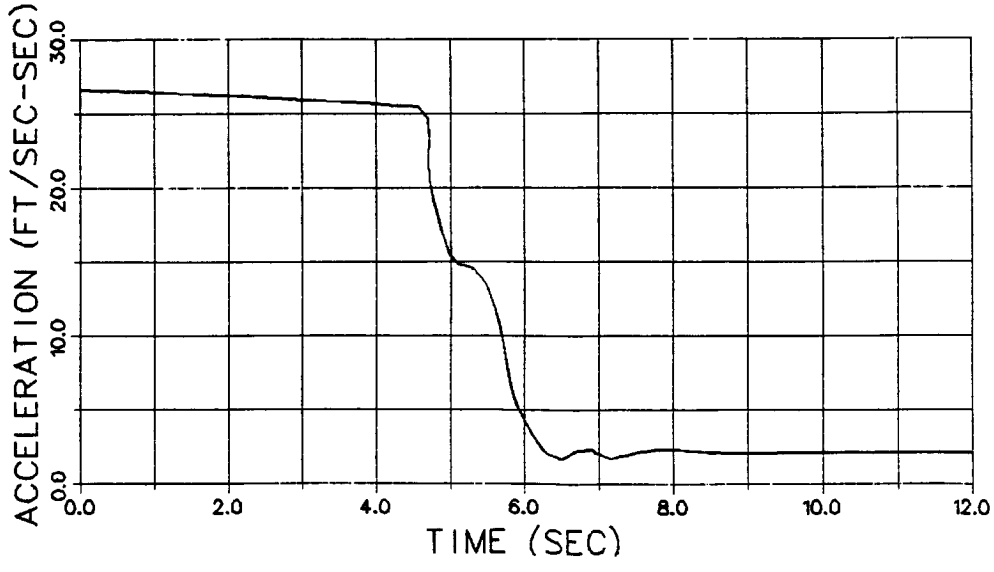

Figure I-2, Takeoff Time History for Φ=1.73 (Continued).

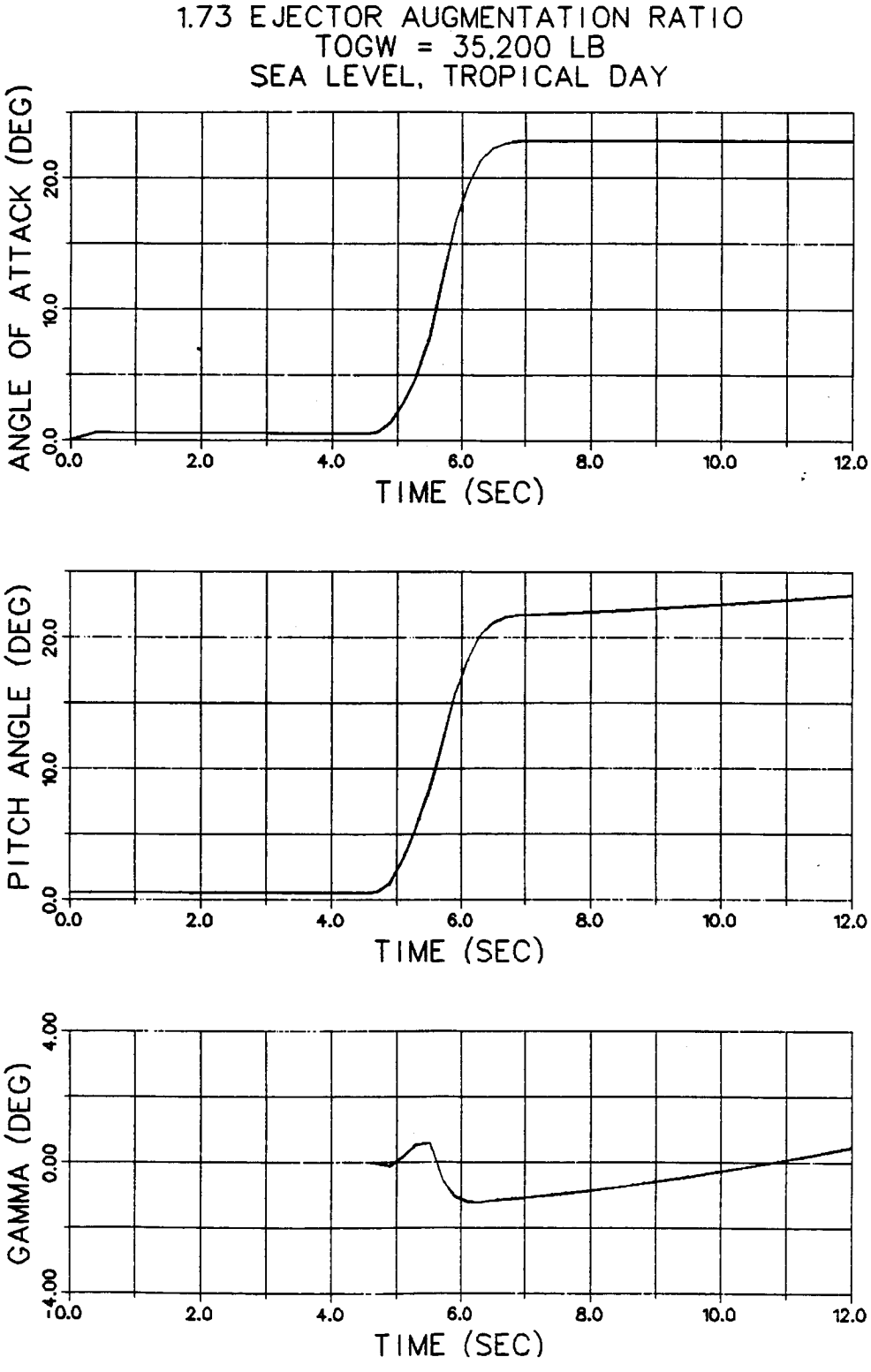

Figure I-2, Takeoff Time History for Φ=1.73 (Continued).

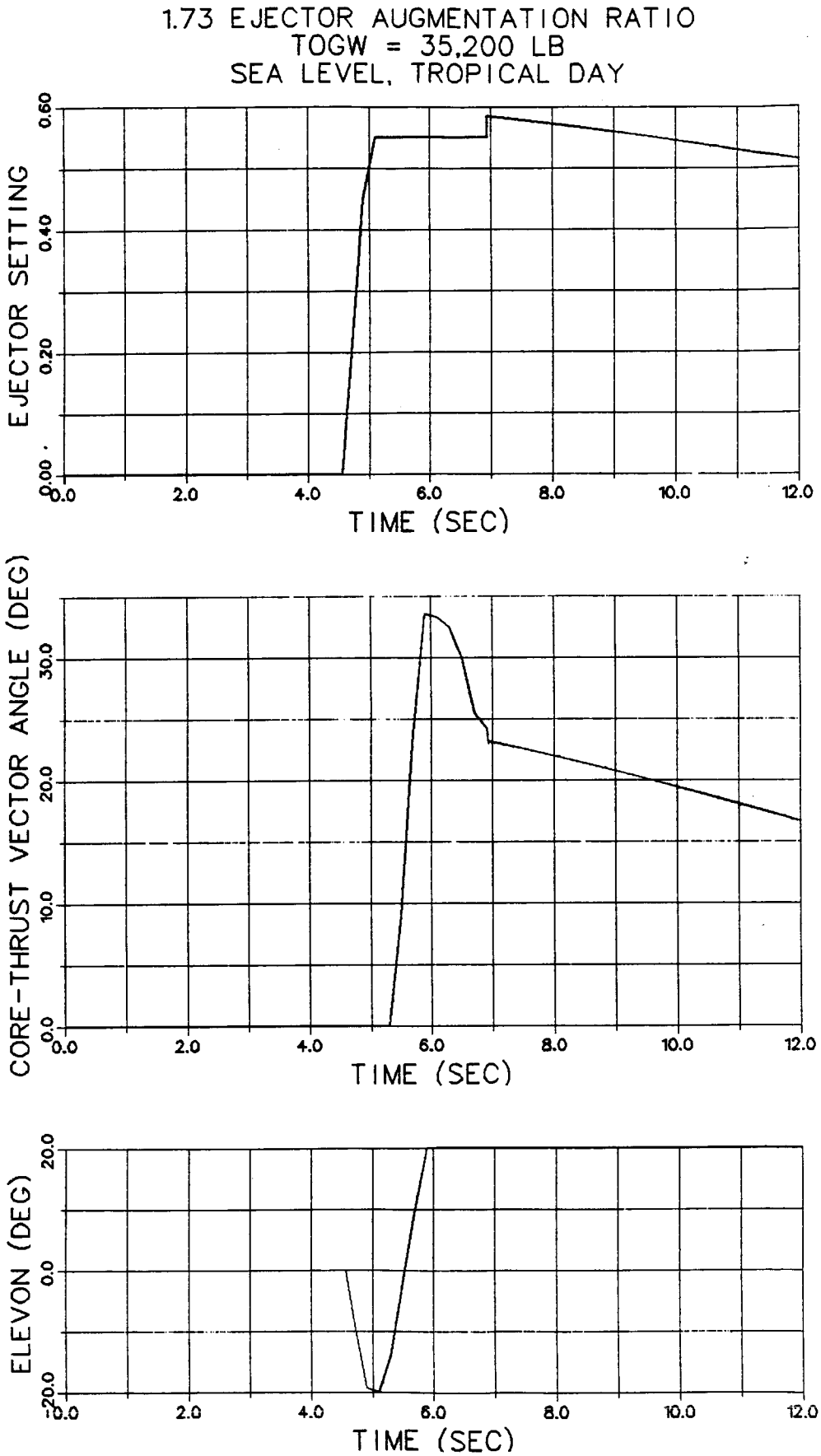

Figure I-2, Takeoff Time History for Φ=1.73 (Continued).

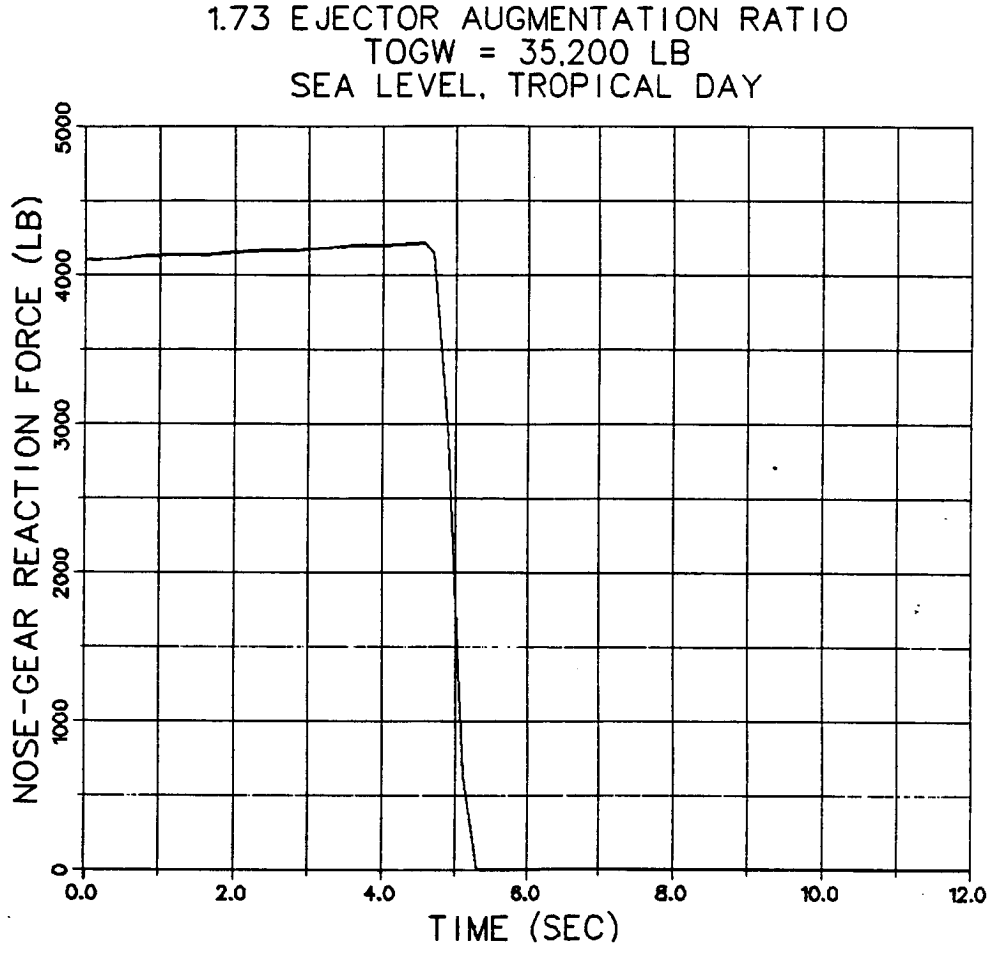

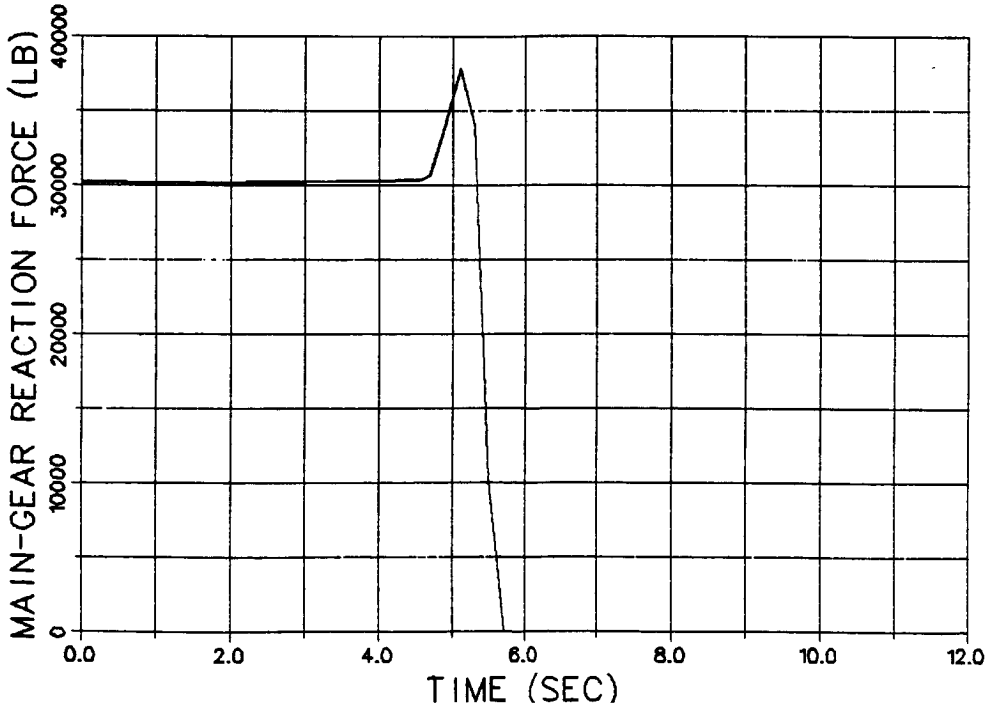

Figure I-2, Takeoff Time History for Φ=1.73 (Concluded).

APPENDIX J

Non-Afterburning Takeoff Histories

Time-history plots of pertinent parameters for the baseline E-7 performing field takeoffs using four combinations of aft and core afterburning are shown in Figure J-1.

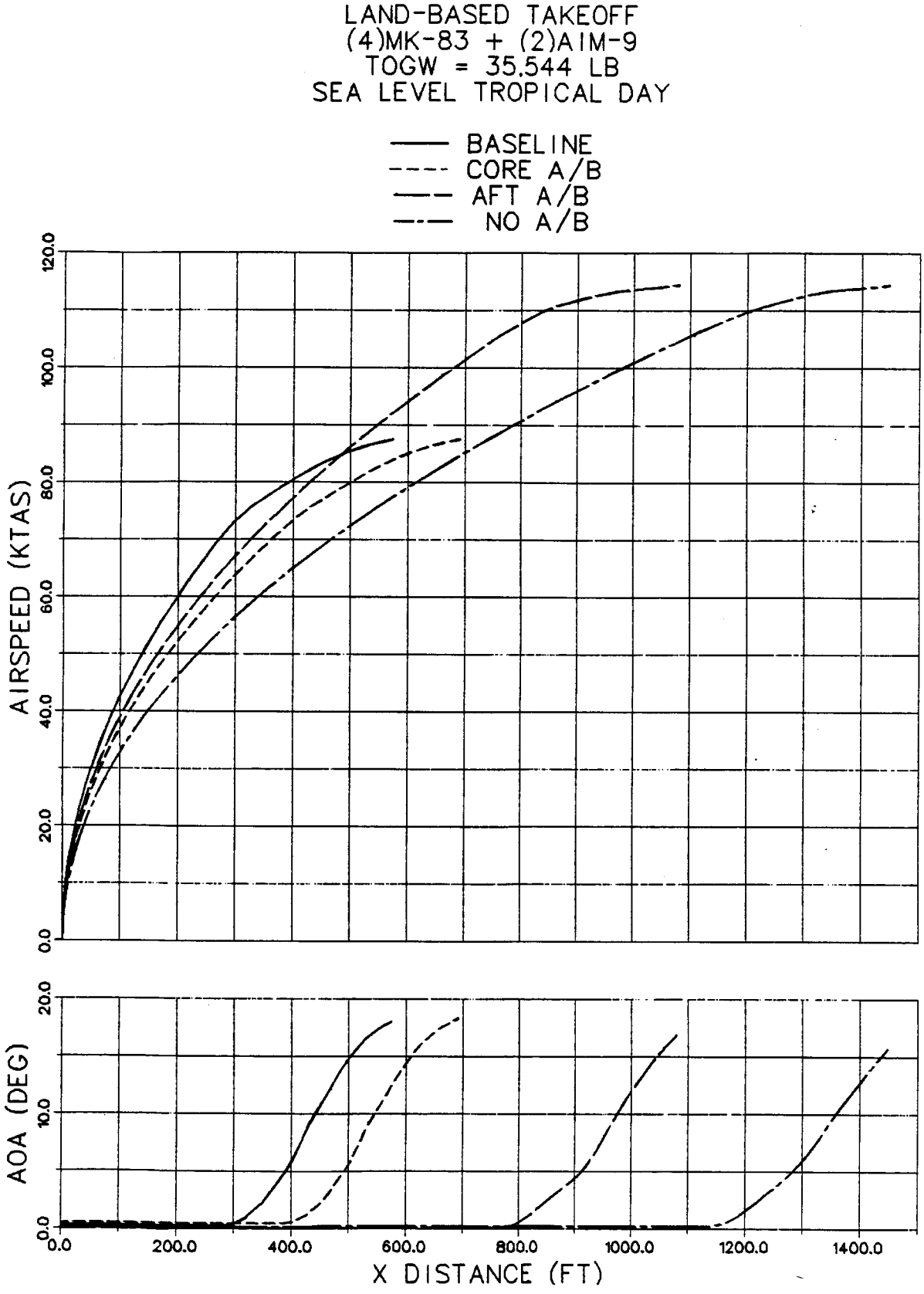

Figure J-1, Takeoff Time Histories for Non-Afterburning Combinations.

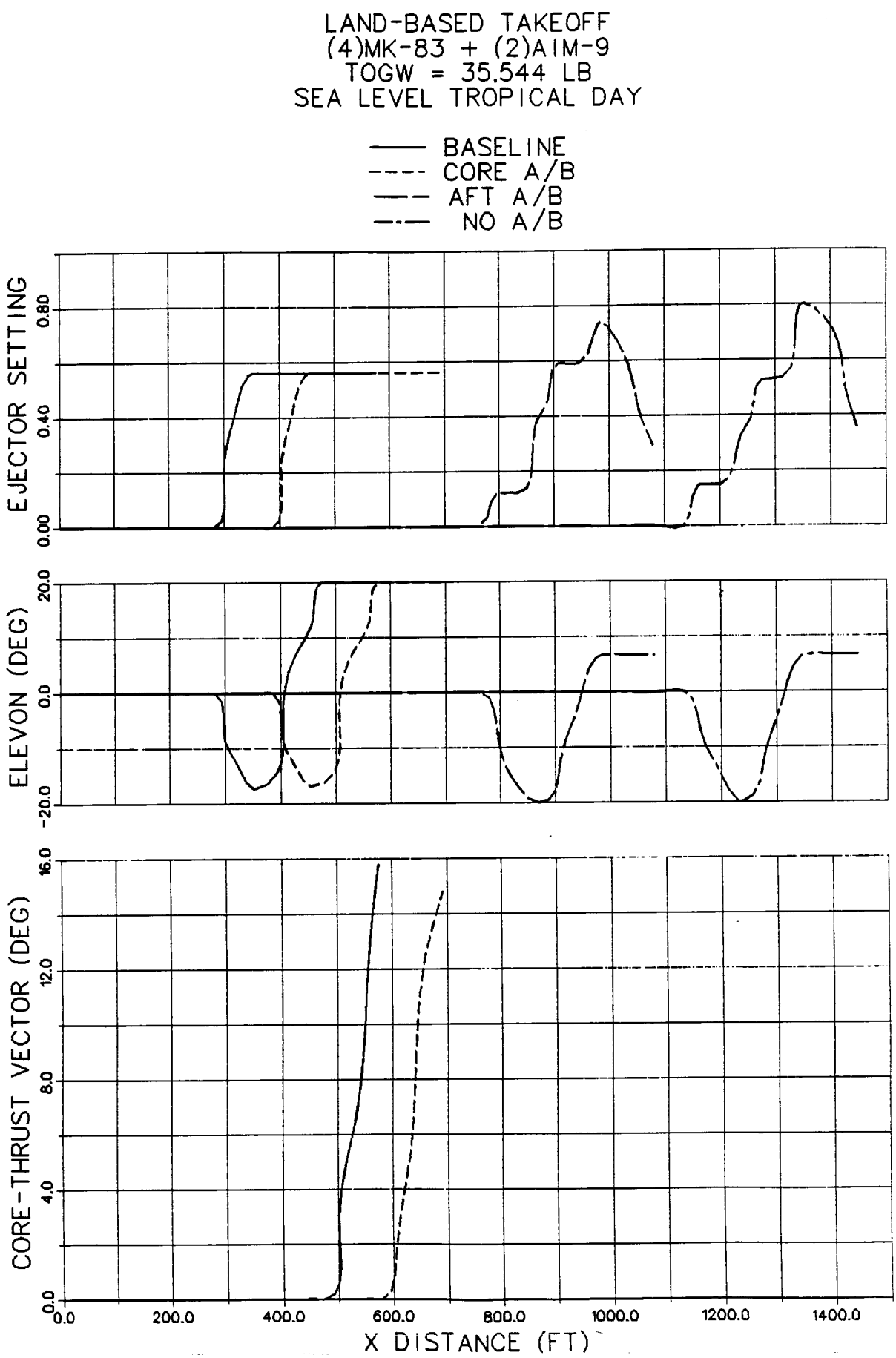

Figure J-1, Takeoff Time Histories for Non-Afterburning Combinations (Continued).

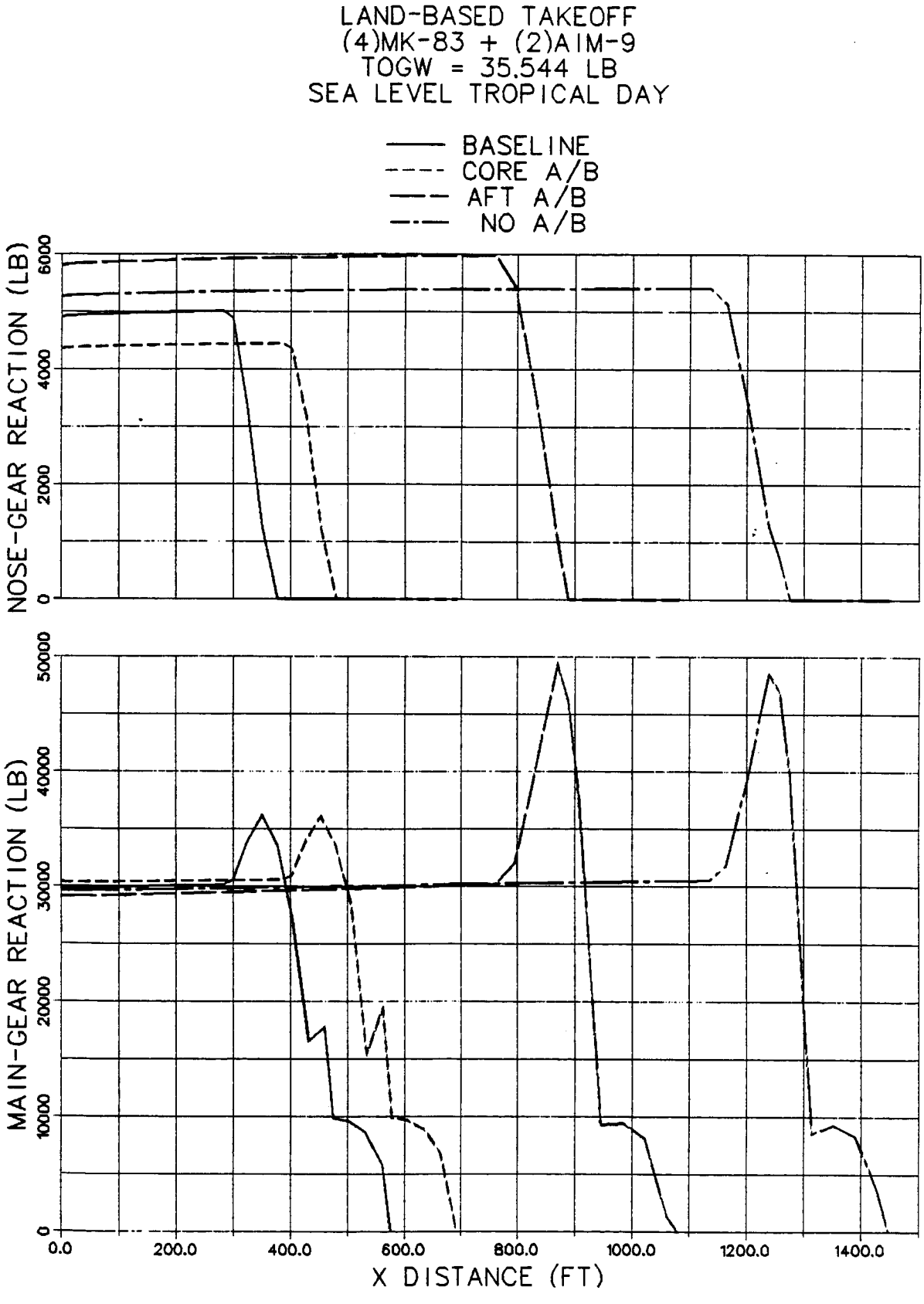

Figure J-1, Takeoff Time Histories for Non-Afterburning Combinations. (Concluded)

APPENDIX K

Non-Ejector Takeoff Histories

Time-history plots of pertinent parameters for the E-7 with a vectorable aft nozzle performing a carrier takeoff at STO weight without activating ejector thrust are shown in Figure K-1. Similar plots for static pitches of 4.6 and 9.1 deg are shown in Figures K-2 and K-3 respectively.

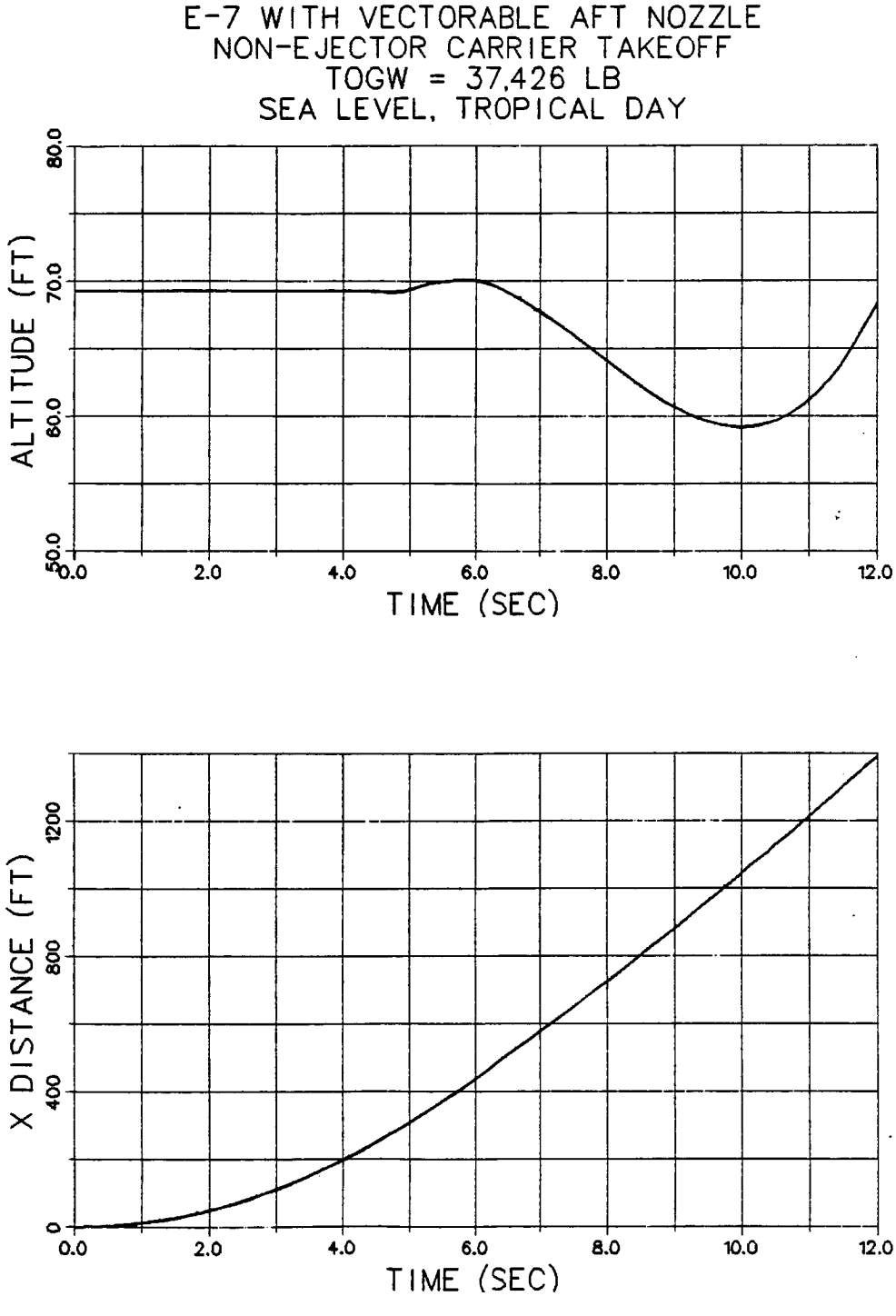

Figure K-1, Non-Ejector-Takeoff Time History.

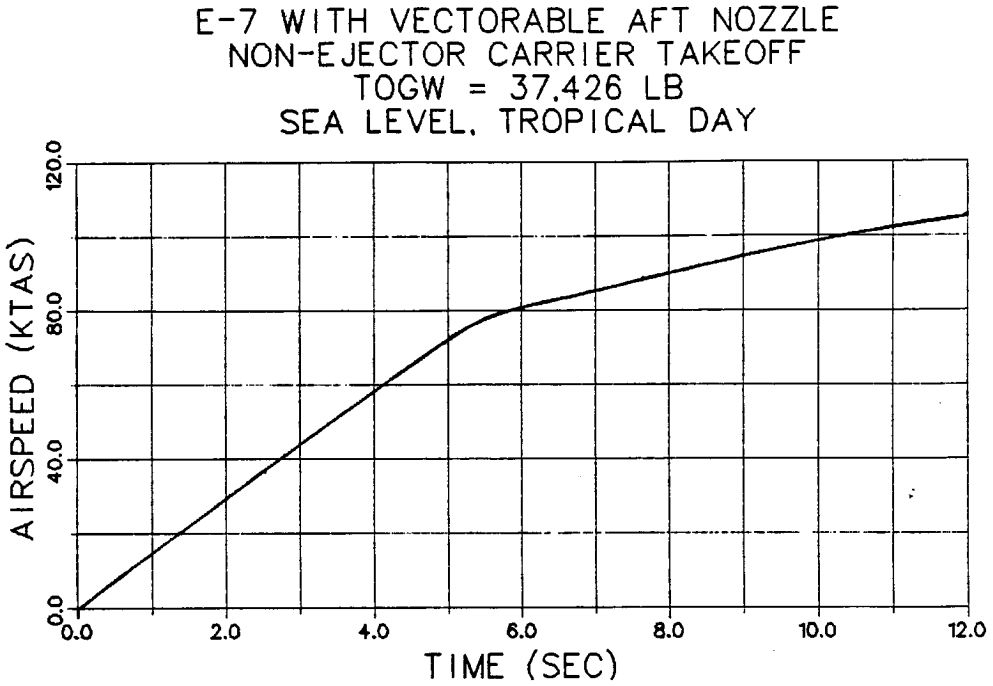

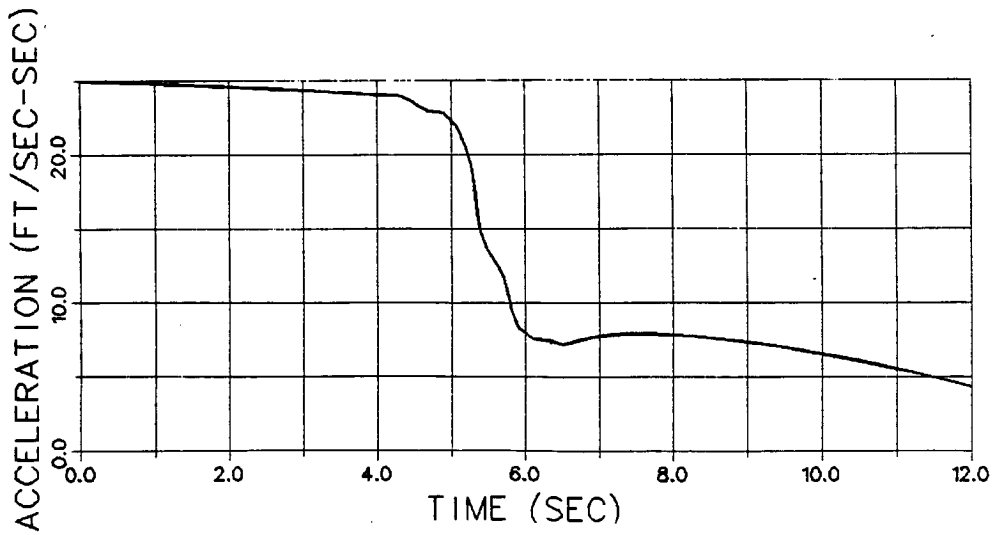

Figure K-1, Non-Ejector-Takeoff Time History (Continued).

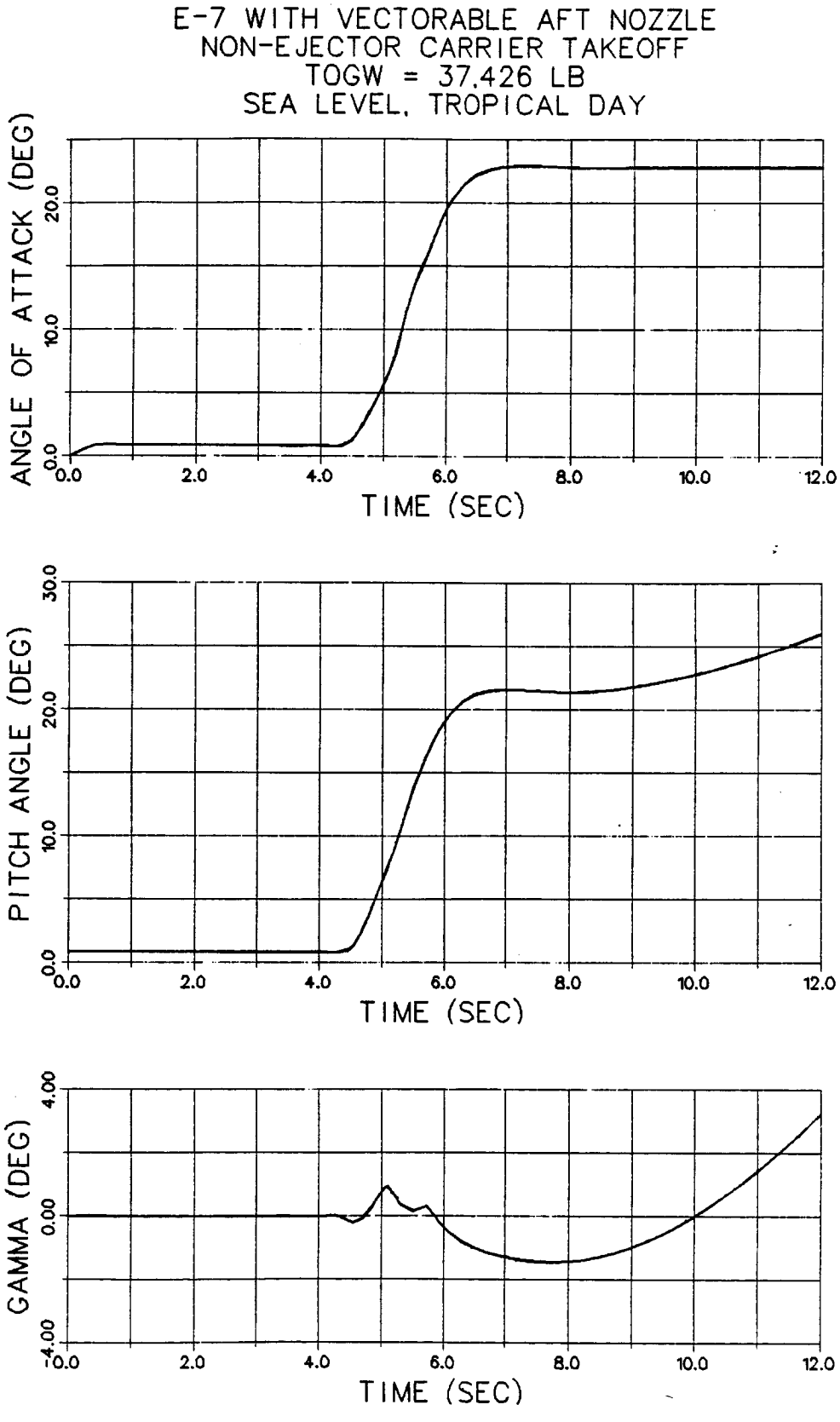

Figure K-1, Non-Ejector-Takeoff Time History (Continued).

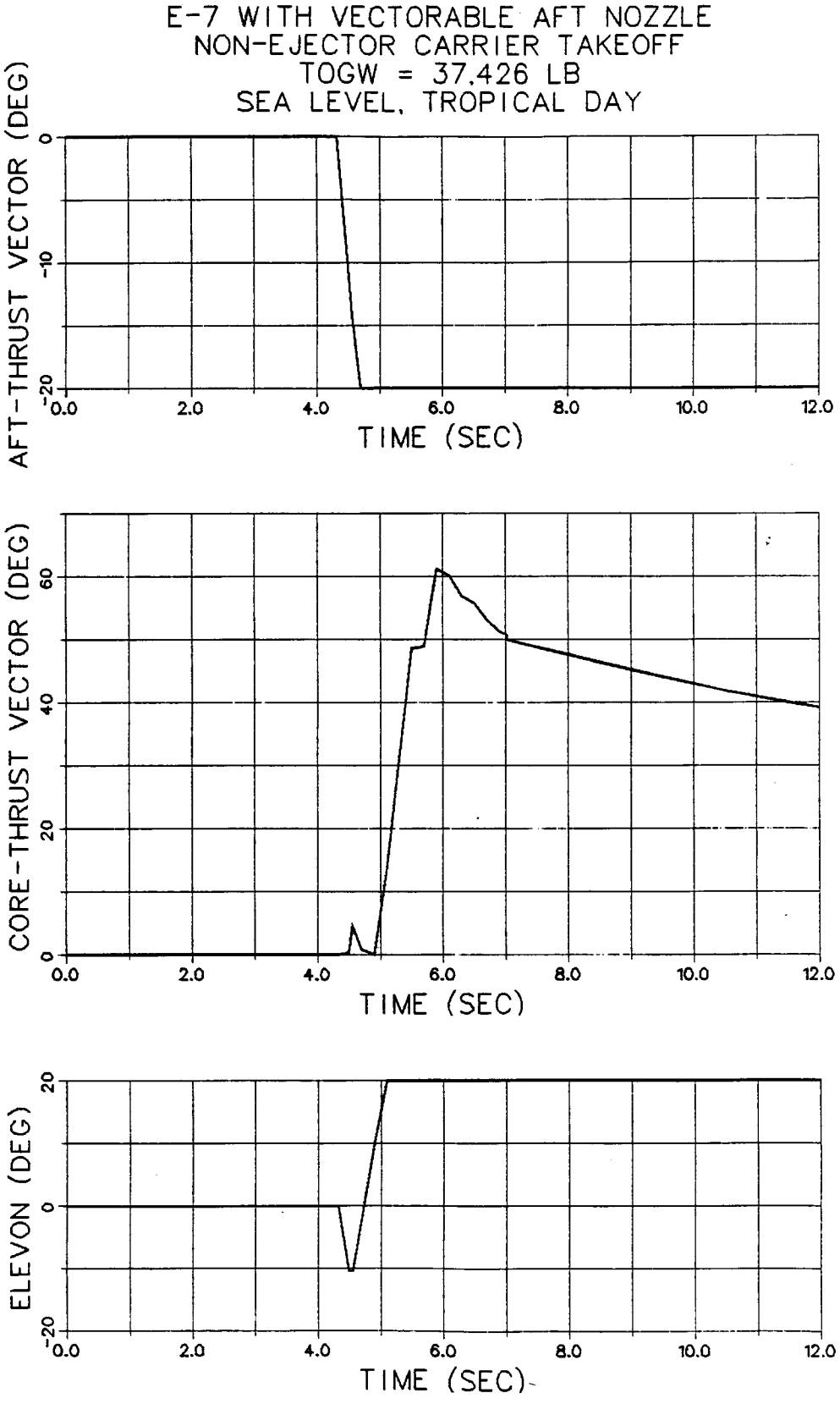

Figure K-1, Non-Ejector-Takeoff Time History (Continued).

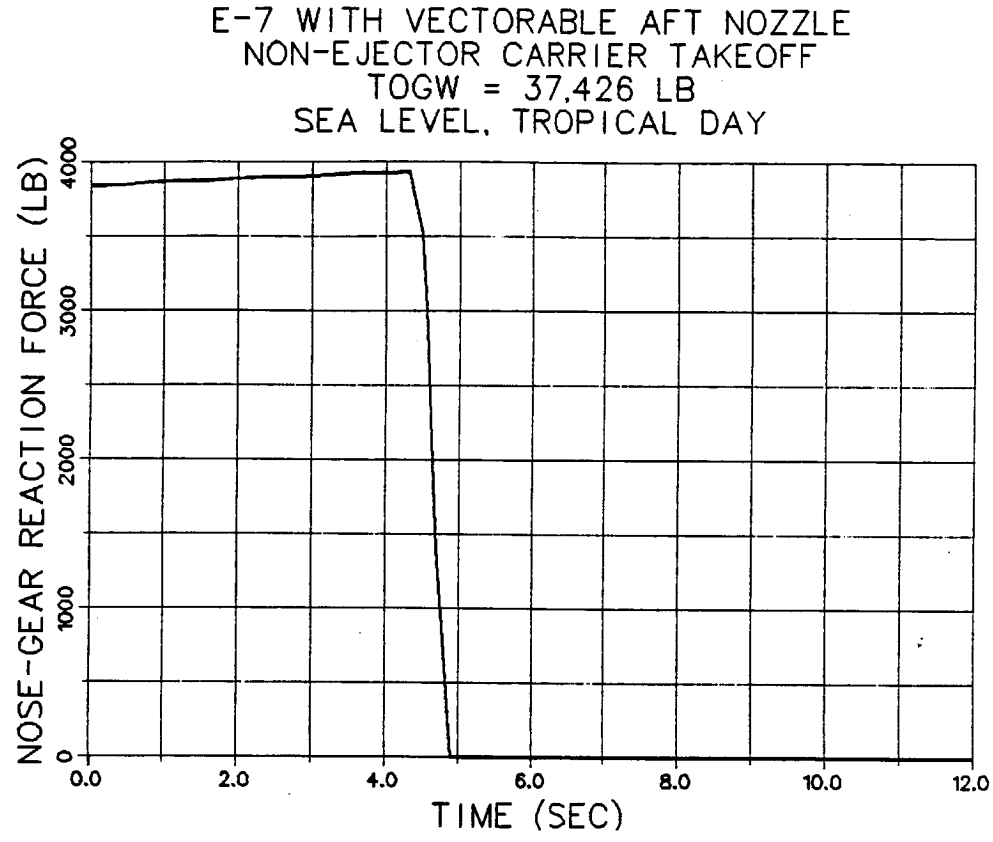

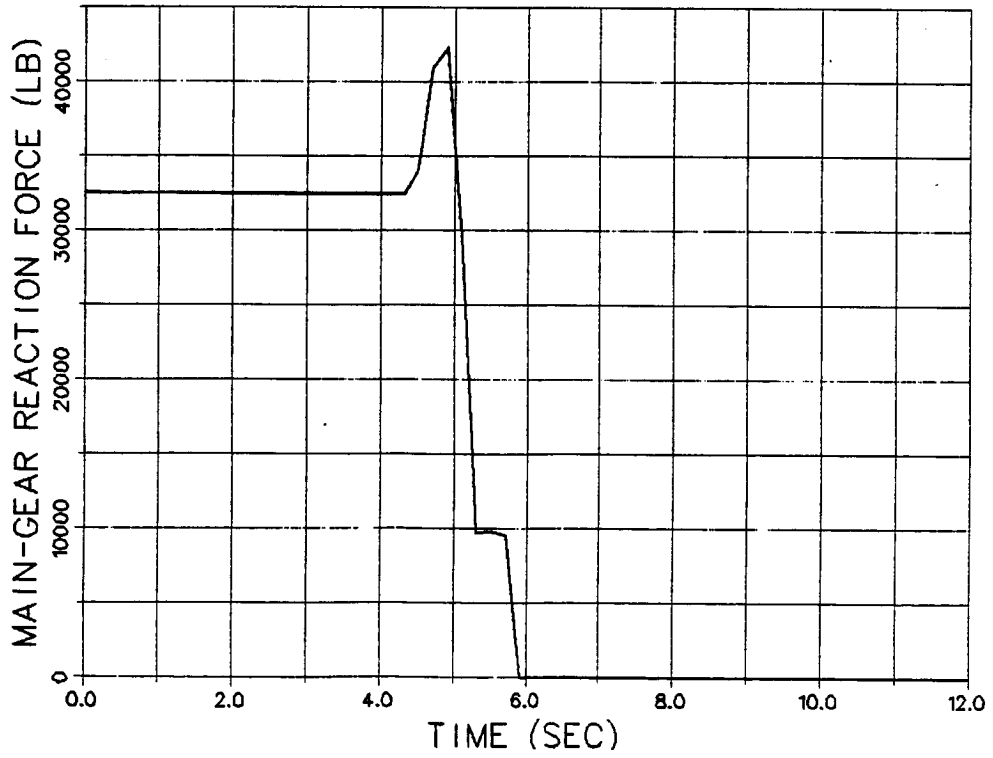

Figure K-1, Non-Ejector-Takeoff Time History (Concluded).

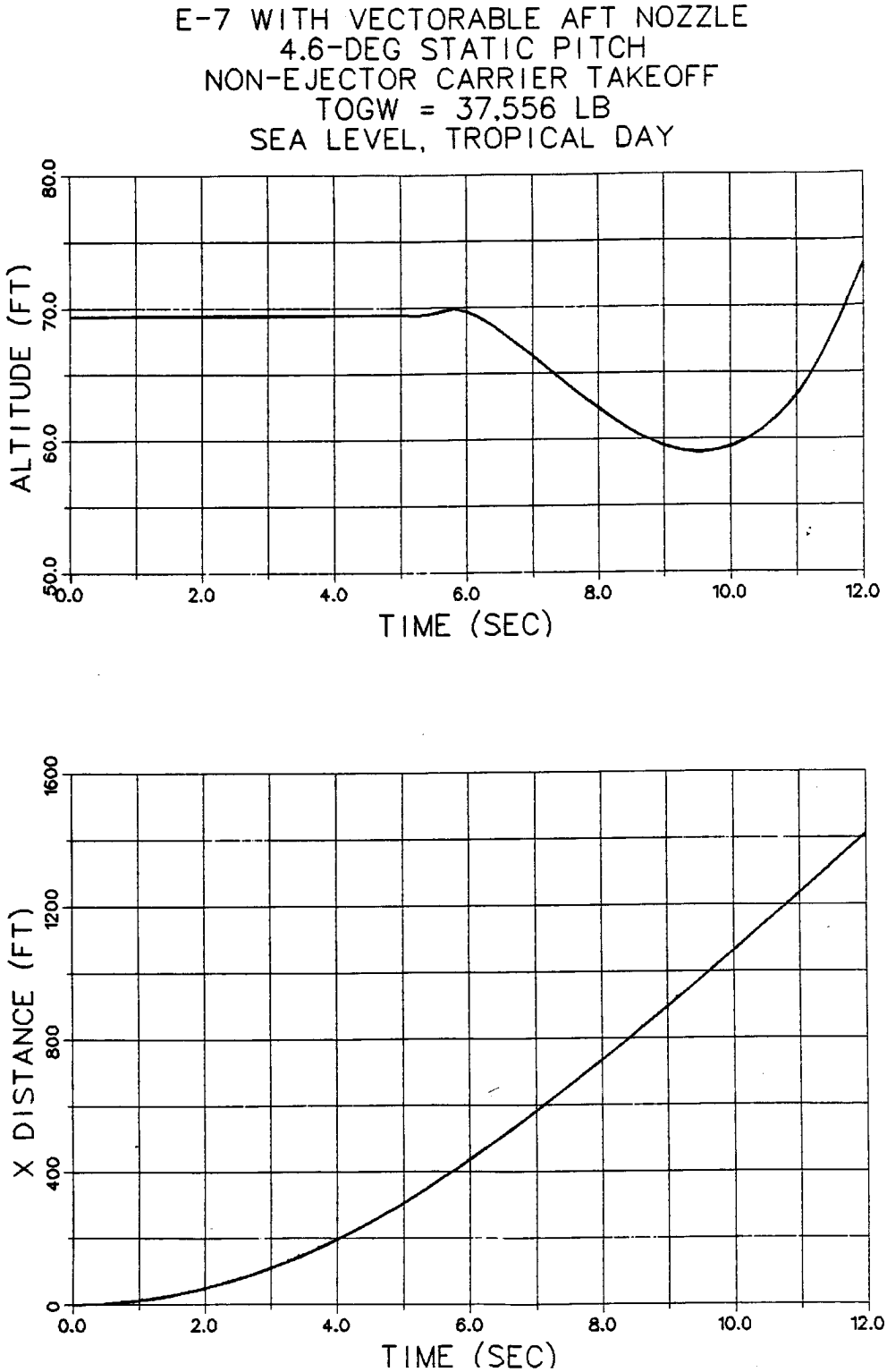

Figure K-2, Non-Ejector-Takeoff Time History for 4.6-Deg Static Pitch.

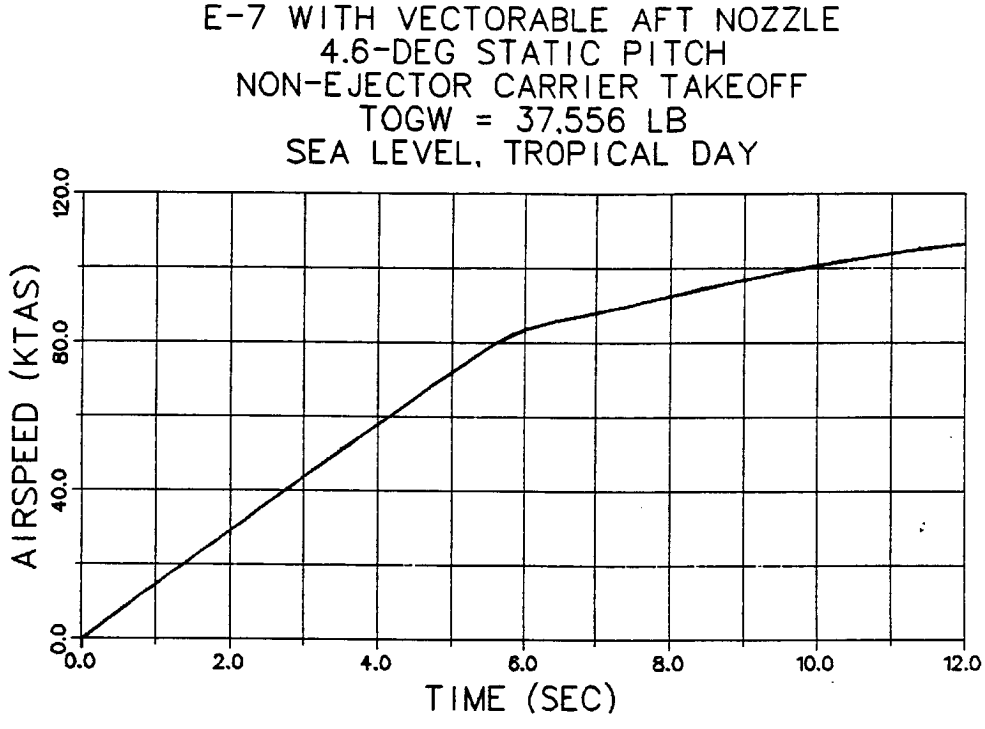

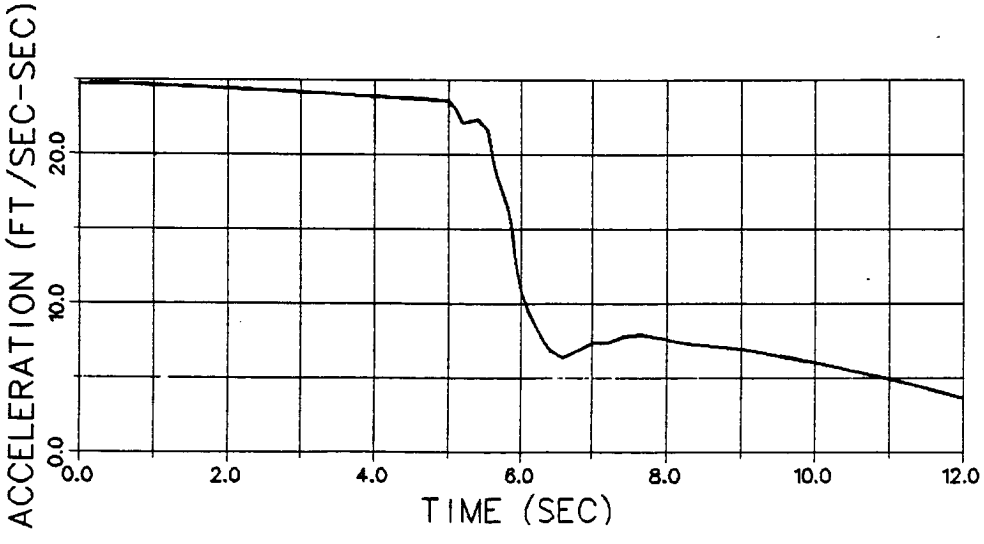

Figure K-2, Non-Ejector-Takeoff Time History for 4.6-Deg Static Pitch (Continued).

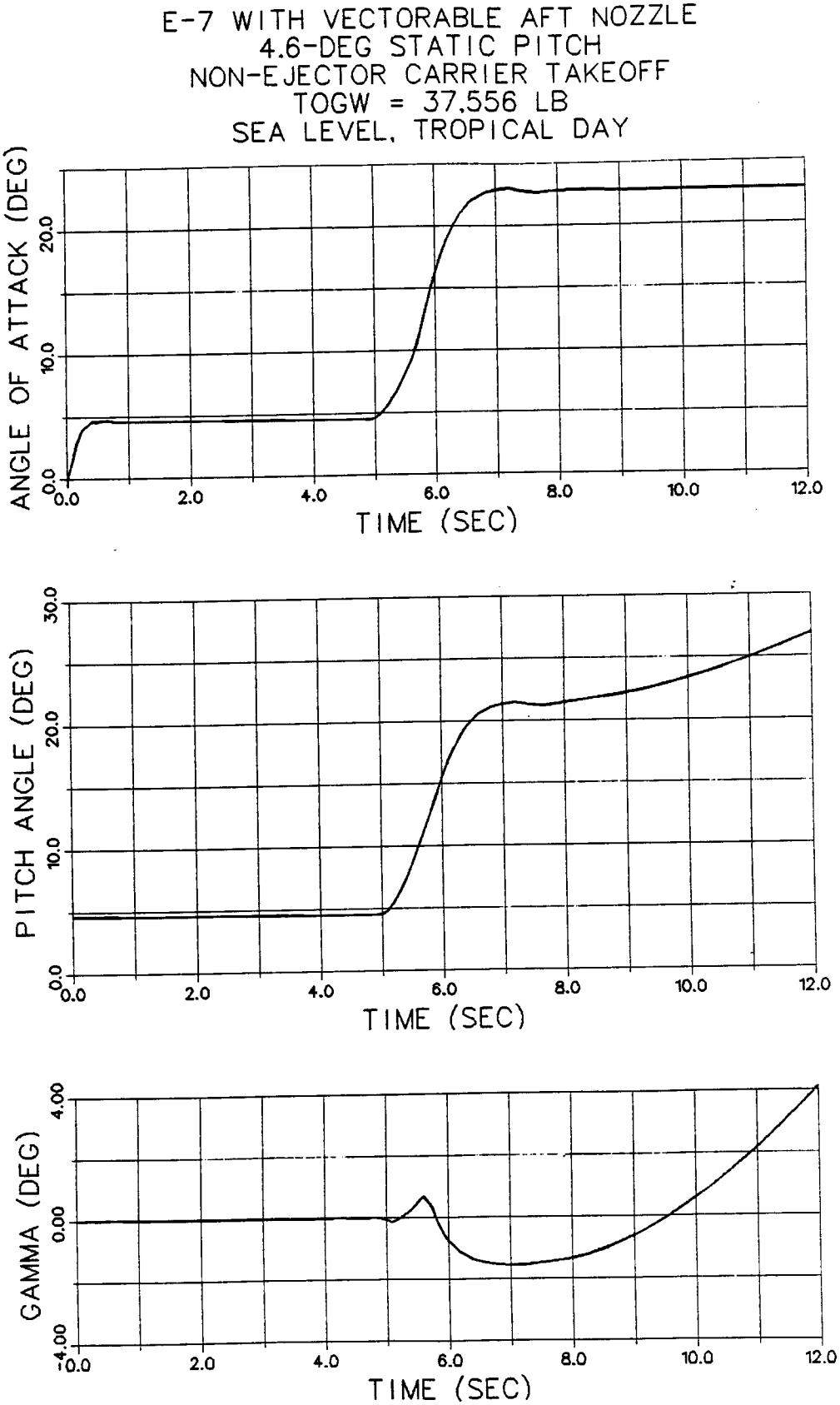

Figure K-2, Non-Ejector-Takeoff Time History for 4.6-Deg Static Pitch (Continued).

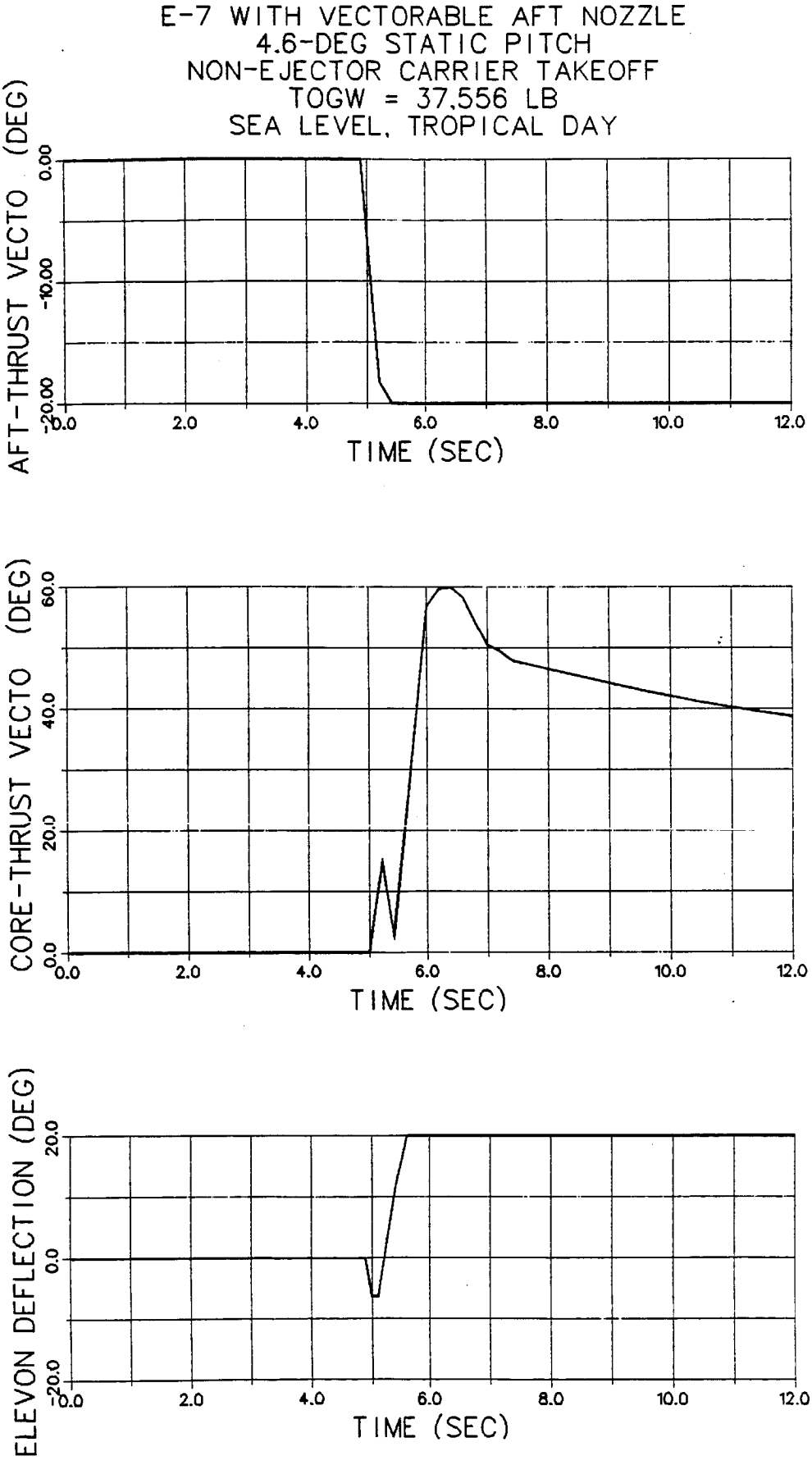

Figure K-2, Non-Ejector-Takeoff Time History for 4.6-Deg Static Pitch (Continued).

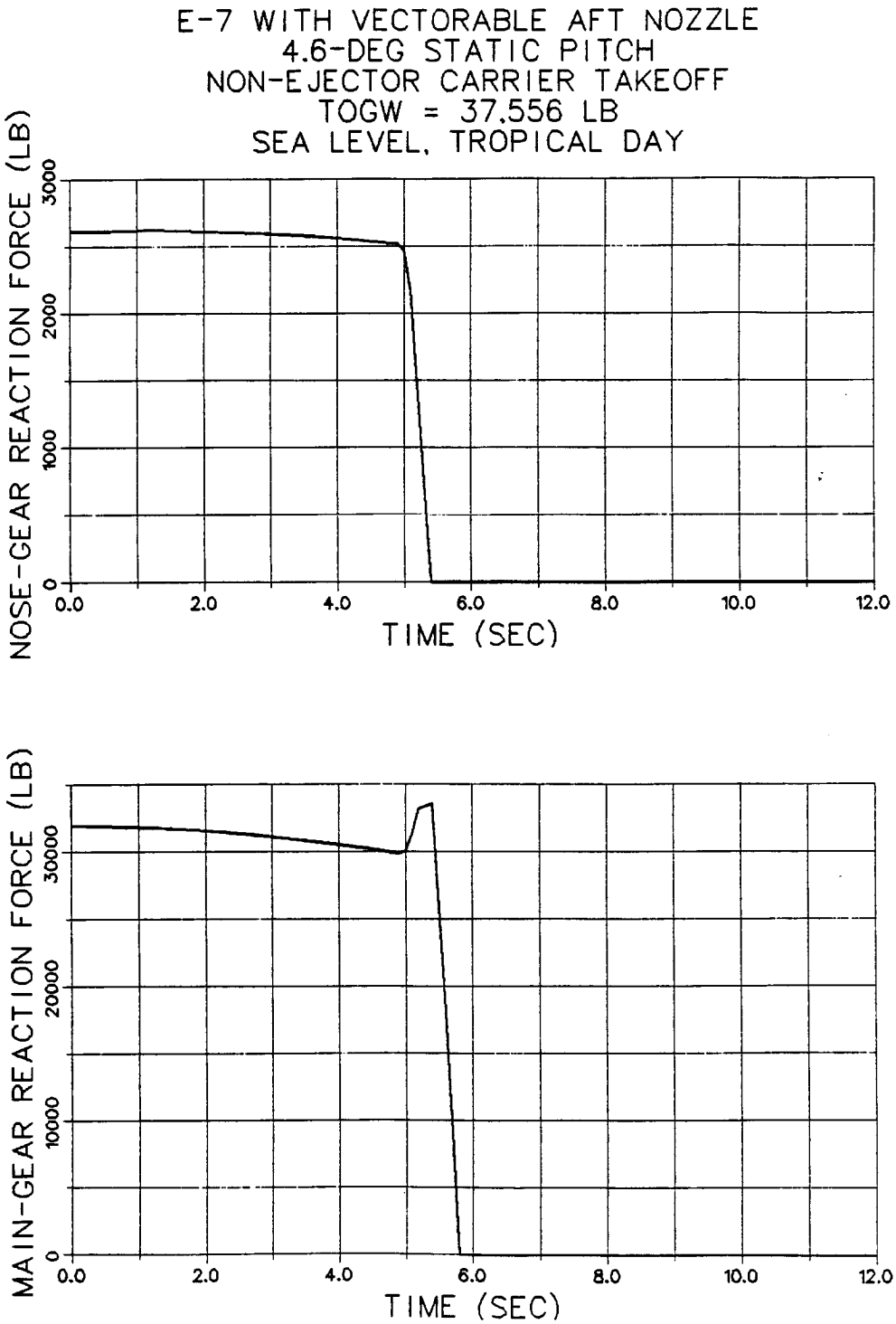

Figure K-2, Non-Ejector-Takeoff Time History for 4.6-Deg Static Pitch (Concluded).

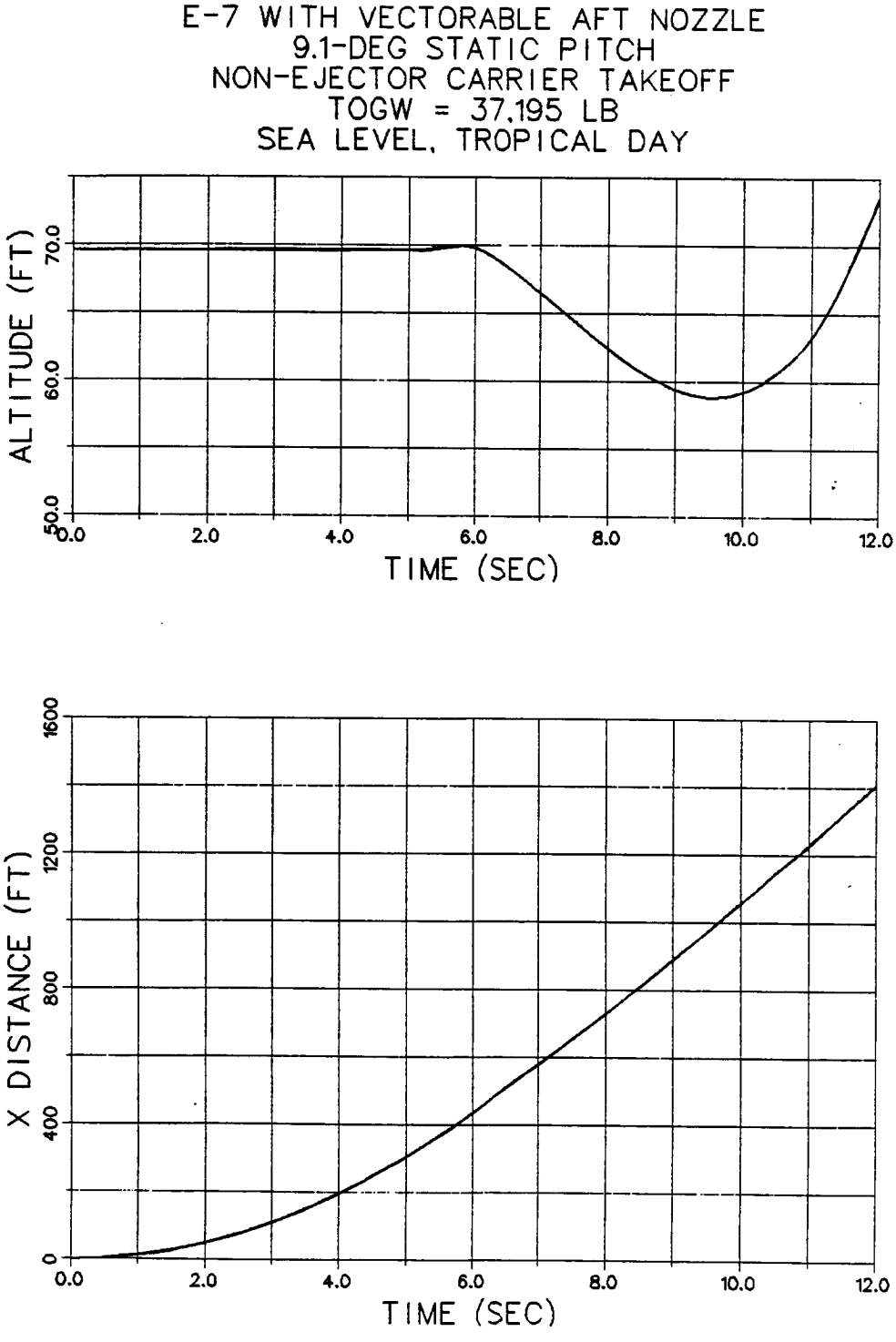

Figure K-3, Non-Ejector-Takeoff Time History for 9.1-Deg Static Pitch.

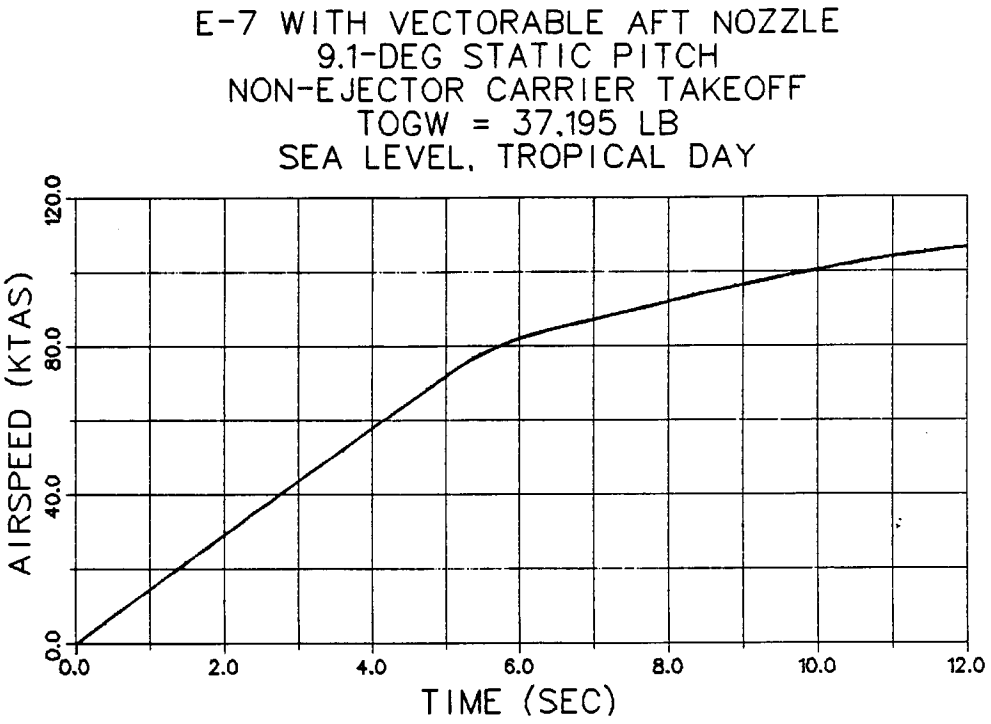

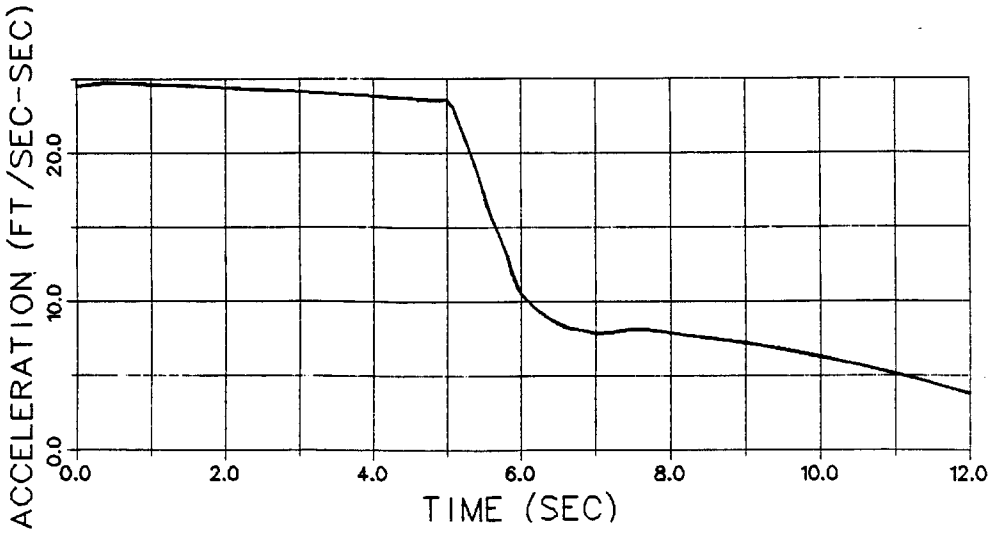

Figure K-3, Non-Ejector-Takeoff Time History for 9.1-Deg Static Pitch (Continued).

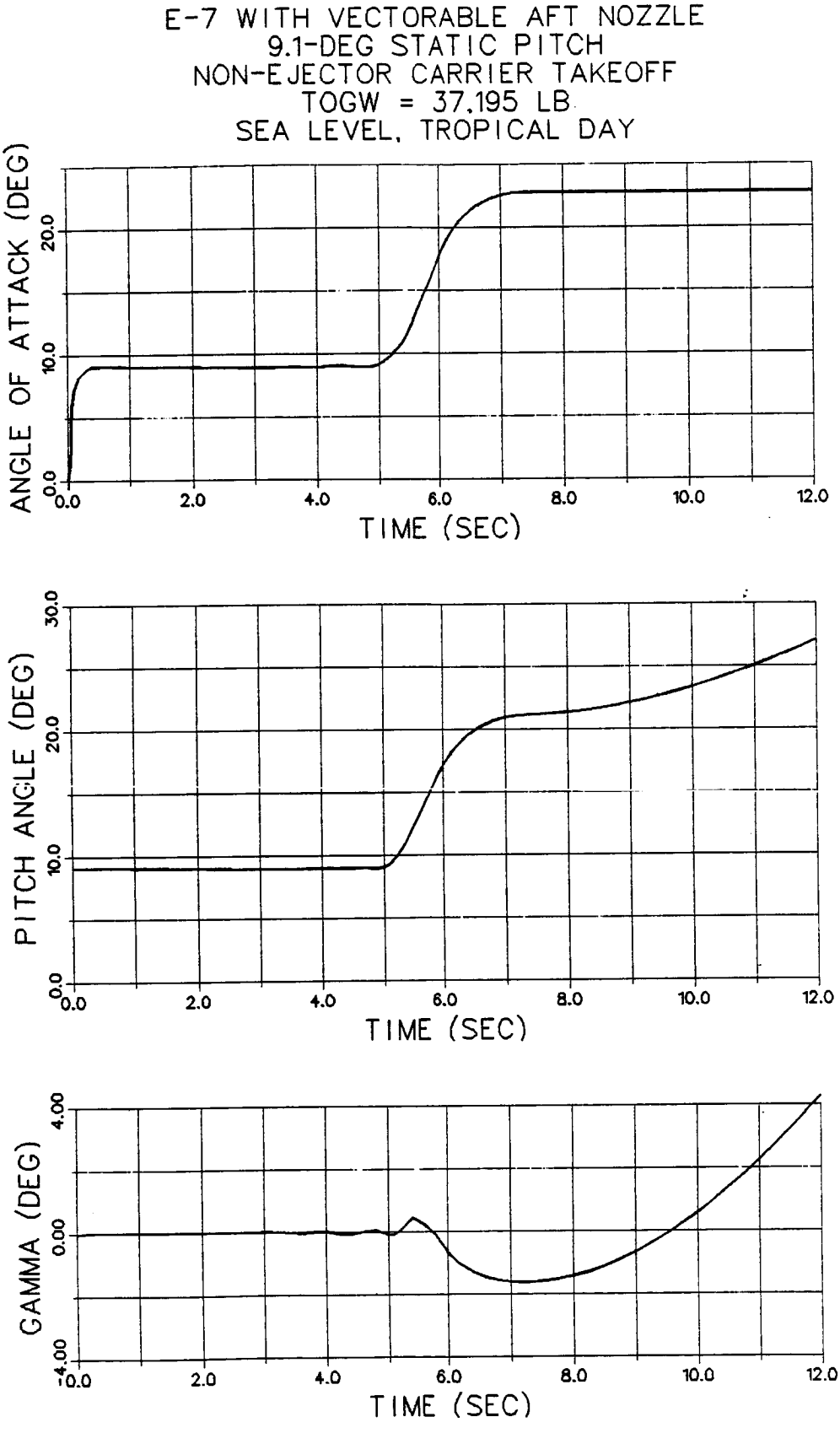

Figure K-3, Non-Ejector-Takeoff Time History for 9.1-Deg Static Pitch (Continued).

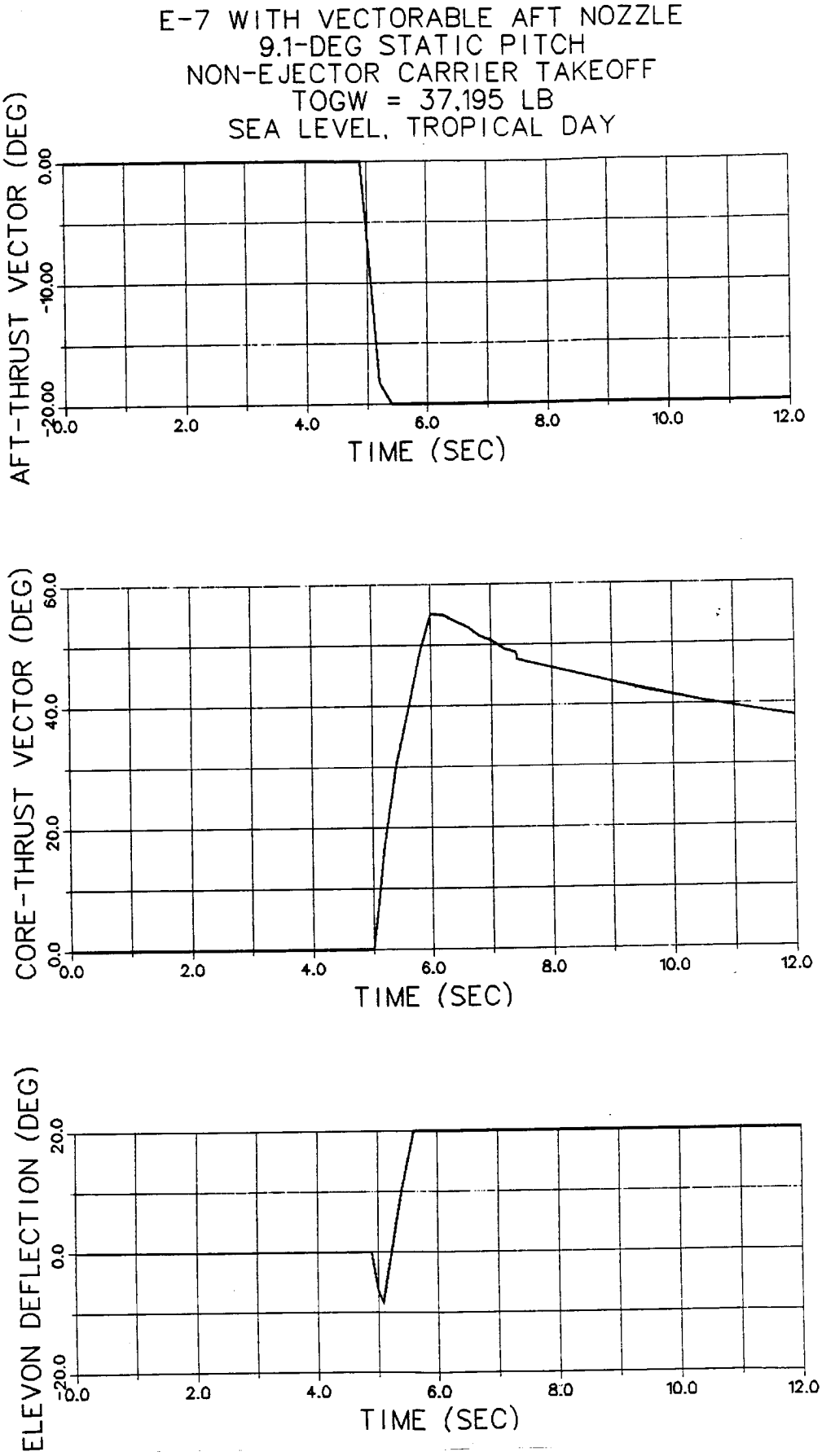

Figure K-3, Non-Ejector-Takeoff Time History for 9.1-Deg Static Pitch (Continued).

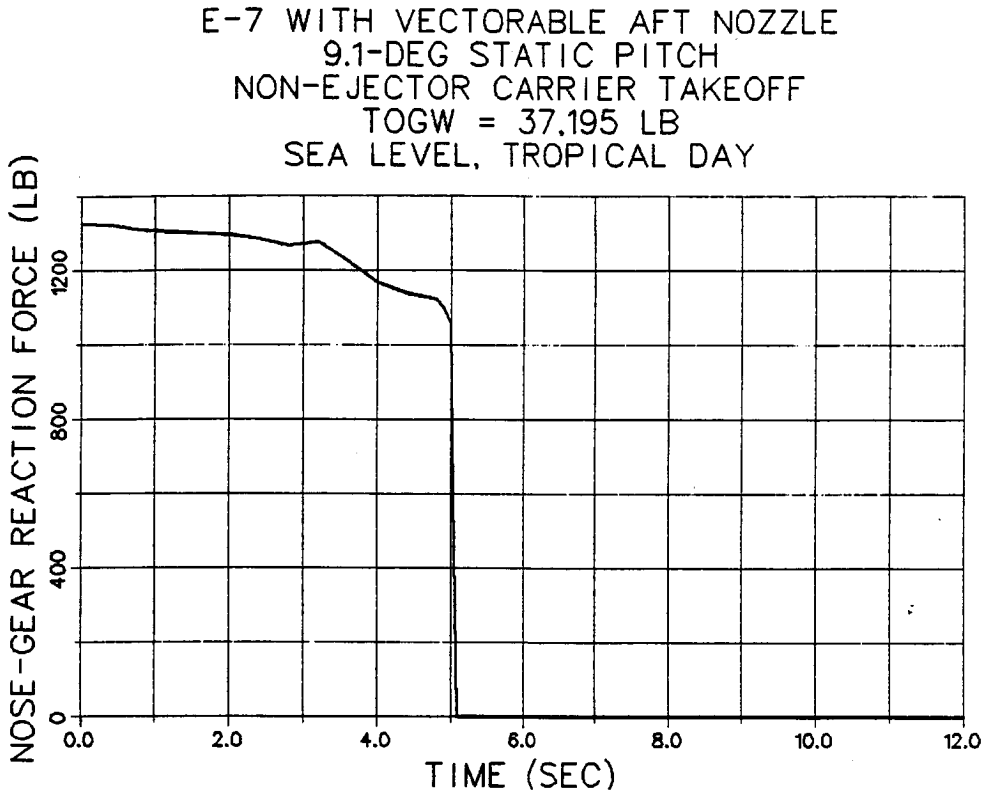

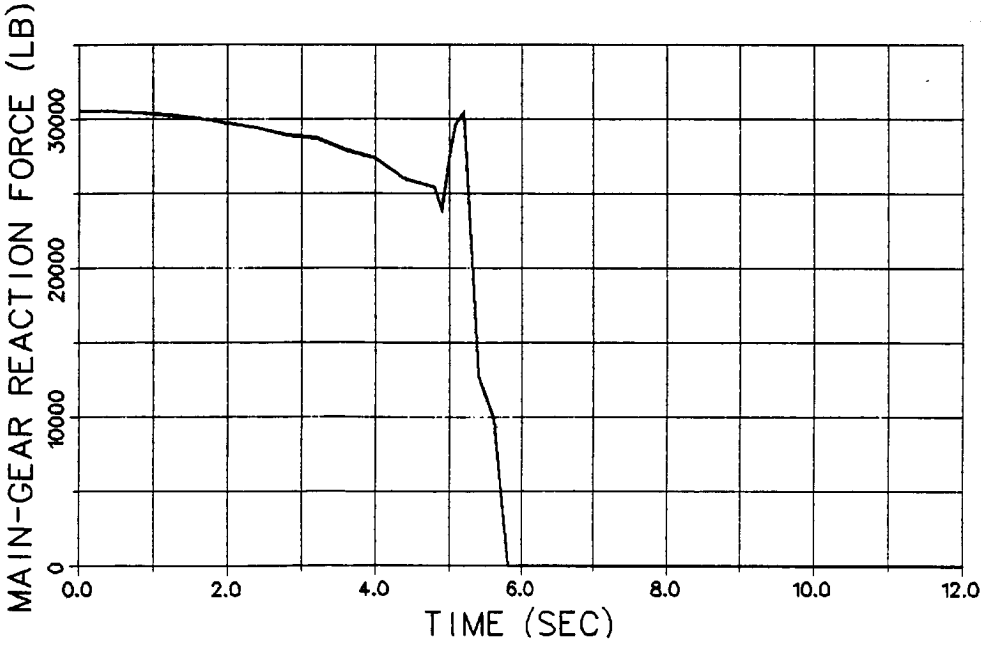

Figure K-3, Non-Ejector-Takeoff Time History for 9.1-Deg Static Pitch (Concluded).

APPENDIX L

International System of Units

U.S. Customary Units have been used for dimensional quantities throughout the report text. Table H-1 provides conversion factors to the International System (SI) of units taken from Reference 14.

Table L-1, SI Units Conversions.

To Convert From	To	Multiply By
ACCELERATION		
foot/second^2	meter/second^2	3.048 E-01
AREA		
foot^2	meter^2	9.290 304 E-02
inch^2	meter^2	6.4516 E-04
DENSITY		
lbm/inch^3	kilogram/meter^3	2.767 990 5 E+04
lbm/foot^3	kilogram/meter^3	1.601 846 3 E+01
slug/foot^3	kilogram/meter^3	5.153 79 E+02
ENERGY		
British thermal unit	joule	1.055 056 E+03
foot lbf	joule	1.355 817 9

Table L-1, SI Units Conversions (Continued).

To Convert From	To	Multiply By
FORCE		
lbf (pound force, avoirdupois)	newton	4.448 221 615 260 5
LENGTH		
foot	meter	3.048 E-01
inch	meter	2.54 E-02
nautical mile (U.S.)	meter	1.852 E+03
statute mile (U.S.)	meter	1.609 344 E+03
MASS		
pound mass, lbm (avoirdupois)	kilogram	4.535 923 7 E-01
slug	kilogram	1.459 390 29 E+01
POWER		
foot lbf/second	watt	1.355 817 9
horsepower (550 foot lbf/second)	watt	7.456 998 7 E+02
PRESSURE		
atmosphere	newton/meter^2	1.013 25 E+05
inch of mercury (32°F)	newton/meter^2	3.386 389 E+03
inch of mercury (60°F)	newton/meter^2	3.376 85 E+03
inch of water (39.2°F)	newton/meter^2	2.490 82 E+02

Table L-1, SI Units Conversions (Continued).

To Convert From	To	Multiply By
inch of water (60°F)	newton/meter^2	2.4884 E+02
lbf/foot^2	newton/meter^2	4.788 025 8 E+01
lbf/inch^2 (psi)	newton/meter^2	6.894 757 2 E+03
millibar	newton/meter^2	1.00 E+02
millimeter of mercury (0°C)	newton/meter^2	1.333 224 E+02
torr (0°C)	newton/meter^2	1.333 22 E+02
SPEED		
foot/second	meter/second	3.048 E-02
kilometer/hour	meter/second	2.777 777 8 E-01
knot (international)	meter/second	5.144 444 444 E-01
mile/hour (U.S. statute)	meter/second	4.4704 E-01
TEMPERATURE		
Celsius (t_C)	kelvin (t_K)	$t_K=t_C+273.15$
Fahrenheit (t_F)	kelvin	$t_K=(5/9)(t_F+459.67)$
Fahrenheit	Celsius	$t_C=(5/9)(t_F-32)$
Rankine (t_R)	kelvin	$t_K=(5/9)t_R$
VISCOSITY		
foot^2/second	meter^2/second	9.290 304 E-02
lbm/foot second	newton second/meter^2	1.488 163 9
lbf second/foot^2	newton second/meter^2	4.788 025 8 E+01
slug/foot second	newton second/meter^2	4.788 025 8 E+01

Table L-1, SI Units Conversions (Concluded).

To Convert From	To	Multiply By
VOLUME		
foot^3	meter^3	2.831 684 659 2 E-02
gallon (U.S. liquid)	meter^3	3.785 411 784 E-03
inch^3	meter^3	1.638 706 4 E-05

REFERENCES

1. Garland, D. B., Static Tests of the J-97 Powered, External Augmentor V/STOL Wind Tunnel Model, DeHavilland Report DHC-DND 77-4, February 1978.

2. Garland, D. B., Phase 1 Wind Tunnel Tests of the J-97 Powered, External Augmentor V/STOL Model, DeHavilland Report DHC-DND 79-4, September 1979.

3. Garland, D. B., and Harris, J. L., Phase 2 and 3 Wind Tunnel Tests of the J-97 Powered, External Augmentor V/STOL Model, DeHavilland Report DHC-DND 80-1, March 1980.

4. Gilbertson, F. L., and Garland, D. B., Static Tests of the J-97 Powered, External Augmentor V/STOL Model at the Ames Research Center, DeHavilland Report DHC-DND 80-2, 1980.

5. Foley, W. H., et al, Study of Aerodynamic Technology for Single-Cruise-Engine V/STOL Fighter Attack Aircraft, NASA CR 166268, February 1982.

6. Beard, B. B., and Foley, W. H., An Engine Trade Study for a Supersonic STOVL Fighter/Attack Aircraft, NASA CR 166304, March 1982.

7. Salguero, D. E., MAPS Handbook, Mission Analysis and Performance System, General Dynamics Report FWD-MRA-2100, October 1980.

8. Beissner, F. L., Jr., Ground Effects on Lift and Drag, General Dynamics Report FWD-MRA-1185, October 1958.

9. 1/14.92-Scale Model 200 Test Data From Calspan 8-Foot Transonic Wind Tunnel (T04-103), unpublished.

10. Convair 218 Navy Strike Fighter, General Dynamics Convair Division Report PSA-74-1002, 15 July 1974, (Confidential)

11. Tyler, S. P., Test Report of Transonic and Supersonic Wind Tunnel Tests of a 1/14.92-Scale Model 218 Airplane, General Dynamics Convair Division Report TR-74-200-08, December 1974.

12. Haldy, J. V., Additional Low-Speed Wind-Tunnel Tests of the General Dynamics 1/14.92-Scale Model 200 Aircraft ...., General Dynamics Convair Division Report GDLST-651, 1974.

13. NATOPS Flight Manual, Navy Model AV-8A and TAV-8A Aircraft, NAVAIR 01-av8a-1, 15 January 1978.

14. Mechtly, E. A., The International System of Units: Physical Constants and Conversion Factors, NASA SP-7012, 1973.

1. Report No.	2. Government Accession No.	3. Recipient's Catalog No.
NASA CR 177330		

4. Title and Subtitle	5. Report Date
Parametric Study of Supersonic STOVL Flight Characteristics	January 1985
	6. Performing Organization Code
7. Author(s)	8. Performing Organization Report No.
David C. Rapp	
9. Performing Organization Name and Address General Dynamics Corp., Forth Worth Div. P.O. Box 748 Fort Worth, Texas 76101	10. Work Unit No. JO 6490
	11. Contract or Grant No. NAS2-11753
12. Sponsoring Agency Name and Address National Aeronautics & Space Administration Washington, D.C. 20546	13. Type of Report and Period Covered Contractor Report
	14. Sponsoring Agency Code RTOP 533-02-51

15. Supplementary Notes

Point of Contact: Technical Monitor, George H. Kidwell, MS 237-11
Ames Research Center, Moffett Field, CA 94035
(415) 694-5886 or FTS 464-5886

16. Abstract

A number of different control devices and techniques are evaluated to determine their suitability for increasing the short takeoff performance of a supersonic short-takeoff/vertical landing (STOVL) airplane. Analysis was based on a rigid-body mathematical model of the General Dynamics E-7, a single engine configuration that utilizes ejectors and thrust deflection for propulsive lift. Alternatives that were investigated include increased static pitch the addition of a close-coupled canard, use of boundary layer control to increase the takeoff lift coefficient, and the addition of a vectorable aft fan air nozzle. Other performance studies included the impact of individual E-7 features, the sensitivity to ejector performance, the effect of removing the afterburners, and a determination of optional takeoff and landing transition methods. The results pertain to both the E-7 and configurations other than the E-7. Several alternatives were not as well-suited to the E-7 characteristics as the world be to an alternative configuration, and vice versa. A large amount of supporting data for each analysis is included.

17. Key Words (Suggested by Author(s))	18. Distribution Statement
Supersonic STOVL Parametric Analysis Aircraft Performance	Unclassified Subject category 05

19. Security Classif. (of this report)	20. Security Classif. (of this page)	21. No. of Pages	22. Price*
Unclassified	Unclassified	229	

*For sale by the National Technical Information Service, Springfield, Virginia 22161

PRECEDING PAGE BLANK NOT FILMED